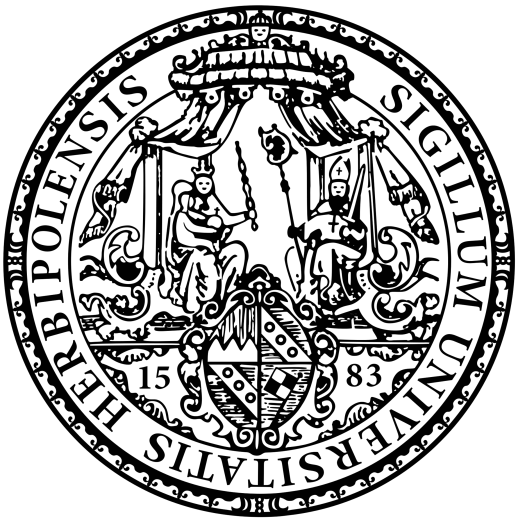

Development of techniques for studying the platelet glycoprotein receptors GPVI and GPIb localisation and signalling

• • •

Entwicklung von Methoden zur Untersuchung zur der Lokalisation und Signaltransduktion der Thrombozytenrezeptoren GPVI und GPIb

Doctoral thesis for a doctoral degree
at the Graduate School of Life Sciences,
Julius-Maximilians-Universität Würzburg,

Section Biomedicine

submitted by

Raluca Alexandra Iulia Neagoe

From Campina, Romania

Würzburg, 2022

Joint PhD Degree between the

University of Birmingham

Institute of Cardiovascular Sciences

and the

Julius-Maximilians-Universität Würzburg

Institute of Experimental Biomedicine

Submitted on:

Members of the Thesis Committee:

Chairperson:	Prof. Dr. Thomas Dandekar
Primary Supervisor:	Prof. Dr. Bernhard Nieswandt
Supervisor (Second):	Dr. Natalie S. Poulter
Supervisor (Third):	Prof. Dr. David Stegner
Supervisor (Fourth):	Prof. Dr. Katrin G. Heinze

Date of Public Defence:

Date of Receipt of Certificate:

Summary

Platelets play an important role in haemostasis by mediating blood clotting at sites of blood vessel damage. Platelets, also participate in pathological conditions including thrombosis and inflammation. Upon vessel damage, two glycoprotein receptors, the GPIb-IX-V complex and GPVI, play important roles in platelet capture and activation. GPIb-IX-V binds to von Willebrand factor and GPVI to collagen. This initiates a signalling cascade resulting in platelet shape change and spreading, which is dependent on the actin cytoskeleton. This thesis aimed to develop and implement different super-resolution microscopy techniques to gain a deeper understanding of the conformation and location of these receptors in the platelet plasma membrane, and to provide insights into their signalling pathways. We suggest *direct* stochastic optical reconstruction microscopy (*d*STORM) and structured illumination microscopy (SIM) as the best candidates for imaging single platelets, whereas expansion microscopy (ExM) is ideal for imaging platelets aggregates. Furthermore, we highlighted the role of the actin cytoskeleton, through Rac in GPVI signalling pathway. Inhibition of Rac, with EHT1864 in human platelets induced GPVI and GPV, but not GPIbα shedding. Furthermore, EHT1864 treatment did not change GPVI dimerisation or clustering, however, it decreased phospholipase Cγ2 phosphorylation levels, in human, but not murine platelets, highlighting interspecies differences. In summary, this PhD thesis demonstrates that; 1) Rac alters GPVI signalling pathway in human but not mouse platelets; 2) our newly developed ExM protocol can be used to image platelet aggregates labelled with F(ab') fragments.

Zusammenfassung

Thrombozyten, spielen in der Hämostase eine entscheidende Rolle, indem sie die Blutstillung bei Gefäßverletzung vermitteln. Sie sind jedoch auch an pathologischen Prozessen wie zum Beispiel der Thrombose und Entzündungen beteiligt. Bei einer Gefäßverletzung spielen zwei Glykoproteinrezeptoren eine wichtige Rolle bei der Adhäsion und Aktivierung von Thrombozyten: der GPIb-IX-V-Komplex und GPVI. GPIb-IX-V bindet an den von-Willebrand-Faktor und GPVI an Kollagen. Dies initiiert eine Signalkaskade, die zu einer Änderung der Morphologie der Thrombozyten führt, welche vom Aktin-Zytoskelett abhängig ist. Ziel dieser Doktorarbeit war die Entwicklung und Anwendung verschiedener hochauflösender Mikroskopietechniken, um ein tieferes Verständnis der Konformation und Lokalisation dieser Rezeptoren in der Plasmamembran der Thrombozyten zu erlangen und Einblicke in ihre Signalwege zu gewinnen. Hierbei etablierten wir *d*STORM und die *structured illumination microscopy* (SIM) als die geeignetsten Methoden für die mikroskopische Untersuchung einzelner Thrombozyten, während die Expansionsmikroskopie (ExM) ideal für die Darstellung von Thrombozytenaggregaten ist. Darüber heben unsere Ergebnisse zur Funktion von Rac im GPVI Signalweg die wichtige Rolle des Aktin-Zytoskeletts hervor. Die Hemmung von Rac mit EHT1864 in menschlichen Thrombozyten induzierte das Abscheiden (*shedding*) von GPVI und GPV, nicht jedoch von GPIbα. Darüber hinaus blieb die GPVI-Dimerisierung und GPVI-Clusterbildung durch EHT1864-Behandlung unverändert, jedoch verringerte sich die Phosphorylierung der Phospholipase Cγ2 in humanen, aber nicht in murinen Thrombozyten, was Unterschiede zwischen den Spezies aufzeigt. Zusammenfassend zeigen die Ergebnisse dieser Doktorarbeit, dass; 1) Rac den GPVI-Signalweg in humanen aber nicht in murinen Thrombozyten beeinflusst; 2) unser neu entwickeltes ExM-Protokoll zur Darstellung von F(ab')-Fragment markierten Thrombozytenaggregaten verwendet werden kann.

Table of Contents

List of Figures

List of Tables

CHAPTER 1

General introduction

1.1 Introduction to platelets

Platelets are small anucleate blood cells that are derived from megakaryocytes (MKs) and play a fundamental role in haemostasis and thrombosis. They were first identified in 1881 by Bizzozero, who observed that they are the first blood cell adhering to the endothelium upon damage (Bizzozero, 1881). After over a century, we have a much deeper understanding of their function in physiological and pathological processes, such as blood clotting or atherosclerosis, respectively (Harrison, 2005).

1.1.1 Platelets biogenesis

MKs are giant cells that have a variety of functions, including platelet formation and the control of hematopoietic stem cells (HSCs). MKs are derived from HSC in a process named megakaryopoiesis, which is regulated by several cytokines, including thrombopoietin (TPO) as the chief regulator (Zucker-Franklin and Kaushansky, 1996). Once the MKs are mature, they move to the sinus of the bone marrow and start the process of releasing platelets. According to the present model, MKs extend cytoplasmic protrusions, named proplatelets across the vessel barrier into the bloodstream (Kowata et al., 2014). However, the signal that induces MKs to produce the protrusions in the right direction is yet unknown, but it is suggested that the modulation of cytoskeletal proteins, including the actin cytoskeleton and microtubules (MTs), may play a role in this polarization (Tilburg et al., 2022). A MT-driven process produces proplatelets which start with the erosion of one of the MKs' poles, producing pseudopodial-like structures that are thin and branch to produce small tubular projections (Thon and Italiano, 2010). It is only at the tip of the proplatelet shaft where platelets are formed, receiving organelles and granules from the MK. Anuclated proplatelets become platelets by detaching from the MK through a process driven by MTs, forming rings that provide platelets with their shape, and supported by the high shear force of the blood flow (Twomey et al., 2019). Further, MTs facilitate the movement of mitochondria and granules into the developing

platelets (Richardson et al., 2005). When platelets are released into the blood, they have a limited life span. In humans, platelets circulate, on average, for 7-10 days at a normal platelet count of 150 – 400 x 10^3 platelets per microliter (Daly, 2011), whereas in mice they circulate for around 4 days at a normal platelet count of 1,000 – 1500 x 10^3 platelets per microliter (Fox et al., 2006). Then phagocytic cells, such as macrophages in the spleen, and Kupffer cells in the liver, remove aged, malfunctioning, or pre-activated platelets from the bloodstream (Quach et al., 2018a). A homeostatic equilibrium between platelet generation and clearance results in a constant number of platelets in circulation.

1.1.2 Platelets structure

Platelets are the second most abundant blood cells. Human platelets measure around 2 μm in diameter, while mouse platelets are even smaller reaching only approximately 1 μm, with an average thickness of 0.5 μm. Human and murine platelets have a volume of 8 fL and 4 fL, respectively (Aurbach et al., 2019, Thon and Italiano, 2010). The platelet structure is schematised in **Figure 1.1**.

Regarding the intracellular structure of platelets, they contain several cellular organelles, granules and mitochondria, and also microtubules and actin filaments. All derive from MKs, as platelets lack a nucleus. Platelet granules are classified into 3 types: α-granules, dense granules and lysosomal granules. α-granules are the most abundant granules (between 50 and 80 per human platelet) and contain several receptors, such as glycoprotein (GP)VI, integrin αIIbβ3, the GPIb-IX-V complex, as well as von Willebrand Factor (vWF), fibrinogen, P-selectin, thrombospondin, and coagulation factors (FV and FIX) (Michelson et al., 2019). Dense granules are smaller and the second most abundant granules (between 3 and 8 per human platelet). They contain high amounts of non-protein molecules that promote platelet activation, for example, adenosine diphosphate (ADP), adenosine triphosphate (ATP) and calcium (Ca^{2+}), amongst others. There are relatively few lysosomes in human platelets (between 0 and 2 per cell) but they play an

important role in extracellular functions, including receptor cleavage and matrix degradation. Lysosomes contain more than 10 acid hydrolases and proteases like cathepsin D (Sevlever et al., 2008). Finally, platelets also present glycosomes, containing glycogen, and mitochondria, which, as in any other cell type, provide energy in the form of ATP, and a dense tubular system that is a residual endoplasmic reticulum from MKs that seems to be empty in platelets (Heijnen and van der Sluijs, 2015, Gremmel et al., 2016, Twomey et al., 2019).

The platelet surface is composed of the plasma membrane, which is a lipid bilayer that plays a key role in platelet activation, as it contains tissue factor (TF), and phosphatidylserine (PS), which upon activation flips to the outer side of the plasma membrane and binds coagulation factors (Reddy and Rand, 2020, Vignoli et al., 2013). On the extracellular side of the plasma membrane, a thick glycocalyx surrounds the platelet, and on the intracellular side, actin filaments and microtubules form the membrane skeleton, which allows platelets to change shape during spreading. Another fundamental component of the plasma membrane is the open canalicular system; folds of the plasma membrane that provide platelets with a larger surface to facilitate spreading (Selvadurai and Hamilton, 2018). Platelets also express a wide range of receptors on their plasma membrane; these are responsible for binding different platelet agonists/ligands, interacting with other cells and pathogens, as well as platelet signalling. Major receptors include integrins, with integrin αIIbβ3 the most abundant platelet receptor. All the integrins have an α- and β-subunit, and they bind to different ligands. Among others, the plasma membrane presents leucine-rich repeat receptors, such as GPIb/IX/V complex and Toll-like receptors, C-type lectin receptors including, P-Selectin and CLEC-2, and receptors belonging to the immunoglobulin superfamily, such as GPVI (Twomey et al., 2019).

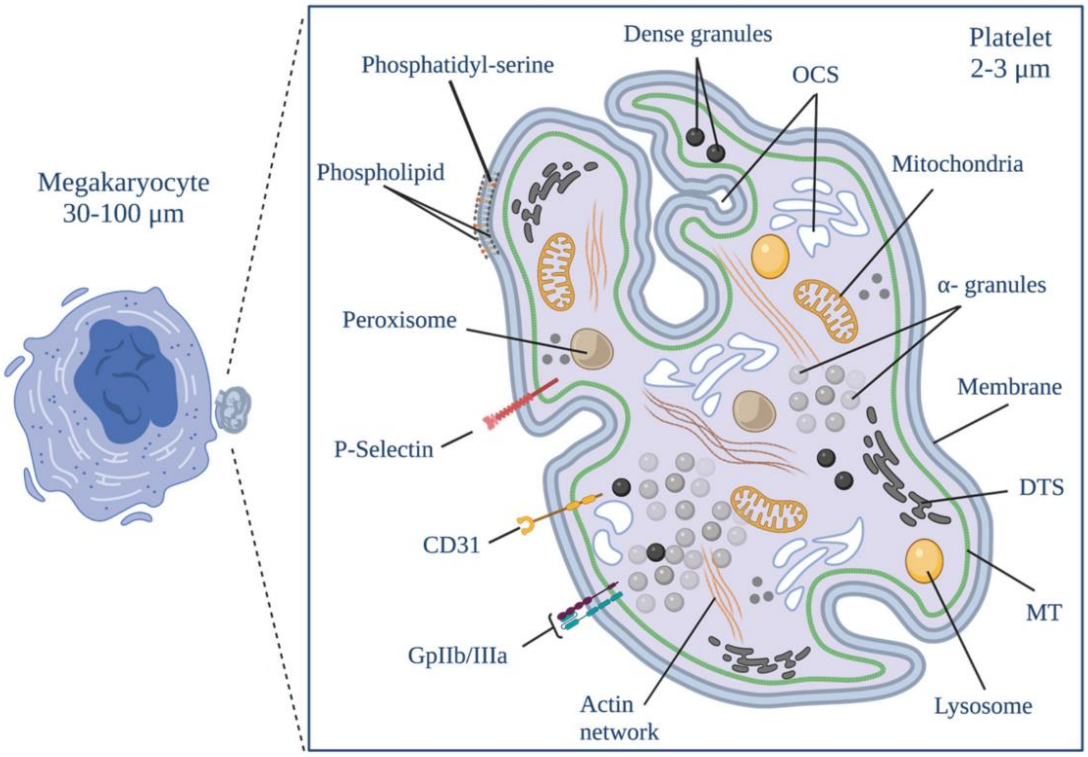

Figure 1.1. The platelet structure. Schematic representation of the platelet structure. The platelet cytosol contains α-granules, dense granules, lysosomes, mitochondria, the dense tubular system (DTS), and the platelet cytoskeleton (actin network and microtubules (MT)). The cytosol is surrounded by the plasma membrane, which presents several receptors GPs and P-selectin, and the membrane has folds named the open canicular system (OCS). Image modified from (Durán-Saenz et al., 2022).

1.1.3 Platelets receptors

Since platelets are primarily responsible for haemostasis, it is not surprising that their main receptors participate in this process, either by activating platelets or by interacting with damaged cell walls and other platelets to build a thrombus. The diversity of receptors present on platelets, along with signalling pathways, underscores the capability to adapt their functions to several situations (Michelson et al., 2019). The main platelet receptors are schematised in **Figure 1.2**.

Integrins

Integrins are noncovalent-associated heterodimers formed by an α- and β-subunit that in resting platelets are found in a low-affinity state, and upon activation change to a high-

affinity state. Platelets have in total 5 integrins, classified into 2 families (β1 and β3) (Shattil and Newman, 2004). The most important ones are integrin αIIbβ3 and α2β1. The most relevant and abundant integrin (and platelet receptor) is the integrin αIIbβ3 (CD41/CD61), also known as the GPIIb-IIIa complex. Platelets express approximately 80,000 molecules, and more than 30,000 molecules can be added to the plasma membrane from the α-granules upon platelet activation (Litjens et al., 2003). The integrin αIIbβ3 binds to fibrinogen, fibrin, vWF, and fibronectin among other ligands. Platelet activation enhances integrin lateral mobility and clustering on the plasma membrane, in addition to conformational alterations (Bennett, 2005). Integrin αIIbβ3 activation and function are described in the following section (**section 1.1.4**). The second most important integrin is α2β1 (CD49b/CD29), also known as GPIa-IIa. In platelets and other cells, it binds to collagen, facilitating platelet adhesion and thrombus stabilisation (Staatz et al., 1989).

Leucine-rich repeat (LRR) family

The GPIb-IX-V complex, the toll-like receptors (TLRs) and the nucleotide-binding oligomerisation domain 2 (NOD2) compose the platelet LRR family, which is characterised by repetitions of 20 to 30 amino acids rich in leucine. The GPIb-IX-V complex is the second most abundant platelet receptor, with approximately 50,000 molecules per platelet (Burkhart et al., 2012), and is formed of the subunits GPIbα, GPIbβ, GPIX in a ratio of 1:2:1, with GPV weakly bound to GPIbα by a transmembrane domain interaction (Li, 2022). GPIbβ is bound to the complex by disulfate bonds; in contrast, GPV is weakly bound by a transmembrane domain interaction to GPIbα (Romo et al., 1999, McEwan et al., 2011, Bendas and Schlesinger, 2022). GPIbα (135 kDa) is the largest component of the complex, followed by GPV (82 kDa), GPIbβ (25 kDa), and GPIX (20 kDa) (Strassel et al., 2004). GPIbα is the main subunit of the complex, and its major ligand is vWF, but it also binds to collagen, thrombin, thrombospondin, kininogen,

and FXI and XII, among other ligands (Andrews and Gardiner, 2016). GPIbα is described in detail in **section 1.3**. TLRs are less abundant in platelets than the GPIb-IX-V complex, but we can find mainly TLR2, TLR4, and TLR9, and they are responsible for binding pathogens and releasing cytokines and chemokines (Hally et al., 2020). With muramyl dipeptide as its ligand, NOD2 is a pattern recognition receptor (Michelson et al., 2019).

Seven transmembrane receptors

The seven transmembrane receptors, also known as G protein-coupled receptors (GPCRs) are the major family of agonist receptors in cells and are particularly prominent in platelets, where they play an essential role in the activation of platelets. There are multiple GPCRs in platelets, with thrombin receptors being the most abundant and important. Thrombin binds to 3 GPCRs: protease-activated receptor (PAR)1 (only in human platelets), PAR3 (only in mouse platelets) and PAR4. All of these PARs are activated by thrombin-mediated cleavage of a part of their N-terminal domain, which reveals a new N-terminal region that functions as a tethered ligand for the receptor (Kahn et al., 1999). The ADP receptors bind to ADP secreted by the dense granules of the platelets. Platelet membranes contain two types of ADP receptors, $P2Y_1$ and $P2Y_{12}$ (guanosine triphosphate coupled protein receptors). There are many other receptors included in this family, such as the glycoprotein and thromboxane (TX) receptors (Rivera et al., 2009).

Immunoglobulin superfamily receptors

The immunoglobulin (Ig) superfamily is a vast set of receptors that play a role in platelet activation and ligand binding. All of these receptors contain at least one Ig domain. This superfamily includes several receptors: GPVI, FcγRIIa, FcεRI, junction adhesion molecules (JAMs), intracellular adhesion molecule 2 (ICAM-2), and G6b-B among others (Michelson et al., 2019). I will focus only on GPVI, the major signalling collagen receptor

in platelets, which, together with the integrin α2β1 is essential for the early stage activation and adhesion of platelets. GPVI contains two extracellular IgG domains, called D1 and D2, and each GPVI molecule is associated with FcRγ-chain, which is responsible for its signalling capabilities (Moroi and Jung, 2004). GPVI is described in detail in **section 1.2**.

C-type lectin receptor family

C-type lectin receptor family is composed of P-Selectin, C-type lectin-like receptor-2 (CLEC-2), cluster of differentiation (CD)72, and some others. All these receptors play a role in adhesion. P-Selectin, also known as CD62P, is stored in α-granules in resting platelets, and upon activation is transferred to the platelet plasma membrane, where approximately 13,000 P-Selectin molecules per platelet can be found (McEver, 2007). CLEC-2's first discovered ligand was the snake venom rhodocytin (Suzuki-Inoue et al., 2006), and its physiological ligand is podoplanin. Interestingly, the blood vessels do not present natural CLEC-2 ligands, therefore the role of this receptor in haemostasis is still under debate (Suzuki-Inoue et al., 2007). However, it is known that CLEC-2 is fundamental for development and preventing blood-lymphatic mixing (Suzuki-Inoue et al., 2010, Finney et al., 2012), thrombosis during inflammation and vascular integrity (Boulaftali et al., 2013, Rayes et al., 2018).

Tetraspanins

As their name describes, tetraspanins (Tspan) contain four membrane-spanning domains. There are several in platelets, but the function of most of them is still poorly understood. Some of the most relevant ones are CD151, which contributes to the outside-in signalling of integrin αIIbβ3 (Lau et al., 2004), and Tspa9 (also known as NET-5), which participates in the activation and lateral diffusion of GPVI along the plasma membrane (Haining et al., 2017). A new tetraspanin subfamily has been identified

recently, termed TspanC8. Three TspanC8 are present in platelets: Tspan14, Tspan15 and Tspan33, and these have been shown to regulate A Disintegrin and metalloproteinase domain-containing protein 10 (ADAM10) activity in platelets (Dornier et al., 2012, Koo et al., 2020). ADAM10 is responsible for receptor shedding and is important for GPVI regulation, as detailed in **Section 1.2.5.**

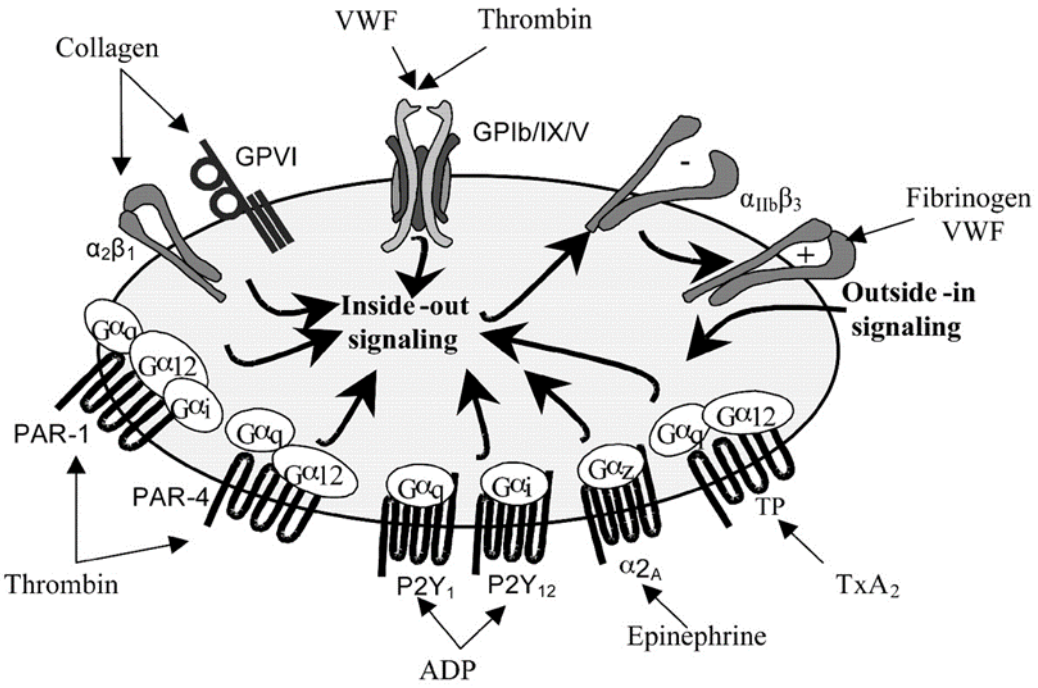

Figure 1.2. Platelet membrane receptors. Schematic representation of the main human platelet receptors and their main ligands: von Willebrand Factor (vWF), collagen, thrombin, fibrinogen and Thromboxane A2 (TxA_2). Image modified from (Rivera et al., 2009).

1.1.4 The role of platelets in haemostasis and thrombosis

In primary haemostasis, platelets aggregate to form a thrombus, in order to prevent blood loss at an injured blood vessel while maintaining normal blood flow. Under healthy conditions, the endothelium does not offer an adhesive surface for platelets, but in places of vascular damage, where the subendothelium is exposed, platelets can adhere to various extracellular matrix (ECM) components, and generate a thrombus. Thrombus formation is accomplished in three phases: platelet adhesion, activation, aggregation

and subsequent thrombus formation (Clemetson, 2012). The multi-step process is illustrated in **Figure 1.3**.

Furthermore, recent studies described a new function of platelets in maintaining vascular integrity and promoting tissue repair. This process is termed inflammation-associated haemostasis, where platelets prevent blood loss on the sites of leukocyte infiltration (Ho-Tin-Noé et al., 2018).

1.1.4.1 Adhesion phase

Following vascular damage, vWF (ECM component) gets immobilised on the exposed collagen, initiating the adhesion process. When exposed to high shear conditions, vWF undergoes a conformational change, making its A1 binding domain available for GPIbα, allowing the tethering of platelets. This is not a stable adhesion and only allows platelets to roll along the endothelium (Cranmer et al., 2011). This facilitates the binding of GPVI and integrin α2β1 to the exposed collagen (Nieswandt and Watson, 2003). Signalling is initiated mainly by GPVI (Nieswandt, 2001), present in a complex with the FcRγ-chain, which contains an immunoreceptor tyrosine-based activation motif (ITAM) (Tsuji et al., 1997). The binding of GPVI-FcRγ-chain to collagen results in the phosphorylation of the ITAM, which causes activation of the spleen tyrosine kinase (Syk). Syk is a kinase and therefore phosphorylates several downstream proteins. The signalling cascade culminates with an increase in cytosolic Ca^{2+} and subsequent platelet shape change, granule secretion, and activation of the integrins α2β1 and αIIbβ3 that strongly bind to collagen, vWF and fibrinogen, leading to a firm adhesion of the platelet (Jarvis et al., 2002).

1.1.4.2 Activation and secretion phase

The secretion process begins when platelets adhere, become activated and change shape through the cytoskeleton, enhancing their adhesion and surface area. Platelets secrete the contents of their α-granules and dense granules such as ADP, TxA_2, vWF

and fibrinogen, in order to amplify platelet activation. ADP binds to its receptors $P2Y_1$ and $P2Y_{12}$, and this leads to an increase of intracellular Ca^{2+}, protein phosphorylation, initial change of shape, and the inside-out activation of integrin αIIbβ3 (Andre et al., 2003). ADP also induces TxA_2 synthesis, a strong platelet agonist that also enhances protein phosphorylation, change of shape, aggregation, and vasoconstriction, which can reduce or stop the blood flow in the affected area (Smyth, 2010). Thrombin is the strongest platelet activator and amplifier of the activation and coagulation cascades. It is currently believed (known as the extrinsic pathway) that TF expressed by endothelial and adjacent cells initiates the coagulation cascade, which involves several factors released by platelets, and results in the production of thrombin from prothrombin (Periayah et al., 2017). Another key role of thrombin is the generation of fibrin, by cleaving fibrinogen, which is essential for thrombus stability (Undas and Ariëns, 2011). PS becomes activated, and then exposed by flipping from the inner to the outer leaflet. PS is important for local thrombus formation as it facilitates the assembly of coagulation complexes (Reddy and Rand, 2020).

1.1.4.3 Aggregation and thrombus formation

The last step of the primary haemostasis concludes with the aggregation of the platelets and thrombus formation. The main receptor involved in this process is the integrin αIIbβ3, which is present in a low-affinity conformation in resting platelets, but upon platelet activation and secretion, it shifts to a high-affinity conformation. As a result of this conformational change, fibrinogen is able to bind to integrin αIIbβ3 forming a bridge between two platelets, causing them to be in close proximity and aggregate. The coagulation cascade completes this process by generating fibrin networks, which increase thrombus stability (Rivera et al., 2009, Twomey et al., 2019).

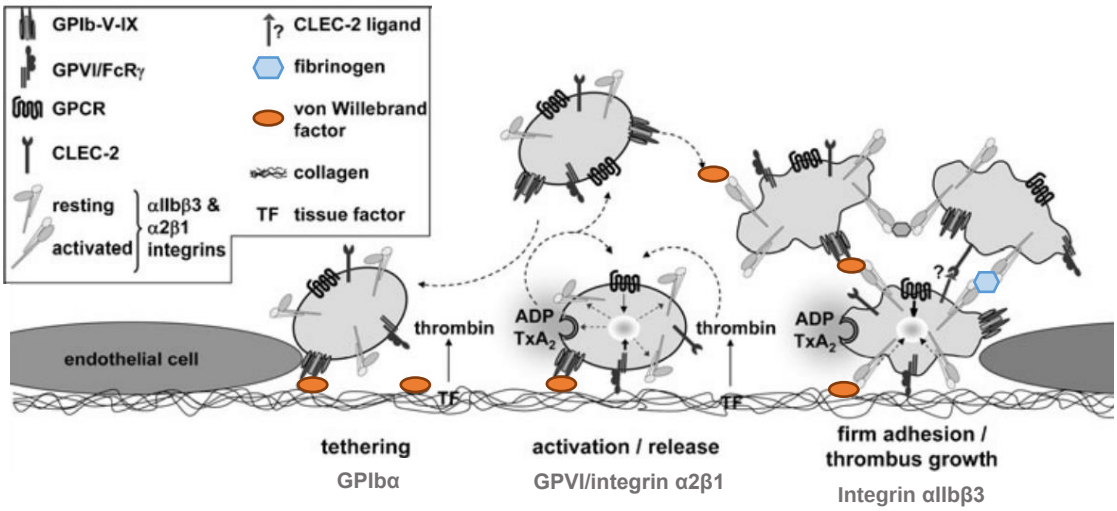

Figure 1.3. Platelet adhesion, activation and aggregation upon endothelium damage. Image showing platelets first tethering upon the binding of GPIbα to vWF, then interacting via GPVI and integrin α2β1 to the exposed collagen fibres, and finally forming aggregates mediated by integrin αIIbβ3. Image modified from (Nieswandt et al., 2011b).

1.1.5 The role of platelets in inflammation and other diseases

Platelets are fundamental for primary haemostasis, but their malfunction can also lead to several disorders. Some conditions are caused by a change in platelet number; a higher than normal platelet count is termed thrombocythemia and causes blood clots that eventually occlude blood vessels and stop the bloodstream (Tefferi and Pardanani, 2019), whereas a lower than normal platelet count leads to thrombocytopenia leaving patients at an increased risk of haemorrhage (Greenberg, 2017). It is well understood that inappropriate activation of platelets can also cause thrombotic disorders, such as myocardial infarction (Smitherman et al., 1981), ischaemic stroke (Nieswandt et al., 2011a), and atherothrombosis (Davì and Patrono, 2007).

Additionally, platelets have a pathological role in sepsis, diabetes mellitus, cancer, and coronavirus disease 2019 (COVID-19), even though they are not well characterised in some cases. (Tyagi et al., 2022). Sepsis is a complex process that triggers an uncontrolled systemic reaction to an infection. Through their haemostatic role, platelets play a significant role in the development of multiple organ failure in sepsis, leading to

disseminated intravascular coagulation (Yaguchi et al., 2004). Diabetes mellitus is a multifactorial disorder closely related to vascular complications. Platelets are involved in the early stages of diabetes, yet, the exact mechanism of action of platelets is unclear. It is known that dysregulation of some signalling pathways occurs in the platelets of diabetic patients, leading to hyperactivation of platelets (Santilli et al., 2015). Platelets also play a role in cancer, due to their capability to regulate the early and late stages of angiogenesis (Wojtukiewicz et al., 2017). Recent studies also demonstrated an important role of platelets in metastasis, where circulating tumour cells can attach to activated platelets and leukocytes, and form heteroaggregates that support the evasion from immune cells (for example natural killer cells) and aids the adhesion to the tumour cells to the endothelium and thereby contribute to metastasis (Nieswandt et al., 1999b, Gay and Felding-Habermann, 2011).

In 2019, a new human virus named severe acute respiratory syndrome coronavirus 2 (SARS-CoV-2) that causes COVID-19 was identified in China (Huang et al., 2020). It was observed that patients with mild symptoms present a slightly higher platelet count, whereas severe patients develop thrombocytopenia (Bi et al., 2020). Aside from respiratory problems, patients were also diagnosed with thrombotic events, ranging from microthrombi to myocardial infarction and stroke. (Boeckh-Behrens et al., 2021). This could be explained by some early findings indicating that platelets from COVID-19 patience experience hyperactivation due to the vessel damage and release of different cytokines and chemokines (Zaid et al., 2020). However, a more recent publication, suggested that COVID-19 patients' platelets are not hyperactivated, but in contrast, they failed to active in response to integrin αIIbβ3 (Weiss et al., 2022). Additionally, patients immunised with some vector-based SARS-CoV-2 vaccines, such as the one generated by Astra-Zeneca (AZD1222, ChAdOx1 nCoV-19, COVID-19 vaccine AstraZeneca)

presented rare thrombotic events including thrombocytopenia and intracranial venous sinus thrombosis (Wolf et al., 2021).

Platelets are implicated in a wide range of diseases, from cardiovascular diseases to inflammatory diseases, which highlights the importance of understanding the activation mechanisms and signalling cascades of platelets to develop drugs that target any of these problems.

1.2 Glycoprotein VI receptor

In 1987, GPVI was identified as the protein recognised by autoantibodies of a patient suffering from autoimmune thrombocytopenic purpura when collagen could not aggregate platelets. (Sugiyama et al., 1987, Moroi et al., 1989). Further studies established GPVI as the main collagen receptor for human and murine platelets (Ichinohe et al., 1997, Nieswandt et al., 2000b). The absence of GPVI does not lead to severe bleeding, but it protects animals against induced thrombosis (Nieswandt et al., 2001, Boylan et al., 2004, Bender et al., 2011). In the development of novel anti-thrombotic agents, GPVI has been targeted because of its efficacy to inhibit thrombosis with virtually no bleeding side effects, as well as its restricted expression in megakaryocytes and platelets (Zahid et al., 2012).

1.2.1 GPVI structure

GPVI is a 64 kDa protein part of the Igs superfamily of receptors (**section 1.1.3**) (Clemetson et al., 1999). There are two Ig C2 loops, named D1 and D2 present in this extracellular domain. The D1 loop contains the collagen-binding domain (CBD) (Smethurst et al., 2004), whereas according to crystallography data the D2 loop contains the dimerisation domain (Slater et al., 2021). These are followed by a mucin stalk region that contains the cleavage site for metalloproteinases, which allows the shedding of the GPVI extracellular domain from the platelet plasma membrane (Ezumi et al., 2000,

Gardiner et al., 2007). Because GPVI lacks catalytic activity, signalling transduction requires to be coupled non-covalently with an FcRγ-chain containing an ITAM, which is defined by two conserved tyrosine residues (YxxI/Lx6-12YxxI/L). The binding site of GPVI and FcRγ-chain is within the transmembrane domain of GPVI via an arginine group (Gibbins et al., 1996). The intracellular domain of GPVI is also known as GPVI-tail, and it is approximately 20 kDa (Arthur et al., 2007). The GPVI-tail is critical for GPVI signalling because of its interaction with the Src family kinases (SFK) Lyn and Fyn (Quek et al., 2000). Additionally, the intracellular domain also contains a calmodulin (CaM) binding site. In resting platelets, CaM is associated with GPVI and dissociates upon activation of GPVI (Andrews et al., 2002). Studies suggest that CaM could be involved in receptor shedding (Bender et al., 2010). The sequence of mouse GPVI is remarkably similar to the human, with roughly 64% identity (Jandrot-Perrus et al., 2000). The biggest difference is the lack of 23 amino acids in the GPVI tail of mouse GPVI, even though no functional significance of this difference has yet been reported. However, some differences in the signalling cascade and shedding mechanisms have been reported (Janus-Bell et al., 2021, Navarro et al., 2022).

1.2.2 GPVI ligands

Although GPVI can bind a variety of endogenous and exogenous ligands, collagen is its major ligand. In the ECM, nine types of collagen are expressed, but GPVI is most reliant on collagen types I and III, as they form fibrils (Jarvis et al., 2002, Jung et al., 2008). Horm collagen is the most frequently used collagen for platelet function assays. It is derived from equine tendons and is primarily composed of collagen type I (Nieswandt and Watson, 2003). GPVI has a higher affinity for collagen as a dimer than as a monomer (Miura et al., 2002, Jung et al., 2012). For many years, the binding site of collagen to GPVI was not clear. The crystal structure of GPVI bound to homotrimeric collagen peptides was published this year by Feitsma et al., which shows collagen binding to the

β-sheet of the D1 domain of GPVI (Feitsma et al., 2022). Recently, two additional physiological ligands of GPVI were discovered, fibrin (Alshehri et al., 2015a, Mammadova-Bach et al., 2015) and fibrinogen (Mangin et al., 2018). There is still a debate on how fibrin and fibrinogen bind to GPVI (Slater et al., 2019). First, it was demonstrated that only dimeric GPVI binds to immobilised fibrinogen and fibrin (Induruwa et al., 2018), however, Mangin et al. suggested that fibrinogen activates only human, but not murine platelets, by binding to monomeric GPVI (Mangin et al., 2018). Additionally, GPVI has several other endogenous ligands such as fibronectin, vitronectin, adiponectin and amyloid peptide Aβ40 (Michelson et al., 2019).

Regarding the exogenous ligands, GPVI is known to bind to collagen-related peptide (CRP), convulxin (CVX) and sulfated polysaccharides including fucoidans and dextran-sulfate (Alshehri et al., 2015b). CRP is the most frequently used synthetic GPVI agonist, and it was created after discovering that collagen contains repeated glycine-proline-hydroxyproline (GPO) motifs (Morton et al., 1995a). CRP consist of a repetition of ten GPOs and can activate platelets specifically via GPVI, but not integrin α2β1. A recent crystallographic study demonstrated that CRP also binds GPVI in the D1 region (Horii et al., 2006). The snake venous toxin CVX is a natural but exogenous ligand of GPVI, and one of the most potent agonists.

1.2.3 GPVI signalling in platelets

As previously described in section 1.2.1, GPVI does not have a signalling motif, therefore it requires to be associated with FcRγ-chain for signal transduction. The dimerisation of GPVI leads to the phosphorylation of the tyrosine residues within the FcRγ-chain ITAM by SFKs (mainly Lyn and Fyn) that are associated with GPVI (Quek et al., 2000, Suzuki-Inoue et al., 2002). These phosphorylated residues serve as docking sites for Syk, another kinase that undergoes auto-phosphorylation (Poole et al., 1997). By phosphorylating the linker for activation of T-cells (LAT), Syk initiates a phosphorylation

cascade in which many proteins and adapters are phosphorylated and recruited, thus forming the LAT signalosome (Pasquet et al., 1999, Hughes et al., 2008). One of the most important components of the signalosome is the phospholipase C (PLC)γ2, which is recruited to the plasma membrane by LAT and SH2-domain-containing leukocyte phosphoprotein of 76 kD (SLP-76) (Gross et al., 1999). GPVI signalling is illustrated in **Figure 1.4**.

PLCγ2 is a protein that hydrolyses phosphatidylinositol 4,5-bisphosphate (PIP_2) into inositol 1,4,5-trisphosphate (IP_3) and diacylglycerol (DAG) (Quek et al., 2000). The generated IP_3 molecules bind to IP_3 receptors, and act as Ca^{2+} channels, and Ca^{2+} is realised from the intracellular reserves (DTS and dense granules) to the platelet cytosol, which results in the integrin αIIbβ3 activation (Varga-Szabo et al., 2009). DAG activates a series of molecules, with protein kinase C (PKC) being the most important one, as it controls granule secretion (Werner and Hannun, 1991, Kishimoto et al., 1980). Subsequently, platelets release the content of their dense- and α-granules, most notably ADP, which amplifies and sustains platelet activation (Harper and Poole, 2010). PLCγ2 activity downstream of GPVI is also regulated by Bruton tyrosine kinase (Btk) (Quek et al., 1998), and by small Rho GTPase Rac1, since it has been demonstrated that Rac1-deficient platelets present impaired IP_3 production and Ca^{2+} mobilisation. Nevertheless, the exact mechanism by which Rac1 controls PLCγ2 is not clear, as PLCγ2 phosphorylation levels were unaltered in Rac1 deficient murine platelets (Pleines et al., 2009).

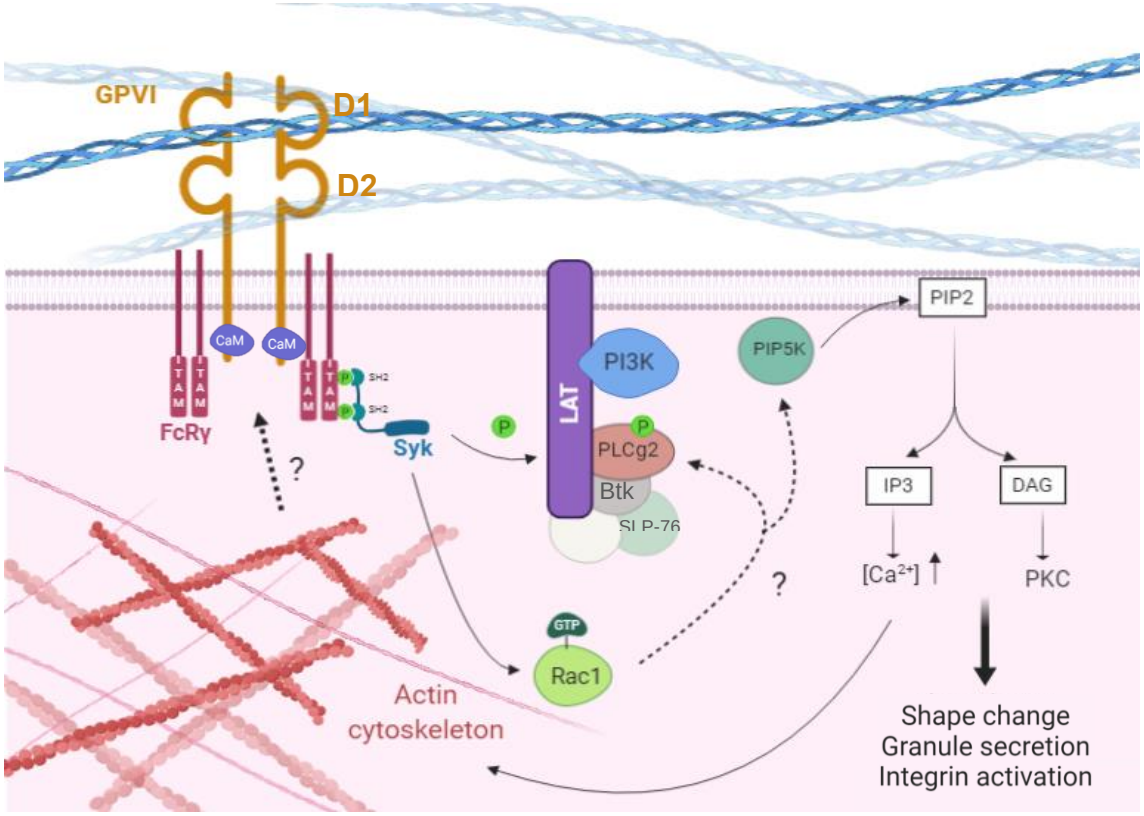

Figure 1.4. GPVI signalling pathway. Schematic representation of GPVI binding its main ligand, collagen via the immunoglobulin domain D1. GPVI forms a complex with the FcRγ-chain and initiates a signalling cascade that begins with phosphorylation of Syk, which in turn induces phosphorylation of many proteins, including LAT. This activates and recruits a series of adaptor and effector molecules that lead to the phosphorylation and activation of PLCγ2, which mediates an increase of Ca^{2+} influx and PKC activation producing a change in platelet shape, granule secretion and integrin αIIbβ3 activation. Rac1, is a small Rho GTPases also activated downstream of GPVI signalling, and possible plays has a role in PLCγ2 activation and/or phosphorylation. Image created with Biorender.

1.2.4 GPVI dimerisation and clustering

An extensive literature debate has been going on since the turn of the century about the conformation (monomeric *vs* dimeric) of GPVI in resting and activated platelets, and whether it changes when platelet activation is induced by GPVI agonists (Clark et al., 2021a). The first authors to report on this topic were Muira et al. in 2002, who found that fibrillar collagen binds selectively to dimeric, but not monomeric GPVI. This conclusion was based on experiments with a dimeric GPVI construct expressed in HEK293T cells, named GPVI-Fc_2, which is a recombinant fusion protein that binds two GPVI molecules via the Fc region of an IgG (Miura et al., 2002). Four years later, the first reported

crystallography structure of GPVI suggested that GPVI forms a dimer back-to-back via the β-sheets of the D2 domain (Horii et al., 2006). The same group also reported that, in solution, GPVI molecules were monomers, and that dimerisation might occur in the platelet plasma membrane due to a weak interaction induced by a high density of GPVI (Horii et al., 2006). Bioluminescence resonance energy transfer (BRET) on HEK293T cells expressing GPVI revealed that GPVI was present as a mixture of monomers and dimers, and this ratio did not change in response to collagen or CVX stimulation, meaning that GPVI ligands do not induce receptor dimerisation (Berlanga et al., 2007). This result was also confirmed years later by our group also using BRET on HEK293T cells (Clark et al., 2021b).

Previous studies have been limited by the fact that they were conducted on cell lines expressing GPVI. A dimer-specific F(ab') fragment, m-Fab-F, was developed by Jung et al., allowing the study of GPVI conformation on platelets, and they found that high concentrations of m-Fab-F blocked collagen-induced platelet aggregation (Jung et al., 2009). In contrast to previous findings, they demonstrated that platelet activation induces GPVI dimerisation from approximately 30% in resting platelets to 40% in CRP-activated platelets (Jung et al., 2012). In a similar study, Loyau and co-authors developed another dimer-specific antibody, 9E18, which doubled its signal upon platelet activation with thrombin and vWF, supporting the idea that GPVI dimerises upon activation (Loyau et al., 2012). The controversy in the literature and the few studies performed on platelets show that further research is needed to understand GPVI dimerisation on human and murine platelets.

Higher-order clustering of GPVI on the platelet plasma membrane was first reported in 2007, (Berlanga et al., 2007). Additionally, CVX is able to cluster up to eight GPVI molecules, explaining how it induces such a strong platelet activation (Horii et al., 2009). However, the deeper understanding of GPVI clustering started with the development of

super-resolution microscopy techniques. Poulter and co-workers were the first to visualise GPVI clusters in human platelets (Poulter et al., 2017). This finding was confirmed by two additional studies from our group in Birmingham. We demonstrated that GPVI clusters colocalise with areas where tyrosine-phosphorylated proteins such as Syk and LAT are enriched, and this enrichment together with increased intracellular Ca^{2+} is sustained for up to 3 hours in platelets (Pallini et al., 2021). Furthermore, GPVI clusters along immobilised collagen fibres were not disrupted by inhibiting phosphorylation of Syk and LAT, suggesting that they are not disrupted once they have formed (Pallini et al., 2021). The second study demonstrated that neither adenosine nor forskolin affected GPVI clustering along immobilised collagen fibres, although both inhibited platelet aggregation by inhibiting the supplementary action of TxA_2 (Clark et al., 2019). Overall, these novel insights demonstrate that GPVI clustering is a robust process that is difficult to disrupt, but the exact mechanism of how clustering occurs remains elusive.

1.2.5 GPVI downregulation and shedding

To avoid thrombotic complications, platelet activation must be tightly regulated by various mechanisms. Under normal conditions, endothelial cells release prostacyclin (PGI_2) and nitric oxide that maintain platelets in a resting state (Radomski et al., 1987). However, platelet activation can also be inhibited by receptors containing tyrosine-based inhibition motifs (ITIMs). For many years, it was believed that PECAM-1 was the only ITIM-receptor found in platelets (Jackson et al., 1997). However, further studies revealed that platelets contain other ITIM-receptors, including G6b-B (Newland et al., 2007, Coxon et al., 2017). A reduction in platelet activation is also achieved by targeting the collagen receptor GPVI, thereby regulating the adhesion and activation of platelets.

GPVI expression can be reduced either by internalising the receptor or by shedding of the extracellular domain, both processes remove the receptor from the platelet surface (Rabie et al., 2007). Internalisation of the GPVI-FcRγ-chain complex via cAMP-

dependent endocytosis is a way to store and recycle GPVI molecules that can reappear in the plasma membrane (Takayama et al., 2008), whereas shedding is the irreversible proteolysis of the GPVI ectodomain. The shedding releases a soluble GPVI (sGPVI) fragment of 55 kDa into the plasma, while the remaining transmembrane and intracellular domains, known as GPVI-tail (approximately 10 kDa), remain anchored to the platelet plasma membrane (Gardiner et al., 2004). It has been shown that ADAM10 regulates GPVI shedding in human platelets, whereas ADAM10 and ADAM17, together with other metalloproteinases, are critical in murine platelets, showing the first difference between human and mice in this mechanism (Bender et al., 2010). However, the cleavage site of ADAM10 is conserved in both human and mouse GPVI molecules in the stalk region of the ectodomain (Gardiner et al., 2007).

GPVI shedding inducers can either be GPVI ligands, pathological shear or antibodies. Since Src and Syk inhibitors block GPVI shedding, ligand-induced receptor release requires the activation of tyrosine kinases, while activation of integrin αIIbβ3 is dispensable (Gardiner et al., 2004). Additionally, different ligands induce different degrees of GPVI shedding, with CVX-induced shedding being stronger than collagen- and CRP-induced shedding (Andrews et al., 2007). GPVI ligand-induced shedding also requires the dissociation of CaM from the receptor endodomain (Andrews et al., 2002), probably to physically allow ADAM10 to reach its cleavage site.

GPVI ectodomain shedding can be triggered solely by exposure of platelets to pathological shear rates, as suggested by the presence of sGPVI in the plasma of patients with atrial fibrillation and acute coronary syndrome (Bigalke et al., 2009). In the plasma of healthy donors, the level of sGPVI was around 20 ng/mL, independent of age and gender (Al-Tamimi et al., 2009b). However, patients from the intensive care unit who suffered from acute brain injury, thermal injury, and elective cardiac surgery among others showed an increase of 50% in sGPVI levels (Montague et al., 2018). Increased

levels of sGPVI were also found in patients with disseminated intravascular coagulation, mediated by FXa as an anti-coagulation mechanism (Al-Tamimi et al., 2011). Another disease characterised by GPVI loss and increased sGPVI levels is lymphoproliferative disorder, a type of cancer (Qiao et al., 2013). Therefore, sGPVI levels can be used as a marker for platelet activation in the detection of thrombotic and inflammatory diseases.

GPVI shedding can also be induced *in vitro* by antibodies against GPVI, such as 9O12, which activates human platelets in a FcγRIIA-dependent manner (Lecut et al., 2003), and 1G5, which is known to activate human platelets in a FcγRIIA-independent manner (Al-Tamimi et al., 2009a). A murine GPVI antibody, JAQ1, can also induce GPVI shedding *in vivo* in mouse models lacking ADAM10 and ADAM17, suggesting the possible role of other metalloproteinases in this process (Nieswandt et al., 2001, Bender et al., 2010).

To date, the biological function and physiological relevance of GPVI shedding is still under debate. The current hypothesis is that there is an ideal GPVI surface density for each person in order to maintain vascular integrity. A change inducing high surface density of GPVI may relate to increased thrombotic risk, whereas a decrease of GPVI in the platelet plasma membrane may be associated with a risk of bleeding. Further research is needed to understand the exact mechanism of GPVI shedding.

1.3 GPIb-IX-V complex

The critical role of the GPIb-IX-V receptor complex in haemostasis was discovered in patients with Bernard-Soulier syndrome, a bleeding disorder associated with thrombocytopenia, caused by mutations in the genes for GPIbα, GPIbβ, and GPIX (Bernard and Soulier, 1948, Jenkins et al., 1976). The GPIb-IX-V complex, particularly GPIbα, is essential in haemostasis because it is the first receptor to reversible attach to vWF exposed in damaged endothelium (Nurden and Caen, 1975). Besides haemostasis,

GPIb-IX-V has also been linked to thrombopoiesis, platelet clearance, and thrombocytopenia, among others.

1.3.1 GPIb-IX-V complex ligands

GPIb-IX-V complex is part of the LRR receptors family of receptors. For more information about the structure of the GPIb-IX-V complex, refer to **section 1.1.3**.

The main ligand of the complex is vWF, which binds to GPIbα. vWF is present in the plasma (secreted by endothelial cells) and platelet α-granules (Andrews et al., 1997). Soluble vWF in the plasma does not have a strong affinity for GPIbα, but when immobilised onto collagen at sites of vascular injury and exposed to high shear rates, it undergoes a conformational change that makes its A1 binding domain available for GPIbα, allowing the platelets to decelerate onto damaged endothelium (Berndt et al., 2001). The binding of vWF to GPIbα results in platelet aggregation and/or clearance (Deng et al., 2016, Chow et al., 1992). As an auto-regulatory mechanism, the exposure of vWF to high shear also unfolds its A2 domain, allowing ADAMTS13 to cleave it, thereby reducing its affinity for GPIbα and releasing adherent platelets (Dong, 2005). Deficiencies in vWF, such as those caused by vWF disease, result in bleeding, whereas deficiencies in ADAMTS13 result in thrombotic diseases (Emmer et al., 2016).

The GPIb-IX-V complex also enhances platelet activation at low, but not high concentrations of α-thrombin (Ruggeri et al., 2010). The GPIbα extracellular domain, named glycocalicin, contains the binding site for thrombin and vWF (Jandrot-Perrus et al., 1992). Additionally, thrombin is responsible for the cleavage of GPV, but not GPIbα (Berndt and Phillips, 1981). There are different manners in which GPIb-IX-V can mediate thrombin-induced platelet activation. GPIbα could act as an adaptor facilitating the cleavage of PAR-1 mediated by thrombin (Vu et al., 1991, De Candia et al., 2001), or shedding of the GPV extracellular domain may crosslink GPIbα subunits leading to a stronger response to thrombin (Ramakrishnan et al., 2001). The GPIb-IX-V complex has

other ligands, including collagen, which binds to GPV and supports platelet adhesion and aggregation mediated by GPVI and integrin α2β1 (Moog et al., 2001), and integrin Mac-1, important for platelet leukocyte aggregates (Simon et al., 2000).

1.3.2 GPIb-IX-V complex signalling pathway

There is a big controversy in the literature regarding GPIb-IX-V complex signalling. Previous studies reported that the binding of vWF to GPIbα induces platelet activation via tyrosine phosphorylation of kinases like Src, Lyn, Syk and PLCγ2, concluding on increased cytosolic Ca^{2+} levels, integrin αIIbβ3 activation, and platelet aggregation (Asazuma et al., 1997, Marshall et al., 2002). As this complex does not possess tyrosine kinase activity, it remains unclear how it would activate the kinases that trigger platelet activation (**Figure 1.5**). However, according to Kuwahara et al. the binding of GPIbα to vWF that allows platelet adhesion is independent of intracellular calcium increase, which is an indicator of platelet activation (Kuwahara et al., 1999). A hypothesis is that the GPIb-IX-V complex could only contribute to the signalling cascade by supporting the signalling of GPVI-FcRγ-chain and/or FcγRIIA. In immunoprecipitation studies, the GPIb-IX-V complex interacts with GPVI on the plasma membrane of resting and activated platelets (Arthur et al., 2005), and with the FcRγ-chain on platelets activated with vWF (Falati et al., 1999). Recently, a study using mice lacking the intracellular domain of GPIbα showed an impaired platelet activation and aggregation upon stimulation with the GPVI ligand CRP, supporting the hypothesis that GPIbα is involved in GPVI signalling (Constantinescu-Bercu et al., 2021). FcγRIIA contains an ITAM domain, which enables it to have tyrosine kinase activity, and additionally, some studies reported that it colocalises with the GPIb-IX-V complex in the plasma membrane (Sullam et al., 1998, Sun et al., 1999). Therefore, the GPIb-IX-V complex could also participate in this signalling pathway. In order to understand whether the GPIb-IX-V complex activates or

supports any signalling pathways and leads to platelet activation, further research is needed.

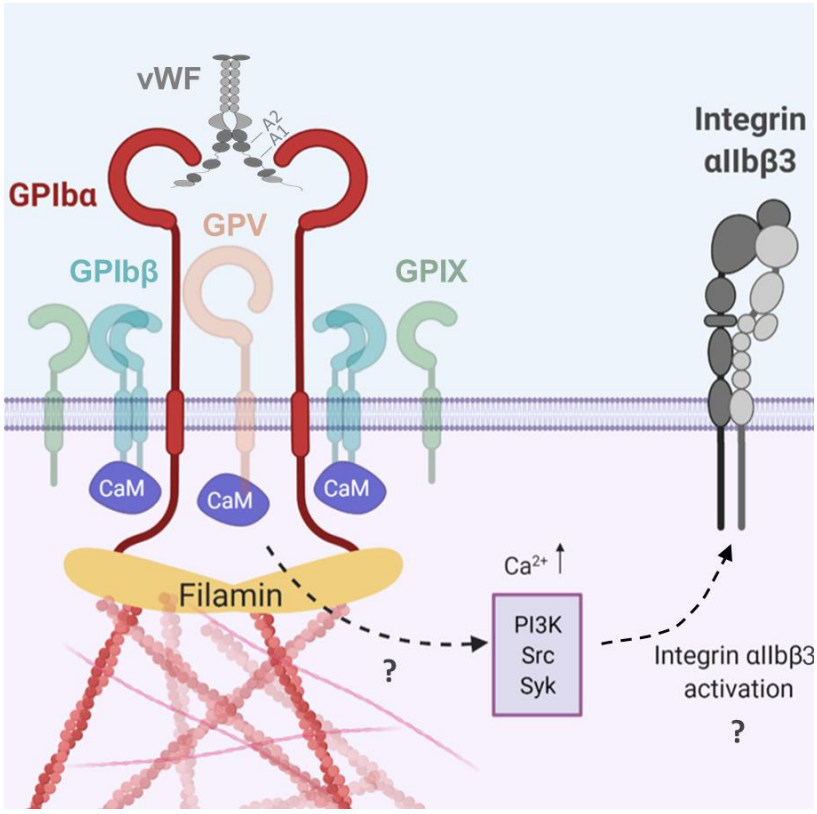

Figure 1.5. GPIb-IX-V receptor complex signalling pathway. Image represents the binding of GPIbα, main subunit of the GPIb-IX-V complex to vWF. The intracellular domain of GPIbα is bound to calmodulin (CaM) and filamin, which connects this receptor complex to the actin network. It is yet not clear whether GPIbα induces any signalling pathway, and therefore the activation of the integrin αIIbβ3. Image generated using Biorender.

1.3.3 GPIb-IX-V complex shedding

In this section, we will focus only on the shedding of GPIbα and GPV. The extracellular domain of GPIbα, known as glycocalicin, contains two mechanosensory domains (MSD), one at the juxtamembrane region (Zhang et al., 2015), and one at the N-terminal, where ligands are bound, known as leucine-rich repeat domain (LRRD) (Ju et al., 2015). In resting platelets, the MSD is folded, and the binding of vWF to the LRRD and high shear unfolds it (Bendas and Schlesinger, 2022). Glycocalicin is found at a relatively high concentration in the plasma of healthy donors (Coller et al., 1984), supporting the theory

that GPIbα is constitutively shed in resting platelets by the metalloproteinase ADAM17 (Bergmeier et al., 2004). The cleavage site of ADAM17 is located in the MSD near the plasma membrane, which is accessible when the MSD is folded in resting platelets. When GPIbα binds to its ligand and the MSD is unfolded, ADAM17 has better access to the cleavage site, and therefore GPIbα shedding increases (Zhang et al., 2015). As treatment with CCCP, an artificial ageing agent, causes GPIb shedding, constitutive cleavage of GPIbα is believed to be a hallmark event of platelet ageing, indicating platelet lifespan (Bergmeier et al., 2003). This goes in line with the fact that GPIbα is involved in the clearance of platelets (Beardsley and Ertem, 1998).

In regards to GPV cleavage, thrombin is responsible for cleaving it from the plasma membrane, as previously described. However, it is shed also by ADAM10 and ADAM17 in a different cleavage site than by thrombin (Rabie et al., 2005, Gardiner et al., 2007). The presence of soluble GPV in plasma and the absence of constitutive GPV degradation indicate platelet activation in diseases like angina pectoris (Atalar et al., 2005). Additionally, GPV can also be shed by the GPVI agonists CVX (Gardiner et al., 2007) and CRP (Rabie et al., 2005), as well as by the inhibition of CaM, as in the case of GPVI, by mediating the activity of the ADAM metalloproteinases (Rabie et al., 2005).

1.3.4 The relevance of the GPIb-IX-V complex in platelet clearance

Platelet clearance is an important physiological process that removes modified or aged platelets from blood circulation. The clearance of platelets seems to be regulated by the GPIb-IX complex, as there is no clear evidence that GPV plays a role in this process (Bendas and Schlesinger, 2022). Patients with immune thrombocytopenia, who have autoantibodies against GPIb, show enhanced platelet clearance (Beardsley and Ertem, 1998). Currently, there are two proposed models to explain the role of the GPIb-IX complex in platelet removal from the bloodstream.

The first model describes GPIbα clustering as the mechanism responsible for the clearance (Shrimpton et al., 2002). It is well known that vWF can cluster GPIbα molecules from the same platelet, or crosslink GPIbα from adjacent platelets, as it has multiple binding sites that can bind to several GPIbα molecules (Gitz et al., 2013). Different anti-GPIbα antibodies that bind to two GPIbα molecules can also induce this dimerisation. Several studies demonstrated that injection of monoclonal anti-GPIbα antibodies causes fast platelet depletion in mice *in vivo* (Cadroy et al., 1994, Bergmeier et al., 2000, Cauwenberghs et al., 2000). However, only the IgG and $F(ab')_2$, but not the F(ab') fragments induce the platelet clearance machinery, suggesting that a bivalent structure and dimerisation of GPIbα is needed (Nieswandt et al., 2000a, Cauwenberghs et al., 2000). These antibodies need high shear to induce the dimerisation, like vWF (Quach et al., 2018b), and only induce the dimerisation if they bind to the LRRD domain and not to the juxtamembrane domain (Bergmeier et al., 2000, Liang et al., 2016). However, there are some reservations regarding the GPIbα clustering model, since it has yet to be explained why antibodies binding GPIbα at the MSD do not drive platelet clearance, and what the exact mechanism by which antibodies trigger platelet activation and depletion is.

Deng et al. (2016) suggested the second model, known as the trigger model (**Figure 1.6**), which attributes a main role to the MSD in platelet clearance. As previously described, the binding of vWF (or antibodies) to the LRRD of GPIbα at physiological shear rates creates a pulling force that enables the unfolding of the MSD. This novel model proposes that the unfolding of the MSD exposes a trigger sequence, containing only 10 amino acids, that is found between the transmembrane domain and the MSD. Then, the extension of the trigger sequence induces platelet activation by increasing P-Selectin levels and phosphatidylserine (PS) exposure, and most importantly, glycans on the platelet surface are desialylated (loss of sialic acid residues) (Deng et al., 2016,

Zhang et al., 2015). The desialysation is crucial for platelet removal as it allows the exposure of galactose residues, which are recognised by Ashwell-Morell receptor (AMR) present in hepatocytes, and leads to platelet recognition, internalisation and clearance (Sørensen et al., 2009, Grozovsky et al., 2015).

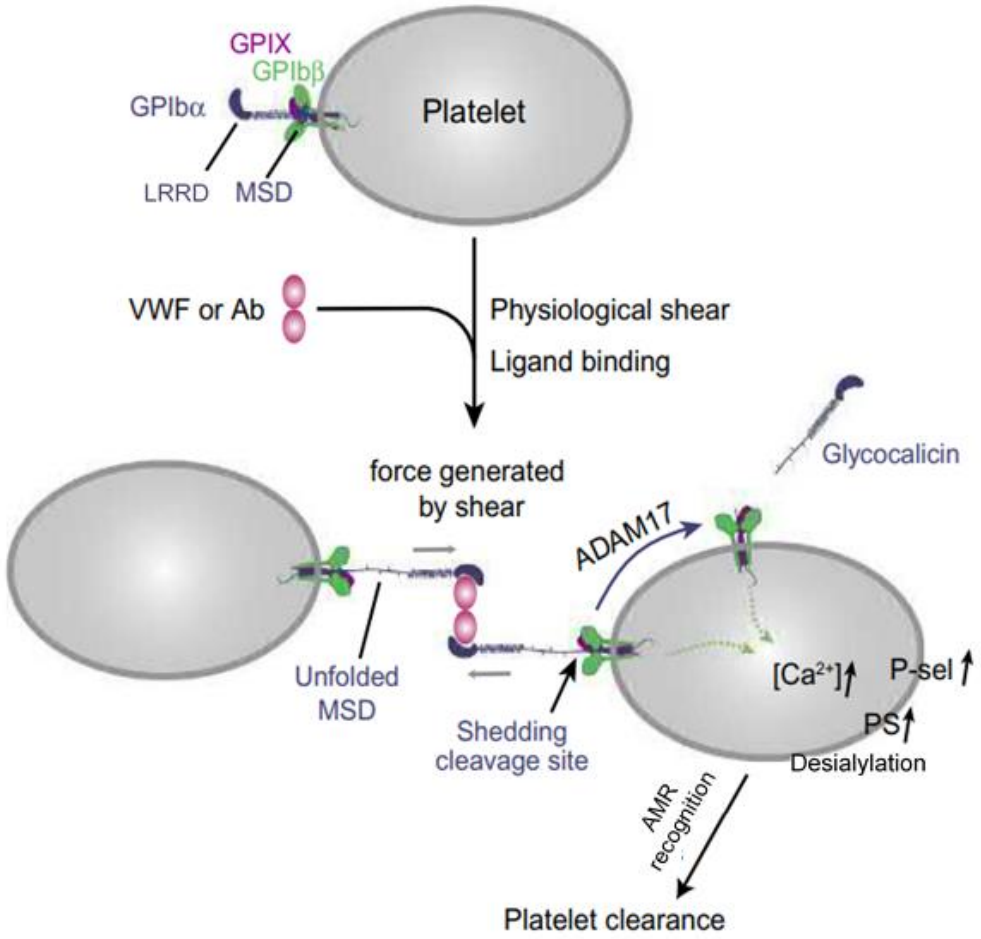

Figure 1.6. GPIbα shedding induced by the trigger model. Image illustrating the binding of a dimeric ligand (vWF or dimeric antibody (IgG or F(ab')$_2$ fragment)) to GPIbα, which, together with high shear rates induces the unfolding of the MSD domain. Consequently, GPIbα is shed from the platelet plasma membrane by the metalloproteinase ADAM17, resulting in P-Selectin expression, PS exposure and desialysation. Image modified from (Michelson et al., 2019).

GPIbα is the main receptor involved in this process since it contains approximately 80% of the sialic acid present on the platelet plasma membrane (Sørensen et al., 2009). The unfolding of the MSD also enhances the affinity of ADAM17 to bind to the MSD, resulting in GPIb shedding and the release of glycocalicin (Deng et al., 2016). Upon cleavage, the trigger sequence is exposed and this has been associated with an increased platelet

clearance (Bergmeier et al., 2003, Chen et al., 2016). However, it is not the only receptor involved; transgenic mice lacking almost all of the GPIbα ectodomain, which is exchanged by the interleukin 4 receptor (IL-4R), but still containing the trigger sequence, present platelet clearance, albeit at a slower rate than in wild-type mice (Deng et al., 2016, Chen et al., 2022). Some evidence suggest that other glycosylated receptors, such as integrin αIIbβ3 can also bind to AMR (Hoffmeister et al., 2003).

1.4 The role of the actin cytoskeleton in platelet signalling

The actin cytoskeleton is essential for platelet biogenesis, and activation. An actin filament is 7 nm wide, and is mostly responsible for forming the cytoplasmic network, which provides resting platelets together with microtubules and other cytoskeletal components the support needed to maintain the discoid shape and the structure when exposed to high shear rates, and serves as a structure for organelles and other compartments to attach (Thomas, 2019). The actin cytoskeleton dynamics enable platelets to change shape rapidly upon activation by polymerisation, resulting in filopodia and lamellipodia formation, allowing the platelet to spread. In this section, I will focus on the connection of the actin cytoskeleton in with the GPIb-IX-V complex and GPVI.

The actin cytoskeleton supports and modulates the GPIb-IX-V complex. The intracellular domain of GPIbα associates with filamin-A, and this interaction is essential for anchoring the whole GPIb-IX-V complex to the membrane skeleton and therefore supporting platelet adhesion under high shear stress (Williamson et al., 2002). The interaction of GPIbα to filamin-A is crucial for protein trafficking from the cytosol to the plasma membrane, as well as for a correct platelet size (Kanaji et al., 2012). Also, the actin cytoskeleton supports the clustering/centralisation of the whole complex upon thrombin stimulation, using myosin II and filamin-A as adapters (Kovacsovics and Hartwig, 1996b). The actin cytoskeleton can also affect GPVI signalling, as blocking actin polymerisation with cytochalasin D or latrunculin A impairs platelet spreading and reduces dimerisation

and cluster formation of GPVI on collagen and CRP surfaces (Poulter et al., 2017). However, in a different study, blocking actin polymerisation did not impair GPVI signalling or aggregation response to GPVI ligands (Pollitt et al., 2010). Therefore, further research is needed to comprehend the linking effect of the actin cytoskeleton on GPVI signalling, dimerisation and clustering.

However, the effect of GPVI activation on the actin cytoskeleton is well known. Upon GPVI-mediated platelet activation, the actin cytoskeleton undergoes a reorganisation, altering platelet morphology, leading to an increase in the platelet surface area that enhances their interactions with the ECM and other platelets (Hensler et al., 1992). In order to spread, platelets create finger-like structures, named filopodia, and sheet-like processes, named lamellipodia (Aslan et al., 2012). The Ras homolog (Rho) GTPases family are the major regulators of actin remodelling in platelets in response to several agonists. RhoA, RhoB, cell division cycle 42 (Cdc42) and Ras-related C3 botulinum toxin substrate (Rac) form the Rho family in platelets. Platelet contractility, change of shape and thrombus stability are modulated by RhoA, via its role in actomyosin contractility (Klages et al., 1999, Pleines et al., 2012). RhoA is not necessary for platelet spreading, but it is required for full activation of integrin αIIbβ3 and clot retraction (Pleines et al., 2012). Recent studies on RhoB function suggest that it can also contribute to platelet function downstream of GPVI signalling (Englert et al., 2022). Cdc42 modulates granule secretion and spreading (Pleines et al., 2010), but its precise role remains unclear. Some authors demonstrated that the absence of Cdc42 in platelets inhibits filopodia formation on CRP- and fibrinogen-coated slides (Akbar et al., 2011), whereas others suggested that Cdc42 is not involved in filopodia formation of platelets spread on CRP and fibrinogen but is involved on vWF-coated surfaces (Pleines et al., 2010). This suggests a role of Cdc42 downstream of GPIbα signalling. Rac is necessary for lamellipodia formation during the spreading of platelets on surfaces coated with collagen,

fibrinogen and vWF (McCarty et al., 2005). The role of lamellipodia formation regulated by Rac in platelets is still under study. Older publications demonstrated that Rac1 is required for supporting aggregation by maintaining the stability of the aggregates (Akbar et al., 2007, McCarty et al., 2005), whereas a recent study suggests that lamellipodia are not essential for thrombus formation and stability (Schurr et al., 2019). In several other cell types, lamellipodia are essential for cell migration (Krause and Gautreau, 2014). A similar phenomenon has been demonstrated in platelets, where lamellipodia formation is necessary for platelets migration to sites of infection and clearing the vasculature of bacteria (Gaertner et al., 2017). Furthermore, lamellipodia-dependent migration detects inflammatory lesions on the endothelium and plugs them, preventing micro-bleeds and bacterial spread (Nicolai et al., 2020). There are 3 isoforms of Rac. Murine platelets express only Rac1 (McCarty et al., 2005), whereas human platelets express mainly Rac1, but also a small amount of Rac2 (Burkhart et al., 2012). A wide range of receptors in platelets can activate Rac, suggesting that Rac could be present in different pools that regulate different platelet functions (Aslan and McCarty, 2013). Stimulation of GPCRs, including PAR and $P2Y_{12}$, with thrombin or ADP activates PLCβ, which supports Rac activation (Offermanns et al., 1997). Additionally, SFKs activated downstream GPVI and integrin αIIbβ3 also mediate Rac activation (Akbar et al., 2007, McCarty et al., 2005), together with 14-3-3ζ, an adapter protein that is coupled to GPIbα in resting platelets and releases the receptor upon vWF binding and thereby modulates Rac activity. Once activated, some studies demonstrated that Rac1 is essential for PLCγ2 activation and also that it supports integrin αIIbβ3 activation (Pleines et al., 2009, Stefanini et al., 2012). However, there is still little evidence detailing Rac's involvement downstream of all of these signalling pathways, as well as how it can facilitate PLCγ2 and integrin αIIbβ3 activation.

1.5 Super-resolution microscopy techniques for platelet imaging

Different microscopy techniques have been used to study platelets' ultrastructure and molecules. Platelets were first identified in 1881 by Giulio Bizzozero using traditional light microscopy (Bizzozero, 1881). Despite the limitations of light microscopy, many significant advances have been achieved using this technique, such as identifying abnormalities in platelet shape and size, which is helpful for the diagnosis of disorders (Greinacher et al., 2017) and characterising the role of the actin cytoskeleton in platelet spreading (Thomas et al., 2007). However, the resolution achieved by standard light microscopy is determined by the wavelength of light and therefore restricted to approximately 200 nm. Electron microscopy (EM) is one means of overcoming this restriction. EM employs a beam of electrons providing the highest resolution to date, with outstanding visualisation of platelet ultrastructural details, including the platelet cytoskeleton and granules (White, 1981, Italiano et al., 1999). Nevertheless, it does not provide information about the dynamics of the molecules, as live imaging is not possible. To overcome this limitation, fluorescence microscopy can be used as multiple molecules can be labelled at the same time and their dynamics can be tracked in real-time (Falati et al., 2002). However, the diffraction limit of a fluorescence microscope is approximately 250 nm laterally and approximately 500 nm axially. This represents a limiting factor for the visualisation of small molecules, such as the actin filaments (7 nm in diameter), microtubules (25 nm in diameter) or plasma membrane receptors that are significantly smaller than the diffraction limit of the microscope, which makes imaging small cells such as platelets even harder. The diffraction limit (d) is defined as the distance that two objects must at least have to be distinguishable in an optical device. It solely depends on the wavelength of light (λ) divided by twice the numerical aperture (NA) of the objective, as described in the following equation (Abbe, 1873):

$$\mathrm{d} = \frac{\lambda}{2\mathrm{NA}} \qquad \text{(Equation 1)}$$

Super-resolution (SR) techniques are relatively new imaging modalities that revolutionised the microscopy field by surpassing the optical diffraction limit (Hell and Wichmann, 1994). Different SR microscopy techniques (**Figure 1.7**) break the diffraction limit in different manners and each of them additionally provides different advantages to imaging, such as reduction of photobleaching or multi-colour imaging.

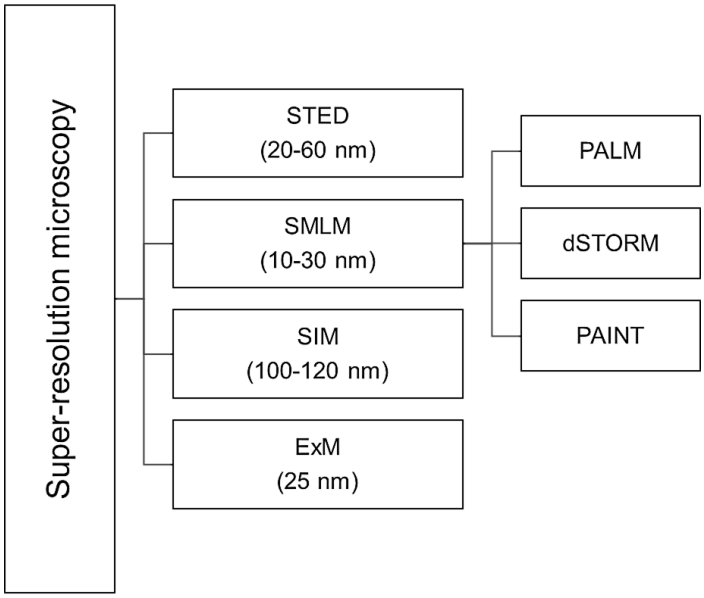

Figure 1.7. Summary of the main super-resolution (SR) microscopy methods. Each SR microscopy method includes the highest spatial resolution that it can achieve. Stimulated emission depletion (STED), single-molecule light microscopy (SMLM), structured illumination microscopy (SIM), expansion microscopy (ExM), photoactivated localisation microscopy (PALM), direct stochastic optical reconstruction microscopy (STORM) and Points accumulation for imaging in nanoscale topography (PAINT).

Stimulated emission depletion (STED) was one of the first SR microscopy method, developed by Hell in 1994 (Hell and Wichmann, 1994). Stochastic optical reconstruction microscopy (STORM) (Rust et al., 2006) together with photoactivated localisation microscopy (PALM) (Betzig et al., 2006) were the first single-molecule light microscopy (SMLM) techniques allowing the visualisation of single fluorophores with relatively simple wide-field microscopy setups.

1.5.1 *d*STORM

*d*STORM relies on labelling proteins of interest with antibodies tagged with a fluorophore. It then uses a reducing buffer that drives the fluorophores into an inactive dark state when a high-powered laser is applied (Rust et al., 2006). The fluorophores then stochastically drop out of this dark state, emitting photons, which can be captured on a sensitive camera (**Figure 1.8**). This method breaks the diffraction limit as almost all fluorophores are switched off, and at any time few of them that are switched on and emit a photon that can be detected and their localisation pinpointed with high accuracy (Heilemann et al., 2008). For *d*STORM, the fluorophore choice is important, and Alexa Fluor 647 is the ideal choice because it presents high levels of blinking (Dempsey et al., 2011). Overlapping thousands of frames in which different subsets of fluorophores are emitting, we obtain *d*STORM images that are then reconstructed in order to obtain the final image, which is composed of a point cloud of the localisations of all the different fluorescent blinks detected during the image acquisition. *d*STORM reaches a spatial resolution of between 10-50 nm (Thorley et al., 2014) which is the highest spatial resolution compared to the other methods mentioned in this thesis, and one of the highest to date for light microscopy. However, its main disadvantages are that the sample can be photobleached as the method needs 100% laser intensity, flat samples, with molecules closed to the coverslip are more amenable to the technique as the TIRF mode is often used to increase the signal-to-noise ratio, and the post-reconstruction of the images is extensive and laborious (Tam and Merino, 2015). Despite these limitations, *d*STORM has been used in numerous studies in the last years to give insights into platelet structure and signalling. The localisation of platelet receptors, including the highly abundant integrin αIIbβ3, was investigated using *d*STORM (Poulter et al., 2015), as well as the clustering of several receptors. For the analysis of clusters in platelets, Ripley's K-function was widely used in the past to study integrin, CLEC-2, and GPVI clustering in

platelets (Pollitt et al., 2014, Poulter et al., 2015, Poulter et al., 2017), but also for instance, in T cells to image LAT, CD45 and LcK (Williamson et al., 2011, Rossy et al., 2013). However, several recent studies demonstrated that the density-based analysis approach (DBSCAN), is a better alternative for cluster analysis of GPVI along collagen fibres than Ripley's K-function since it analyses the entire image instead of a small region of interest (Pallini, 2020) (Clark et al., 2019). Additionally, *d*STORM was employed in platelet to image areas of tyrosine phosphorylation events accumulation in actin nodules (Poulter et al., 2015), and also the whole platelet actin cytoskeleton was characterised (Lickert et al., 2018).

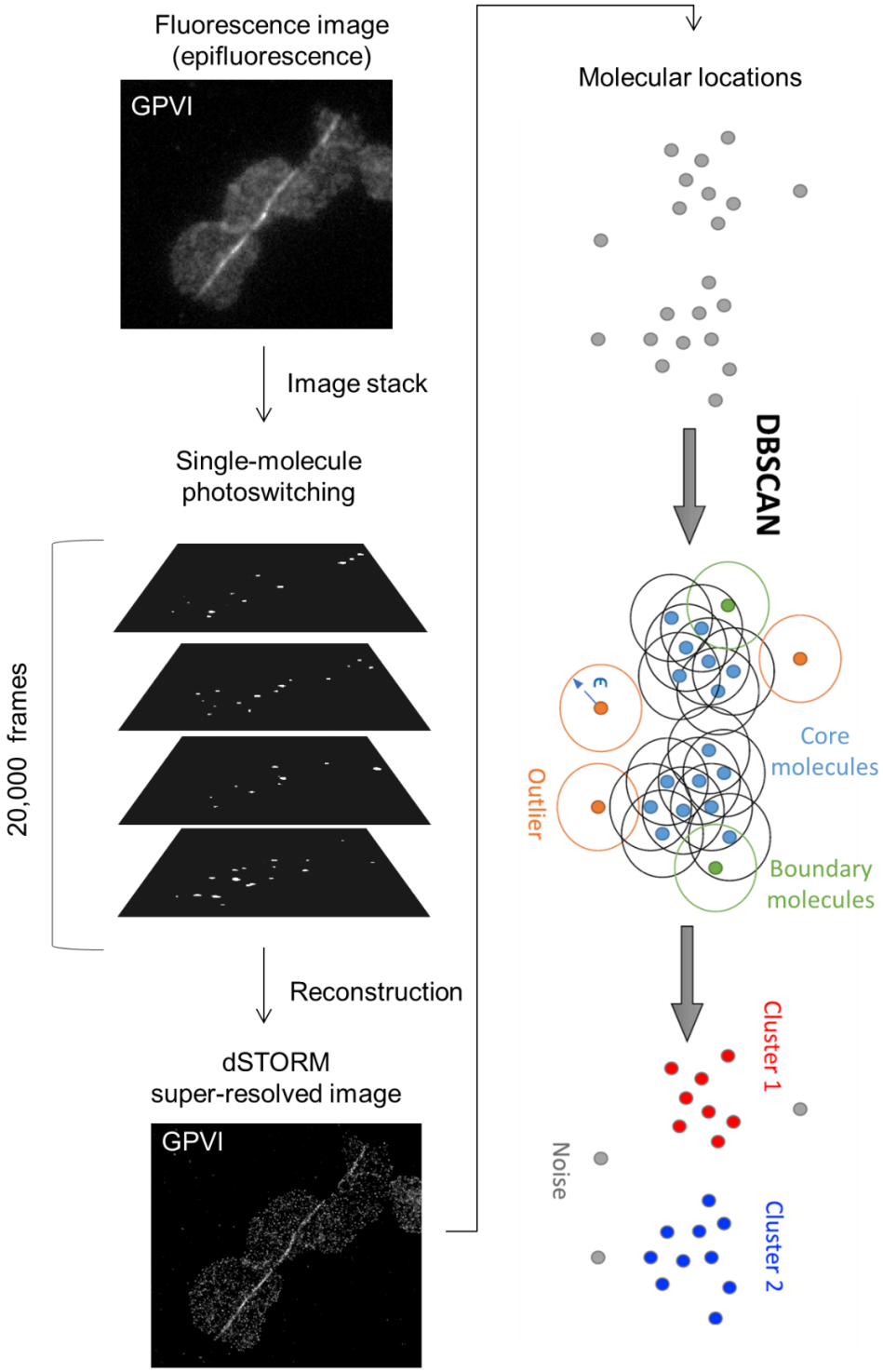

Figure 1.8. The basic principle of *d*STORM and cluster analysis. An overview of the imaging, reconstruction and density-based clustering analysis (DBSCAN). The sample is labelled with an antibody against the target protein (GPVI), then 20,000 frames are acquired, and in each of the frames, a different set of molecules is in a bright state. Then, the image is reconstructed, obtaining a map with the precise location of the GPVI molecules (super-resolved image). The molecular locations are processed, first correcting the drift and chromatic aberrations, and then the cluster analysis is performed, grouping a set of molecules that are neighbours into clusters. The DBSCAN scheme was modified from (Khater et al., 2020).

1.5.2 Structured illumination microscopy (SIM)

SIM principle was also developed at the end of the last century as a SR microscopy method (Neil et al., 1997). The breakage of the diffraction limit in this method is achieved by illuminating the sample with a pattern (known linear grid) that projects fine details into the image plane that can be observed (known as Moiré pattern) (Gustafsson, 2000). The linear grid is rotated and shifted along its diffraction direction, obtaining different Moiré patterns. Typically, 15 images with different illumination patterns (usually 5 lateral shifts from 3 different angles), where different fluorophores are covered and uncovered by the grid, are recorded (**Figure 1.9**). The final images are obtained by mathematically deconvolving the signal with the acquisition software, using the Fourier transformation (Demmerle et al., 2017). SIM improves resolution by approximately 2-fold compared to conventional light microscopy, reaching a spatial resolution of ~ 100 nm (Valli et al., 2021). The principal advantages of SIM are that the samples are prepared like for standard fluorescence microscopy (any dye can be used) and imaging reconstruction is fast. However, data reconstruction is also one of their main drawbacks, as it relies on complicated computational procedures that the software applies, which could lead to artefacts if the user is not well-trained and does not recognize them (Heintzmann and Huser, 2017). SIM has also been used in the platelet field to image changes in the actin cytoskeleton during spreading, when proteins involved in the regulation of the actin cytoskeleton, such as Wiskott-Aldrich syndrome protein (WASP) and actin-related protein 2/3 complex (Arp2/3) are disrupted (Poulter et al., 2015, Kahr et al., 2017). Additionally, SIM was used to study the immunomodulatory role of CLEC-2 (Bourne et al., 2021).

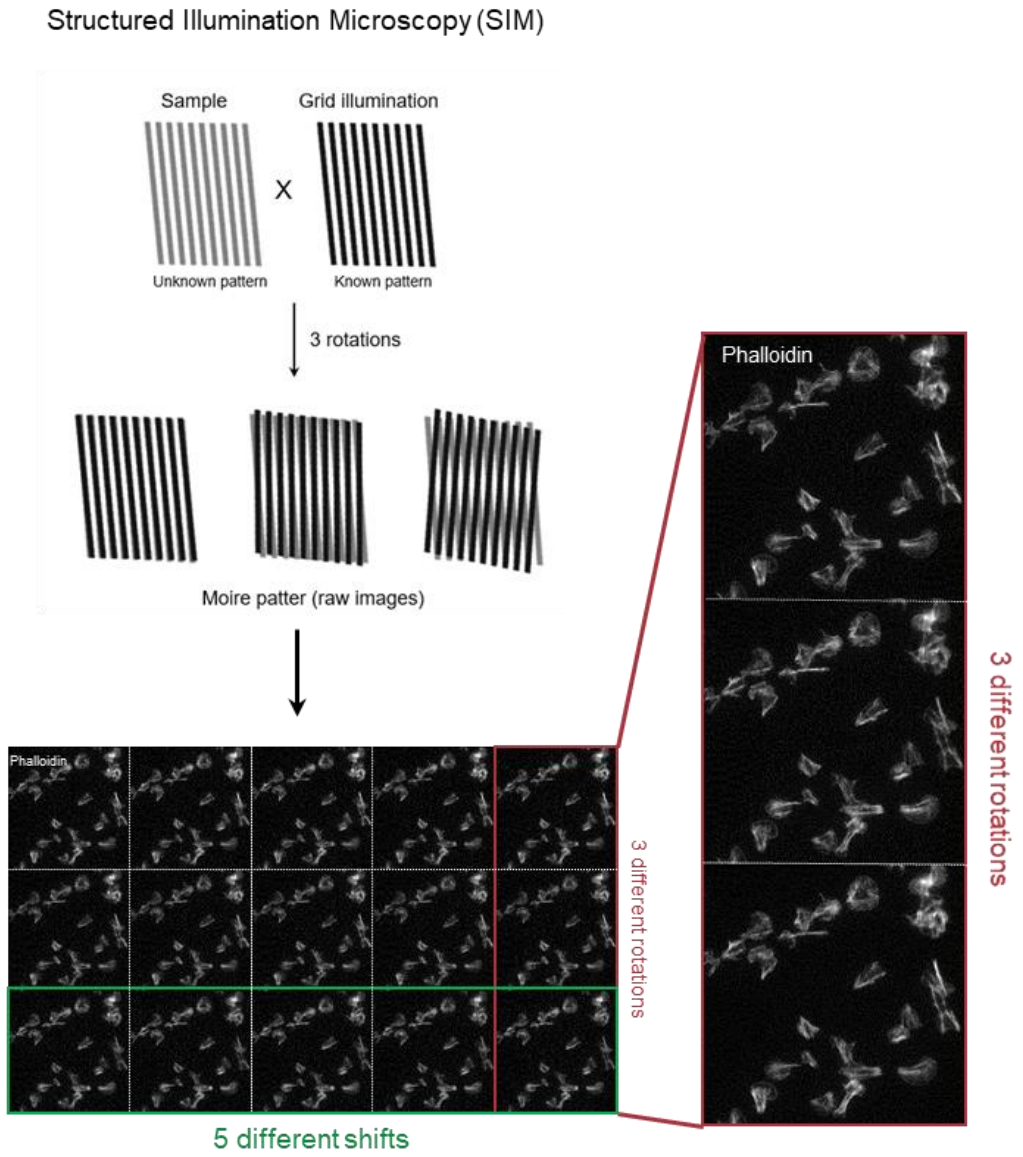

Figure 1.9. SIM image acquisition overview. Individual images are illuminated with a structured pattern (grid), and captured by rotating the grid three times and shifting it five times. This generates the Moiré pattern, in which not the entire sample is illuminated. Afterwards, a computer algorithm produces a super-resolution image, with a resolution of around 100 nm, from the 15 raw images.

1.5.3 Point accumulation in nanoscale topography (PAINT)

PAINT is another SR microscopy method, developed by Sharonov and Hochstrasser (2006). In this method fluorophores photoswitching does not occur. However, blinking relies on the transient immobilisation of fluorophores that are free in solution and then bind their target molecule, for a short period (**Figure 1.10**). As fluorophores diffuse fast

in solution, they only appear as background and can only be localised when they temporally bind their target (Sharonov and Hochstrasser, 2006). PAINT has evolved into several different approaches. The first and most prominent one is DNA-based PAINT (DNA-PAINT) which uses short DNA oligomers (up to ten nucleotides long) to provide the transient but specific interaction that is needed for PAINT (Jungmann et al., 2010). There are two DNA oligomers, one known as the docking strand, that is fixed and bound to the target protein, and the other one, called the imager strand is found in solution conjugated to a fluorophore and transiently binds the docking strand (Jungmann et al., 2010). Exchange-PAINT follows the same principle as DNA-PAINT but employs several DNA oligomer sequences that allow the observation and localisation of multiple targets, which is achieved by the exchange of the buffer that contains different imager strands (Jungmann et al., 2014). An alternative method is quantitative PAINT (qPAINT) which allows quantitative counting of the stoichiometry using single strands kinetics that is identified because of the known origami structure created with DNA (Jungmann et al., 2016). One of the main benefits of DNA-PAINT is that photobleaching does not occur, as the fluorophore coupled to the imager strand can be constantly renewed with the addition of fresh buffer containing more of the imager strand. The greatest advantage of this technique compared to any other SR approach is that by Exchange-PAINT up to eight different targets can be visualised in the same sample, using the same fluorophore to overcome chromatic aberration (Jimenez et al., 2020). Regarding disadvantages, images can have a high background noise as the fluorophores (coupled to the imager strands) are free in the imaging buffer, and the labelling is complicated, as normal antibodies and fluorophores cannot be used. In order to perform the labelling, first DNA oligomers need to be synthesised and then coupled to antibodies and fluorophores for creating the docking and imager strand respectively (Lee et al., 2020). PAINT is widely used in several cell lines, however, it has barely been used in platelet research to date. An interesting study was performed to compare the radius of microtubules obtained with

*d*STORM and PAINT, showing that DNA-PAINT surprisingly produced larger linkage errors than *d*STORM (Früh et al., 2021).

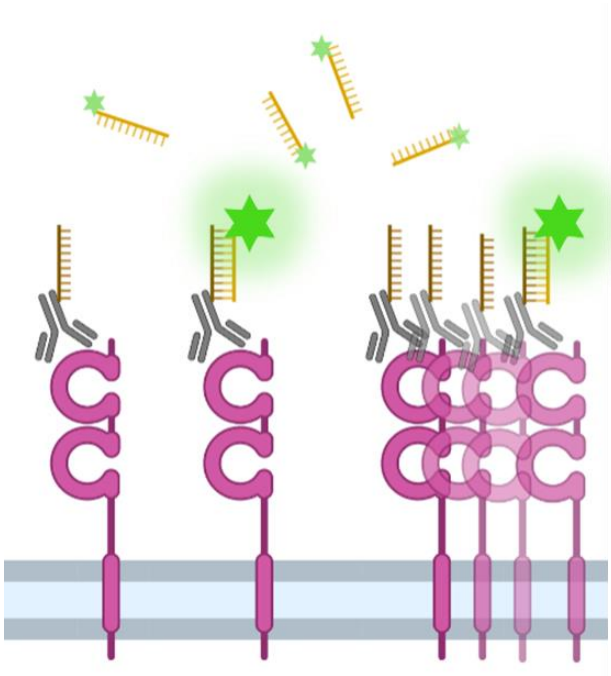

Figure 1.10. The blinking principle of DNA-PAINT microscopy. The sample is labelled with an antibody against the targeted receptor. The antibody is coupled with a docking strand (dark brown). During imaging, the sample is treated with the imaging buffer that contains the imaging strand (yellow, coupled with a fluorophore). Since the imaging strand in solution diffuses rapidly, it is not captured by the camera, and it is only captured when it binds the docking strand effectively. Image generated using Biorender.

1.5.4 Expansion microscopy (ExM)

Expansion microscopy is the newest SR microscopy method, developed by Boyden, Chen and co-authors, in 2015. Whereas the previously cited SR microscopy methods obtained a higher resolution by implementations in the microscope (e.g. SIM) or the labelling strategy (e.g. DNA-PAINT), in expansion microscopy the improvement is obtained by physically expanding the sample (in both lateral and axial directions) and to be imaged on a standard fluorescence microscope (Chen et al., 2015).

The principle of expansion microscopy consists of five steps; sample fixation, labelling, linking (not always), gelation, digestion and expansion, some steps may vary depending

on the protocol (**Figure 1.11**). Many variations and improvements of the original expansion protocol have been published in the last few years (Tillberg et al., 2016, Chang et al., 2017, Gambarotto et al., 2019). A complete description of variations in the ExM protocol can be found in Chapter 5. Depending on when the staining step is performed, all the new ExM protocols can be categorised into two groups; pre-gelational staining or post-gelational staining methods (**Figure 1.11**). In pre-gelational staining, the sample is originally fixed with paraformaldehyde (PFA) (Chen et al., 2015), but several recent studies have demonstrated that glyoxal produces brighter images than PFA (Truckenbrodt et al., 2018, Heil et al., 2022). Then, the sample is labelled, and linked to the gel. The linking was originally performed using glutaraldehyde (Chen et al., 2015), however, according to a recent study, the fluorescence signal is better preserved with Acryloyl-X (AcX) (Tillberg et al., 2016). In pre-gelation ExM protocols, this anchoring process is critical for the preservation of fluorophores. Then, the gelation process starts using a monomer solution that contains acrylamide and the cross-linker. The sample is embedded in the gel once it has been polymerised. Then, the digestion is performed using enzymes, such as proteinase K (Truckenbrodt et al., 2018) and Lys-C (Tillberg et al., 2016). Finally, the sample expansion occurs by incubating the gel in water overnight. The post-gelational staining was developed by Gambarotto et al. (2019), and it is known as ultra-expansion microscopy (U-ExM). In contrast to the pre-gelation protocol, the sample here is fixed with a mixture of formaldehyde and acrylamide, and labelling occurs at the end of the protocol after the sample has been embedded in the gel and expanded, therefore fluorophores do not need to be linked. The other most significant difference is that the sample is not digested, but denatured using detergents, such as sodium dodecyl sulfate (SDS) (Gambarotto et al., 2019). Due to the fact that fluorophores are not degraded during the several steps of the expansion protocol, Gambarotto and co-authors achieved higher retention of fluorescent signal with this approach. In the last years, this method has been optimised and used for the imaging of several samples by different

groups. It has been extensively used for visualising from nanoscale structures such as mitochondria (Suofu et al., 2017) and cytoskeleton filaments (Halpern et al., 2017) to brain tissue for studying the neuron synapses in numerous mouse models, including *Drosophila* (Jiang et al., 2018) and zebrafish (Freifeld et al., 2017).

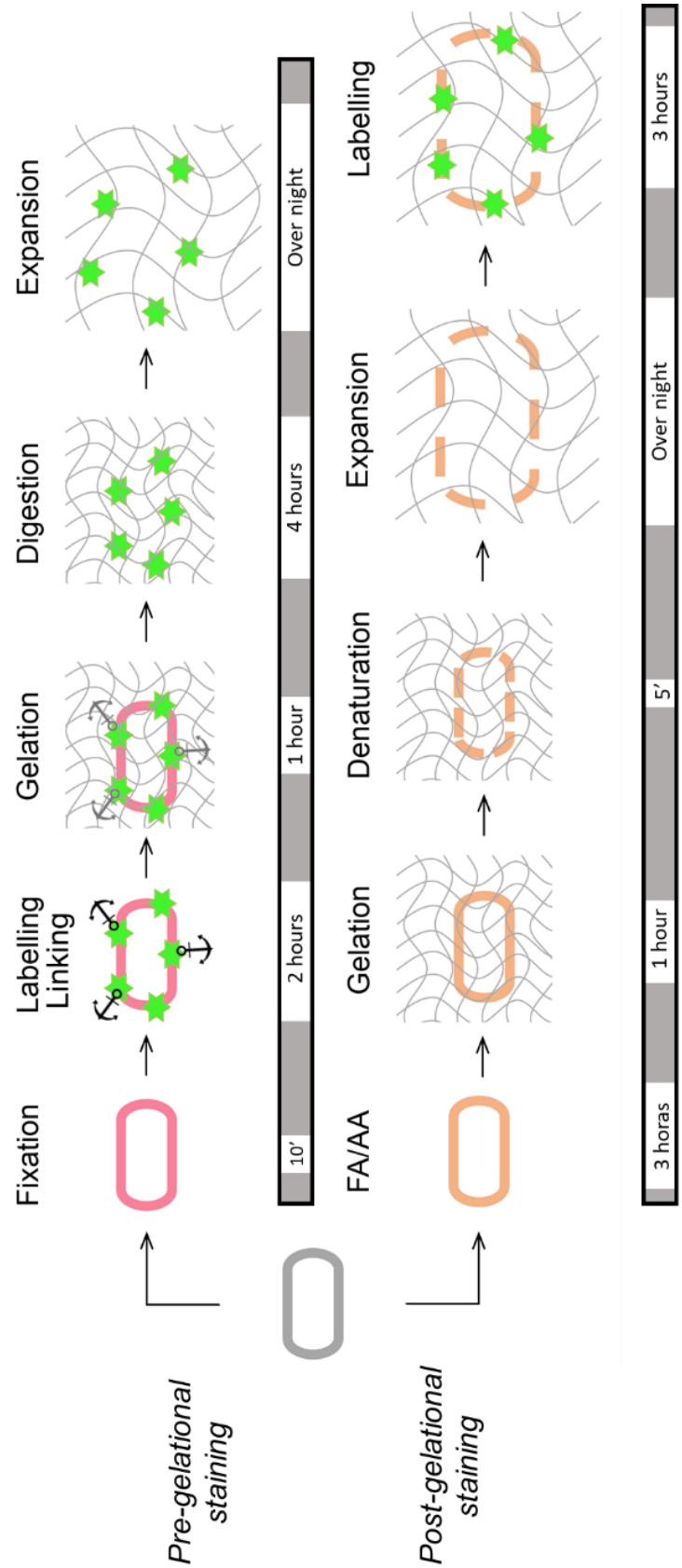

Figure 1.11. Expansion microscopy step-by-step. Diagram representing both expansion microscopy approaches; pre- and post-gelational staining ExM, including the incubation time of each step.

1.6 Aims of the thesis

Platelet glycoprotein receptors play vital roles in the function of platelets, and the GPIb-IX-V receptor complex and GPVI are two of the most important ones. GPVI downstream signalling has been studied in the literature, but less is known about GPVI and GPIb-IX-V complex organisation and conformation on the plasma membrane. This thesis aims to develop super-resolution microscopy techniques to enable the investigation of the receptors and reveal novel biological functions. The specific aims of this thesis were:

1. To understand the conformation and localisation of GPVI in resting human platelets, and to investigate whether or not its conformation changes upon platelet activation.
2. To study the effect of inhibiting Rac, a small Rho GTPase that regulates the actin cytoskeleton, on GPVI location, conformation and signalling pathway in human platelets.
3. To develop an expansion microscopy (ExM) protocol that can label platelets with antibody F(ab') fragments in order to understand GPIb conformation and location on single platelets and aggregates and its interaction with GPVI.

CHAPTER 2

Materials and methods

2.1 Materials

2.1.1. Reagents

Tables 2.1 and **2.2** contain information about commercial primary and secondary antibodies and **Table 2.3** about in-house-made antibodies used for flow cytometry, immunofluorescence and Western blotting. **Table 2.4** describes agonists and inhibitors and **Table 2.5**, the chemicals used for expansion microscopy protocols. The Rac1 activation assay kit was obtained from Cell Biolabs (Exeter, UK). The rest of the reagents are described within the thesis. If unstated, the reagents were purchased from Sigma-Aldrich (Poole, UK).

Table 2.1. Primary antibodies

Commercial primary antibody	Host species	Use	Supplier
α-hCD41/CD61- AF647 conjugated (PAC-1)	Mouse	FACS: 1:50	BioLegend (San Diego, USA)
α-hCD42P- APC conjugated (α-GPIbα)	Mouse	FACS: 1:50	Thermo Fisher (Waltham, USA)
α-h-CD62P-FITC conjugated (α-P-Selectin)	Mouse	FACS: 1:50	BD Biosciences (San Diego, USA)
α-FcRγ	Rabbit	IF: 1:200 WB: 1:500	Merck Millipore (Abingdon, UK)
α-GAPDH	Rabbit	WB: 1:1000	Cell Signaling Technology (Hitchin, UK)
α-hGPVI-PE conjugated (HY101)	Mouse	FACS: 1:50	BD Biosciences (San Diego, USA)
α-LAT	Rabbit	IF: 1:200 WB: 1:500	Millipore Merck (Abingdon, UK)
α- PLCγ2 (B-10)	Mouse	IF: 1:200 WB: 1:500	Santa Cruz Biotechnology (Dallas, USA)
α-PLCγ2 (AB-753)	Rabbit	WB: 1:500	Sigma-Aldrich (St. Louis, USA)
α-phosphotyrosine (4G10)	Mouse	WB: 1:1000	Merck Millipore (Abingdon, UK)
α-phospho-LAT Tyr200	Rabbit	IF:1:500	Abcam (Cambridge, UK)

		WB: 1:500	
α-phospho-PLCγ2 Tyr1217	Rabbit	IF: 1:200 WB: 1:125	Cell Signaling Technology (Hitchin, UK)
α-phospho-PLCγ2 Tyr759	Rabbit	WB: 1:500	Santa Cruz Biotechnology (Dallas, USA)
α-phospho-Syk Tyr525-526	Rabbit	IF: 1:250 WB: 1:500	Cell Signaling Technology (Hitchin, UK)
Phalloidin-AF488 conjugated		IF: 1:500	Invitrogen (Carlsbad, USA)
α-Syk (4D10)	Mouse	IF: 1:200 WB: 1:200	Santa Cruz Biotechnology (Dallas, USA)
α-Tubulin	Mouse	IF: 1:500 WB: 1:1,000	Cell Signaling Technology (Hitchin, UK)

FACS: Flow cytometry, IF: immunofluorescence, WB: Western blot

Table 2.2. Secondary antibodies

Commercial secondary antibody	Host species	Use	Supplier
α-mouse-AF568 conjugated	Goat	IF: 1:300	Invitrogen (Paisley, UK)
α-mouse-AF647 conjugated	Goat	IF: 1:300	Invitrogen (Paisley, UK)
α-rabbit-AF488 conjugated	Goat	IF: 1:300	Invitrogen (Paisley, UK)
α-rabbit-AF647 conjugated	Goat	IF: 1:300	Invitrogen (Paisley, UK)
Mouse IgG-HRP conjugated	Sheep	WB: 1:10,000	GE Healthcare (Bucks, UK)
Rabbit IgG-HRP conjugated	Donkey	WB: 1:10,000	GE Healthcare (Bucks, UK)

IF: immunofluorescence, WB: Western blot

Table 2.3. In-house generated antibodies

In-house generated antibody	Clone	Antigen	Reference
α-GPIbα IgG	92H12	GPIbα	Unpublished, provided by Prof B. Nieswandt
p0p4 F(ab')fragment and IgG	15E2	GPIbα	(Bergmeier et al., 2000)
p0p5 F(ab')fragment and IgG	13G12	GPIbα	(Bergmeier et al., 2000)
p0p6 IgG	56F8	GPIX	(Nieswandt et al., 2000a)
α-hGPVI F(ab') fragment	313A10	GPVI	(Neagoe et al., 2022)
α-hGPVI F(ab') fragment	336E2	GPVI	Unpublished, provided by Prof B. Nieswandt
α-hGPVI F(ab') fragmemt	1G5	GPVI	Provided by Prof E. Gardiner (Canberra, Australia) (Jung et al., 2012)

α-hGPVI cytoplasmic tail IgG	GPVI tail	GPVI	Provided by Prof E. Gardiner (Canberra, Australia) (Al-Tamimi et al., 2009a)
JAQ1 IgG	98A3	GPVI	(Nieswandt et al., 2001)
hGPV	10C10	GPV	Unpublished, provided by Prof B. Nieswandt
HEL1 IgG	11F9	CLEC-2	(Brown et al., 2021)
EDL1 IgG	57B10	β3 subunit	(Bergmeier et al., 2000)
MWReg30 IgG	5D7	αIIb subunit	(Nieswandt et al., 1999a)
JON6 IgG	14A3	αIIbβ3	Unpublished, provided by Prof B. Nieswandt
JON/A IgG	4H5	αIIbβ3	(Bergmeier et al., 2002)
WUG 1.9 IgG	5C8	P-Selectin	(Schulte et al., 2003)

Table 2.4. Agonists and inhibitors

Reagent	Target protein	Use	Supplier
4-(2-aminoethyl) benzenesulfonyl fluoride (AEBSF)	Serine protease	2mM	Calbiochem (San Diego, USA)
Aprotinin	Serine protease	10 μg/mL	Sigma-Aldrich (Poole, UK)
Apyrase	ATP	2 U/mL	Sigma-Aldrich (Poole, UK)
Collagen-related peptide (CRP)	GPVI	1, 5 and 10 μg/mL	Invitrogen (Paisley, UK)
EHT1864	Rac1	30 and 50 μM	Tocris Bioscience (Bristol, UK)
Fibrinogen (vWF and plasminogen depleted)	Integrin αIIbβ3	100 μg/mL	Enzyme Research laboratories (Swansea, UK)
GI254023	ADAM10 inhibitor	2 μM	Scientific Laboratory Supplies (Nottingham, UK)
GM6001	Metalloproteinases inhibitor	100 μM	Sigma-Aldrich (Poole, UK)

Horm collagen	GPVI and integrin α2β1	1, 5 and 10 µg/mL	Takeda (Linz, Austria)
Indomethacin	Cycloxygenase	100 µM	Sigma-Aldrich (Poole, UK)
Integrilin	Integrin αIIbβ3	9 µM	Hospital Queen Elizabeth (Birmingham, UK)
Leupeptin	Serine, threonine and cysteine protease	10 µg/mL	Enzo Life Sciences (Exeter, UK)
PAR1 peptide	PAR1	200 uM	Alta Biosciences (Birmingham, UK)
Pepstatin	Aspartyl protease	10 µg/mL	Sigma-Aldrich (Poole, UK)
Prostacyclin	G protein-coupled receptors	0.1 µg/mL	Cayman Chemicals (Cambridge, UK)
Sodium Orthovanadate (Na_3VO_4)	Tyrosine phosphatase	10 µg/mL	Caltag Medsystems (Buckingham, UK)
Thrombin	PAR1 and PAR4		Sigma-Aldrich (Poole, UK)

Table 2.5. Chemicals for expansion microscopy

Reagent	Supplier
Acrylamide (AA)	Sigma-Aldrich (Darmstadt, Germany)
4-(2-hydroxyethyl)-1-Piperazineethanesulfonic acid (HEPES)	Carl Roth (Karlsruhe, Germany)
Acryloyl-X, SE	Thermo Fischer (Waltham, USA)
Ammonium Persulfate (APS)	Carl Roth (Karlsruhe, Germany)
Bovine Serum Albinum	Carl Roth (Karlsruhe, Germany)
EDTA	AppliChem (Darmstadt, Germany)
Ethanol	Sigma-Aldrich (Darmstadt, Germany)
Ethylene Glycol-Bis(β-Aminoethyl ether) N,N,N',N'-tetraacetic Acid (EGTA)	Sigma-Aldrich (Darmstadt, Germany)

Ethylenediaminetetraacetic Acid (EDTA)	AppliChem (Darmstadt, Germany)
Fluoroshield™	Sigma-Aldrich (Darmstadt, Germany)
Glutaraldehyde	Sigma-Aldrich (Darmstadt, Germany)
Glyoxal	Sigma-Aldrich (Darmstadt, Germany)
Guanidine HCl	Sigma-Aldrich (Darmstadt, Germany)
N,N′-Methylenbisacrylamide (BIS-AA)	Sigma-Aldrich (Darmstadt, Germany)
N,N′-Dimethylacrylamide (DMAA)	Sigma-Aldrich (Darmstadt, Germany)
N,N,N′,N′-Tetramethylethylenediamine (TEMED)	Carl Roth (Karlsruhe, Germany)
Poly-D Lysine	MP Biomedicals (Santa Ana, USA)
Proteinase K	Thermo Fischer (Waltham, USA)
Potassium Persulfate (KPS)	Sigma-Aldrich (Darmstadt, Germany)
Sodium Acrylate (SA)	Sigma-Aldrich (Darmstadt, Germany)
Sodium chloride (NaCl)	Carl Roth (Karlsruhe, Germany)
Sodium hydroxide (NaOH)	Carl Roth (Karlsruhe, Germany)
Triton X-100	Carl Roth (Karlsruhe, Germany)
Tween 20	Carl Roth (Karlsruhe, Germany)

2.1.2 Buffers and solutions

Acid-Citrate-Dextrose (ACD) buffer, pH 4.5

Trisodium citrate dehydrate	85 mM
Anhydrous citric acid	65 mM
Anhydrous glucose	110 mM

Denaturation buffer, pH 8.0 (for post-gelation labelling ExM)

SDS	200 mM
NaCl	200 mM
Tris-HCl	50 mM

Digestion buffer, pH 8.0 (for pre-gelation labelling ExM)

Tris-HCl, pH 8.0	50 mM
EDTA	1 mM
Triton X-100	0.5 %
Guanidine HCl, pH 8.0	0.8 M
Supplemented with: proteinase K	8 U/mL

***d*STORM buffer, pH 7.5**

Mercaptoethylamine	100 mM
Glucose oxidase	50 µg/mL
Catalase	1 µg/mL

Glyoxal buffer, pH 5.0

Pure ethanol	20% (v:v)
Glyoxal	3.15% (v:v)
Acetic acid	0.7%

Lysis buffer, pH 7.5

Tris-HCl	10 mM
NaCl	150 mM
EDTA	1 mM
Triton X-100	1% (v:v)
Sodium azide	0.02% (v:v)

Supplemented with 1:100 protease inhibitor cocktail containing:

Na_3VO_4	200 mM
AEBSF	20 mg/ml
Aprotinin	10 mg/ml
Leupeptin	1 mg/ml
Pepstatin	2.5 mg/ml

Monomer solution (for 4x post-gelation labelling ExM)

SA	19% (wt:v)

AA	10 % (wt:v)
BIS-AA	0.1% (wt:v)
Supplemented with:	
APS	0.5% (v:v)
TEMED	0.5% (v:v)

Monomer solution (for 10x pre-gelation labelling ExM)

DMAA	2.67% (wt:wt)
SA	0.64% (wt:wt)
Supplemented with:	
KPS	0.36% (v:v)
TEMED	0.4% (v:v)

Monomer solution (for 10x post-gelation labelling ExM, T-REX)

SA	1.1 M
AA	2 M
BIS-AA	0.003% (wt:v)
Supplemented with:	
APS	0.1% (v:v)
TEMED	0.1% (v:v)

Phosphate buffered saline (PBS)

NaCl	137 mM
KCl	2.7 mM
KH_2PO_4	1.5 mM
Na_2HPO_4	8 mM

5x SDS sample buffer

Sodium dodecyl sulfate (SDS)	10 mg/ml
Glycerol	50% (v:v)
Stacking buffer	25% (v:v)
2-mercaptoethanol	25% (v:v)
Brilliant Blue	Small amount

Stripping buffer in TBS-T

SDS	2% (wt:v)
2-mercaptoethanol	1 % (v:v)

50x Tris-acetate-EDTA (TAE) buffer

Tris base	0.2 M
EDTA	10% (from 0.5 M)
Acetic acid	5.7%

TRIS-buffered saline (TBS), pH 7.3

NaCl	137 mM
Tris-HCl	20 mM

TBS-T buffer

Tween-20	0.1% (v:v)
In TBS	

Tyrode's-HEPES buffer, pH 7.3

NaCl	129 mM
Na_2HPO_4	0.34 mM
KCl	2.9 mM
$NaHCO_3$	12 mM
HEPES	20 mM
Glucose	5 mM
$MgCl_2$	1 mM

2.2 Methods

2.2.1 Generation of mutant mice

Mice lacking Rac1 in megakaryocytes and platelets were generated using the Pf4-Cre system (Tiedt et al., 2007). The mice had the Rac1 gene flanked by loxP sites, and they were crossed with transgenic mice that carried the Pf4-Cre transgene, obtaining Rac1

knock-out mice (Rac1(fl/fl)/Pf4-Cre+). Additionally, control mice (Rac1 (fl/fl)/Pf4-Cre-) deriving from the same breeding pairs were used as a control for wild-type platelets. Furthermore, knockout (KO) and wildtype (WT) mice were tested for the presence of the Rac1 protein by Western blotting of platelets lysates using an α-Rac1 antibody, as described in section 2.2.7.4. Mice with part of the GPIbα extracellular domain replaced by human interleukin-4 receptor α (IL-4Rα) were obtained as previously described (Kanaji et al., 2002) using as background C57BL/6J mice from Charles River (Sulzfeld, Germany).

2.2.2 Mouse genotyping

Wild type and Rac1 deficient mice were genotyped by incubating an ear clipping in DNA lysis buffer (Viagen Biotech, Los Angeles, USA) supplemented with proteinase K for 2 h at 56 °C and stirring at 1,200 rpm. The reaction was finalised by incubating the sample for 30 min at 85 °C. Then, a polymerase chain reaction (PCR) was performed to determine the presence of PF4-Cre transgene as below described, for 50 µL sample preparation:

2 µL	DNA sample
5 µL	10x DreamTaq buffer
5 µL	$MgCl_2$ (25 mM)
2 µL	dNTPs (10 µM)
2 µL	Primer 1 (dilution 1:10 from stock 1 µg/µL)
2 µL	Primer 2 (dilution 1:10 from stock 1 µg/µL)
0.5 µL	DreamTaq DNA polymerase
31.5 µL	H_2O

Primers for Pf4-Cre

Pf4-Cre forward 5’ CCC ATA CAG CAC ACC TTT G 3’
Pf4-Cre reverse 5’ TGC ACA GTC AGC AGG TT 3’

PCR program for Pf4-Cre

96°C	3:00 min	1 cycle
94°C	0:30 min	35 cycles
94°C	0:30 min	
94°C	0:45 min	
94°C	3:00 min	1 cycle
94°C	∞	

Expected band size

Wildtype	No PCR product
Pf4-Cre positive	450 base pairs (bp)

2.2.3 Agarose gel electrophoresis

The PCR product was separated on 1% agarose gel, which was prepared by diluting 4 g agarose in 400 mL Tris-acetate-EDTA (TAE) buffer and boiled until agarose was dissolved. Midori Green (Biozym Scientific, Oldenburg, Germany) was added to the gel solution to visualize the DNA. Samples were loaded into the agarose gel together with a marker ranging from 100 to 10,000 bp and the gel was run for 30 min at 140 Volts. The gel was imaged with a gel documentation system E.A.SY. Doc plus equipped with a CCD camera (Herolab GmbH, Germany).

2.2.4 Expression constructs

Human untagged GPVI expression construct was generated in the peGFP vector using human GPVI cDNA as a template and was obtained from colleagues from Prof Steve Watson's laboratory (University of Birmingham, UK). Human untagged FcRγ-chain expression construct cloned in the pcDNA3 vector, human Syk expression construct cloned in the pEF6 vector containing a Myc epitope, and human LAT expression

construct cloned in the peGFP vector containing a Myc epitope, as well as a GFP tag, were obtained from Dr Michael Tomlinson (University of Birmingham, UK).

2.2.5 Cell culture and transfections

Human embryonic kidney (HEK)-293T cells were grown in Dulbecco's Modified Eagle Medium (DMEM; Merck, UK), which contained 1% penicillin, 1% streptomycin, 1% glutamine and 10% fetal bovine serum, at 37 °C and 5% CO_2. The adherent HEK293T cells were incubated with Trypsin and Ethylenediaminetetraacetic acid (EDTA) for 5 min at 37 °C, diluted in DMEM, and then seeded at a concentration of 3 x 10^5 cells/well in a 6-well plate. When the seeded cells reached a confluence of 50%, there were transfected by adding to each of the 50 µL serum-free DMEM, 0.25 µg DNA and 0.76 µL polyethyleneimine (PEI), and the cells were incubated overnight at 37 °C and 5% CO_2. The following day, cells were washed with PBS, and 150 µL of cold lysis buffer was added to each well. Samples were first incubated with the lysis buffer for 20 min on ice and then, transferred to an Eppendorf tube and centrifuged at 14,000 rpm for 15 min at 4 °C. Supernatant containing the cell lysate was collected, and the lysis process was finished by the addition of 5x SDS sample buffer, and incubation of the sample for 15 min on ice. Samples were denatured at 100 °C for 5 min, and centrifuged at 1,500 x g for 10 minutes at 4 °C, obtaining the final cell lysate. Finally, the transfection was verified by Western blotting for the proteins of interest.

2.2.6 Blood collection and platelet preparation

2.2.6.1 Preparation of human washed platelets

Blood samples were collected from healthy donors that gave their consent in accordance with the Declaration of Helsinki, and the licence number: ERN_11-0175 was granted by the University of Birmingham ethical committee. Blood was drawn via venepuncture and collected into 10% (v:v) sodium citrate solution, then additional 10% (v:v) (acid-citrate-dextrose) ACD buffer was added to the blood. Whole blood was centrifuged at 200 x g

for 20 min at room temperature (RT) in order to obtain platelet-rich plasma (PRP). PRP was centrifuged at 1,000 x g for 10 min at RT in the presence of prostacyclin (0.1 µg/mL) to obtain platelets. The resulted platelet pellet was resuspended in modified Tyrode's-HEPES buffer containing ACD and prostacyclin (0.1 µg/mL) before centrifugation at 1,000 x g for 10 min at RT. The final pellet containing washed platelets was resuspended in modified Tyrode's-HEPES buffer. Platelet count was measured using the Coulter Z_2 Particle Counter (Beckman Coulter Ltd, UK) and platelets were resuspended to the desired concentration in Tyrode's-HEPES buffer and were allowed to rest for 30 min at RT.

2.2.6.2 Preparation of mouse washed platelets

Blood samples were collected from mice anaesthetised in isoflurane and bled from the retroorbital plexus. The blood (up to 1 mL) was collected in a tube containing 300 µL heparin (20 U/mL, pH 7.3) diluted in Tris-buffered saline (TBS). Whole blood was spun down at 800 rpm for 6 min at RT. The upper phase was transferred to a new tube with additional 300 µL heparin (20 U/mL, pH 7.3) diluted in TBS and centrifuged again at 800 rpm for 6 min at RT in order to obtain PRP. PRP was then supplemented with prostacyclin (0.1 µg/mL) and apyrase (0.02 U/mL), and centrifuged at 2,800 rpm for 5 min at RT. The final pellet containing platelets was resuspended in Tyrode's-HEPES buffer, with additional prostacyclin (0.1 µg/mL) and apyrase (0.02 U/mL) and centrifuged again at 2,800 rpm for 5 min at RT. After the final wash, platelet count was measured using the KX-21 Sysmex Cell Counter (Sysmex Europe, Germany) and platelets were resuspended in Tyrode's-HEPES buffer to the desired concentration and were allowed to rest for 30 min at 37 °C.

2.2.7 Platelets function assays

2.2.7.1 Platelet aggregation

For analysis of platelet aggregation upon stimulation, human and murine washed platelets were diluted to 2 x 10^8 platelets/mL. Aggregometry traces were obtained using a Chrono-Log Optical aggregometer (Labmedics, UK) or Fibrintimer 4 channel aggregometer (APACT, Germany) while stirring at 1,200 rpm constantly. Platelets were pre-incubated with different concentrations of EHT1864 (3, 10, 30 and 50 µM) and/or Cytochalasin D (10 µM) for 5 minutes at 37 °C under static conditions. Then, GPVI agonists Horm collagen and CRP (1, 5 or 10 µg/mL) induced platelet aggregation. Aggregation traces were monitored for 6 min after the addition of the agonists, and the maximum aggregation (Amax) was measured. The blank sample was obtained by measuring in an aggregometer cuvette only Tyrode's-HEPES buffer.

2.2.7.2 Platelet spreading

Platelet spreading assays were performed to measure platelet function and capability to form filopodia and lamellipodia. Human and murine washed platelets were diluted to 2 x 10^7 platelets/mL. Coverslips were coated with Horm collagen (10 µg/mL) or fibrinogen (100 µg/mL) overnight at 4 °C. The following day the coverslips were blocked with fatty-free bovine serum albumin (BSA) (5 µg/mL) for 1 h at RT. Control coverslips were only coated in BSA. When stated, platelets were pre-incubated with EHT1684 (30 or 50 µM) for 10 min at 37 °C. Later, platelets were spread for 30 min at 37 °C on the coated coverslips. Spread platelets were fixed with 10% (v:v) formalin solution for 10 min at RT. Then, platelets were permeabilised with 0.1% Triton X-100 for 5 min, washed 3 times with 1X phosphate buffered saline (PBS) and blocked with 1 % BSA supplemented with 2% goat serum for 1 h at RT. Platelets were then stained for actin with Alexa Fluor (AF)-488® phalloidin (1:500), and with different primary and fluorescent labelled secondary antibodies according to the different experiments. Stained platelets were washed 3 times

with PBS and mounted on slides using Hydromount solution (National Diagnostics, USA), except the dishes for super-resolution microscopy that were stored in PBS at 4°C until they were imaged.

2.2.7.3 Platelet lysate preparation and GPVI shedding

Human and murine platelets were diluted to 5 x 10^8 platelets/mL and placed in a thermomixer rack (Eppendorf, Germany) incubated with integrilin (9 μM), in the presence or absence of the metalloproteinases inhibitors GM6001 (250 μM) or GI254023X (2 μM) for 10 min at 37 °C under static conditions. Platelets were then pre-incubated with or without EHT1864 (30 or 50 μM) for 10 min at 37 °C under static conditions. Later, platelets were stimulated with vehicle (PBS) or CRP (5 μg/mL) for 3 min and stirred at 900 rpm. For GPVI cleavage assay, platelets were supplemented from the beginning with 2 mM $CaCl_2$ and as a positive control for shedding, platelets were treated with N-ethyleimide (NEM; 2 mM) for 1 h at 37 °C under stirring conditions (900 rpm). Sample preparation was terminated by the addition to the platelets of 5x SDS sample buffer supplemented with 500 Mm dithiothreitol (DTT) and incubation of the sample for 15 min on ice. Samples were denatured at 100 °C for 5 min and centrifuged at 1,500 x g for 10 minutes at 4 °C, obtaining finally the platelet lysate.

2.2.7.4 SDS-PAGE and Western blotting

Platelet lysates were loaded into commercial NuPAGE 4-12% Bis-Tris Plus (Invitrogen, UK) gels and additionally, one lane was loaded with a broad range of colour pre-stained protein standard (New England, UK) that was used to evaluate proteins' molecular weight (MW). Proteins were separated by sodium sulfate-polyacrylamide gel electrophoresis (SDS-PAGE) using NuPAGE MOPS running buffer (Invitrogen, UK). Then, the transfer of the proteins onto polyvinylidene difluoride (PVDF) membrane (Trans-Blot Turbo RTA Midi LF PVDF transfer kit, Bio-Rad, Hemel Hempstead, UK) was performed using a Bio-Rad semi-dry transfer system (Bio-Rad, UK) for 10 min at 25

Volts. PVDF membrane was then blocked in 4% (w:v) BSA dissolved in TBS-T for 1 h at RT and then, incubated at 4°C overnight with primary antibody diluted in 4% (w:v) BSA dissolved in TBS-T. The following day, membranes were washed 3 times with TBS-T buffer and then incubated with horseradish peroxidase (HRP) conjugated anti-rabbit or mouse secondary antibody (1:10,000 dilution in TBS-T) for 1 h at RT. Membranes were developed using ECL-Super Signal West Pic Plus chemiluminescence substrate (ThermoFisher Scientific, USA) and scanned using the Odyssey Fc System (LI-COR Biosciences, USA). For loading control, membranes were washed 3 times with TBS-T and then incubated twice with stripping buffer for 15 min at 80 °C. To remove the stripping buffer, PVDF membranes were washed 3 times with TBS-T for 10 min, blocked in 4% (w:v) BSA dissolved in TBS-T and incubated with loading control antibodies (GAPDH, tubulin or total LAT) overnight at 4 °C. The following day, the procedure was the same as above. The quantification of the band intensity was analysed using Image Studio Lite v5.2 software. The results were transferred to Excel (Microsoft, Redmond, WA, USA) and the relative values were normalised to the loading controls, GAPDH, tubulin or pan-LAT. Next, the values were also normalised to the vehicle control CRP-stimulated sample. The percentage of GPVI shedding was calculated as follows (equation 2):

$$\% \text{ Shed} = [\text{GPVI tail} / (\text{GPVI full length} + \text{GPVI tail})]$$

2.2.7.5 Flow cytometry

Human and murine washed platelets were diluted to 2 x 10^7 platelets/mL and pre-incubated for 10 min at 37 °C with vehicle (PBS) or EHT1864 (30 or 50 µM). Platelets were then left unstimulated or stimulated using agonists against GPVI (CRP) or GPCRs such as thrombin, ADP and the TxA_2 analogue U46619 for 7 min at 37 °C followed by 7 min at RT. Staining of the platelets was performed as described in the following subsections according to the different assays. Staining was stopped by adding 500 µL

PBS to the samples. Human samples were measured using a CytoFLEX flow cytometer (Beckman Coulter, USA) and the analysis was performed using its acquisition software CytoExpert (Beckman Coulter, USA), while murine samples were measured using a FACS Celesta cytometer (BD Biosciences, Germany) and the analysis was performed using the FACSDiva software (BD Biosciences, Germany). In all the flow cytometry assays, platelet populations were gated according to their size using forward scatter (FSC) *vs* side scatter (SSC).

2.2.7.5.1 Platelet activation

Platelet activation was monitored by P-selectin exposure and integrin αIIbβ3 activation. Unstimulated and stimulated human platelets were incubated with 10 µL of anti-human FITC-labelled anti-P-selectin and Alexa Fluor® 647 conjugated anti-human activated CD41/CD61 (clone: PAC-1) antibodies. Resting and activated murine platelets were labelled with 10 µL of anti-mouse FITC-labelled anti-P-selectin (clone: WUG1.9) and anti-mouse anti-activated integrin αIIbβ3 (clone: JON/A) antibodies. Their MFI was determined by flow cytometry as described above (section 2.2.7.5).

2.2.7.5.2 Platelet glycoprotein expression

Surface expression of the main glycoproteins on resting and activated platelets was performed by labelling the platelets with antibodies against GPVI, GPV, GPIbα, CLEC-2 and integrin β3 subunit conjugated with FITC, PE or APC and determining their MFI by flow cytometry as described above (section 2.2.7.5).

2.2.7.5.3 Fluorescence resonance energy transfer (FRET) in platelets

To study GPVI dimerisation and clustering, flow cytometric FRET analysis was performed in human platelets. During FRET it is assumed that there is an energy transfer from an excited donor fluorophore (AF-488) to an acceptor fluorophore (AF-546) when both fluorophores are closer than 10 nm together (Hochreiter et al., 2019). Platelets were pre-treated with EHT1864 when cited, unstimulated or stimulated with CRP and labelled

with 50 µg/mL of anti-human-GPVI F(ab') fragment 313A10 conjugated with Alexa Fluor® 488 (as the donor fluorophore), with Alexa Fluor® 546 (as the acceptor fluorophore) or unlabelled. As a negative control for the FRET assay, the integrin αIIbβ3 and GPIX were used as they are not known to interact to form a dimer, but both are highly expressed on the platelet surface. The following antibodies were used: anti-integrin αIIbβ3 (clone: MWReg30) labelled with Alexa Fluor® 488 and anti-GPIX (p0p6) labelled with Alexa Fluor® 546. For the flow cytometric FRET, the FACSAria (BD Biosciences, USA) flow cytometer was used, and the analysis was performed using the FACSDiva software (BD Biosciences, USA). When the MFI of each sample was determined, the FRET efficiency (E) was calculated as a reduction in the MFI of the donor in the presence of the acceptor divided by the MFI of the donor alone, as described in the following equation (equation 3):

$$E = 1 - \frac{MFI_{Donor + Acceptor} - MFI_{background}}{MFI_{Donor} - MFI_{background}}$$ (Vereb, 2011)

2.2.8 Microscopy

2.2.8.1 Epifluorescence microscopy

Platelets were spread on 13 mm #1.5 glass coverslips (VWK, UK) coverslips, uncoated or coated with collagen or fibrinogen. Samples were imaged using a Zeiss Axio Observer 7 epifluorescence microscope (Carl Zeiss, Germany) equipped with a Plan-Apochromat 63x/1.4 numerical aperture (NA) oil objective lens, Hamamatsu ORCA Flash 4 LT sCMOS camera, Colibri 7 LED light source and, Zeiss GFP/FITC Filter Set 38 HE and Cy5/647 Filter Set 50. Platelets were stained with phalloidin-Alexa Fluor® 488 and with different primary antibodies against the protein of interest, then incubated with secondary antibodies labelled with Alexa Fluor® 647 and/or 594. The images were taken at optimal exposure time and consistent within the same experiment. For each condition, at least 5

separate fields of view (FOVs) were acquired using the Zeiss software Zen Pro v2.3 and the analysis was performed using ImageJ v2.0 (NIH, Bethesda, USA).

2.2.8.2 Scanning electron microscopy (SEM)

Glass coverslips were coated with 0.01% poly-L-Lysine for 15 min at RT on an orbital shaker at medium speed and then dried for 2 hours at 60 °C. During the coverslips drying, washed platelets were adjusted to 2.5 x 10^8 platelets/mL in Tyrode's buffer and placed in the aggregometry cuvette. Washed platelets were stimulated with 50 µg/mL isotype IgG control or α-GPIbα IgG antibodies, and incubated for 10 min at 37 °C under stirring conditions in the aggregometer (1,200 rpm). Samples were then fixed by adding the sample volume of 2x fixation buffer (5% glutaraldehyde in cacodylate buffer; 100 mM sodium cacodylate-HCl pH 7.4) for 15 min at 37 °C. Carefully, fixed platelets were placed on the coated coverslips, with fresh 1x fixation buffer (2.5% glutaraldehyde in 50 mM cacodylate buffer) added, and they were incubated for 1h at RT. Coverslips were then dehydrated with cacodylate buffer in 30% (15 min), 50% (20 min), 75 % (30 min), 90% (45 min) and 100% (five times, 30 min each) acetone. Samples are then dried out, sputtered with gold/palladium using an SC7620 Sputter Coater (Quorum technologies, UK) and analysed using Phenom Pro Desktop SEM (ThermoFisher Scientific, USA).

2.2.8.3 Super-resolution microscopy

2.2.8.3.1 Direct stochastic optical reconstruction microscopy (*d*STORM)

In order to obtain *d*STORM super-resolved images, platelets were spread on glass bottom dishes (MatTek Corporation, USA) coated with collagen, and blocked in BSA. Samples were imaged using a Nikon N-STORM microscope (Nikon Instruments, New York, USA) in total internal reflection fluorescence (TIRF) and *d*STORM mode using a Plan-Apochromat TIRF 100x/1.4 NA oil objective lens, Perfect Focus System (PFS), Andor iXon Ultra 897 EM-CCD camera and Agilent MLC400 Monolithic Laser Combiner containing 405 nm, 488 nm, 561 nm and 640 nm lasers. Platelets were stained with

phalloidin-Alexa Fluor® 488 and the relevant primary antibodies, then secondary labelled with Alexa Fluor® 647 conjugated antibodies. DIC images were obtained to visualize the collagen fibres. Samples were imaged in oxidizing and reducing buffer (*d*STORM buffer) that promotes the photoswitching of the fluorophores (Goossen-Schmidt et al., 2020). *d*STORM acquisition was obtained for 20,000 frames (9.2 ms exposure time, conversion gain 3), and the sample was illuminated at 640 nm (continuously at 100% laser power) combined with a gradual increase of the 405 nm laser (5% increase every 30 sec) that was used to pump the 647 fluorophore blinking. The 20,000 frames were acquired using Nikon NIS Elements v4.5 software and reconstruction was performed using ThunderSTORM ImageJ plugin (Ovesný et al., 2014).

2.2.8.3.2 DNA points accumulation for imaging in nanoscale topography (DNA-PAINT)

Platelets were spread on glass bottom dishes (MatTek Corporation, USA) coated as detailed above. DNA-PAINT sample preparation was performed as previously described (Schnitzbauer et al., 2017). In summary, platelets were labelled with a primary antibody against the protein of interest, followed by a secondary antibody that was coupled with the docking strand (short DNA sequence). The linking of the docking strand to the secondary antibody was performed using the Thunder-Link PLUS Oligo Conjugation System (Novus Biologicals, USA), following the company protocol. Briefly, the linking protocol was performed by diluting the secondary antibodies to 1 mg/mL and activating them using the kit Antibody Activation Reagent vial for 30 min at RT. During the incubation time, the separating column provided by the kit was desalted and equilibrated by washing it with the kit Wash Buffer at least 4 times. After 30 min activation, activated antibodies were mixed with the different docking strands and went through the separating column previously equilibrated. Wash Buffer was added to the top of the column to push the activated antibody with the docking strand to the base of the column, where it was

collected in a clean tube. When platelets were ready and labelled with the antibody conjugated with a docking strand, and immediately before the imaging, the imaging buffer C (500 mM NaCl in PBS and, supplemented with 0.05% Tween-20, pH 7.2) containing the imager strand (complementary DNA sequence of the docking strand) conjugated with Alexa Fluor® 488 or 647 was added to the MatTek dish and the imaging started. Samples were imaged using a Nikon N-STORM microscope in TIRF mode (Nikon Instruments, New York, USA. See *d*STORM section above for a complete description of the microscope. Images acquisition was obtained for 20,000 frames (300 ms exposure time, conversion gain 3) and illuminated at 488 nm or 640 nm (40% laser power). The images were reconstructed using Nikon NIS Elements v4.5 software.

2.2.8.3.3 Structured illumination microscopy (SIM)

Platelets were spread on 1.5 high tolerance glass coverslip (MatTek Corporation, USA). Samples were imaged using the TIRF-SIM mode on a Nikon N-SIM-S microscope (Nikon Instruments, New York, USA) equipped with a Plan-Apochromat TIRF 100x/1.49 NA oil objective lens, Perfect Focus System (PFS), Cairn TwinCam imaging splitter with two Hamamatsu Flash 4.0 sCMOS cameras and emission filter Chroma ET525/50m and Chroma ET700/75m. Platelets were stained with phalloidin-Alexa Fluor® 488 and the relevant primary antibodies and then labelled with Alexa Fluor® 647 conjugated secondary antibodies. The images were taken at optimal exposure time and consistent within the same experiment. For each condition, at least 5 separate FOVs were acquired and then reconstructed using Nikon NIS-Elements v5 software, using the default settings for SIM.

2.2.8.3.4 Expansion microscopy

In order to obtain super-resolved images, platelets were expanded 4 and 10 times using different expansion microscopy (ExM) protocols. Washed platelets were spread on 12 mm glass coverslips (VWK, UK) coverslips coated with 2 M glycine. Then, for each of

the expansion protocols, platelets were fixed, labelled, and expanded following the protocols described below. All the expanded samples were imaged using a Zeiss LSM 980 Airyscan 2 microscope (Carl Zeiss, Germany) prepared with a Plan-Apochromat 40x/1.2 NA water immersion objective, a laser bed containing 405 nm, 488 nm, 514 nm, 543 nm, 561 nm and 639 nm lasers and 2 PMT detectors. Images were obtained with the ZenBlue software (Carl Zeiss, Germany). The trifunctional linkers used for ExM were obtained from Chrometra and the labelling of the antibodies was performed according to their protocol (Chrometra, The Netherlands). Briefly, mix the activation agent with the antibody, incubate for 1h at 37 °C, and purify the activated antibody through a spin-column. Then, the activated antibody was added to the tube containing the reactive dye (Atto-488 or Atto-546). The mix of the antibody with the dye was incubated overnight at 4 °C, and purified through a spin-column to remove the dye not coupled to the antibody.

2.2.8.3.4.1 4x post-gelational labelling ExM

4x ExM experiments were adapted and modified from Gambarotto et al. ultrastructure expansion microscopy (U-ExM) protocol (Gambarotto et al., 2019). In summary, washed platelets were fixed with a solution containing 0.7% formaldehyde (FA) and 2% acrylamide (AA) in 1x PBS for 3 h at 37 °C and then washed 3 times with 1x PBS. Then, gelation was carried out by adding the U-ExM 4x monomer solution to the coverslips. Gelation proceeded for 1h at 37 °C. Gels denaturation was performed by adding denaturation buffer, first for 15 min at 37 °C shaking. Then samples were boiled for 30 min at 95 °C. Gels were expanded by exchanging water every hour at least 3 times until the gels are 4x bigger than the starting size (from 12 mm to ~ 5 cm). When gels were fully expanded, a piece was cut out and shrank in 1x PBS for 30 min several times. Gels containing the platelets were then stained with primary fluorescently labelled antibodies (10 µg/mL) diluted in 2 % (w:v) BSA in PBS for 3 h at 37 °C and gentle shaking. Labelled

platelets were washed with 1x PBS supplemented with 0.1% Tween-20 for 10 min 3 times. Finally, platelets were again expanded by exchanging water several times.

2.2.8.3.4.2 10x pre-gelational labelling ExM

Pre-gelational labelling 10x ExM experiments were adapted and modified from Truckenbrodt et al. protocol (Truckenbrodt et al., 2019). Briefly, washed platelets were fixed with Glyoxal buffer for 20 min at RT, washed 3 times with 1x PBS, and blocked with 5% (w:v) BSA in PBS for 2 h at RT. Then, platelets were labelled with fluorescently labelled primary antibodies (10 µg/mL) against different glycoproteins for 30 min at 37°C. Labelled platelets were incubated with linking solution Acryloyl-X (0.1 mg/mL) overnight at RT. Gelation was performed by adding the 10x monomer solution and incubating it in a humidified chamber for 48 h at 4 °C. Next, digestion of the sample upon the gelation was induced by incubating the gel in digestion buffer plus additional proteinase K (8 units/mL). The expansion was performed by exchanging the water for the gels at least 4 times every 2 h. The gels should reach a size 10x bigger than the starting size (from 12 mm to ~ 12 cm).

2.2.8.3.4.3 Mix-Match 10x post-gelational labelling ExM

We have created a new expansion microscopy protocol that expands the platelets 10x and allows a post-gelation labelling. This protocol was created by combining and modifying pieces from two existing protocols (Gambarotto et al., 2019, Damstra et al., 2022), for that reason we have named our protocol Mix-Match Expansion microscopy (MM-ExM). Washed platelets were fixed with 0.7 % FA and 1% AA in 1x PBS for 3h h at 37 °C and then washed 3 times with 1x PBS. Gelation started by placing the coverslip with the platelets upside-down in 50 µL 10x T-REX monomer solution for 1h at 37 °C. Digestion was performed by adding the denaturation buffer for 15 min at 37 °C, shaking and then boiling the samples for 5 min at 95 °C. Once the samples were denaturised, we proceeded with the expansion by exchanging water until the gels reached a size 10x

bigger than the initial size (~ 12 cm). The following day, the gels were shrunk in PBS and small pieces were extracted in order to perform the labelling. Labelling was performed by incubating small pieces of gels for 3 h at 37 °C (with gentle shaking) with different fluorescently labelled antibodies (10 µg/mL) against platelet receptors. Afterwards, gels were washed with PBS containing 0.1% Tween-20 for 10 min 3 times. The last step was to re-expand the gel pieces by exchanging water at least 4 times every 1 – 2 hours. This method was developed together with Prateek Gupta, from Prof Heinze laboratory.

2.2.9 Image analysis

2.2.9.1 Platelet spreading data analysis

In order to quantify in an automated manner epifluorescence images of spread platelets, pixel classifier software ilastik (Sommer et al., 2011) was used to perform platelet binary segmentation and then, platelet count and surface area were analysed using KNIME software (Berthold et al., 2009). Platelets were manually selected in 10 random images per experiment in order to train ilastik software to differentiate platelets. To separate spread platelets that were touching other platelets, the centre of the platelets was manually selected using a KNIME workflow developed in our lab (Pike et al., 2021). Only objects bigger than 1 μm^2 were considered for the platelet analysis. Data generated in Knime was exported to Excel for further analysis.

2.2.9.2 *d*STORM data reconstruction

The 20,000 frames obtained from the *d*STORM imaging were reconstructed in order to obtain the final super-resolved image using ThunderSTORM plugin for ImageJ (Ovesný et al., 2014). The settings used in the reconstruction and post-processing analysis were; Gaussian PSF model and maximum likehood estimator to fit the position of the fluorescent molecules, drift correction and photon intensity filter (>1000 photons). Further, to minimise artefacts, detection within 20 nm from another detection in two consecutive frames were merged as a single detection. Gaussian filter was applied to

visualise the reconstructed images that represent individual fluorescent blinking events, which are referred to as detections.

2.2.9.3 Clustering analysis

Single-level cluster analysis of GPVI was performed on reconstructed *d*STORM Density-Based Spatial Clustering of Applications with Noise (DBSCAN) (Ester et al., 1996), which was applied to group detections into clusters. DBSCAN was implemented in KNIME software (Berthold et al., 2009). For the clustering analysis, the following settings were used; the radius of the local neighbourhood was adjusted to 50 nm and the minimum number of reachable detection was set to 10. In order to calculate cluster area, detections that were within a radius of 50 nm from each other were considered as part of the same cluster. Cluster density was calculated as the number of detections per cluster divided by the cluster area. The clustering analysis was performed with the help of Dr Jeremy Pike (University of Birmingham, UK).

2.2.10 Statistical analysis

Data analysis was performed using Prism v8.0.2 software (GraphPad Software, California, USA). All data are shown as mean ± standard deviation (SD) unless otherwise stated. The number of replicates and statistical tests used for each experiment were detailed in the figure legends. Significance was reached with a p-value < 0.05.

CHAPTER 3

Development of methods to study GPVI conformation, localisation and signalling

Based on: Clark, J. C., **Neagoe, R. A. I**., Zuidscherwoude, M., Kavanagh, D. M., Slater, A., Martin, E. M., Soave, M., Stegner, D., Nieswandt, B., Poulter, N. S., Hummert, J., Herten, D. P., Tomlinson, M. G., Hill, S. J., & Watson, S. P.. (2021). Evidence that GPVI is Expressed as a Mixture of Monomers and Dimers, and that the D2 Domain is not Essential for GPVI Activation. Thrombosis and Haemostasis, 121(11), 1435–1447.

This Chapter contains self-citations. I performed the flow cytometry-based FRET assay, analysed the FRET results, wrote the corresponding method and result section, and helped with the editing of the manuscript. JCC performed the rest of the experiments, analysed data and wrote the manuscript. MZ performed experiments and provided supervision, DMK designed experiments and performed FCS experiments. AS, EMM, MGT design constructs and experiments and edited the manuscript. MS provided reagents and constructs. DS, BN, NSP provided reagents and edited the manuscript. JH and DH developed algorithms for the photobleaching image analysis and analysed data. SJH and SPW provided supervision and funding, and wrote and edited the manuscript.

3.1 Introduction

GPVI is the main collagen receptor in platelets, and therefore, it has a potential role as an anti-thrombotic target (Gardiner et al., 2014). Hence, it is crucial to know its conformation in the platelet in order to be able to design effective inhibitory agents. GPVI conformation was unknown for many years until Horii et al. published the first time its crystal structure, showing a back-to-back dimer (Horii et al., 2006). More recently, another domain-swapped dimeric structure was identified (Slater et al., 2021) demonstrating that GPVI can form a dimer. However, whether this occurs with the full-length protein in a platelet, or whether it is important for signalling is debated (Clark et al., 2021a). Different studies have used dimeric GPVI-specific antibodies to understand GPVI conformation and showed that GPVI can be found partly as dimers in platelets (Jung et al., 2012, Loyau et al., 2012). We selected fluorescence resonance energy transfer (FRET) (Matkó et al., 1994) in combination with flow cytometry to study GPVI conformation, dimerisation and oligomerisation.

Flow cytometry-based FRET is a powerful method to detect protein-protein interaction, changes in dimerisation/oligomerisation and protein-folding dynamics (Nagy et al., 2005, Okamoto and Sako, 2017). Proteins are labelled with two different fluorophores, called acceptor and donor respectively, and the transfer of energy (fluorescence) from the donor to the acceptor can be quantitated and is a measure of how close the two proteins are. FRET efficiency (E) is the quantum yield of the energy transfer transition, that describes a process of energy transfer of an electron based on dipole-dipole interactions that happen from an excited fluorescent molecule (donor fluorophore) to an acceptor molecule (acceptor fluorophore) (**Figure 3.1A**) (Förster, 1948). In order for this to occur, the donor emission spectrum should overlap with the acceptor excitation spectrum and the molecules should be separated by less than 10 nm (**Figure 3.1B**) (Lakowicz, 2006).

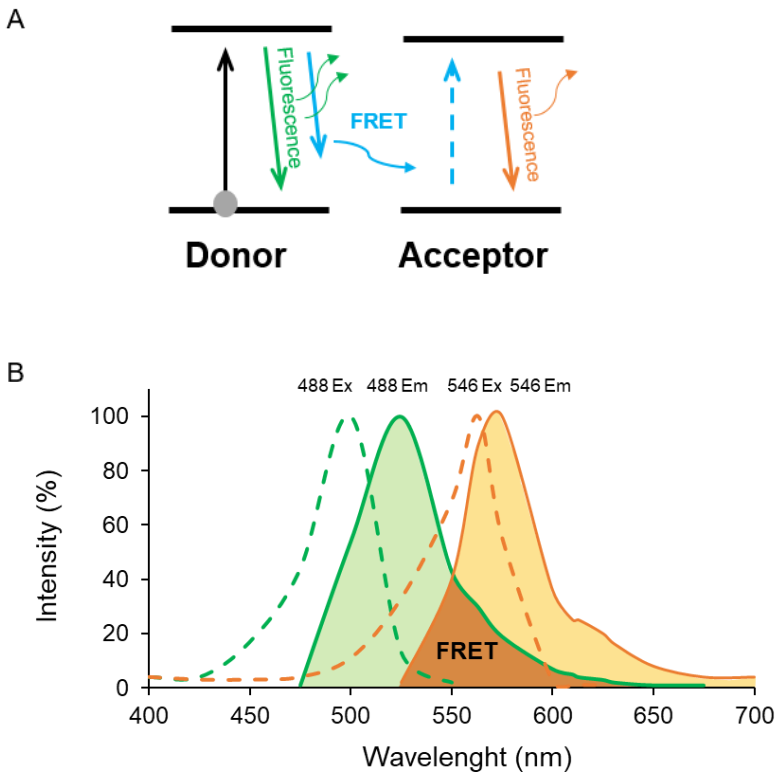

Figure 3.1. The principle of FRET. (**A**) Jablonski diagram describing the FRET mechanism. When the donor electron is excited, then falls back to the ground state realising energy as a photon (donor fluorescence), but the energy can also be transferred to a neighbour electron (less than 10 nm apart) that would get excited and therefore also release a photon (acceptor fluorescence). (**B**) Excitation and emission spectrum of Alexa Fluor 448 (green) and 546 (orange) fluorophores, acting as a FRET pair. Spectra overlap corresponds to FRET (dark orange).

When FRET occurs, the emission of the donor fluorophore, manifested as fluorescence, has a lower intensity, and therefore the emission of the acceptor fluorophore is greater (Vereb, 2011). Many fluorophores, which spectrums overlaps, can be used as FRET pairs. One of the most optimal pairs is Alexa Fluor 488 and Alexa Fluor 546. Alexa Fluor 488 is commonly used since it is very bright and has a long lifetime (Horváth et al., 2005). Using simulation prediction models, a study reported that a mix of monomers and dimers reach an efficiency of 30% while only dimers got up to 70% FRET efficiency (King et al., 2017). Nevertheless, the FRET efficiency in cells is significantly lower than in simulated models, for example, integrin α4β1 in leukocytes, a well-known dimer, reached an

efficiency of only 37% using flow cytometric FRET (Sambrano et al., 2018). In this Chapter, flow cytometric FRET has been used to study the conformation of the platelet GPVI receptor in resting and CRP-stimulated human platelets.

Flow cytometry-based FRET is a useful technique to determine the conformation of the molecules, however, it gives no spatial information on the receptor in individual cells. In order to have a precise knowledge of the localisation of the molecules, super-resolution (SR) microscopy methods can be used. The development of SR microscopy techniques has overcome several limitations of traditional light microscopy, as they break the diffraction limit of light meaning that single molecules can be resolved down to approximately 20 nm (Hell and Wichmann, 1994). Among all the SR microscopy techniques, SIM and *d*STORM have been the greatest employed in platelet research. SIM has shown unique insights into the actin cytoskeleton (Poulter et al., 2015), and co-clustering into α-granules (Kamykowski et al., 2011). Using *d*STORM, great advances have been made in understanding GPVI clustering. It was first shown by Poulter et al. that GPVI clusters along the collagen fibres, and that some of these GPVI are dimeric (Poulter et al., 2017). Additionally, recent studies have tried to understand what is the signalling pathway driving GPVI clustering. These have demonstrated the inhibition of two of the main kinases downstream of GPVI; Syk and Src do not alter GPVI clustering after the clusters have formed (Pallini et al., 2021). Additionally, neither adenosine nor the adenylyl cyclase-activating compound forskolin affect GPVI clustering (Clark et al., 2019). Therefore, there is not yet a clear mechanism describing how GPVI clustering is controlled.

3.2 Aims

This Chapter contains the establishment and verification of the methods that have been further used in Chapter 4, where we focused on the biological relevance of the results. In the literature, there was no agreement on whether GPVI is a monomer or dimer. Therefore, the goals of this Chapter were:

1. Understanding the conformation of GPVI in human platelets, investigating whether GPVI is present as a monomer or dimer in resting platelets and analysing its conformation change upon GPVI-ligand stimulation.
2. Studying GPVI and the proteins downstream of GPVI signalling cascade location in human platelets. For this reason, we have optimised the use of several super-resolution microscopy techniques, which allowed us to obtain a clear idea of the distribution of proteins involved in the GPVI signalling pathway.

3.3 Results

3.3.1 Evaluation of flow cytometry-based FRET efficiency

In order to evaluate the FACS-FRET method that we intended to use for studying GPVI dimerisation, we studied the detectable FRET efficiency of known monomers and dimers on the platelet surface. Integrins are transmembrane glycoprotein heterodimers, which remain as heterodimers regardless of whether the platelet is in a resting or activated state (Bennett, 2005). Integrin αIIbβ3 is the most abundant receptor on the platelet plasma membrane, expressing around 80,000 copies per platelet (Wagner et al., 1996). These characteristics make this protein an excellent option to be used as a positive control for the assay. To assess the FRET efficiency of integrin αIIbβ3, mouse platelets were labelled with MWReg30 antibody (known to bind the αIIb subunit) conjugated with Alexa Fluor 488 (donor), and JON6 antibody (not known the exact binding epitope in the integrin αIIbβ3) conjugated with Alexa Fluor 546 (acceptor). First, the mean fluorescence intensity (MFI) of MWReg30, the donor, was measured by flow cytometry (**Figure 3.2Ai**). Platelets were unstimulated or stimulated with 10 µg/mL CRP, and labelled with MWReg30-AF488 (donor alone), or MWReg30-AF488 + JON6-AF546 (donor in the presence of the acceptor). To obtain FRET efficiency, MFI of the donor in the presence of the acceptor was divided by the fluorescence of the donor alone, as explained in equation 3 (**Figure 3.2Aii**). The result suggests that the FRET efficiency of the heterodimer αIIbβ3, is approximately 45% and 50% in resting and CRP stimulated platelets, respectively. There is no significant difference between FRET efficiency of resting and stimulated platelets, as the integrin stays as a heterodimer in both inactive and active conformation.

For the negative control, integrin αIIbβ3 and GPIX, two highly-abundant glycoproteins in the platelet surface that are not known to dimerise (Heil et al., 2022), were chosen. GPIX was labelled with p0p6 antibody conjugated with Alexa Fluor 488, and αIIb subunit of the

integrin with MWReg30 antibody conjugated with Alexa Fluor 546. Then, MFI of the donor was measured by flow cytometry, using p0p6-AF488 (donor alone), or p0p6-AF488 + MWReg30-AF546 (donor in the presence of the acceptor) (**Figure 3.2Bi**). FRET efficiency was calculated as described above. FRET efficiency of GPIX and integrin αIIbβ3, two glycoproteins not dimerising, was 7% (**Figure 3.2Bii**).

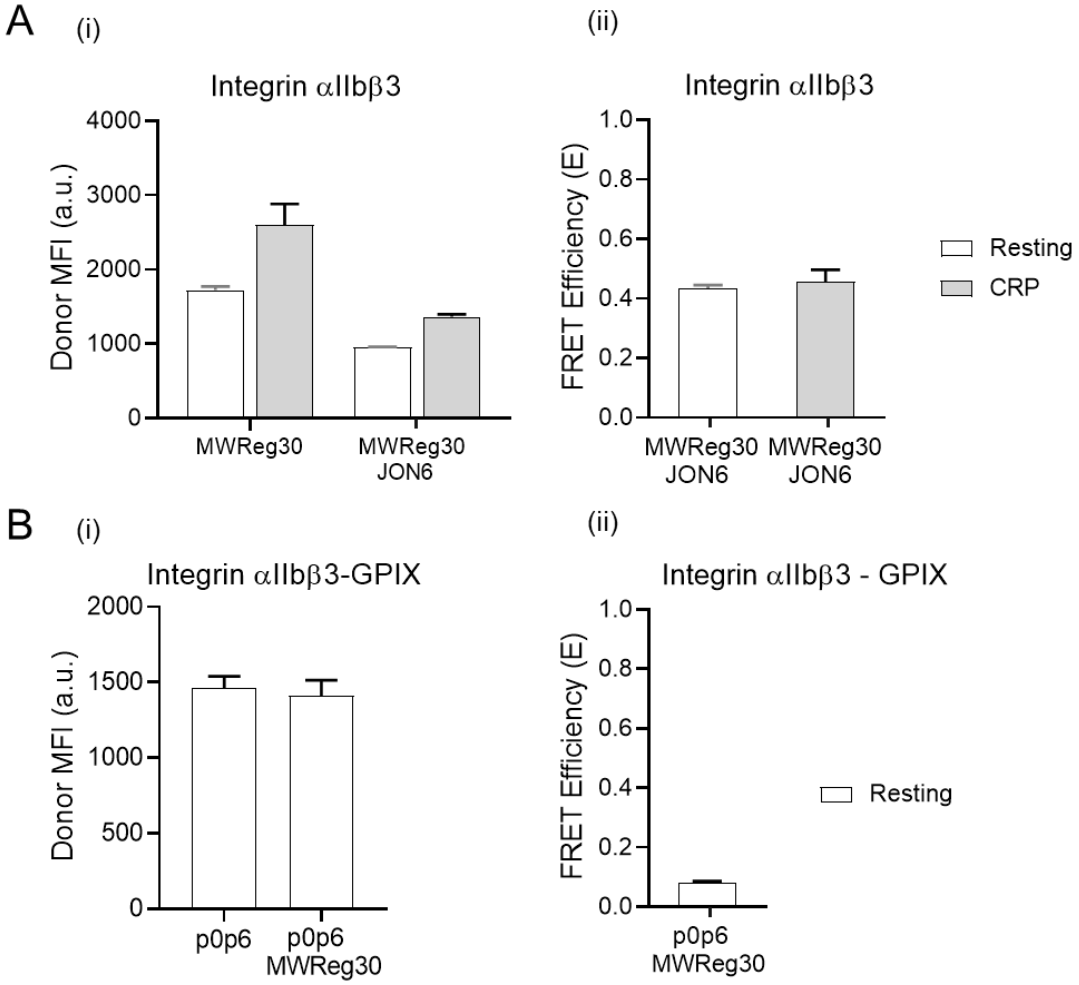

Figure 3.2. Positive and negative controls for the FRET assay. (**A**) For the positive control, the heterodimeric integrin αIIbβ3 was used. Murine platelets were labelled with anti-αIIbβ3 IgG antibodies; MWReg30-AF488 (donor) and JON6-AF546 (acceptor). Platelets were resting (white) or stimulated with 10 µg/mL CRP (grey) for 10 min at 37°C. (Ai) The mean fluorescent intensity (MFI) of donor alone (MWReg30) and donor in the presence of the acceptor (MWReg30 + JON6) was measured by flow cytometry. (Aii) The FRET efficiency was calculated as a difference in the MFI of the donor in the presence of the acceptor divided by the MFI of the donor alone in resting (white) and activated cells (grey) (n=2). (**B**) For the negative control, resting platelets were stained for GPIX (p0p6-AF488; donor) and integrin αIIbβ3 (MWReg30-AF546; acceptor). (Bi) The MFI of the donor alone (p0p6) and the donor in the presence of the acceptor (p0p6 + MWReg30) was measured by flow cytometry. (Bii) The FRET efficiency for GPIX and integrin αIIbβ3 was calculated as described in (Aii) (n=2).

3.3.2 Optimisation of GPVI labelling with antibodies for flow cytometry-based FRET

GPVI was labelled using different in-house-made antibodies prepared in the laboratory of Prof Nieswandt that have been previously characterised by other laboratory members. The three anti-GPVI antibodies tested for the experiment were the following clones: 313A10, 336E2 and JAQ1. It is known that all of them bind the extracellular domain of GPVI, however, exact epitopes have not yet been identified. To avoid cross-linking errors and to improve the sensitivity of antigen detections, all anti-GPVI antibodies used were F(ab') fragments instead of IgGs. As their binding epitope is not known, to verify that CRP does not compete for the same epitope as the antibodies, GPVI was measured under 3 conditions in human platelets: 1) resting platelets labelled with 313A10, 336E2 or JAQ1; 2) platelets labelled with each antibody prior to stimulation with CRP; 3) platelets stimulated with CRP, and then labelled with each antibody. The fluorescence intensity of each antibody was analysed by flow cytometry (**Figure 3.3A**). Preliminary data suggests that the 313A10 signal was not different between platelets labelled with the anti-GPVI antibody before, or after CRP stimulation, indicating that CRP binds to a different site on GPVI to that of antibody 313A10. Additionally, when platelets were stimulated with CRP, regardless of whether it was before or after antibody labelling, the fluorescence intensity increased, suggesting GPVI levels increase post-activation, as previously shown (Moroi et al., 2020). Studying 336E2, in the preliminary results, we observed that the levels of detectable GPVI decreased when samples were labelled with the antibody fragment and then stimulated with CRP, making this clone unsuitable for this assay, and indicating that it might bind close to the CRP binding epitope. The third antibody verified, JAQ1, showed the same dynamic as 313A10; GPVI expression increased in CRP-stimulated samples and did not alter depending on whether the antibody fragment was added before or after CRP stimulation. However, for JAQ1 the MFI was considerably lower than for 313A10. All these early findings together made

313A10 the best candidate for the FRET assay. However, a higher number of replicates would be necessary to firmly conclude that 313A10 is the best candidate.

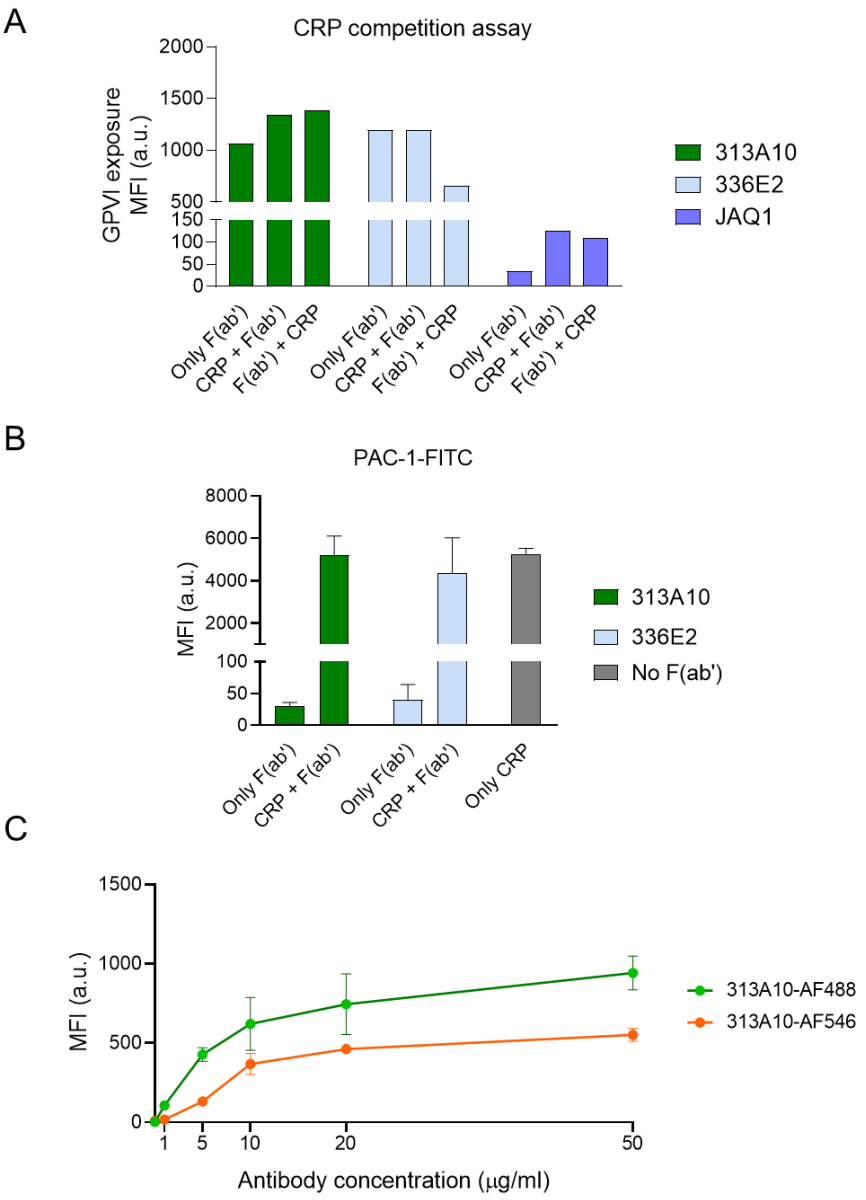

Figure 3.3. Validation of antibodies for the FRET assay. (**A**) Platelets were unstimulated, pre- and post-stimulated with CRP (10 µg/mL) for 10 min at 37°C, to validate that the antibody does not block the CRP binding site of GPVI. Platelets were labelled for 10 min at RT and 10 min at 37°C with 3 different in-house-made F(ab') fragments against GPVI; 313A10, 336E2 and JAQ1 conjugated with Alexa-Fluor 488 (10 µg/mL). Using a flow cytometer, the MFI of each antibody was measured (n=1). (**B**) Platelets were resting or pre-stimulated with CRP (10 µg/mL) for 10 min at 37°C, and later incubated with anti-GPVI F(ab') fragments 313A10 and 336E2 (10 µg/mL) for 10 min at RT. Then, platelets were stained with anti-human activated integrin αIIbβ3 (PAC-1) antibody conjugated with FITC, and PAC-1 MFI was measured by flow cytometry. n=3 ± SD. (**C**) Platelets were resting, and then labelled with 313A10 F(ab') fragments conjugated with Alexa-Fluor 488 or 546 using different concentrations (0-50 µg/mL). MFI of 313A10-AF488 and 313A10-AF546 was measured by FACS. n=3 ± SD.

Further, we studied whether 313A10 alters platelet activation. Data was collected by labelling human platelets with PAC-1 antibody conjugated with FITC and measuring the MFI by FACS (**Figure 3.3B**). PAC-1 recognises the active conformation of the integrin αIIbβ3 and therefore represents platelet activation. It was observed that neither 313A10, nor 336E2 activates resting platelets. Additionally, neither of the antibodies blocked the activation of platelets mediated by CRP. Yet, 313A10 was the selected antibody for this assay.

Finally, a titration assay for 313A10 was performed. Based on the results, the concentration at which 313A10 saturated GPVI could be determined. Resting and CRP-activated human platelets were labelled with up to 100 µg/mL 313A10 conjugated with Alexa Fluor 488 and 546 (donor and acceptor fluorophore, respectively), and the MFI was measured by flow cytometry (**Figure 3.3C**). Saturation was reached at 5 µg/mL for 313A10-AF546, and at 50 µg/mL for 313A10-AF488. To use the same concentration for both antibodies, 50 µg/mL was selected as the saturation concentration for further experiments.

3.3.3 GPVI is expressed as a mix of monomers and dimers in resting and CRP-stimulated platelets

Flow cytometry-based FRET was used to study the conformation of GPVI after we had established positive and negative controls, and also identified an antibody (313A10) with a high MFI that does not block CRP binding nor CRP-induced activation. We labelled human platelets with 50 µg/mL 313A10-AF488, 313A10-AF546 and 313A10 unlabelled F(ab') fragments in the combinations detailed below. Then, platelets were stimulated with 10 µg/mL CRP. This assay measured the MFI of resting and CRP-stimulated platelets. For calculating the FRET efficiency (equation 3), we need; 1) platelets labelled with 313A10-AF488 + 313A10-AF546 (donor in the presence of the acceptor; FRET condition) and 2) platelets labelled with 313A10-AF488 + 313A10-unlabelled (simulating

the donor alone condition) (**Figure 3.4A**). Since we have the same antibody in two different colours targeting the same epitope, in theory, 50% of GPVI will always be labelled with the donor fluorophore and the other 50% with the acceptor fluorophore (FRET condition). By labelling the platelets with 313A10-AF488 + 313A10-unlabelled, we obtained theoretically 50% of GPVI labelled with the donor fluorophore, whereas the other 50% is unlabelled, which is crucial for calculating FRET efficiency, so 50% of the GPVI is labelled with the donor fluorophore in both conditions. As another point to consider, using only 313A10-AF488 as the condition of the donor alone would have labelled 100% of GPVI with the donor fluorophore, making this condition incomparable to the FRET condition.

In the presence of the donor and acceptor fluorophores (313A10-AF488 + 313A10-AF546), there was a similar and significant decrease in the MFI of the donor fluorophore alone in both resting and CRP-activated platelets compared to the labelling with the donor fluorophore alone (313A10-AF488). From the MFI obtained, the FRET efficiency for GPVI was calculated to be 32% and 33% for resting and CRP-activated platelets, respectively (**Figure 3.4B**).

The calculated FRET efficiency for GPVI was between the FRET efficiency obtained for the integrin dimers (approximately 50%) and the FRET efficiency of proteins which are abundant but not known to form dimers and therefore act as a proxy for monomers (7%). This indicates that GPVI can be found as a mixture of monomers and dimers in resting and activated platelet and that the dimerisation does not increase significantly when the platelets are activated.

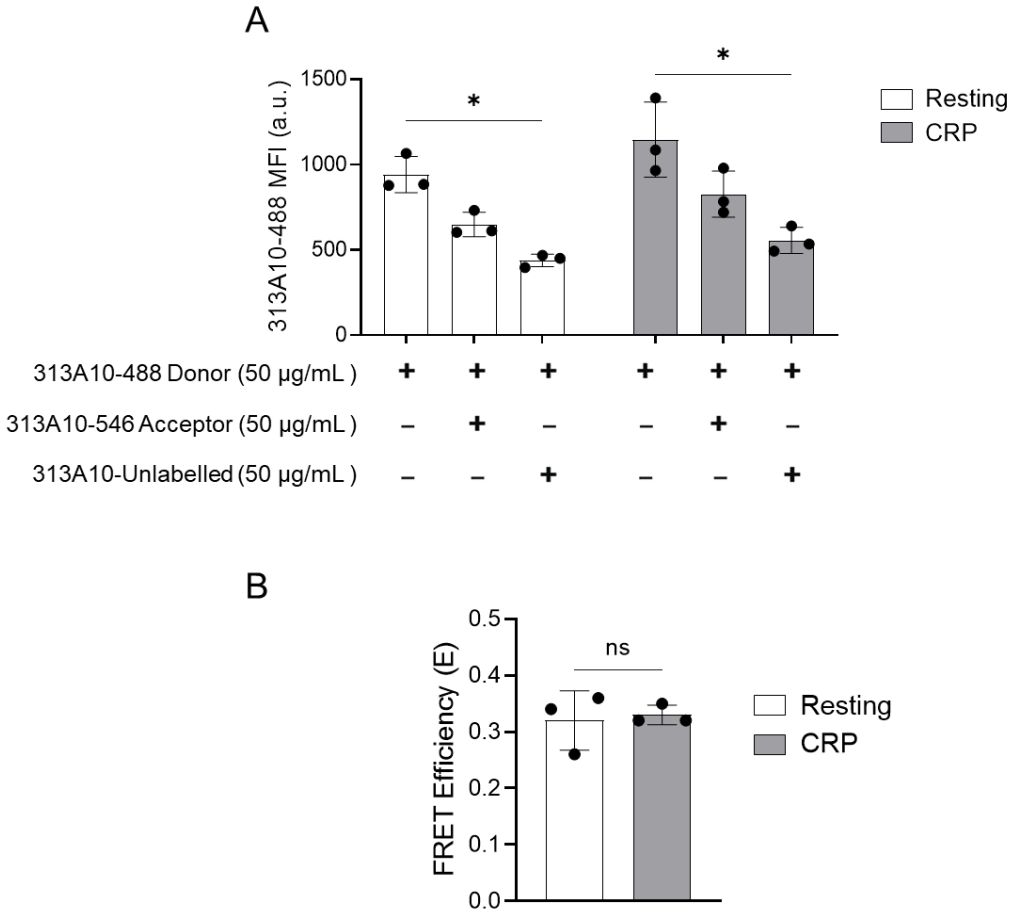

Figure 3.4. GPVI is present in human platelets as a mixture of monomers and dimers. (**A**) Human resting (white) and 10 µg/mL CRP-stimulated (grey) platelets were stained with 50 µg/mL anti-GPVI F(ab') fragments. Platelets were labelled with only 313A10-AF488 (donor fluorophore), 313A10-AF488 and 313A10-AF546 (acceptor fluorophore), or 313A10-AF488 and 313A10-unlabelled (control). The MFI of the donor fluorophore (AF488) was measured in all the samples by flow cytometry (n=3). Mean ± SEM, * $p < 0.05$ by two-way ANOVA. (**B**) FRET efficiency of GPVI in resting (white) and 10 µg/mL CRP-activated platelets (dark grey), and of integrin αIIbβ3 (MWReg30-AF488) and GPIX (anti-GPIX-AF546) (light grey) was calculated as a difference in the MFI of the donor in the presence of the acceptor divided by the MFI of the donor alone (n=2-3). Mean ± SEM, * $p < 0.05$ by one-way ANOVA, ns (not significant). Figure adapted from (Clark et al., 2021b).

3.3.4 Validating the specificity of antibodies for microscopy

Techniques such as microscopy rely on the labelling of proteins using antibodies. To be sure that you are detecting and studying the protein of interest, the antibodies need to be specific to that protein and function well in the assay that they are being used in. This project is interested in the platelet receptor GPVI and its downstream signalling proteins, FcRγ, Syk and LAT. To determine the specificity of antibodies against these proteins that

will be used in subsequent results chapters, we expressed our proteins of interest in human embryonic kidney 293T (HEK-293T) cells since these cells are easily transfected, and they do not have an endogenous expression of the platelet proteins we are interested in. HEK-293T cells were transfected with plasmids containing GPVI GFP-tagged, FcRγ untagged, and Syk and LAT myc-tagged, and untransfected HEK-293T cells were used as a negative control. The expression of these proteins of interest was verified by epifluorescence microscopy. For GPVI also intrinsic GFP signal was recorded. Transfection with the GPVI-GFP plasmid resulted in high transfection efficiency as evidenced by the presence of GFP in the cells (green channel; **Figure 3.5A**). The anti-GPVI antibody 1G5 (magenta channel; **Figure 3.5A**) only labelled cells that were also green, indicating specificity for the expressed GPVI protein. A non-specific binding of 1G5 antibodies was not observed in untransfected cells. The antibodies against FcRγ (**Figure 3.5B**), Syk (**Figure 3.5C**) and LAT (**Figure 3.5D**) also bind specifically to transfected cells, and no unspecific signal was detected in untransfected cells for these antibodies.

Next, we validated the ability of the antibodies to bind to the same proteins in platelets. The same antibodies were used to stain human platelets on non-coated and collagen-coated glass coverslips. We observed that platelets spread on an uncoated surface presented a homogeneous distribution of GPVI, FcRγ, Syk and LAT within the platelet (**Figure 6A**). However, as expected, in platelets spread on collagen, GPVI and FcRγ were densely located along the collagen fibres, whereas Syk and LAT continued to be uniformly distributed along the platelet (**Figure 3.6B**).

All of this information combined led us to the conclusion that the tested antibodies are specific for the target protein and are suitable to use in further experiments.

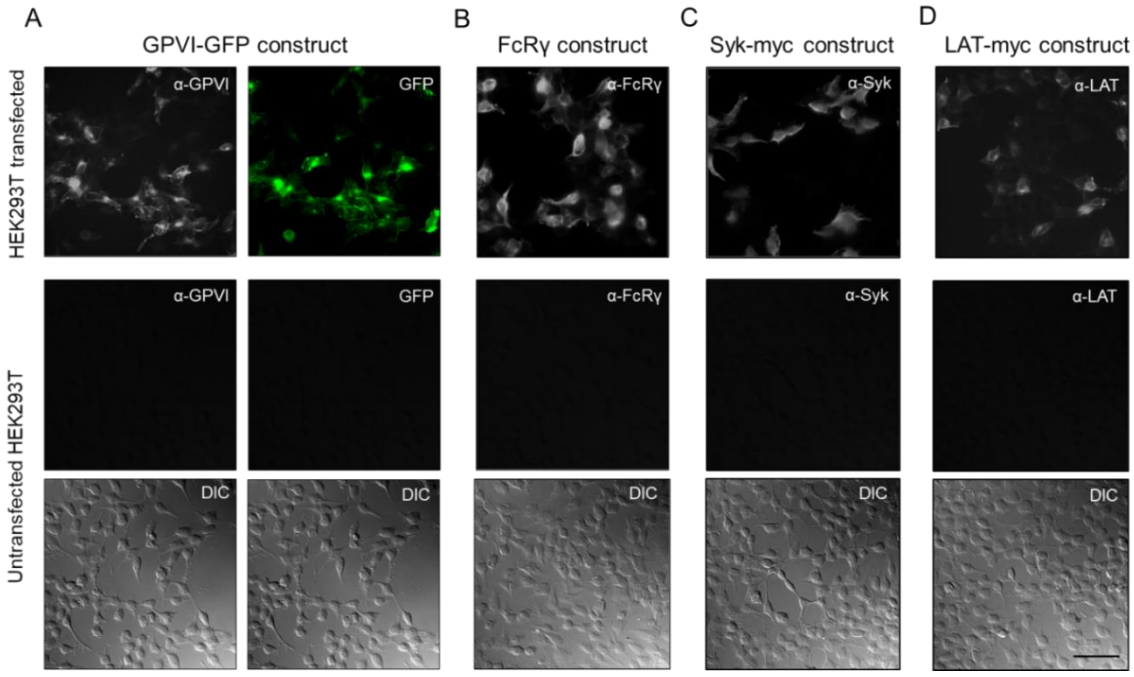

Figure 3.5. Validation of antibodies using HEK-293T cells. HEK-293T cells were transfected with GPVI GFP-tagged, FcRγ untagged, Syk and LAT myc-tagged constructs or untransfected to study antibodies specificity. Transfected and untransfected cells were stained with primary antibodies against the expressed proteins; anti-GPVI (clone 1G5) (**A**), anti-FcRγ (**B**), anti-Syk (**C**) and anti-LAT (**D**), and with secondary antibodies conjugated with Alexa Fluor 647. The fluorescence images from the two upper rows were obtained in the 647-channel using epifluorescence microscopy. Additionally, for GPVI samples the 488-channel was also recorded to visualise the GFP signal. The presence of untransfected HEK-293T cells is shown in the bottom row (DIC images) (n=2). In total, at least 10 fields of view were acquired for each sample. Scale bar: 50 μm.

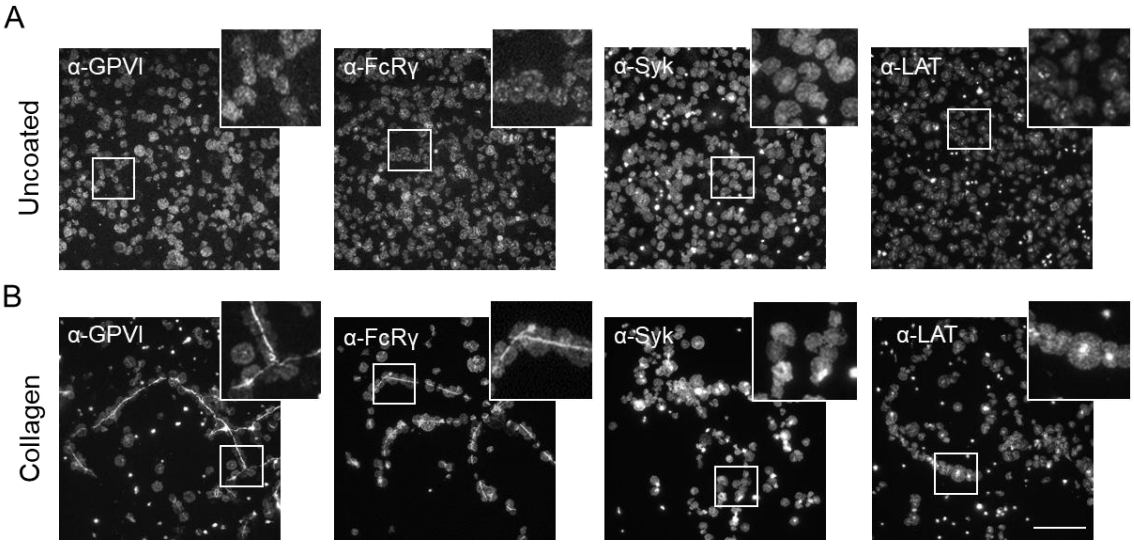

Figure 3.6. Validation of antibodies using human platelets. Single colour epifluorescence imaging of human platelets spread on uncoated (**A**) and collagen-coated slides (**B**). Platelets were spread for 30 min at 37°C. Next, samples were labelled using primary antibodies against GPVI

(clone 1G5), FcRγ, Syk, and LAT, and then with anti-mouse and anti-rabbit secondary antibodies conjugated with Alexa Fluor 647 (n=3). In total, at least 10 fields of view were acquired for each sample. All the images include a magnification box to mark the location of the protein along collagen fibres or homogenously distributed. Scale bar: 50 µm.

3.3.5 Comparing different super-resolution microscopy methods for platelets staining

After successfully testing antibodies against GPVI, FcRγ, Syk, and LAT using epifluoresence microscopy, we investigated the distribution of these proteins employing super-resolution microscopy technologies such as SIM, *d*STORM, and PAINT. Human platelets were spread on collagen-coated slides and stained with the same antibodies previously tested. SIM is one of the most common and practical super-resolution microscopy methods and thus has been employed in platelets previously (Poulter et al., 2015, Westmoreland et al., 2016). However, it has not been employed to investigate in detail the GPVI intracellular signalling pathway. Our results showed a clear distribution of GPVI and FcRγ along the collagen fibres, obtaining a greater resolution than with conventional fluorescence microscopy (**Figure 3.7A,B**). Regarding Syk and LAT, we observed more distinct punctate structures than with epifluoresence microscopy, which would be more useful for colocalisation studies, but in this case does not reveal any further patterns of localisation (**Figure 3.7A,B**). These findings are in line with previous literature (Pallini, 2020), where it was also shown that GPVI colocalised mainly along the collagen fibres, whereas total Syk and LAT were uniformly distributed in those platelets. Furthermore, in Chapter 4 (Figure 4.11), we study the localisation of phosphorylated Syk in platelets spread on collagen-coated slides, to compare it with the localisation of total Syk.

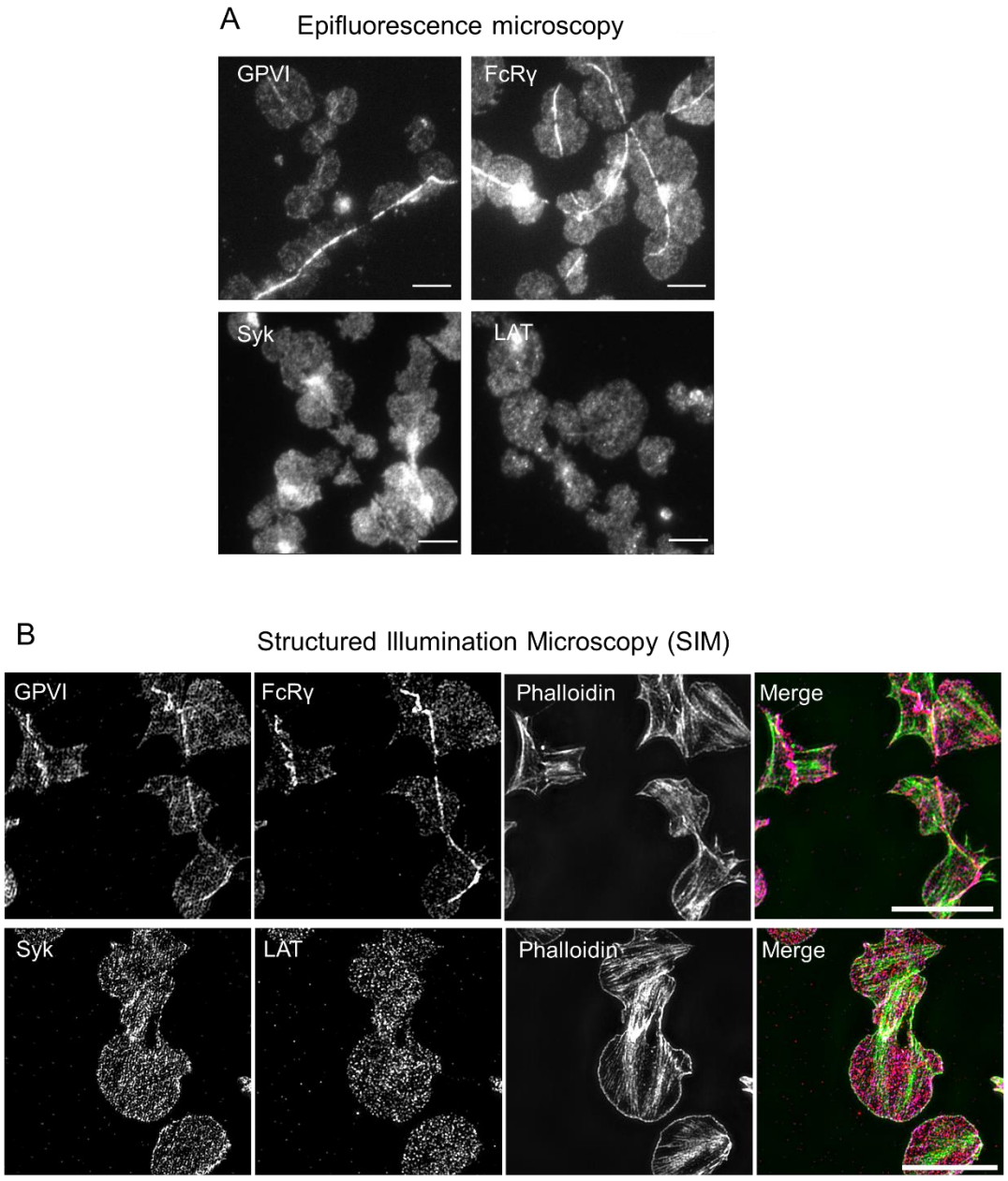

Figure 3.7. SIM provides a higher resolution on the distribution of GPVI, FcRγ, Syk and LAT compared to conventional fluorescence microscopy. Super-resolution imaging of platelets using N-SIM. Washed human platelets were spread on collagen-coated glass-bottom coverslips for 30 min at 37°C and stained with primary antibodies for GPVI (1G5), FcRγ, Syk, and LAT, and then with anti-mouse Alexa Fluor 647 (for GPVI and Syk) and anti-rabbit Alexa Fluor 546 (for FcRγ and LAT) secondary antibodies and phalloidin-AF488 to label F-actin as detailed in images. (**A**) Single-colour epifluorescence imaging of spread platelets illustrates the location of GPVI and some of the proteins downstream of its signalling pathway. In total, at least 10 fields of view were acquired for each sample (n=3). Scale bar: 10 µm. (**B**) Triple-colour structured illumination microscopy (SIM) imaging shows the location of GPVI, FcRγ, Syk and LAT in super-resolution, acquired using the Nikon SIM microscope. Super-resolution image reconstruction was performed by the Nikon NIS Elements SIM. The merged images highlight the location of some proteins along the collagen fibres. In total, at least 10 fields of view were acquired for each sample (n=3). Scale bar: 10 µm.

Other SR microscopy techniques, such as *d*STORM and PAINT, are part of the single-molecule light microscopy (SMLM) category, which are microscopy techniques that allow the visualisation of single molecules, and therefore give a higher resolution than SIM. We compared *d*STORM and DNA-PAINT to determine which SR microscopy technique is more suitable for imaging platelets. *d*STORM has been widely used for platelet imaging, emphasising on receptor clustering (Pollitt et al., 2014, Poulter et al., 2017, Clark et al., 2019, Pallini et al., 2021) and cytoskeleton organisation (Mayr et al., 2018, Chung et al., 2021). Conversely, DNA-PAINT has been barely used in platelet research, although it has big potential (Brockman et al., 2020). On collagen-coated coverslips, platelets were stained for tubulin and Syk (**Figure 3.8**). Microtubules were chosen, as their structure is well studied in platelets (Patel-Hett et al., 2008), and the original PAINT protocol was developed by imaging microtubules (Jungmann et al., 2014), so it provided a good indicator of whether the technique was working. Additionally, we labelled Syk to confirm which methods would be more suitable for imaging intracellular proteins involved in the GPVI signalling pathway that we are interested in. To verify the quality of the images, and detect artefacts SQUIRREL software (Culley et al., 2018) was applied. SQUIRREL downscales super-resolved images and compares them with their diffraction-limited wide-field images. The software detects artefacts that SR methods create during the reconstruction process. As a result, we obtained an error map and the Resolution Scaled Pearson (RSP) coefficient, which is calculated from the Pearson correlation between reference (wide-field) and super-resolution (downscaled super-resolved) images, with values in the interval of -1 and 1. The greater the RSP, the better the agreement, with 1 being the perfect structural match. The advantage of SQUIRREL is that the quality of various images from different single-molecule super-resolution methods can be compared using the RSP coefficient (Culley et al., 2018). As a result, apparently by eye, the staining for tubulin and Syk was satisfactory for both *d*STORM and PAINT (**Figure 3.8A**). However, after employing SQUIRREL, we noticed from the

error map and RSP value generated by the software that DNA-PAINT causes more inaccurate images than *d*STORM, showing a lower RSP coefficient (**Figure 3.8 B**).

Overall, our results demonstrate that SIM and *d*STORM are the most efficient and accurate methods to be used for imaging platelets. PAINT has great potential, however, the imaging and reconstruction were not as precise as for *d*STORM and will need further development for our cells and labels.

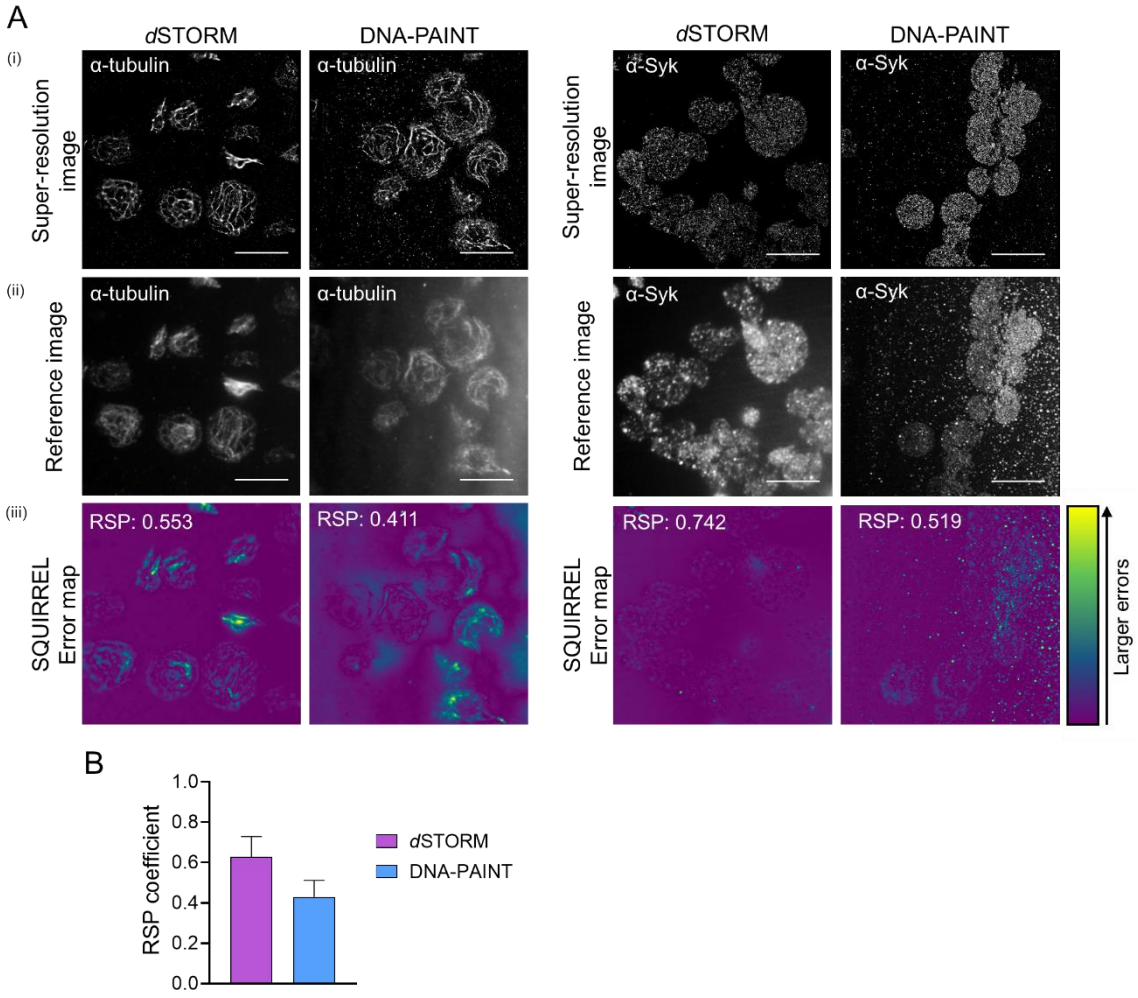

Figure 3.8. As a platelet imaging tool, *d*STORM imaging provides fewer artefacts compared to DNA-PAINT. Single-molecule super-resolution imaging of platelets and SQUIRREL analysis. Washed human platelets were spread on collagen-coated (10 µg/mL) glass bottom coverslips for 30 min at 37°C and stained with primary antibodies against tubulin (left panel) and Syk (right panel). Samples were secondarily stained with antibodies conjugated with Alexa Fluor 647. (**A**) Representative images of platelets acquired according to each protocol (*d*STORM and DNA-PAINT) with the Nikon *d*STORM microscope. (Ai) Reconstructed images were analysed by SQUIRREL software, using an (Aii) reference image creating an (Aiii) error map showing the resolution scaled Pearson (RSP) coefficient (bottom). RSP coefficient represents a value from -1

to 1, being 1 the perfect reconstruction, and the error map shows in yellow structures present in the reference image that are absent in the super-resolved image. (**B**) Bar graph of the quantification of RSP coefficient of platelets stained for tubulin and imaged with *d*STORM and DNA-PAINT techniques (n = 2). Scale bar: 10 μm.

3.4 Discussion

The aim of this chapter was to study the conformation and localisation of GPVI and proteins downstream in the GPVI signalling pathway. This included the establishment of FACS-FRET, a technique that allowed us to understand GPVI conformation as a change in dimerisation/oligomerisation of the protein of interest. In addition, different super-resolution methods, including SIM, *d*STORM, and PAINT have been established, using the validated antibodies, to study GPVI and different protein distribution on platelets.

Previous studies have shown discrepancies in GPVI conformation. Generating a GPVI dimer-specific antibody, several groups demonstrated that GPVI is present on platelets as dimers (Jung et al., 2009, Loyau et al., 2012). Moroi et al., using their antibody found that GPVI is 30% dimeric in resting platelets, and upon stimulation, with CRP the dimerisation increases to 40% (Jung et al., 2012). In addition, in our group in Birmingham, Clark et al. confirmed by bioluminescence resonance energy transfer (BRET) that GPVI can be expressed as monomers and dimers in cell lines transfected with GPVI (Clark et al., 2021b). However, a study with human platelets was missing. We performed flow cytometry-based FRET to study GPVI conformation in resting and CRP-activated human platelets. To prove the assay, we used a well-known and abundant platelet dimer receptor, integrin αIIbβ3, as a positive control. We obtained a FRET efficiency of approximately 45%. Even though in simulated models dimers obtained a FRET efficiency of 70% (King et al., 2017), in leukocytes the integrin α4β1 reached a FRET efficiency of 37% (Sambrano et al., 2018), validating, therefore, our positive control with the platelet integrin αIIbβ3. For the negative control, we used the integrin αIIbβ3 and the glycoprotein GPXI, as they are both highly expressed on platelets plasma

membrane but are not known to form dimers so acted as a monomer for the purpose of this assay. We obtained a FRET efficiency of 7%, which is consistent with the 5% obtained in another study for the negative control with monomers (Škerle et al., 2020). Once our positive and negative controls were validated, we moved forward to analyse the conformation of GPVI. We showed a FRET efficiency of 32% and 33% in resting and CRP-stimulated platelets, respectively. Based on the fact that dimers have a FRET efficiency of 45% while monomers have a FRET efficiency of 7%, GPVI's FRET efficiency of 33% suggests that GPVI is present as a mixture of monomers and dimers in resting and CRP-activated platelets. Our finding supports and completes the BRET study performed in our group in Birmingham in cell lines concluding that GPVI exists as a mixture of monomers and dimers in human platelets, and that dimer proportion is not affected by platelet activation (Clark et al., 2021b). Our results, are also in line with the previous findings of (Berlanga et al., 2007), however, they are in contrast to what was observed previously by (Jung et al., 2012), which showed a significant increase in GPVI dimerisation when platelets were activated with CRP. Moreover, our results suggest that GPVI dimerisation alone is not essential for the amplification of the signal transduction in the downstream pathway and, in the final stage, of platelet activation. Additionally, since resting platelets already present a high proportion of dimers, it is more likely that it is the clustering of the dimers by the ligand which is required for signal amplification and platelet activation.

Next, a variety of super-resolution microscopy methods were also developed to investigate the localisation of proteins involved in the GPVI signalling pathway. First, HEK-293T cells expressing GPVI, FcRγ, Syk and LAT, and later human platelets were used to demonstrate the specificity of antibodies against those proteins. By conventional epifluorescence microscopy, we observed that GPVI and FcRγ were located mainly along collagen fibres, whereas Syk and LAT were uniformly distributed. However, the

resolution of epifluorescence microscopy was not enough to determine a pattern in their distribution. For this reason, we established SIM, *d*STORM and PAINT imaging in platelets. For the first time, SIM was used to visualise these proteins in platelets. SIM's increased resolution demonstrated that GPVI and FcRγ, unlike Syk and LAT, exhibited enhanced localisation along the collagen fibre, which is consistent with diffraction-limited microscopy. While the resolution increased, no additional information was gained regarding global Syk and LAT location, as no pattern was recognised, however, it is possible that no pattern was discernible.. By using SMLM, such as *d*STORM and PAINT together with the cluster analysis we could study the size of Syk and LAT clusters at the collagen fibres, and gain further information about these proteins, therefore we optimised these SMLM methods for platelets imaging.

*d*STORM has been used by our group and others to study platelet proteins location for many years (Poulter et al., 2017, Clark et al., 2019, Pallini et al., 2021). In this study, we compared *d*STORM with PAINT, since PAINT offers more advantages than *d*STORM. In theory, Exchange-PAINT is capable of labelling a large number of molecules with a single fluorophore, thereby removing chromatic aberrations and reducing photobleaching. Alternatively, there is quantitative (q)PAINT, which theoretically provides real protein numbers, but requires tedious optimisations and controls, making it difficult to implement (Jungmann et al., 2016). As for now, *d*STORM is only a qualitative method that provides relative numbers for comparing treatments, although recent publications are working on getting quantitative information from it (Patel et al., 2021). All of these advantages could convert PAINT into a good replacement for *d*STORM (Molle et al., 2016). To perform the comparison, platelets were labelled for tubulin, well characterised by *d*STORM and PAINT, and Syk, an example protein that we are interested in and has a homogenous distribution on the platelet membrane. According to SQUIRREL software, PAINT causes more artefacts in the image reconstruction than

*d*STORM for both proteins, which could be caused by a longer exposition time required for the acquisition of PAINT images. Yet, this finding goes in line with a study published by Früh et al. during the preparation of this thesis, in which they compared the resolution and size of microtubules obtained from *d*STORM and PAINT and demonstrated that with *d*STORM the images are more accurate (Früh et al., 2021).

Overall, the findings of this Chapter demonstrate that GPVI is present as a mixture of monomers and dimers in resting and CRP-activated human platelets, with no increase detected upon stimulation, and that SIM and *d*STORM are appropriate super-resolution microscopy methods for platelet imaging. Flow cytometry-based FRET, SIM and STORM will be further used in Chapter 4, to study GPVI conformation, and distribution of GPVI, FcRγ, Syk and LAT upon inhibitory treatments, in order to understand further their biological relevance.

CHAPTER 4

The effect of Rac inhibition on GPVI signalling in human platelets is through GPVI shedding and reduction in PLCγ2 phosphorylation

Based on: **Neagoe, R.A.I**, Gardiner, E. E., Stegner, D., Nieswandt, B., Watson, S. P., & Poulter, N. S. (2022). Rac Inhibition Causes Impaired GPVI Signalling in Human Platelets through GPVI Shedding and Reduction in PLCγ2 Phosphorylation. International journal of molecular sciences, 23(7), 3746.

This Chapter contains self-citations. I performed all the experimental work, acquired and analysed data, and wrote the manuscript. EEG provided antibodies. DS, BN, SPW provided antibodies, supervision, funding, and edited the manuscript. NSP designed experiments, provided supervision, funding, and wrote and edited the manuscript.

4.1 Introduction

During platelet activation, the actin cytoskeleton undergoes extensive reorganisation, leading to filopodia and lamellipodia formation, and platelet spreading. The Rho family of GTPases have been shown to drive actin remodelling in platelets in response to several agonists, and is critical for the control of the actin dynamics (Aslan and McCarty, 2013). Rac is a member of the Rho family GTPases, together with Cdc42 and Rho (Goggs et al., 2015), and like other GTPases, can be found in two conformations, active (bound to GTP), and inactive (bound to GDP) (De Toledo et al., 2003). In platelets, Rac is activated by collagen binding to GPVI (Pleines et al., 2009) and integrin α2β1 (Morton et al., 1995b), or by thrombin (Pandey et al., 2009). There are 3 isoforms of Rac, but the most abundant in murine and human platelets is Rac1 (McCarty et al., 2005, Burkhart et al., 2012). The most studied function of Rac in platelets is its role in lamellipodia formation (McCarty et al., 2005, Pleines et al., 2009, Schaks et al., 2021). Additionally, it is known to be a key regulator of platelet aggregation and dense granule secretion (Akbar et al., 2007). Rac's significance in the different phases of platelet activation remains poorly understood. Pleines et al. (2009) reported that Rac1 knock-out platelets present an impaired PLCγ2 activation, however, the phosphorylation status of this protein was not affected in murine platelets. In line with these results, Guidetti et al. showed that Rac1 inhibition downstream the integrin α2β1 did not alter PLCγ2 phosphorylation, but caused an impaired activation and binding to fibrinogen of integrin αIIbβ3 (Guidetti et al., 2009). This data complements an *in vitro* study where it was shown that Rac1 can activate PLCγ2 (Piechulek et al., 2005). Despite the promising role of Rac downstream the GPVI signalling cascade, data showing the effect of Rac in PLCγ2 in human platelets was still missing.

Studying the effect of Rac on human platelets is important, since mice with Rac1 deficient platelets are prevented from arterial thrombosis (Pleines et al., 2009), and therefore

effective pharmacological inhibitors are required. EHT1864 is one of the widely used commercial Rac inhibitors that inhibits the GTP loading of Rac (Shutes et al., 2007). It was previously demonstrated that concentrations over 100 μM EHT1864 generate off-target effects including cell apoptosis (Dütting et al., 2015), thus we limited our research to a maximum of 50 μM EHT1864, which has been proved to be effective in platelets (Pollitt et al., 2010). For all experiments in this chapter, we used 30 μM and 50 μM EHT1864, except for the spreading assay, where 30 μM was the maximum dose. This could be explained by the fact that on spread platelets, the effect of the inhibitor is stronger since it targets single platelets, with 30 μM enough to inhibit lamellipodia formation. In other assays, such as aggregation, platelets become activated and aggregate, generating a strong wave of secondary mediators and therefore requiring a higher dose of the inhibitor (50 μM EHT1864).

In view of these considerations, we chose to investigate the role of Rac in human platelets, focusing on its effect on GPVI organisation and clustering, and the downstream signalling pathway.

4.2 Aims

This Chapter aimed to study the effect of the inhibition of Rac in GPVI-dependent signalling in human platelets by using the Rac-specific inhibitor EHT1864. EHT1864 was chosen since it is the most selective, with the fewest off-target effects of all the Rac inhibitors currently available. We have investigated Rac's role in GPVI clustering by *d*STORM, GPVI conformation by FACS-FRET, and the GPVI signalling pathway by flow cytometry and Western blotting.

4.3 Results

4.3.1 EHT1864 inhibits Rac activation and causes dose-dependently impaired human platelet aggregation

To study the effect of EHT1864 on Rac activation, we performed a pull-down assay with control and EHT1864-treated human platelet lysates using beads coupled with the p21 binding domain (PBD) of the p21 activated kinase 1 (PAK), which specifically recognises only Rac bound to GTP (active form). The absence of active Rac1 on platelets treated with 30 µM and 50 µM EHT1864 was confirmed by Western blot analysis (**Figure 4.1A**). Pleines et al. have demonstrated in previous studies that Rac1 knock-out mice present impaired murine platelet aggregation only in response to GPVI agonist, but not to thrombin or ADP (Pleines et al., 2009). To verify the effect of EHT1864 in response to GPVI agonists on human platelets, we stimulated platelets with low- and high-dose collagen and collagen-related peptide (CRP). By aggregometry, EHT1864-treated platelets showed a dose-dependent significant reduction in platelet aggregation with 50 µM EHT1864 (**Figure 4.1B, C**).

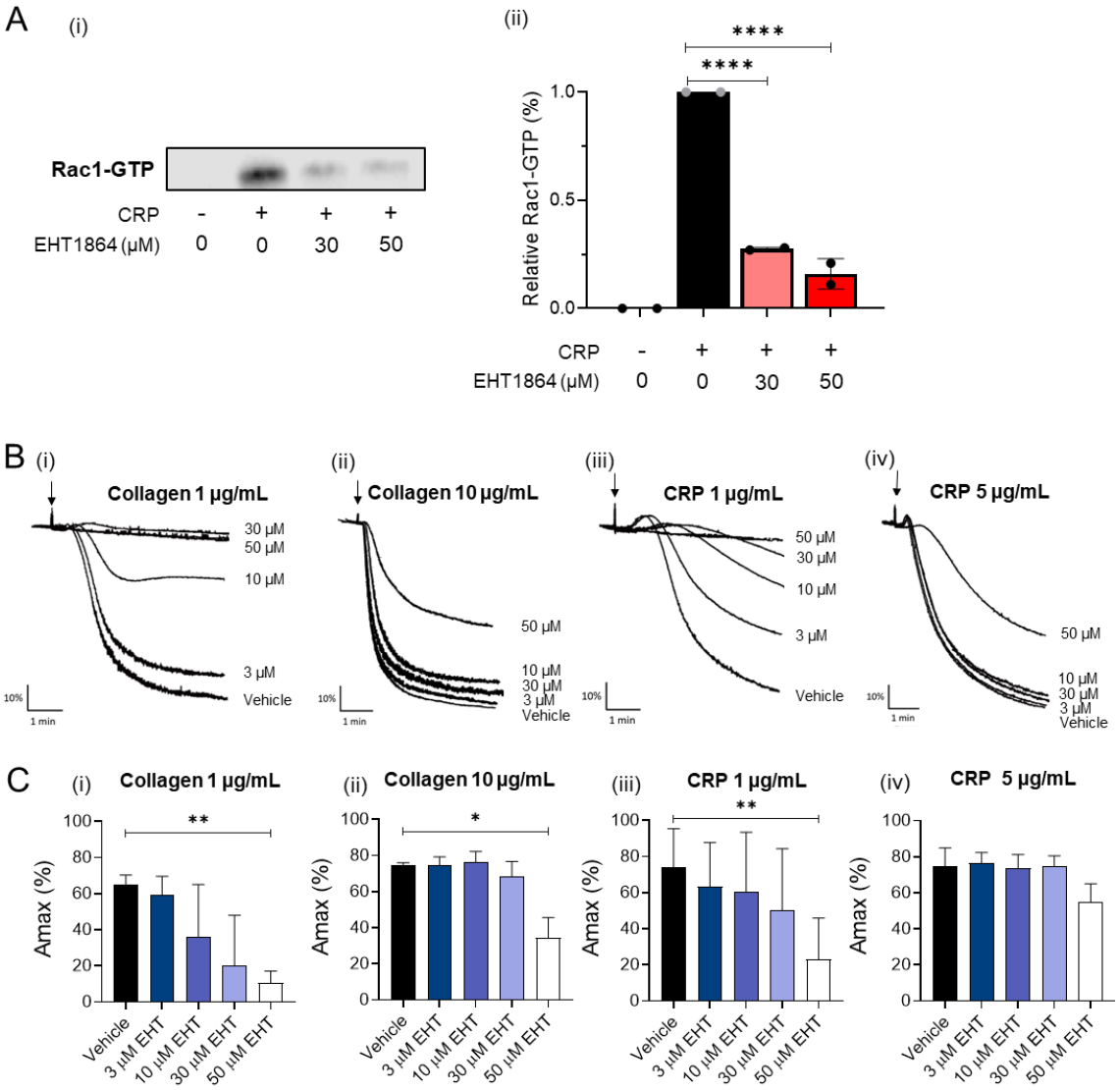

Figure 4.1. EHT1864 causes Rac1 inactivation and impaired GPVI-mediated aggregation on human platelets. (**A**) Quantification of active Rac, GTP-bound. (Ai) Representative Western blot image of Rac1-GTP of human platelets pre-treated with EHT1864 (30 and 50 μM) and stimulated with or without CRP (5 μg/ml), and (Aii) quantification of the relative percentage of Rac1-GTP ± SD. (n=2), **** P < 0.0001. (**B**) Dose-dependent inhibition of platelet aggregation caused by EHT1864 (0-50 μM) on human platelets stimulated with GPVI agonist Horm collagen or collagen-related peptide (CRP) was recorded by light transmission aggregometry. Representative aggregation traces of platelets stimulation with (Bi) 1 μg/mL and (Bii) 10 μg/mL Horm collagen, and (Biii) 1 μg/mL and (Biv) 5 μg/mL CRP. (**Ci-Civ**) Bar graph of quantification of platelets aggregation assay. Results are given as a mean percentage (%) of Maximal Amplitude (Amax) ± SD. (n=3), * P < 0.05, ** P < 0.01, by paired t-test (comparing vehicle vs EHT1864 treated platelets). Image obtained from (Neagoe et al., 2022).

It is known that the actin cytoskeleton plays a role in platelet aggregation, however its precise role is unclear. The inhibition of the cytoskeleton polymerization with Cytochalasin D blocks human platelet aggregation induced by GPVI agonists (Mistry et al., 2000, Pollitt et al., 2010). Conversely, Cytochalasin D enhances platelet aggregation upon stimulation with GPIbα ligand vWF (Mistry et al., 2000). Our aggregometry data agrees with the literature, demonstrating that at low-dose collagen stimulation, Cytochalasin D (1-10 μM) completely blocks platelet aggregation (**Figure 4.2Ai, Bi**), however, with 10 μg/mL collagen, even a high concentration of Cytochalasin D (10 μM) has no effect on the aggregation (**Figure 4.2Aii,Bii**). To investigate the possibility that Rac may enhance the effect of Cytochalasin D, we have measured the aggregation of platelets incubated with Cytochalasin D (10 μM) and different concentrations of EHT1864 (3-50 μM) (**Figure 4.2Aii**). Surprisingly, EHT1864 does not cause any additional inhibition on Cytochalasin D pre-treated platelets, indicating that the effect of EHT1864 might be mediated by the actin cytoskeleton.

4.3.2 EHT1864 blocks lamellipodia formation on human platelets

According to the literature, Rac1 knockout platelets do not form lamellipodia, but only adhere to the surface and develop filopodia (McCarty et al., 2005). To study the effect of Rac inhibition on human platelet spreading, we spread the platelets on uncoated, collagen- (10 μg/mL), and fibrinogen-coated (100 μg/mL) slides, labelled the F-actin with phalloidin-AF488 and studied the platelet morphology and cytoskeleton by epifluorescence microscopy (**Figure 4.3Ai**). The results confirmed that in human platelets the adhesion was unaltered by Rac inhibition (**Figure 4.3Aii**), however, the platelet surface area decreased in platelets treated with EHT1864 on all surfaces (**Figure 4.3Aiii**). In order to investigate the reduction in surface area in more detail, the platelets were analysed for the four stages of spreading: 1) adhered but not spread (compact shape); 2) filopodia extensions; 3) filopodia and lamellipodia extensions; 4) fully spread

with actin stress fibres. Whilst all surfaces showed a significant reduction in the percentage of platelets that were fully spread, collagen showed the greatest effect of Rac inhibition, with over 50% of the platelets adhering but not spreading (**Figure 4.3Aiv**).

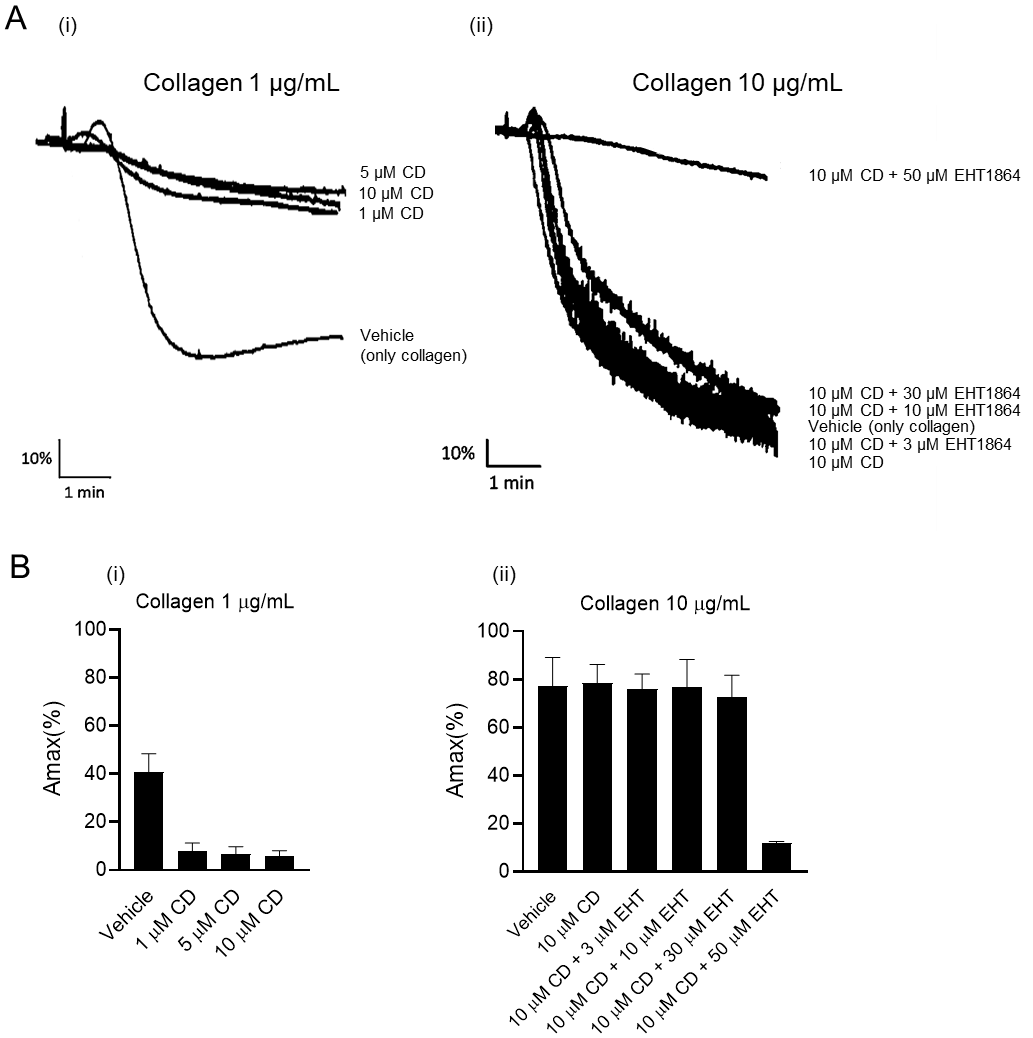

Figure 4.2. The effect of Cytochalasin D on human platelet GPVI-mediated aggregation. (**A**) Dose-dependent inhibition of platelet aggregation caused by (Ai) only Cytochalasin D (0, 1, 5 and 10 µM), or (Aii) 10 µM Cytochalasin D with additional EHT1864 (0-50 µM) on human platelets pre-activated with Horm collagen (1 and 10 µg/mL). Representative aggregation traces were recorded by light transmission aggregometry. (**Bi-Bii**) Bar graph of quantification of platelets aggregation assay. Results are given as a mean percentage (%) of Maximal Amplitude (Amax) (n=2).

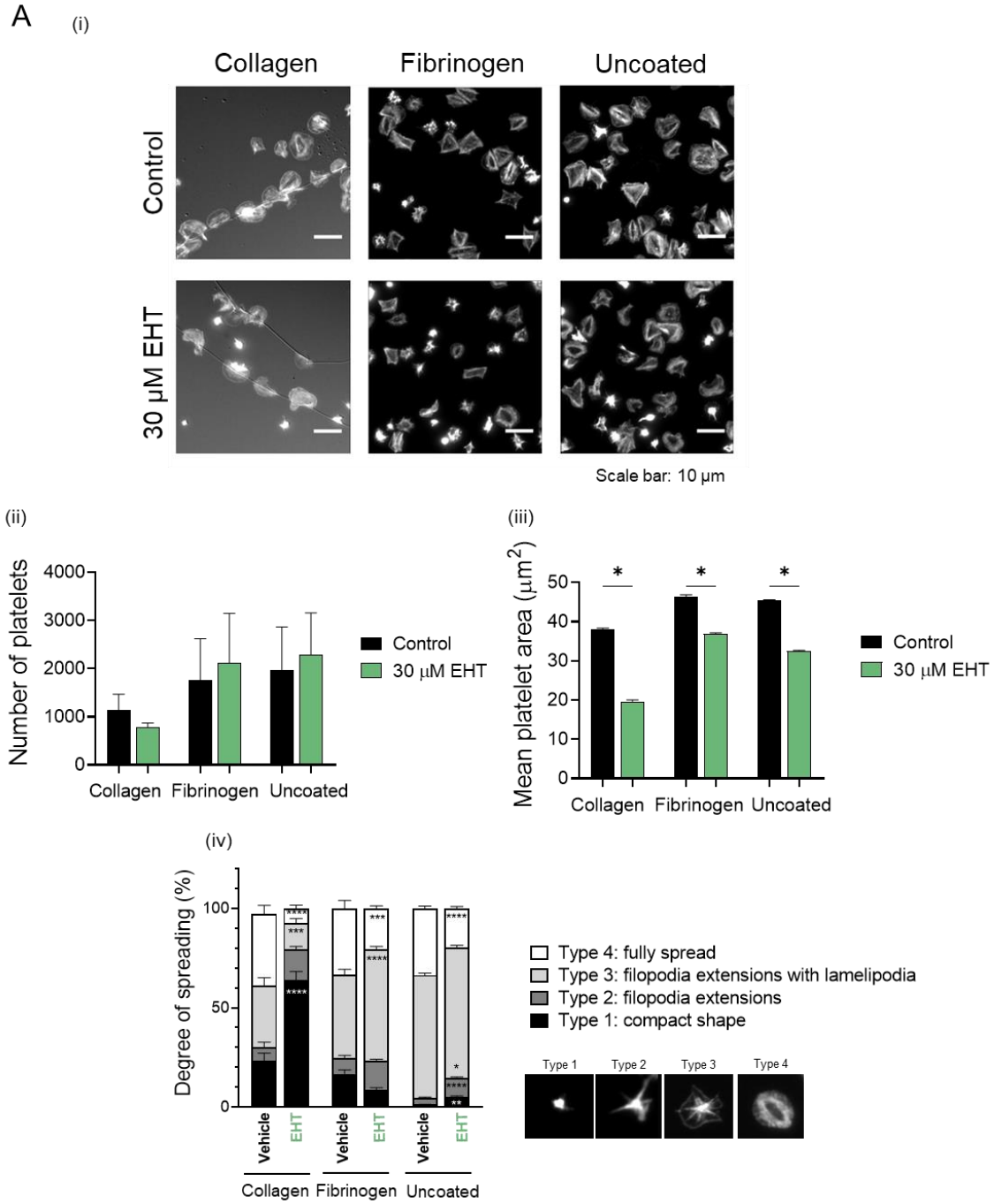

Figure 4.3. Rac inhibition causes impaired spreading on human platelets. (**A**) Washed human platelets were pre-incubated with vehicle (PBS) or 30 μM EHT1864 and spread for 30 min on uncoated, collagen-, or fibrinogen-coated slides. (Ai) Representative immunofluorescence images of spread platelets stained for actin with phalloidin-AF488 imaged with an epifluorescence microscope. (Aii) Bar graph of the number of adherent platelets, (Aiii) mean platelet area, and (Aiv) percentage of spread platelets at different stages; type 1: compact shape, without lamellipodia or filopodia, type 2: only filopodia extensions, type 3: filopodia and lamellipodia extensions, and type 4: fully spread platelets (n=3). Data represented as mean ± SEM, * $P < 0.05$, ** $P < 0.01$, **** $P < 0.0001$ by paired t-test (comparing vehicle vs EHT1864-treated platelets). Image obtained from (Neagoe et al., 2022).

4.3.3 Rac is not essential for GPVI cluster formation

Our group has previously reported that GPVI clusters along collagen fibres in platelets spread on Horm collagen (Poulter et al., 2017), and also more recently, in platelet adhering to and forming thrombi on collagen under flow (Jooss et al., 2022). In order to determine what role, if any, Rac plays in GPVI clustering on collagen, super-resolution microscopy of GPVI, in combination with the Rac inhibitor EHT1864 was used.

By single-molecule super-resolution *d*STORM imaging, GPVI localisation and clustering were analysed in human platelets untreated or pre-treated with 30 μM EHT1864 and spread on a collagen-coated surface by immunolabelling with an anti-GPVI F(ab') fragment (clone 1G5). The quantitative cluster analysis based on density-based spatial clustering of applications with noise (DBSCAN), in which each GPVI cluster was coloured, was used to analyse GPVI clusters. We observed from the reconstructed super-resolved images (**Figure 4.4Ai**) and DBSCAN cluster plots (**Figure 4.4Aii**) that Rac inhibition had no impact on GPVI localisation along collagen fibres, as GPVI clusters were still concentrated along fibrous collagen. Moreover, according to the DBSCAN analysis, on EHT1864-treated platelets, the number of detections, cluster density, and cluster area decreased, however, the decrease was insufficient to reach significance (**Figure 4.4Bi-iv**). Of note, DBSCAN quantitative analysis measures relative differences between different samples, not absolute numbers. These findings reveal that EHT1864 had no effect on GPVI clustering along fibrillar collagen.

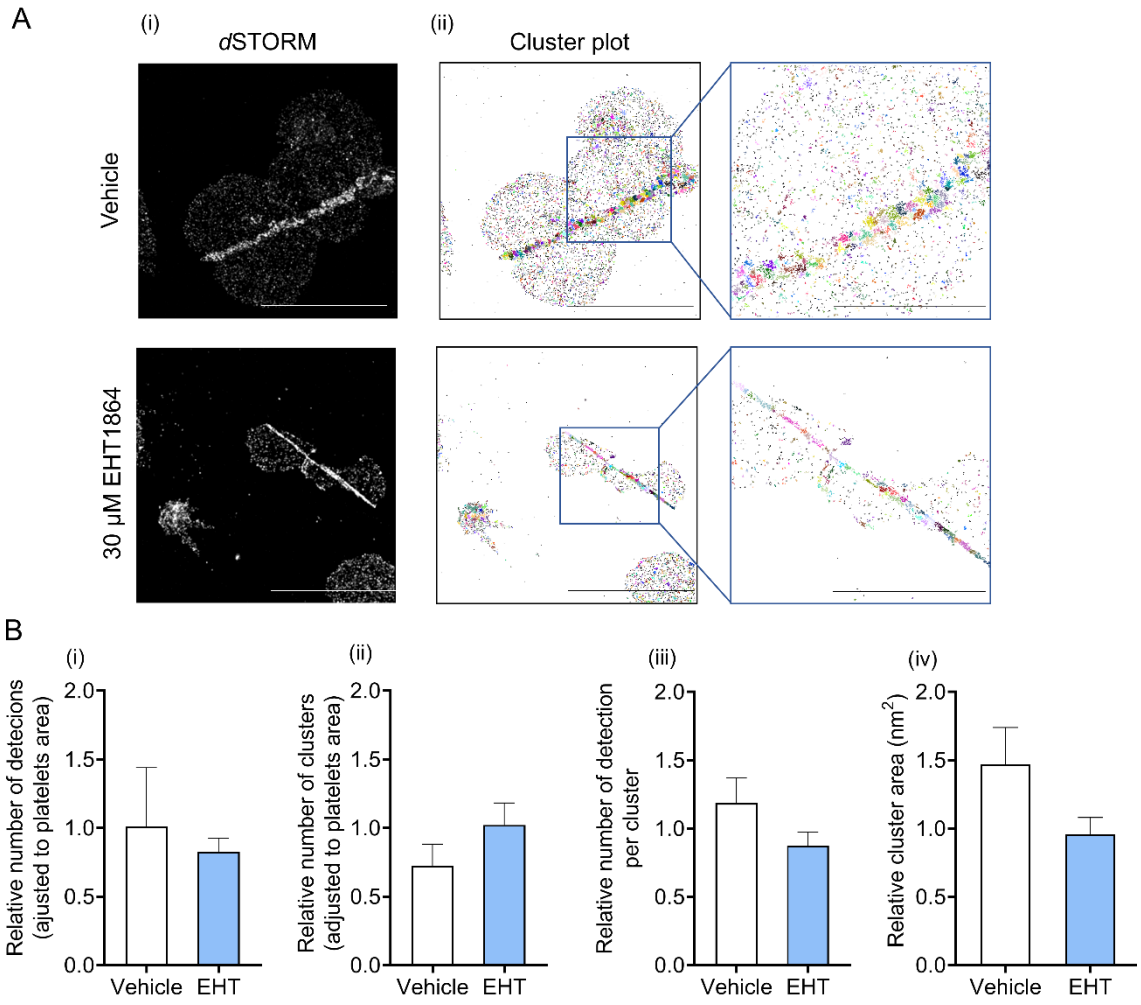

Figure 4.4. *d*STORM cluster analysis shows that Rac inhibition does not alter the GPVI cluster in platelets adhering to immobilised Horm collagen. (**A**) Washed human platelets were treated with vehicle (PBS) or 30 μM EHT1864, labelled against GPVI using 1G5 F(ab') fragment (2 μg/mL), spread for 30 min at 37 °C on a collagen-coated glass-bottom slide, stained with a secondary antibody conjugated with Alexa Fluor 647, and imaged using the Nikon N-STORM microscope. (Ai) Representative *d*STORM reconstructed images. Scale bar: 10 μm. Reconstruction was performed recording 20,000 frames per image and using the ImageJ ThunderSTORM plugin. (Aii) Representative DBSCAN-based cluster plot in which individual clusters are differently coloured. The left panels have a scale bar of 10 μm, and the middle and right panels have a scale bar of 5 μm. (**B**) Bar graphs of the relative number of (Bi) detections, (Bii) clusters, (Biii) detections per cluster, and (Biv) cluster area (n = 3). Data represented as mean ± SEM. Image obtained from (Neagoe et al., 2022).

4.3.4 EHT1864 does not alter GPVI dimerisation on resting and CRP-stimulated human platelets

To investigate whether Rac plays a key role in GPVI dimerisation, human platelets were analysed by FACS-FRET. The FACS-FRET assay was described in the results in Chapter 3, showing the implementation of the method including as a dimer control the integrin αIIbβ3, where a FRET efficiency of 45% was reached, and a monomer control with the integrin αIIb-subunit and GPIX, obtaining a FRET efficiency of 7%. We have also reported in Chapter 3 that by FACS-FRET, in both resting and CRP-stimulated human platelets, the FRET efficiency of GPVI is approximately 30%, meaning that it is present as a mix of dimers and monomer, and that proportion does not change upon platelet stimulation (Clark et al., 2021b).

To study the possible effect of Rac inhibition on GPVI dimerisation, due to its role in the rearrangement of the actin cytoskeleton, we have used the same approach as before, using flow cytometric FRET and labelling GPVI with F(ab') fragments conjugated with two different fluorophores, AF488 (donor) and AF546 (acceptor). Despite Rac inhibition, FRET efficiency for resting and CRP-stimulated platelets was 25-30% (**Figure 4.5**).

These data indicate that EHT1864 did not affect GPVI conformation/dimerisation after stimulation with the GPVI agonist CRP, indicating that Rac is not involved in these processes. This is consistent with the observation that Rac inhibition does not alter GPVI clustering either, concluding that Rac has no detectable role in GPVI dynamics.

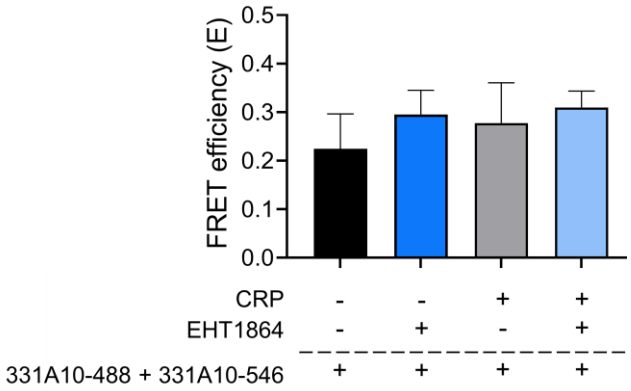

Figure 4.5. Rac does not alter GPVI oligomerisation on human platelets. FRET efficiency of GPVI on human platelets that were pre-incubated with vehicle (PBS) or 30 μM EHT1864 for 10 min at 37 °C, unstimulated or stimulated with 10 μg/mL CRP and stained with anti-human GPVI (clone 313A10) F(ab') fragment (n=3). Mean ± SEM, by paired t-test. Image modified from (Neagoe et al., 2022).

4.3.5 The effect of EHT1864 on human platelet activation and glycoprotein expression

As Rac plays a key role in human platelet aggregation upon GPVI ligands stimulation but did not significantly alter GPVI dimerisation and clustering, we decided to study further the role of Rac in platelet activation and GPVI signalling. Platelet activation was analysed by staining platelets for the active form of the integrin αIIbβ3 (clone PAC-1) and α-granules secretion (P-selectin). Platelets were stimulated with 5 μg/mL CRP, causing platelet activation as detected by flow cytometry with PAC-1 (**Figure 4.6Ai**) and P-selectin exposure (**Figure 4.6Aii**). Rac's role was analysed by pre-incubating the samples with EHT1864. We observed on CRP-activated platelets that 30 μM and 50 μM EHT1864 caused a 2- and 4-fold reduction, respectively, in the integrin αIIbβ3 activation and a reduction trend, yet not significant, in α-granules secretion. The reduction in platelet activation caused by Rac could explain the loss of aggregation induced by GPVI agonists.

Next, we studied whether Rac affects glycoprotein expression on human platelets by flow cytometry. We observed that GPVI plasma membrane abundance increased upon

CRP-induced activation of platelets. Surprisingly, 50 μM EHT1864 not only prevented the GPVI surface expression increase but also caused a significant reduction in its levels on CRP-stimulated samples. Additionally, treatment with 50 μM EHT1864 in resting platelets resulted in a slight decrease in GPVI levels (**Figure 4.6Aiii**). There was also observed a substantial decrease in surface expression levels of GPV in CRP-stimulated platelets pre-treated with 50 μM EHT1864 (**Figure 4.6Aiv**). However, the expression levels of GPIbα (**Figure 4.6Av**), integrin β3-subunit (**Figure 4.6Avi**), and CLEC-2 (**Figure 4.6Avii**) were unaffected by Rac inhibition.

The fact that only GPVI and GPV surface expression levels were reduced, but not the other examined glycoproteins, shows that the Rac mechanism is specific towards these two receptors.

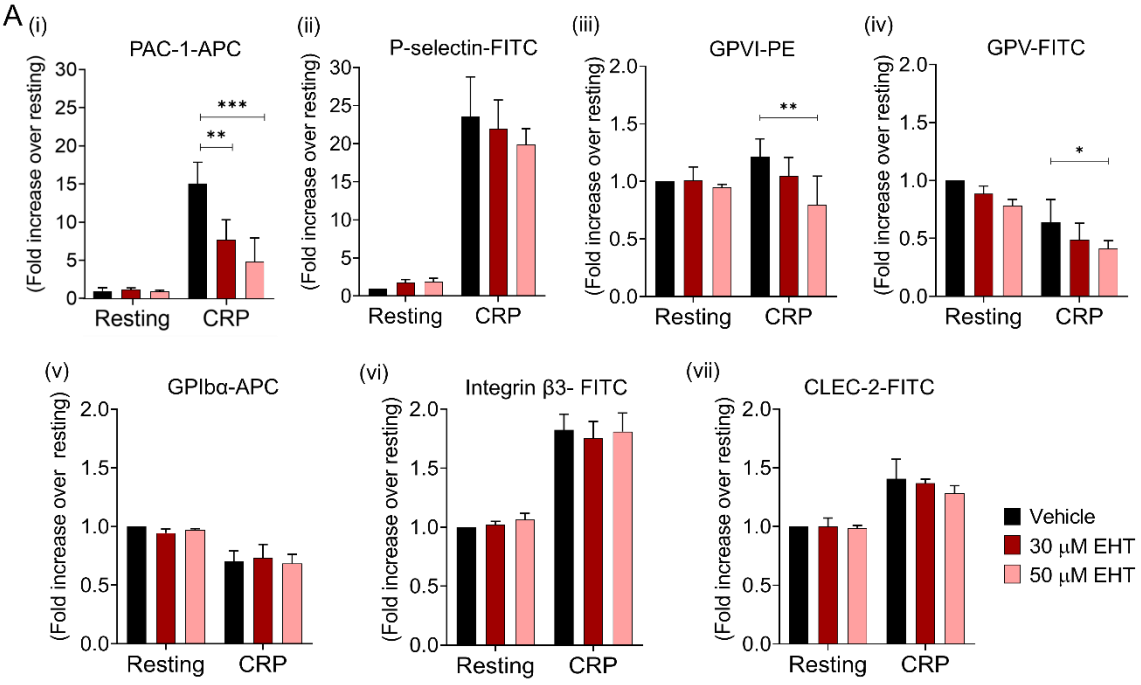

Figure 4.6. EHT1864 induces dose-dependent impaired platelet activation and glycoprotein exposure. (**A**) Quantitative analysis of flow cytometry data of washed human platelets pre-incubated with vehicle (PBS), and 30 and 50 μM EHT1864, unstimulated or stimulated with 5 μg/mL CRP. Platelets were labelled with primary antibodies conjugated with FITC, PE or APC (as stated in the figure) against (Ai) activated integrin αIIbβ3 (clone PAC-1), (Aii) P-Selectin, (Aiii), GPVI (clone HY101), (Aiv) GPV, (Av) GPIbα, (Avi) integrin-β3 subunit, and (Avii) CLEC-2 (n=3). Mean ± SD * P < 0.05, ** P < 0.01, *** P < 0.001 by two-way ANOVA (comparing vehicle versus EHT1864-stimulated platelets). Image obtained from (Neagoe et al., 2022).

4.3.6 Rac inhibition causes GPVI shedding through ADAM10

In section 4.3.5, we observed that Rac inhibition reduced the expression levels of GPVI upon CRP stimulation, suggesting that this glycoprotein was being shed or internalised. This also happened to GPV, but in this Chapter, we will focus on GPVI and suggest further research into GPV reduction.

GPVI removal from the platelet surface can occur via two mechanisms, mainly receptor shedding (Bender et al., 2010), but also internalisation could occur (Nieswandt et al., 2001). To confirm that the cause of GPVI reduction is receptor shedding, we performed Western blotting with resting and CRP-activated human platelets using an antibody (GPVI-tail) that recognises the cytosolic tail of GPVI that remains anchored to the plasma membrane after the extracellular domain of the receptor has been cleaved (Al-Tamimi et al., 2009a). For the shedding assay, we used the thiol-modifying agent N-ethylmaleimide (NEM), which induces GPVI cleavage, as a positive control. We observed that both resting and CRP-activated platelets, presented a significant increase in the GPVI-tail fraction (approximately 10-kDa) when treated with 50 μM EHT1864 (**Figure 4.7 Ai, Bi**). Treatment with GM6001 (broad matrix metalloproteinase inhibitor) (**Figure 4.7 Aii, Bii**) and GI254023X (metalloproteinase ADAM10 specific inhibitor) (**Figure 4.7 Aiii, Biii**) blocked the shedding induced by EHT1864.

These findings suggest that GPVI shedding by ADAM10 may be responsible for at least part of the reduced platelet activation observed in EHT1864-treated platelets.

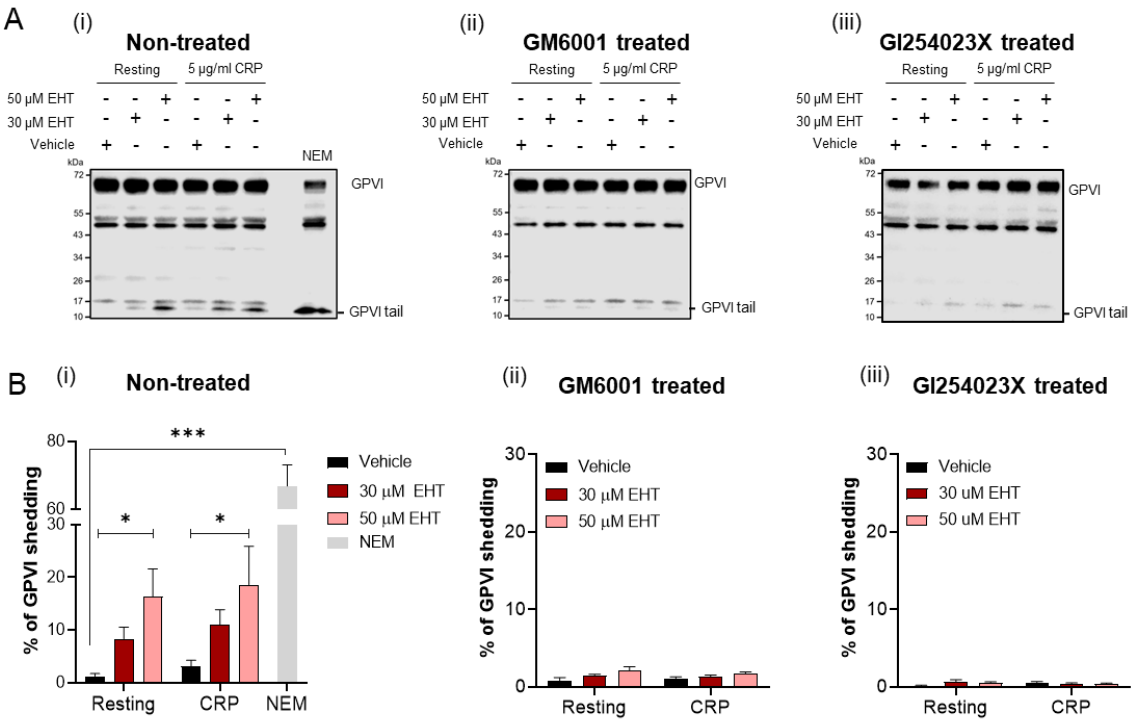

Figure 4.7. EHT1864 induces GPVI shedding through ADAM10. Human washed platelets were pre-incubated with 30 and 50 µM EHT1864 and stimulated with vehicle (PBS) or 5 µg/mL CRP. (**A**) Representative Western blot images of platelets (Ai) non-treated, or treated with (Aii) 250 µM GM6001 (broad metalloproteinase inhibitor) and (Aiii) 2 µM GI254023X (ADAM10-specific inhibitor), developed using a GPVI tail antibody. (**B**) Quantification of the percentage (%) of GPVI shedding on (Bi) non-treated, (Bii) 250 µM GM6001-treated, and (Biii) 2 µM GI254023X-treated human platelets (n=3). Data presented as mean ± SEM * $P < 0.05$, *** $P < 0.001$ by two-way ANOVA (comparing vehicle versus EHT1864-stimulated platelets). Image modified from (Neagoe et al., 2022).

4.3.7 The effect of EHT1864 on the phosphorylation of proteins involved in the GPVI signalling pathway

After confirming that EHT1864 induces GPVI shedding, which could partially explain the reduction in platelet aggregation caused by Rac inhibition, we examined tyrosine phosphorylation levels of the main proteins downstream GPVI in order to validate whether Rac inhibition is initiating a disruption that causes impaired platelet activation.

To confirm the results of Pleines et al. (2009) that the absence of Rac1 in murine platelets did not affect PLCγ2 phosphorylation levels, we Western blotted *Rac1*$^{-/-}$ platelets, resting or stimulated with CRP (5 µg/mL), with the phospho-specific antibody PLCγ2 pY1216.

We observed that p-PLCγ2 levels did not differ from the wild-type platelets (**Figure 4.8A**). We wanted to investigate further if the same occurs on human platelets. By total tyrosine phosphorylation assay using human platelets, we found no obvious reduction in any protein band size upon Rac inhibition, except for the 155-kDa band, corresponding to PLCγ2 (**Figure 4.8B**). To verify this finding, we performed Western blotting assays against our proteins of interest; PLCγ2, Syk and LAT. We found a significant reduction in PLCγ2 phosphorylation levels of about 30% and 40% in human CRP-activated platelets pre-treated with 30 μM and 50 μM EHT1864, correspondingly (**Figure 4.8Ci, Di**). We evaluated p-PLCγ2 levels in human platelets treated with the metalloproteinase inhibitor GM6001 to verify whether GPVI cleavage and therefore, reduction of GPVI surface expression was the cause of the impaired PLCγ2 phosphorylation. We observed that by blocking GPVI shedding with GM6001, we maintained a significant decrease in p-PLCγ2 levels in EHT1864 treated platelets (**Figure 4.8Cii, Dii**). Additionally, we studied the phosphorylation levels of two key proteins in the GPVI signalling pathway that are upstream of PLCγ2; Syk and LAT. We observed that EHT1864 did not induce a significant reduction in either p-Syk (**Figure 4.8Diii**) or p-LAT (**Figure 4.8Div**) levels. These results suggest that Rac is downstream of Syk and LAT, but upstream of PLCγ2 in the GPVI signalling pathway and it affects p-PLCγ2 levels.

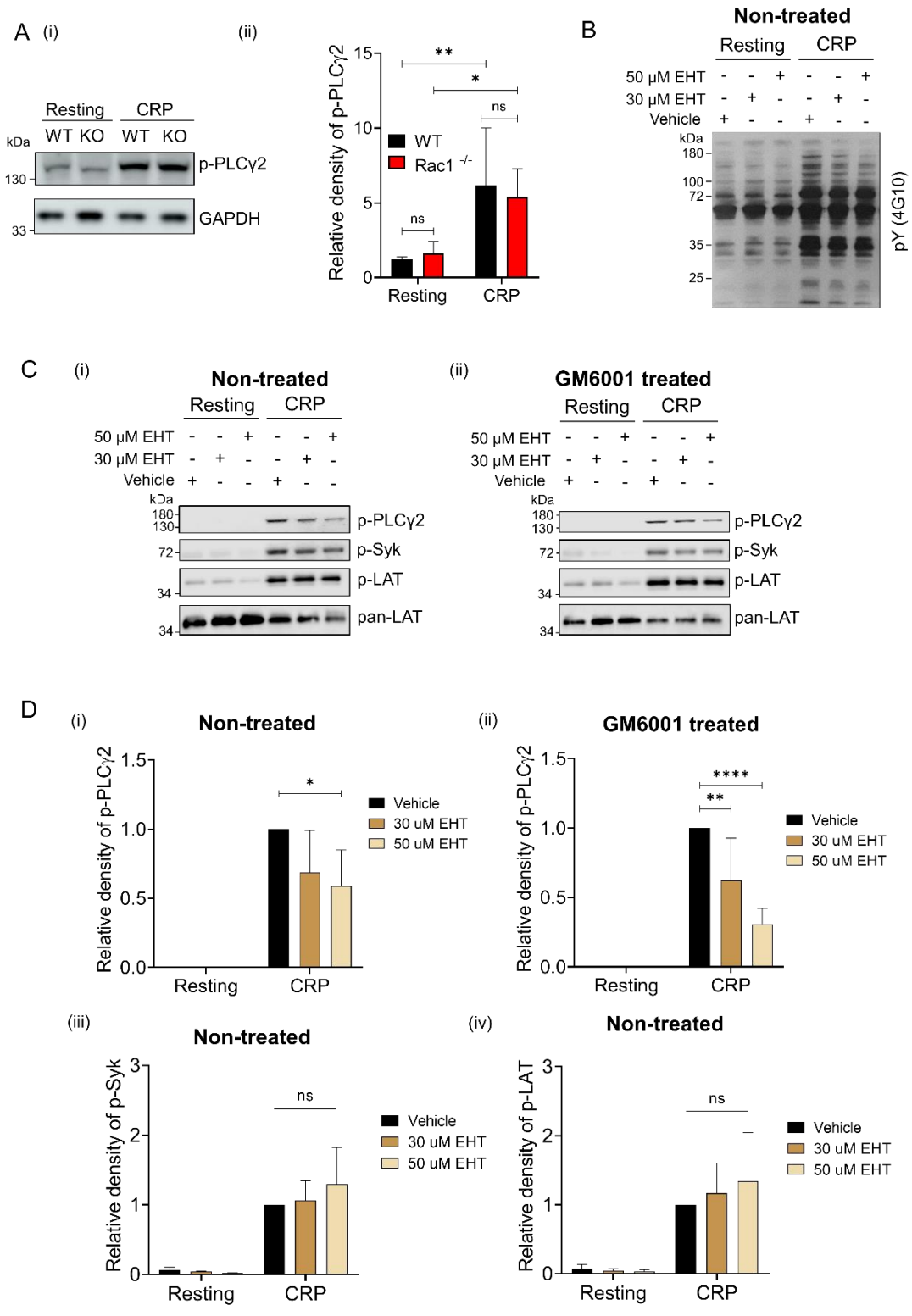

Figure 4.8. EHT1864 causes impaired PLCγ2 phosphorylation only in human platelets. (**A**) Analysing the phosphorylation levels of PLCγ2 on *Rac1*$^{-/-}$ platelets. (Ai) Representative Western Blot image of the phosphorylation levels of PLCγ2 Y1216 on resting and 5 μg/mL CRP-stimulated mouse platelets. GAPDH was used as a loading control. (Aii) Quantification of phosphorylated PLCγ2 band intensity (n = 3). (**B**) Determination of whole-cell tyrosine phosphorylation of human

platelets treated with EHT1864 (30 and 50 μM) and stimulated with vehicle or 5 μg/mL CRP. (**C**) Determination of the phosphorylation levels of PLCγ2, Syk and LAT in human platelets. Representative images of Western blots immunoblotted with antibodies specific for phosphorylated PLCγ2 (pY1216), Syk (pY525/6), and LAT (Py200) on (Ci) non-treated and (Cii) 250 μM GM6001-treated human platelets. Pan-LAT was used as the loading control. (**D**) Normalised quantification of band intensities of p-PLCγ2 in (Di) non-treated and (Dii) GM6001-treated human platelets, and (Diii) p-Syk and (Div) p-LAT in non-treated human platelets (n=3). Mean ± SD * $P < 0.05$, ** $P < 0.01$, *** $P < 0.001$, **** $P < 0.0001$ by two-way ANOVA (comparing vehicle versus EHT1864-stimulated platelets). Image modified from (Neagoe et al., 2022).

4.3.8 The effect of EHT1864 on the location of proteins involved in the GPVI signalling pathway

We next investigated whether EHT1864 plays a role in the localisation of proteins downstream in the GPVI signalling pathway, including Rac. Human platelets were immunolabelled with antibodies against GPVI (clone: 1G5), FcRγ, Syk, LAT, and Rac1, spread on a collagen-coated glass slide, and imaged using the super-resolution microscopy method structured illumination microscopy (SIM), validated in Chapter 3 for platelet imaging. We observed that control platelets have a distribution of GPVI and FcRγ mainly along the collagen fibre, as previously described (section 3.3.5). To evaluate the effect of Rac inhibition, platelets were incubated with 30 μM EHT1864. As a result of the EHT1864 treatment, platelets did not fully spread, developing only filopodia extension or maintaining a compact shape (**Figure 4.9**). GPVI and FcRγ appeared to also cluster along collagen fibres on EHT1864-treated platelets, however, because of their partial limitation on spreading, containing only filopodia, the visualisation was difficult even using super-resolution microscopy. The localisation of these proteins became even harder when platelets maintain their compact shape and do not spread (**Figure 4.9Ai-ii**). Similarly, when Syk and LAT were imaged, in control platelets they present a homogenous distribution as previously described (section 3.3.5), and their location was difficult to distinguish in platelets with impaired spreading due to EHT1864 treatment (**Figure 4.9Aiii-iv**).

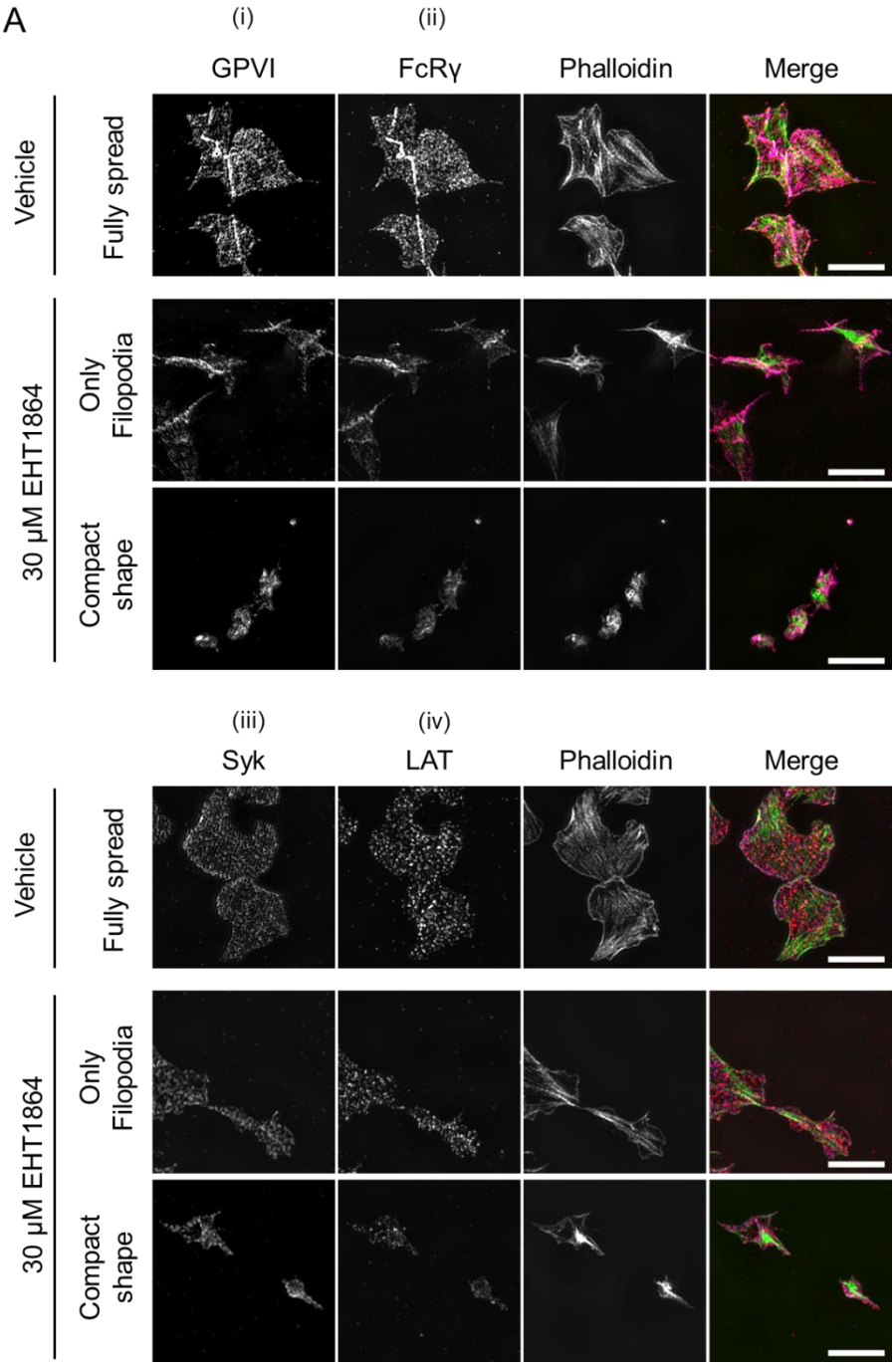

Figure 4.9. Rac inhibition does not alter the localisation of proteins downstream of GPVI. (**A**) SIM super-resolved images of human washed platelets pre-incubated with vehicle (PBS) or 30 μM EHT1864, spread on collagen (10 μg/mL), and labelled with antibodies against (Ai) GPVI (clone 1G5) (magenta), FcRγ (pink), Syk (magenta), and LAT (pink). Triple-colour structured illumination microscopy (SIM) images showing fully spread (top rows), partially spread forming only filopodia (middle rows) and non-spread (bottom rows) platelets, were acquired using the Nikon SIM microscope. Super-resolution images were reconstructed using the Nikon acquisition software. Additionally, F-actin was labelled with phalloidin-Alexa Fluor 488 (green). The merged images highlight the location of some proteins along the collagen fibres. In total, at least 10 fields of view were acquired for each sample (n=3). Scale bar: 10 μm.

Next, SIM was used to image human platelets labelled for Rac1, untreated or treated with 30 μM EHT1864, and spread on collagen- and fibrinogen-coated slides (**Figure 4.10**). In neither collagen nor fibrinogen surfaces EHT1864 affected Rac1 location, which was homogenously distributed in the platelet. Interestingly, we observed actin nodules on spread platelets on fibrinogen-coated slides, which were maintained upon EHT1864 incubation, and Rac1 partially colocalised with them (**Figure 4.10**).

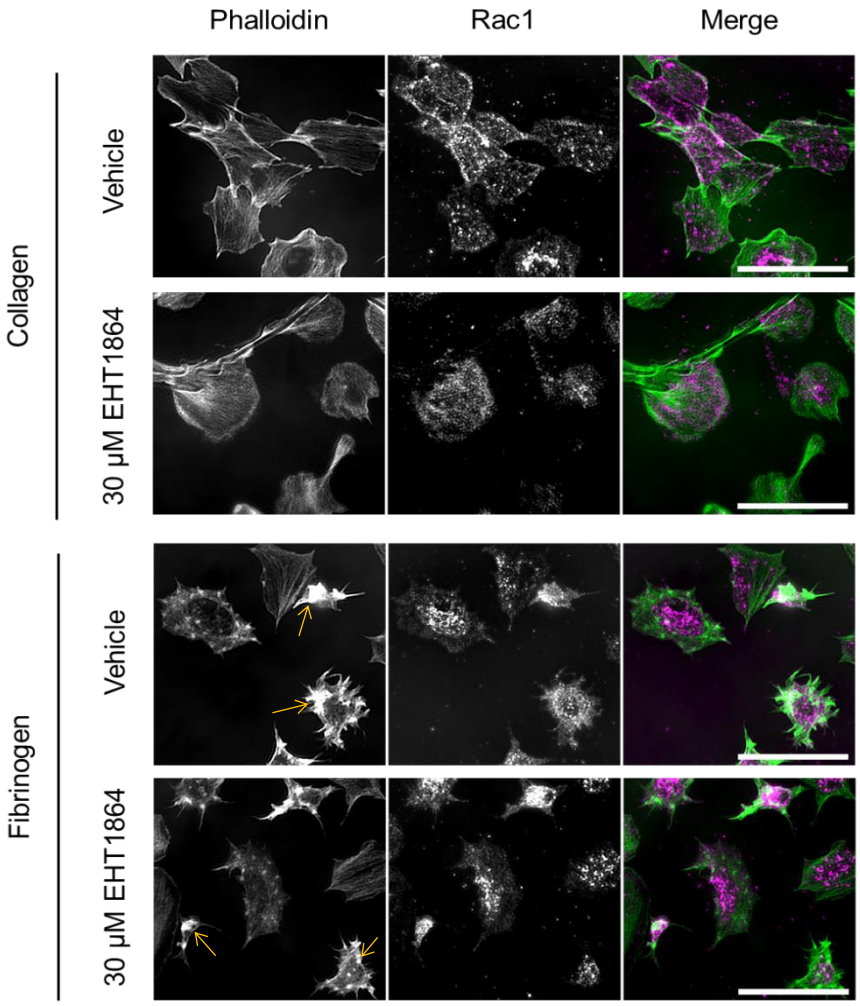

Figure 4.10. EHT1864 does not alter Rac distribution on human platelets. (**A**) SIM super-resolved images of human washed platelets pre-incubated with vehicle or 30 μM EHT1864, spread on collagen (10 μg/mL) (top panel) or fibrinogen (100 μg/mL) (bottom panel), and labelled with a primary antibody against Rac1, and a secondary antibody conjugated with Alexa Fluor 647 (magenta). F-actin was labelled with phalloidin-Alexa Fluor 488 (green) and some of the actin nodules are marked with yellow arrows. Dual-colour structured illumination microscopy (SIM) images were acquired using the Nikon SIM microscope. Super-resolution images were reconstructed using the Nikon acquisition software. The merged images highlight the location of

Rac1 within platelets. In total, at least 10 FOVs were acquired for each sample (n=3). Scale bar: 10 μm.

As the phosphorylation level of Syk was not modified by EHT1864 (section 4.3.7), we investigated whether its location might be altered. The epifluorescence microscopy analysis showed that phosphorylated Syk was present along collagen fibres independently of EHT1864 treatment, but the compact shape of the platelets made the analysis challenging. (**Figure 4.11**).

These findings conclude that Rac does not play a key role in the localisation of proteins downstream in the GPVI signalling pathway. However, Rac is necessary for platelet spreading. Its inhibition by EHT1864 makes it difficult to visualise intracellular proteins and to distinguish any particular change in the distribution upon EHT1864 treatment.

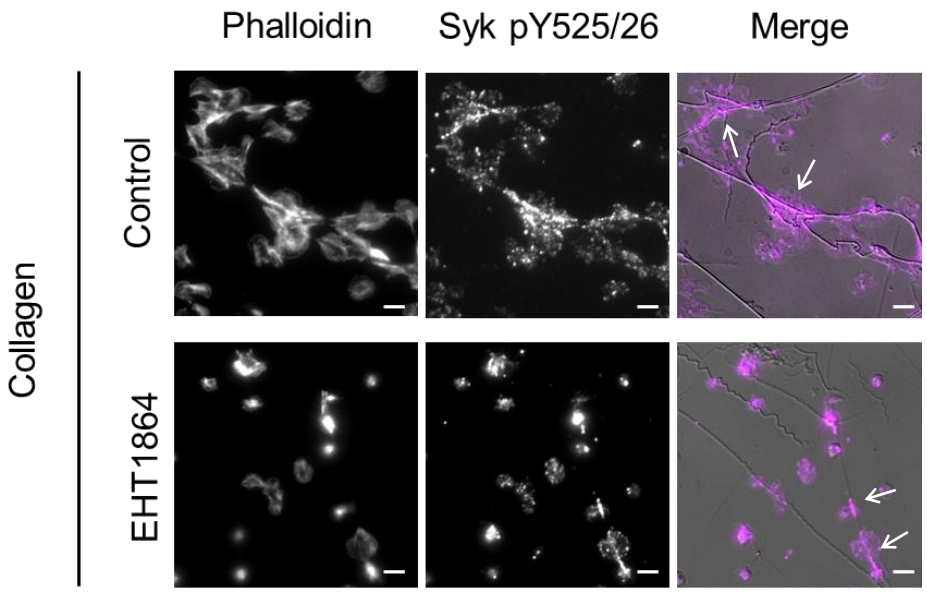

Figure 4.11. Rac inhibition does not alter the localisation of p-Syk along the collagen fibres on human platelets. Human platelets were spread on collagen-coated slides, pre-incubated with 50 μM EHT1864, and imaged by epifluorescence microscopy. From left to right, representative images of platelets stained with phalloidin-Alexa Fluor488, a primary antibody against phosphorylated Syk (pY525/26) and a secondary antibody conjugated with Alexa Fluor 647, and the merge of anti-phosphorylated-Syk and DIC images. Arrows are marking phosphorylated Syk enrichment along fibrous collagen. Scale bar: 10 μm.

4.4 Discussion

In this Chapter, we investigated the effect of the small Rho GTPase Rac on human GPVI localisation, clustering, shedding, and downstream signalling. The role of Rac in human platelets was assessed by using a Rac-specific inhibitor, EHT1864. Most of the experiments in this Chapter were designed to study the effect of Rac on human platelets, which was partially unknown, and to compare it with its effect on murine platelets, which has been extensively studied using Rac1 deficient platelets by several groups in the past.

The results from this study demonstrated that Rac inhibition altered platelet spreading, by blocking lamellipodia formation, and reduced platelet aggregation and PLCγ2 phosphorylation. Murine platelets deficient in Rac1 were also found to be involved in these processes (Pleines et al., 2009, McCarty et al., 2005). Surprisingly, unlike in mouse platelets, Rac1 controls the tyrosine phosphorylation of PLCγ2 (Y1216) in human platelets. Additionally, we found that Rac is also involved in GPVI shedding in human platelets, but it does not alter GPVI clustering or dimerisation in response to collagen and CRP.

NSC23766 and EHT1864 are the most commonly used inhibitors to block Rac activation. NSC23766 binds the groove of Rac1 that is recognised by its guanine nucleotide exchange factors (GEFs), preventing the exchange of GDP to GTP (Gao et al., 2004), whilst EHT1864 binds all the Rac isoforms and leads to allosteric inhibition of GDP to GTP exchange, inhibiting, therefore, Rac (Désiré et al., 2005). NSC23766 has been previously employed in other studies to demonstrate that inhibition of Rac causes a defect in human platelet secretion and aggregation in response to collagen and atherosclerosis plaque, which is also a collagen-rich substrate (Pandey et al., 2009, Dwivedi et al., 2010). Using NSC23766 they also discovered a deficiency in thrombin receptor activating peptide (TRAP)-induced platelet aggregation that was not present in mice (Dwivedi et al., 2010), thus revealing the first differences of Rac in platelet activation

between mice and humans. However, for our work, we chose EHT1864 as the inhibitor because it is more selective than NSC23766, and has no side effects if it is employed in concentrations up to 50 μM (Dütting et al., 2015).

Regarding GPVI-induced platelet aggregation and spreading, we confirmed that Rac plays a role in human platelet aggregation, activation and lamellipodia formation, and therefore in the degree of spreading, which goes in line with previous data from Rac deficient platelets (Pleines et al., 2009). We also observed that EHT1864 did not cause any effect on platelets' capacity to attach to various surfaces (uncoated, collagen-, and fibrinogen-coated coverslips), as reported in the literature (Jiroušková et al., 2007). There is evidence that the involvement of Rac in the actin cytoskeleton can affect receptor dynamics (Bai et al., 2018, Li et al., 2019) therefore, we hypothesised that Rac could have a role in GPVI dimerisation and clustering. We employed *d*STORM super-resolution microscopy to image platelets and analyse GPVI distribution. The cluster analysis performed by DBSCAN indicates that Rac inhibition by EHT1864 did not affect the number, area and density of GPVI clusters. As the inhibition of Rac was heterogeneous and did not affect all the platelets to the same degree, as observed in the spreading assay, the clustering analysis was performed on platelets that partially and fully spread (not affected by Rac inhibition). Additionally, it would not be possible to assess the clustering only on platelets partially spread due to technical difficulties. According to our hypothesis, GPVI cluster size is correlated with the degree of platelet activation, so platelets that can fully spread may be able to overcome the inhibitory effects of EHT1864.

Previously, in our group in Birmingham, two studies showed that GPVI clustering was not significantly altered by using Src and Syk inhibitors (Pallini et al., 2021), or adenosine and forskolin (Clark et al., 2019), suggesting that GPVI clustering is a strong and complex process that cannot be disrupted by altering GPVI downstream signalling pathway once the clusters have been formed. In addition, as there is evidence that the actin

cytoskeleton can affect dimer levels, as detected by a dimer-specific antibody using flow cytometry (Poulter et al., 2015), we wanted to test whether Rac plays a role in GPVI dimerisation. Using flow cytometry-based FRET developed in Chapter 3, we found that the fraction of dimers present in either resting or CRP-activated platelets was unaffected by EHT1864, demonstrating that Rac does not play a role in the dimerisation process.

Furthermore, we demonstrated by flow cytometry that EHT1864 caused an impaired platelet activation and a reduction in the exposure levels of two glycoproteins, GPV and GPVI, while others such as CLEC-2 and GPIbα remained unchanged. Despite the interesting fact that GPV expression levels were also reduced by EHT1864, we will focus this Chapter only on GPVI. Of note, our flow cytometric analysis showed a decrease in GPVI exposure only in activated platelets treated with EHT1864, whereas our Western blot analysis, using GPVI tail antibody, showed a significant increase in GPVI shedding in both resting and activated platelets treated with EHT1864. It remains unclear why this occurs, more than simply the differences between these two methods; flow cytometry is less sensitive and employs live cells, whereas Western blotting is more sensitive and uses platelet lysates.

It is known that GPVI is cleaved only by ADAM10, while ADAM10 and ADAM17 can cleave GPV (Gardiner et al., 2007, Matthews et al., 2017). CLEC-2 shedding is independent of ADAM10 (Inoue et al., 2019), and GPIbα is cleaved only by ADAM17 (Matthews et al., 2017). Since ADAM10 is the only metalloproteinase that GPVI and GPV share, we hypothesised that the shedding induced by Rac inhibition is caused by ADAM10. This was confirmed by incubating platelets with GI254023X, an ADAM10-specific inhibitor, with which we observed that we were able to block the shedding. Our findings go in line with the fact that, as shown in tumour cells, Rac regulates CD44 receptor shedding from the plasma membrane through ADAM10 (Murai et al., 2006). Moreover, Rac activity has also been demonstrated to have a function in receptor

shedding in other cell lines (Bai et al., 2018, Wiens et al., 2005). How the inhibition of Rac affects GPVI shedding remains to be elucidated. However, there is work showing that ADAM10 is regulated by a group of transmembrane proteins called tetraspanins (Harrison et al., 2021). In platelets, it has been shown that the ADAM10/Tspan15 complex is responsible for regulating GPVI cleavage (Koo et al., 2022) and proteomic studies have identified Rac1 as a potential interactor of Tspan15 (Koo et al., 2020), which implicates Rac1 in the GPVI shedding pathway. GPVI shedding caused by Rac1 inhibition is a process that is still unclear, and we are unsure whether platelets are less active and then shed GPVI, or if they shed GPVI and are therefore less active. Further research is needed to understand this complex process.

Pleines et al. demonstrated that murine Rac1 deficient platelets present a reduced IP3 production, however, PLCγ2 phosphorylation levels were not altered (Pleines et al., 2009). The finding that p-PLCγ2 levels were unchanged in Rac1 deficient platelets was also shown in this study. Nevertheless, in human platelets we demonstrated that Rac is crucial for PLCγ2 phosphorylation, showing another difference in Rac's role innate to each species. Furthermore, we showed that Rac inhibition does affect the phosphorylation or location of LAT and Syk, proteins upstream of PLCγ2 in the GPVI signalling cascade.

In summary, Rac plays an important role not only in human platelet aggregation and lamellipodia formation but also in GPVI shedding and PLCγ2 phosphorylation. Although Rac1 remodels the actin cytoskeleton, it does not significantly disrupt either the clustering and dimerisation of GPVI or the location of proteins downstream of the GPVI signalling, including Syk and LAT. All these findings indicate that the role of Rac in the GPVI signalling varies between species.

CHAPTER 5

Development of ExM to study the localisation of platelet glycoprotein receptors and their conformation

Part of the results shown in this Chapter has been performed together with Prateek Gupta (PG) and Luise Evers (LE). PG and I designed and performed ExM experiments together, and he acquired the microscopy data. LE performed the trifunctional experiments together with me, acquired the microscopy data and analysed the results of that assay.

5.1 Introduction

We demonstrated in the previous Chapters that the visualisation of platelets is challenging due to their small size and the high abundance of receptors in their plasma membrane (Saboor et al., 2013), but this could be, at least partially, overcome by using SR microscopy methods such as SIM and *d*STORM. However, even using these SR methods, non-spread or resting platelets still provide a challenge for assessing receptor/protein distribution as seen in Chapter 4 when Rac inhibition prevented platelet spreading. Recently, a new approach to obtain super-resolved images, known as expansion microscopy (ExM) (Chen et al., 2015) has been developed. Whereas in the conventional SR microscopy techniques the increased resolution is obtained by big advances in the microscopes, with ExM the high resolution is achieved by physically expanding the sample. The main steps of the technique are explained in Chapter 1 (**Figure 1.11**). Since 2015, when the first expansion protocol was developed, different protocols have been established, increasing the resolution reached and adapting to different types of samples. Chen, Tillberg and Boyden obtained a lateral resolution of 70 mm, equivalent to 4x expansion, in the original expansion protocol (Chen et al., 2015), which was improved by iterative expansion microscopy (iExM) (Chang et al., 2017) or 10-times expansion microscopy (10x ExM) (Truckenbrodt et al., 2018) obtaining a lateral resolution of 25 nm using conventional fluorescent microscopes. The increase in the sample size raised the resolution but, unfortunately, also amplified the loss in fluorescence signal. To overcome this problem, recent protocols have focused on reducing the loss of signal by using a different digestion strategy (Tillberg et al., 2016) or labelling the sample once it has been expanded (post-expansion labelling), to avoid the destruction of the fluorophores during digestion (ultrastructure expansion microscopy; U-ExM) (Gambarotto et al., 2019) (**Table 5.1**).

Table 5.1. Comparison of different ExM protocols. A summary of the available protocols for ExM including the developers, expansion factor, linking solution, digestion buffer and staining method.

	Expansion protocol				
	4x ExM	**10x ExM**	**TREx**	**U-ExM**	**MM-ExM**
Developed by	(Tillberg et al., 2016)	(Truckenbrodt et al., 2018)	(Damstra et al., 2022)	(Gambarotto et al., 2019)	(Neagoe et al., in preparation)
Expansion factor	4x	10x	10x	4x	10x
Linking	Acryloyl-X	Acryloyl-X	Acryloyl-X	Acrylamide and formaldehyde	Acrylamide and formaldehyde
Digestion	Proteinase K	Proteinase K	Proteinase K	Digestion buffer	Digestion buffer
Staining	Pre-gelational	Pre-gelational	Pre-gelational	Post-gelational	Post-gelational

The biggest advantage of ExM compared to the single molecule technique *d*STORM, which gives a similar resolution to 10x ExM, is that it does not use TIRF mode. *d*STORM requires TIRF in order to increase the signal-to-noise ratio and image receptors at the adherent plasma membrane. Whilst it is possible to obtain 3D data with *d*STORM (Huang et al., 2008) using astigmatic lenses, it is not ideal for densely packed receptors in platelet aggregates as there will be a lot of overlapping fluorescent 'blinks' making reconstruction of the image difficult. ExM does not have this limitation. Samples can be imaged using confocal microscopy, making it more suitable for imaging samples with densely packed receptors and particularly thicker samples where the protein of interest is not necessarily at the coverslip. Indeed, resolution can still be increased further by imaging ExM samples in combination with other SR microscopy techniques such as SIM (Wang et al., 2018).

Recently, in the Würzburg group, Heil et al. adopted the 10x ExM protocol from Truckenbrodt et al. (2018) to visualise the localisation of the integrin αIIbβ3 in platelets

(Heil et al., 2022). However, the study has several limitations; the 10x ExM Truckenbrodt protocol is long and complicated, and the gel presents low stability, which makes the replication of the experiments tedious. Additionally, this protocol uses a harsh digestion process that complicates the sample imaging because of the fluorophores degradation/loss. In this Chapter, we develop a new expansion microscopy method that combines parts of different published ExM protocols, allowing the platelets to expand 10x but using a soft digestion process, which prevents the loss of fluorescent signal and optimises the process for platelet imaging.

The GPIb-IX-V receptor complex on platelets is composed of GPIbα, GPIbβ, GPIX in the ratio 1:2:1 with GPV weakly associated with it (McEwan et al., 2011). It is the second most highly expressed receptor on platelet with an estimated copy number of 50,000 (Romo et al., 1999) and is important for the capture and tethering of platelets to damaged vessels through its interaction with vWF (Andrews et al., 1997) and platelets clearance (Beardsley and Ertem, 1998). A series of antibodies raised against GPIbα in Prof Nieswandt's laboratory have been shown to cause rapid thrombocytopenia *in vivo* and reduction in platelet count *in vitro* (Bergmeier et al., 2000) when used as whole IgGs, but not F(ab') fragments. However, it is yet unclear what are the molecular pathways or conformational changes driving these processes. Our hypothesis is that the rapid thrombocytopenia occurring upon injection with α-GPIbα IgG antibodies is because of a change in the GPIb-IX-V receptor complex conformation, which could induce platelet GPIbα-dependent non-classical aggregation (nc-aggregation) in the absence of platelet activation. Therefore, ExM is the most suitable technique to assess whether this is occurring as it allows the imaging of thick samples and platelets aggregates.

5.2 Aim

The first aim of this Chapter was to optimise the use of ExM for platelet visualisation stained with F(ab') fragments. F(ab') fragments labelling offers several advantages; decreases the linkage error (error measured by the physical distance between the fluorophore and the target protein/receptor), and avoids nc-aggregates formation, which is essential for studying GPIbα localisation in resting platelets. The second aim of this study was to use ExM to understand the role and conformation/location change of GPIbα in the platelet nc-aggregates formed by the addition of the anti-GPIbα IgG antibodies.

5.3 Results

5.3.1 Validation of the expansion microscopy protocol

In Würzburg, our collaborators (Heil et al., 2022), started optimising the 10x Truckenbrodt protocol for platelets imaging, including glyoxal as a fixative and modifying different incubation times. Our first step was to replicate their data and ensure that the protocol functioned. We stained platelets live for 15 min at 37 °C or post-fixation for 30 min at 37 °C (both pre-gelation) with IgG antibodies against integrin αIIbβ3 (MWReg30) and GPIX (p0p6). Images of live-stained 10x expanded platelets revealed that integrin αIIbβ3 was forming large clusters (**Figure 5.1A, E**), whereas GPIX was found homogeneously expressed, especially in the plasma membrane (**Figure 5.1B, E**), matching the previous results reported by Heil and co-authors. Interestingly, post-fixation staining of integrin αIIbβ3 showed a homogenous distribution of this receptor within the membrane (**Figure 5.1D, F**).

These results suggest that we were able to expand platelets 10x using our modified Truckenbrodt protocol (Heil et al., 2022), and the addition of the anti-integrin αIIbβ3 antibody to live platelets caused this receptor clustering and internalisation. However, this phenome could be avoided by staining the platelets after fixation.

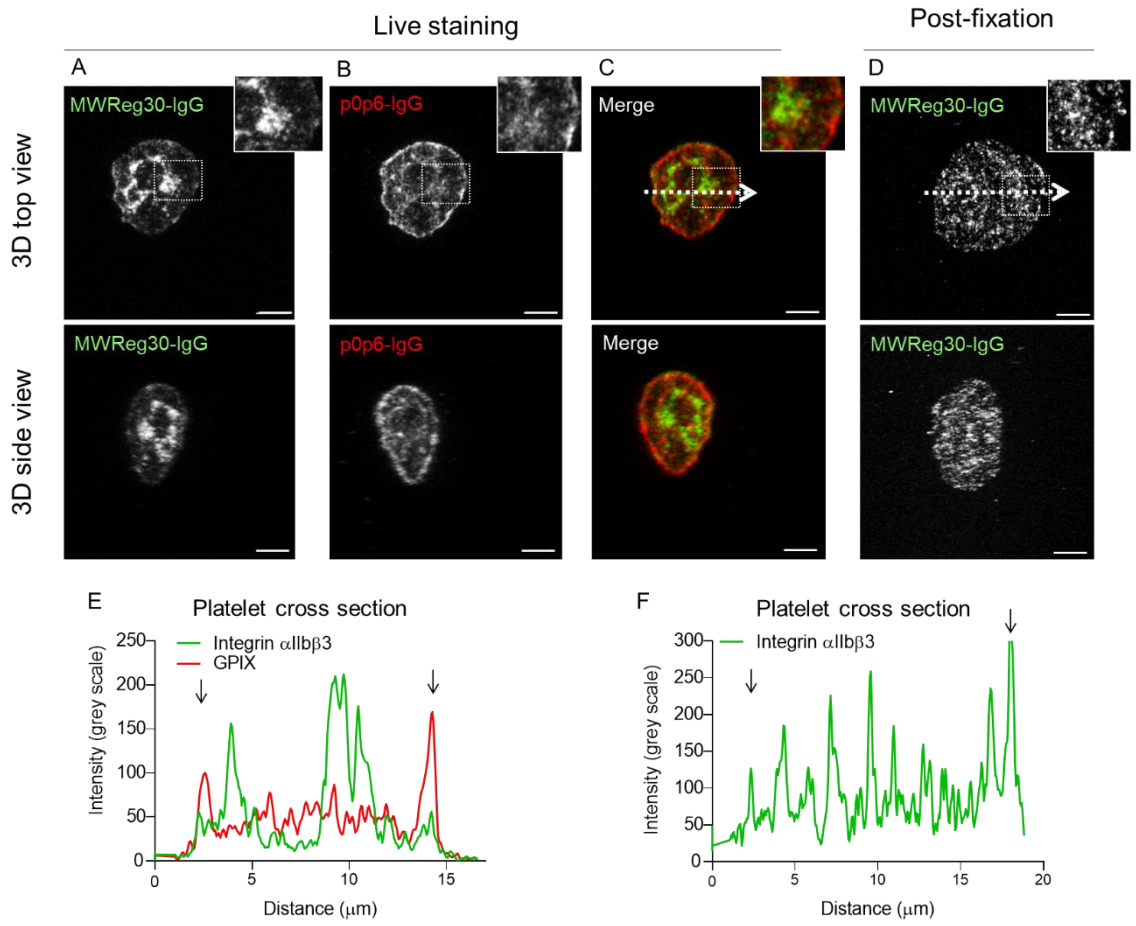

Figure 5.1. Visualisation of 10x expanded platelets in which the anti-integrin αIIbβ3 antibody causes integrin clustering. Murine platelets were attached to glycine-coated slides and expanded 10x following Truckenbrodt et al. protocol. Images were obtained using the AiryScan confocal microscope (Zeiss), and the reconstruction and 3D projections were obtained using Zen Blue software (Zeiss). Representative 3D top (top panel) and side views (bottom panel) of (**A**) live stained platelets (prior to fixation) with an anti-integrin αIIbβ3 IgG antibody (MWReg30) conjugated with Alexa Fluor-488 (green) and (**B**) anti-GPIX IgG antibody (p0p6) conjugated with Alexa Fluor-594 (red), and (**C**) merge 3D projection highlighting the cluster formation of only integrin αIIbβ3. Platelets were also stained after fixation (**D**) with an anti-integrin αIIbβ3 IgG antibody (MWReg30) conjugated with Alexa Fluor-488 (green). White arrows represent the transversal section used in the colocalisation plot, and the images include a magnification box to mark the presence or absence of clustering. Representative line plots of the mean grey value of a transversal section to study the localisation of (**E**) integrin αIIbβ3 and GPIX live stained platelets and (**F**) integrin αIIbβ3 in post-fixed stained platelets. The plasma membrane was represented in both plots with black arrows (n = 3).

5.3.2 Characterising anti-GPIbα antibodies function

In the initial characterisation of the anti-GPIbα antibodies, Bergmeier et al., (2000) observed a significant reduction in platelet count *in vitro* when platelets were treated with an anti-GPIbα monoclonal IgG and measured by flow cytometry. We replicated this experiment and found that the incubation of mouse platelets with antibodies against GPIbα antibodies caused a 75% decrease in the platelet count, with the appearance of larger platelet aggregates visible in the flow cytometry scatter plots (FSC/SSC) (**Figure 5.2A**). Additionally, by aggregometry, we observed that the anti-GPIbα IgG also causes 20% aggregation (**Figure 5.2B**). To confirm that these results were caused by the binding of the antibody to GPIbα, we studied its effect using a transgenic mouse line that has most of the GPIbα extracellular domain replaced by the alpha subunit of the human interleukin 4 receptor (IL-4Rα) (**Figure 5.2C**). Of note, the transgenic receptor still contains a portion of the ectodomain that includes the juxtamembrane mechanosensory domain (MSD) (Kanaji et al., 2002). As expected, using GPIbα-IL-4Rα transgenic platelets, anti-GPIbα IgG did not cause any platelet aggregation (**Figure 5.2B**). Scanning electron microscopy (SEM) was used to image wild-type platelets from the aggregometry cuvette, and we found that anti-GPIbα IgG caused platelets to come close together, but they were still in their resting, discoid form and not activated as when they aggregate, so we called this GPIbα-dependent non-classical aggregation (nc-aggregation) (**Figure 5.2D**).

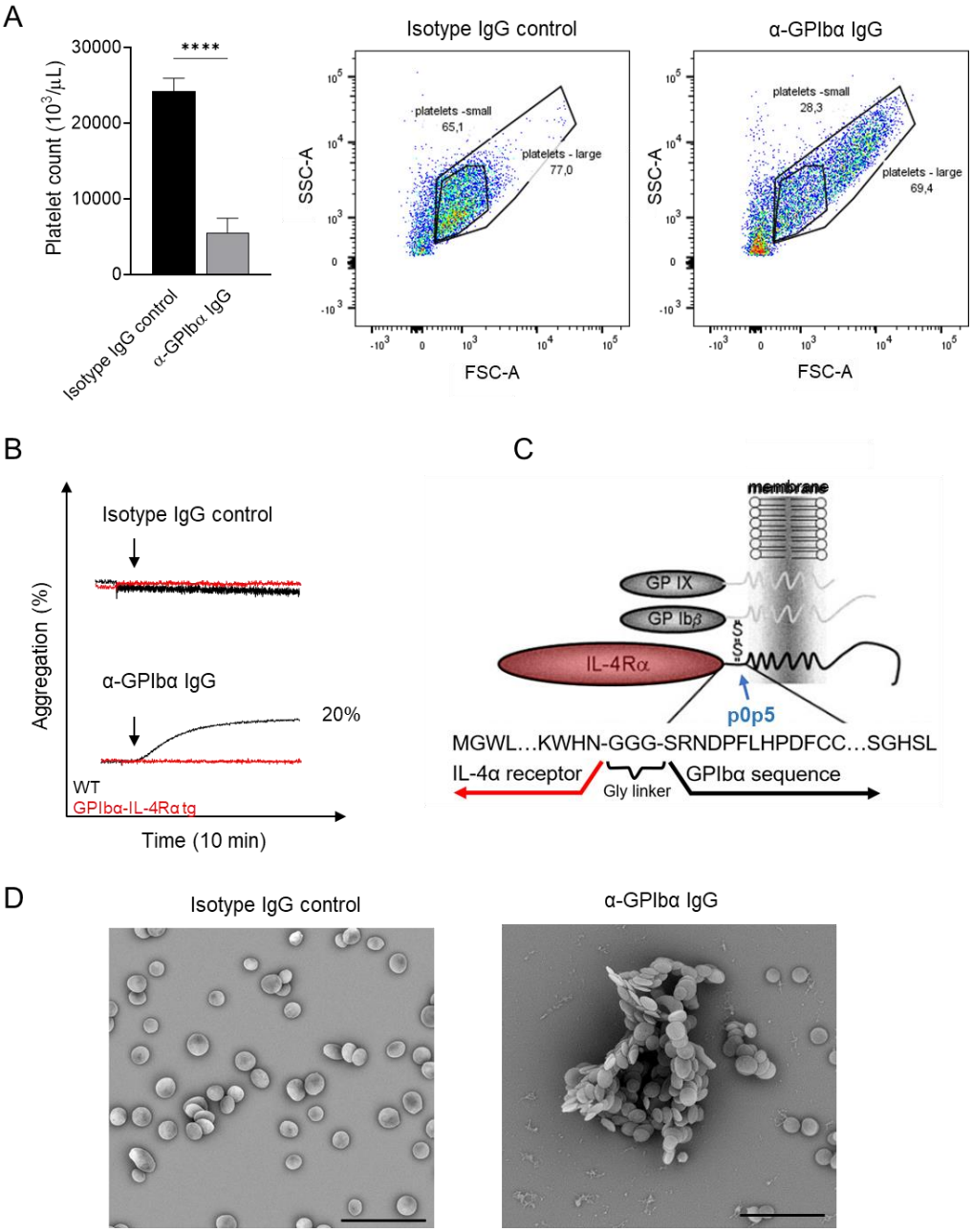

Figure 5.2. Anti-GPIbα IgG antibody induces platelet nc-aggregation. Murine platelets were incubated with 50 µg/mL of the isotype IgG control and anti-GPIbα IgG for 15 min at R.T., and then platelets were placed in the aggregometry cuvette for 10 min with constant stirring at 1,200 rpm to obtain the nc-aggregates. (**A**) Platelet count was measured by flow cytometry gating for platelet size (n=5). Left, bar graph represents platelet count, and right, represents the corresponding FSS/SSC plots. Data represented as mean ± SD. **** < P = 0.0001 by paired t-test. (**B**) Representative aggregation traces of wild-type and GPIbα-IL-4Rα transgenic platelets incubated with 50 µg/mL of isotype IgG control and anti-GPIbα IgG antibody (n = 3). (**C**) Schematic representation modified from (Kanaji et al., 2002) representing GPIbα-IL-4Rα transgenic platelets in which most of the extracellular domain of GPIbα was exchanged by IL-4Rα. IL-4Rα is fused by 3 glycine residues to the remaining 13 residues of the extracellular GPIbα. In addition, the binding site of p0p5 is marked with a blue arrow. (**D**) Representative scanning electron microscopy images of wild-type platelets obtained after the stimulation with isotype IgG

control and anti-GPIbα IgG antibodies after 10 min stirring in the aggregometry cuvette (n = 3). Scale bar: 10 µm.

5.3.3 Validating anti-GPIbα antibodies specificity

To validate our hypothesis that a change in the GPIb-IX-V receptor complex conformation/location occurs when nc-aggregates are induced by anti-GPIbα IgG antibodies, we stained the platelets with anti-GPIbα F(ab') fragments to avoid nc-aggregation formation. Additionally, F(ab') fragments also improve the labelling strategy, as they reduce the linkage errors of IgGs, since they are 3 times smaller than IgGs, and therefore reduce the distance between the fluorophore and the target protein/receptor compared to IgGs. We confirmed anti-GPIbα F(ab') fragments specificity using wild-type and GPIbα-IL-4Rα transgenic mice. First, by flow cytometry, we tested anti-GPIbα F(ab') fragments (p0p4 and p0p5), as a control, we used IgG antibodies against GPIX (p0p6) and integrin αIIbβ3 (MWReg30). We demonstrate that both anti-GPIbα antibodies only bind wild-type platelets, whereas p0p6 and MWReg30 bind both wild-type and transgenic mice (**Figure 5.3A**). By immunofluorescence we showed that anti-GPIbα F(ab') p0p4 does not bind to GPIbα-IL-4Rα transgenic adherent platelets, proving its specificity (**Figure 5.3B, C**). However, p0p5 does bind the transgenic platelets (**Figure 5.3D, E**). This could be explained by the fact that the binding epitope of p0p5 F(ab') is in the extracellular domain close to the plasma membrane, where the transgenic platelet still contains the GPIbα juxtamembrane MSD (**Figure 5.2C**). By flow cytometry, platelets are resting and in solution, therefore the MSD is most likely folded; however, by adhering platelets to the coverslip, GPIbα could be triggered by the interaction with the coverslip or the fixation process, unfolding its MSD and allowing p0p5 to bind the transgenic receptor.

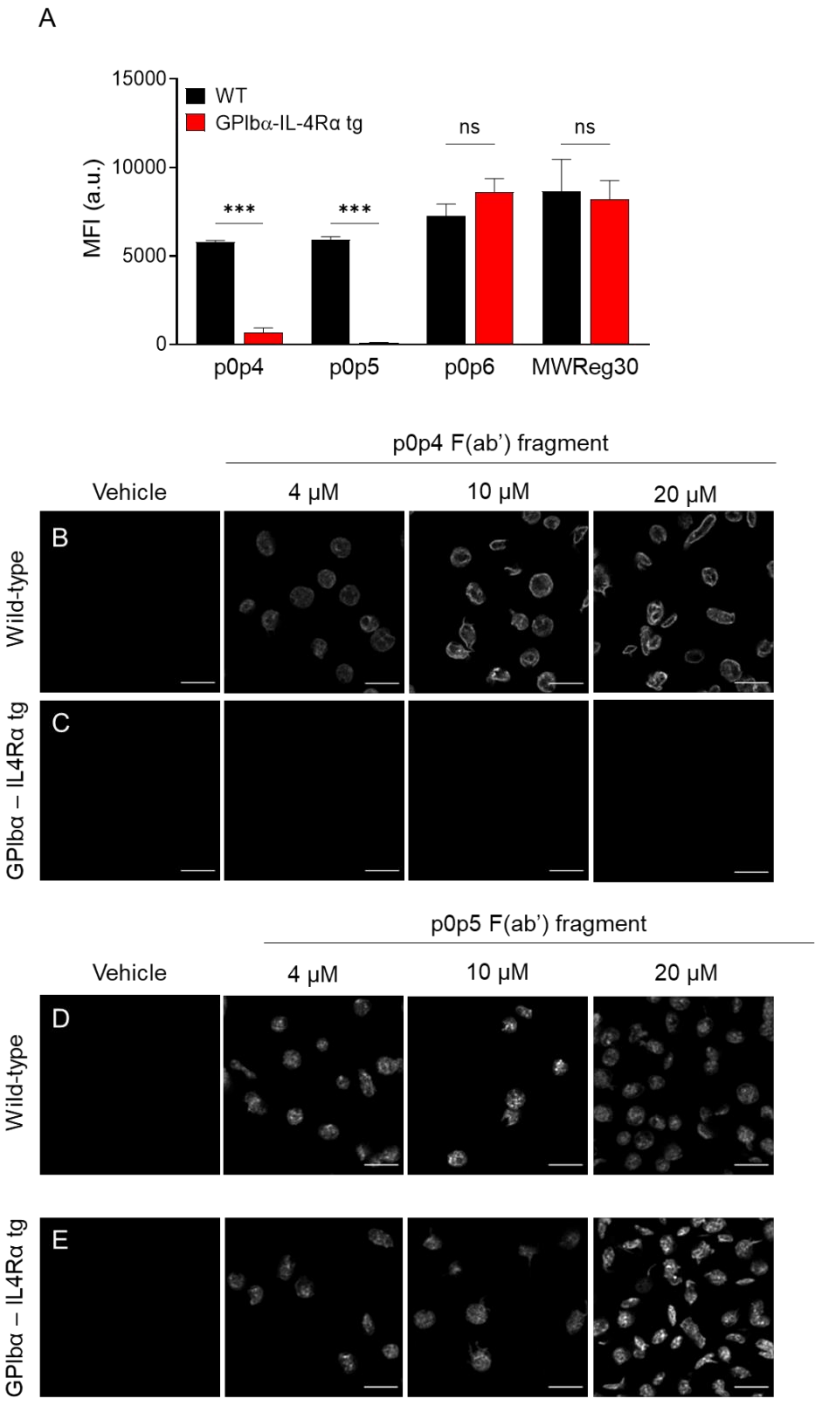

Figure 5.3. GPIbα-IL-4Rα transgenic platelets show antibodies specificity. Murine unexpanded wild-type and GPIbα-IL-4Rα transgenic platelets were labelled with F(ab') fragments against GPIbα in order to test their specificity. (**A**) Flow cytometric analysis of platelets labelled with antibodies against GPIbα (p0p4 and p0p5), GPIX (p0p6) and integrin αIIbβ3 (MWReg30). Data represented as mean fluorescence intensity (MFI) ± SD (n = 3). *** < P = 0.001 (ns; not significant) by paired t-test. Single-colour representative images of the staining performed using vehicle (PBS), p0p4 in (**B**) wild-type or (**C**) GPIbα-IL-4Rα transgenic platelets, and p0p5 in (**D**) wild-type or (**E**) GPIbα-IL-4Rα transgenic platelets. For all the conditions, 4, 10 or 20 μM of the F(ab') fragments were used. (n = 3). Scale bar: 5 μm.

Since protein conformation and epitope exposure can change from cells in solution to adherent cells, these findings demonstrate that microscopy methods are better to demonstrate antibodies specificity when used for imaging. Additionally, we prove that both p0p4 and p0p5 are specific for GPIbα.

5.3.4 Using trifunctional-labelled antibodies to visualise platelets by ExM

After testing the specificity of the antibodies and proving their binding to unexpanded platelets (**Figure 5.4A**), the following step was to confirm that platelets could be stained with IgGs and F(ab') fragments following the two standard protocols with pre-gelational labelling, 4x ExM developed by Tillberg et al., and 10x ExM developed by Truckenbrodt et al. (**Table 5.1**). We fixed the platelets on a lysine-coated coverslip and we observed that the pre-gelational staining with anti-GPIX IgG (p0p6) was successful for 4x and 10x protocols (**Figure 5.4B, C, left**). In contrast, the signal intensity of the p0p4 F(ab') fragment was dim for both conditions, and platelets could not be identified (**Figure 5.4B, C, right**). It was observed that the fluorescence signal of the IgG and F(ab') fragment dropped dramatically during the digestion step of the expansion protocol. (**Figure 5.4E**). After expansion, it was still possible to visualize the IgG signal, but not the F(ab') fragment, because an insufficient signal was detected.

To address this issue we tried trifunctional-conjugated antibodies. Trifunctional anchors were first used by Shi et al. for expansion microscopy to improve the retention of the labelled antibody by avoiding signal loss during the digestion process (Shi et al., 2021). Trifunctional anchors consist of three arms (**Figure 5.4F**): a label that could be a fluorophore such as Atto-488 or Atto-594, meth-acrylamide that anchors to the gel polymer, and a connector that binds to the antibody. We tested labelling p0p6 IgG and p0p4 F(ab') fragment with trifunctional anchors as summarised in **Table 5.2**. We were able to label the IgG obtaining a relatively high degree of labelling (DOL) (1.27), however,

the labelling of the F(ab') fragment was not that successful due to their smaller size and therefore fewer conjugation sites.

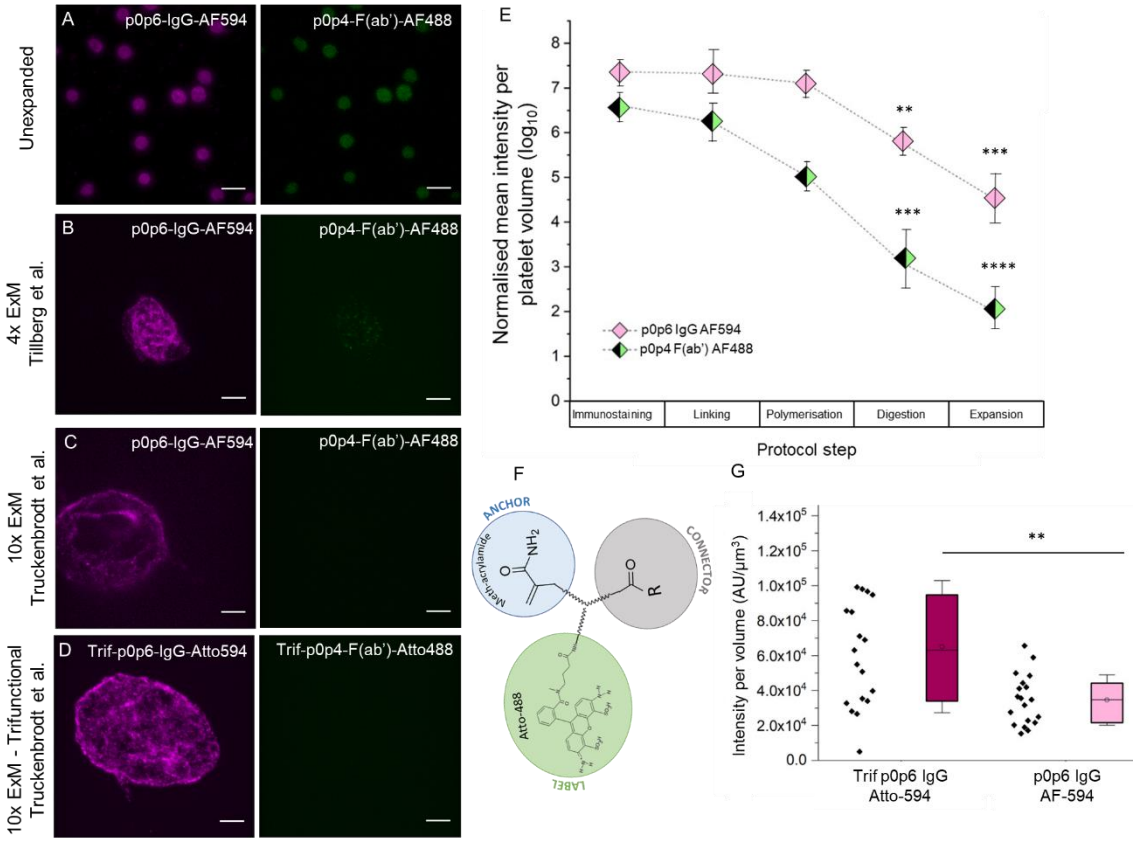

Figure 5.4. Using trifunctional labelled antibodies for expansion microscopy. Two-colour confocal representative images of murine wild-type platelets labelled with an anti-GPIX (p0p6) IgG antibody conjugated with Alexa Fluor-594 (magenta, left) and anti-GPIbα (p0p4) F(ab') fragment conjugated with Alexa Fluor-488 (green, right) in (**A**) unexpanded, (**B**) 4x expanded following Tillberg et al. protocol, and (**C**) 10x expanded platelets following Truckenbrodt et al. protocol. (**D**) Representative images of the trifunctional approach where murine platelets were stained using an antibody against GPIX (p0p6) trifunctionally-conjugated with Atto-594 (magenta, left) and a F(ab') fragment against GPIbα (p0p4) trifunctionally-conjugated with Atto-488 (green, right), and expanding platelets using 10x Truckenbrodt et al. protocol. Scale bar: 5 µm. (**E**) Normalised loss of fluorescent intensity per platelet volume of platelets stained with anti-GPIX (p0p6) IgG antibody conjugated with Alexa Fluor-594 (magenta) and anti-GPIbα (p0p4) F(ab') fragment conjugated with Alexa Fluor-488 (green) after each step (immunostaining, linking, gel polymerisation, digestion and expansion), when platelets were expanded 10x using Truckenbrodt et al. protocol (n = 3). (**F**) Schematic diagram of the trifunctional anchors, containing a connector, an anchor and a label (Atto-488). (**G**) Bar graph showing the fluorescence signal per platelet volume after 10x expansion of platelets labelled with Alexa Fluor-594 (right) or trifunctionally-conjugated with Atto-594 (left) after they were imaged with the same laser intensity (n = 3). Data represented as single points and mean ± SD. ** < P = 0.01, *** < P = 0.001, and **** < P = 0.0001 by paired t-test. Graphs (E) and (G) were kindly provided by Luise Evers.

After several attempts, the F(ab') fragment with 0.22 DOL produced the greatest results (**Table 5.2**). We observed that trifunctional-labelled IgG had a brighter signal in 10x expanded platelets than conventional-labelled IgG, even though its DOL was lower since the fluorophore was retained in the hydrogel because of the trifunctional anchor (**Figure 5.4D, G**). However, the signal intensity of the p0p4 trifunctionally-tagged F(ab') fragment remained too low to visualise (**Figure 4D**). Based on these results, F(ab') fragments cannot be recommended for 4x and 10x expansion pre-gelational labelling protocols, since they are conjugated to fewer fluorophores than IgG, and therefore the harsh digestion of the expansion protocols prevents their visualisation.

Table 5.2. Optimisation of labelling antibodies with trifunctional anchors.

Antibody	Labelling method	DOL	Dye	Visualisation	
				Unexpanded platelets	10x expanded platelets
p0p4 F(ab') fragment	Normal	1.8	AF-488	+	-
	Trifunctional	0.8	Atto-488	+	-
		0.4	Atto-488	+	-
		0.22	Atto-488	+	+
p0p6 IgG	Normal	6.3	AF-594	+++	+++
	Trifunctional	0.66	Atto-594	+++	+++
		1.27	Atto-594	+++	++++

The visualisation parameter is measured as integrated density of the images. Values are ranged as; (-) 0-5,000, (+) 5,001-20,000, (++) 20,001-35,000, (+++) 35,001-50,000, and (++++) >50,000.

5.3.5 Developing a 10x expansion post-gelational protocol to visualise F(ab') fragments using expansion microscopy

In the previous section, we found that labelling platelets with F(ab') fragments before gelation, denaturation, and expansion failed due to signal loss during the process. Therefore we tried another approach named ultrastructure expansion microscopy (U-

ExM) developed by Gambarotto et al., in which platelets are first embedded within the hydrogel, the digestion is replaced by a light denaturation process, the sample is expanded, and the labelling takes place as the last step (Gambarotto et al., 2019) (**Table 5.1**). We observed using Gambarotto's protocol, that 4x expanded platelets were successfully stained with p0p6 IgG (**Figure 5.5A, top**) and p0p4 F(ab') fragment (**Figure 5.5A, bottom**). Due to the still small size of the platelets, the resolution obtained with a 4x expansion of the sample was not sufficient. As a result, we developed a new expansion microscopy protocol in which the sample was expanded 10x, and labelled after gelation and expansion, similar to U-ExM. We named our protocol Mix & Match expansion microscopy (MM-ExM) as we employed the 10x monomer solution from (Damstra et al., 2022), and the fixation and post-gelational labelling of the U-ExM (Gambarotto et al., 2019). To establish and optimise the protocol for platelet imaging by testing different fixation conditions and denaturation times (**Table 5.3**). Finally, platelets were expanded 10 times according to protocol Av (**Table 5.3**), and the staining with IgG, as well as with F(ab') fragments was successful and allowed us to image the platelet receptors (**Figure 5.5B**).

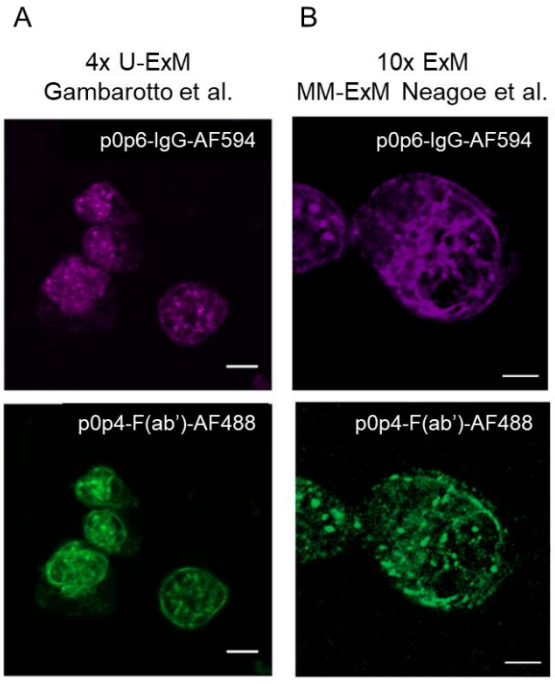

Figure 5.5. Developing a new 10x post-gelational labelling expansion protocol. Comparing two post-gelational protocols, the existing 4x developed by Gambarotto et al. (known as U-ExM), and our 10x protocol, named mix and match expansion microscopy (MM-ExM). Dual-colour confocal representative images of wild-type platelets labelled with an anti-GPIX (p0p6) IgG antibody conjugated with Alexa Fluor-594 (magenta, top) and anti-GPIbα (p0p4) F(ab') fragment conjugated with Alexa Fluor-488 (green, bottom) using (**A**) 4x U-ExM and (**B**) 10x MM-ExM protocols. Scale bar: 5 μm.

Table 5.3. Optimisation of a new post-gelational labelling 10x expansion microscopy protocol.

Protocol	Fixative	Time of fixation	Denaturation	Expansion	Visualisation
Ai	0.7% FA + 1% AA	20 min	95 °C for 5 min	+++	+
Aii	0.7% FA + 1% AA	1 hour	95 °C for 5 min	+++	++
Aiii	0.7% FA + 1% AA	1 hour	95 °C for 5 min	+++	++
Aiv	0.7% FA + 1% AA	1 hour	95 °C for 15 min	+++	++
Aiv	0.7% FA + 1% AA	1 hour	95 °C for 30 min	+++	++
Av	**0.7% FA + 1% AA**	**3 hours**	**95 °C for 5 min**	**+++**	**+++**
Avi	0.7% FA + 1% AA	3 hours	95 °C for 15 min	+++	++
Avii	0.7% FA + 1% AA	3 hours	95 °C for 30 min	+++	++
Bi	1% FA + 1% AA	20 min	95 °C for 5 min	++	+
Bii	1% FA + 1% AA	1 hour	95 °C for 5 min	++	+
Biii	1% FA + 1% AA	1 hour	No denaturation	++	+
Ci	3% Glyoxal + 3 % AA	20 min	95 °C for 5 min	++	+

Protocols are colour-coded by the fixative used. The expansion parameter is measured as expansion factor of the expanded gels. Values are ranged as; (++) 7x-9x expansion and (+++) 10x expansion. The visualisation parameter is measured as integrated density of the images. Values are ranged as; (-) 0-5,000, (+) 5,001-20,000, (++) 20,001-35,000, and (+++) 35,001-50,000.

Another advantage of our MM-ExM protocol was that we obtained platelets that were on average 20 µm in diameter, which is 10-fold larger than the size of unexpanded platelets (2 µm), demonstrating that platelets were consistently 10x larger with our protocol, whereas platelets were 15 µm in diameter on average with the 10x Truckenbrodt protocol (**Figure 5.6**).

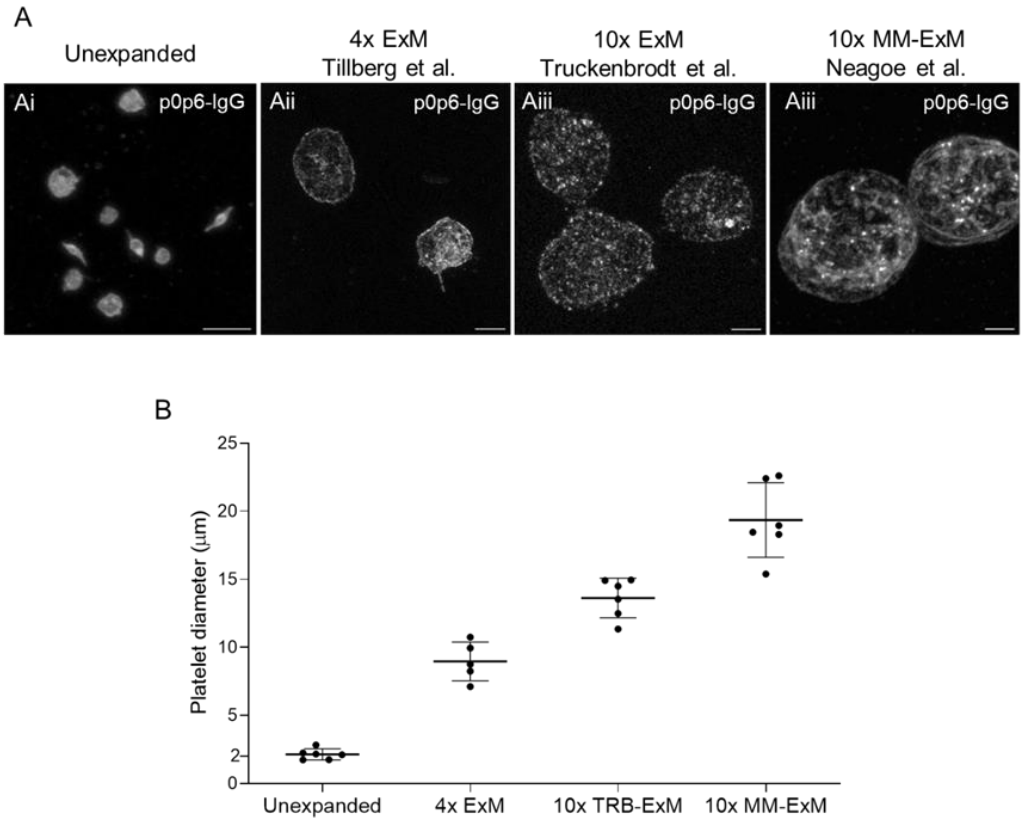

Figure 5.6. Analysing microscopic expansion of different ExM protocols. We examined the microscopic expansion of murine platelets following several expansion protocols. (**A**) Single-colour confocal representative images of platelets (Ai) unexpanded, (Aii) 4x expanded (Tillberg et al. protocol), (Aii) 10x expanded (Truckenbrodt et al. protocol), and (Aiv) 10x expanded following our MM-ExM protocol, and labelled with an anti-GPIX (p0p6) IgG antibody conjugated with Alexa Fluor-594. Scale bar: 5 µm. (**B**) Quantification of platelet diameter of platelets expanded following the protocols described in (A). A total number of 5 platelets was measured from n = 2 experiments.

5.3.6 Visualising from single platelets to nc-aggregates using expansion microscopy

Before, we established the 10x protocol only for resting platelets. Our next step was to expand and visualise activated platelets and nc-aggregates. For the imaging of activated platelets, we pre-activated murine them with thrombin (0.01 U/mL) and spread them on collagen- (10 µg/mL) or fibrinogen-coated (100 µg/mL) slides. We observed that platelets spread on collagen and fibrinogen were able to adhere to the gel and expanded 10 times (**Figure 5.7A**). To visualise nc-aggregates, we incubated resting platelets with the anti-GPIbα monoclonal IgG antibody for 10 min under stirring conditions using the

aggregometry cuvette. When the nc-aggregates were formed, we proceeded with the 10x expansion protocol. Unexpanded nc-aggregated platelets were tightly close together and single platelets were difficult to characterise (**Figure 5.7B**). However, using the 10x expansion protocol, we were able to observe single platelets within nc-aggregates (**Figure 5.7B**).

These results suggest that activated platelets and nc-aggregates could be transferred to the hydrogel and therefore it would be possible to use this microscopy technique as a tool to study the possible conformation change in platelet receptors in nc-aggregates.

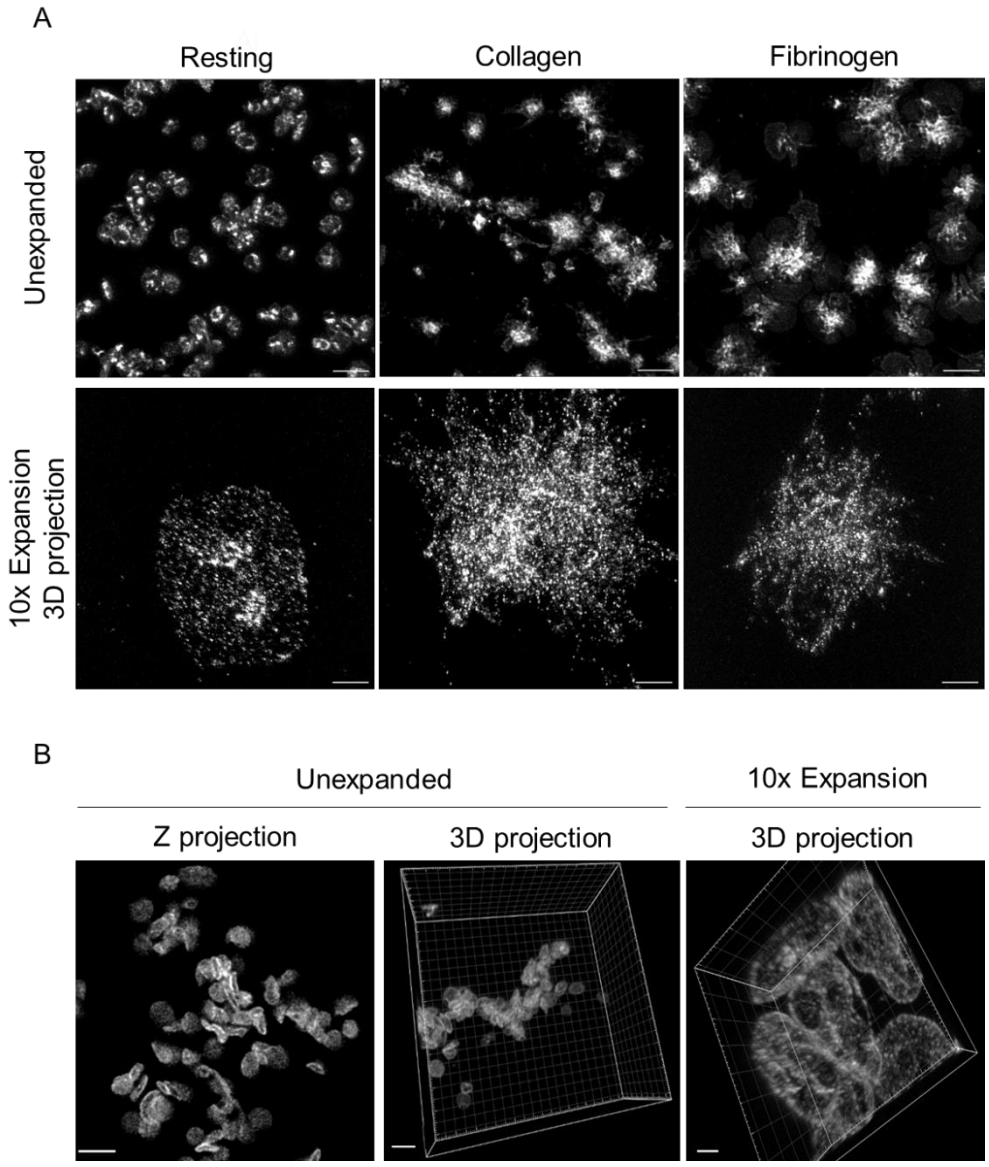

Figure 5.7. ExM of nc-aggregates, and single platelets spread on collagen- and fibrinogen-coated slides. Murine washed platelets were spread on different surfaces and expanded 10x following the 10x MM-ExM protocol. All platelets were stained with an anti-GPIX IgG antibody (p0p6) conjugated with Alexa Fluor-594. Images were obtained using the AiryScan confocal microscope (Zeiss), and the reconstruction and 3D projections were obtained using Zen Blue software (Zeiss). (**A**) Representative images of unexpanded (top) and 10x expanded (bottom) platelets spread on glycine- (left), collagen- (middle) and fibrinogen-coated (right) slides. (**B**) Murine platelets were incubated with 50 µg/mL of an anti-GPIbα IgG for 15 min at R.T., and then platelets were placed in the aggregometry cuvette for 10 min with constant stirring at 1,200 rpm to obtain the nc-aggregates. Then, nc-aggregates were fixed on glycine-coated slides and imaged. Representative images of unexpanded (left) and 10x expanded (right) platelets. Scale bar: 5 µm.

5.3.7 Mapping GPIb-V-IX receptor complex distribution on platelets

Following the establishment of the 10x post-gelational protocol (MM-ExM) and confirming that the nc-aggregates can be transferred into the gel, we proceed to study the distribution of the GPIb-IX-V complex, first on resting platelets. Platelets were stained with two different antibodies in three different combinations (**Figure 5.8A**). The highest colocalisation case was obtained using two different antibodies that bind to different epitopes of GPIbα (**Figure 5.8, case I**). Then, two different subunits of the complex, GPIbα and GPIX, were stained. GPIbα and GPIX have a higher distance and therefore we expected a lower colocalisation for this case (**Figure 5.8, case III**). For our case of study, we labelled GPIbα with the same antibody in two different colours (AF-488 and AF-594) to investigate a change in this receptor distribution (**Figure 5.8, case II**). This provides insights into the dynamic range of the receptors using expansion microscopy.

Using our MM-ExM protocol we stained platelets according to the cases previously described (**Figure 5.8**). It was visible from the 3D projections that p0p4 and p0p5 colocalised (**Figure 5.8B, case I**; represented in yellow), whereas for p0p4 and p0p6 we observed a lower proportion of colocalisation on the images (**Figure 5.8B, case III**). However, in order to verify the expected colocalisation of case I and case III, to obtain the precise colocalisation of case II, and to show that the resolution obtained with our expansion microscopy protocol is sufficient we would need to perform a colocalisation analysis. In the previous study (Heil et al., 2022), they used the 10x Truckenbrodt protocol to study the distribution of integrin αIIbβ3, and the colocalisation analysis was performed using the Manders' colocalisation approach (Manders et al., 1993). We aim to employ the same colocalisation approach to study GPIbα distribution on platelets. However, due to time constraints, the results of the colocalisation analysis cannot be shown in this Chapter.

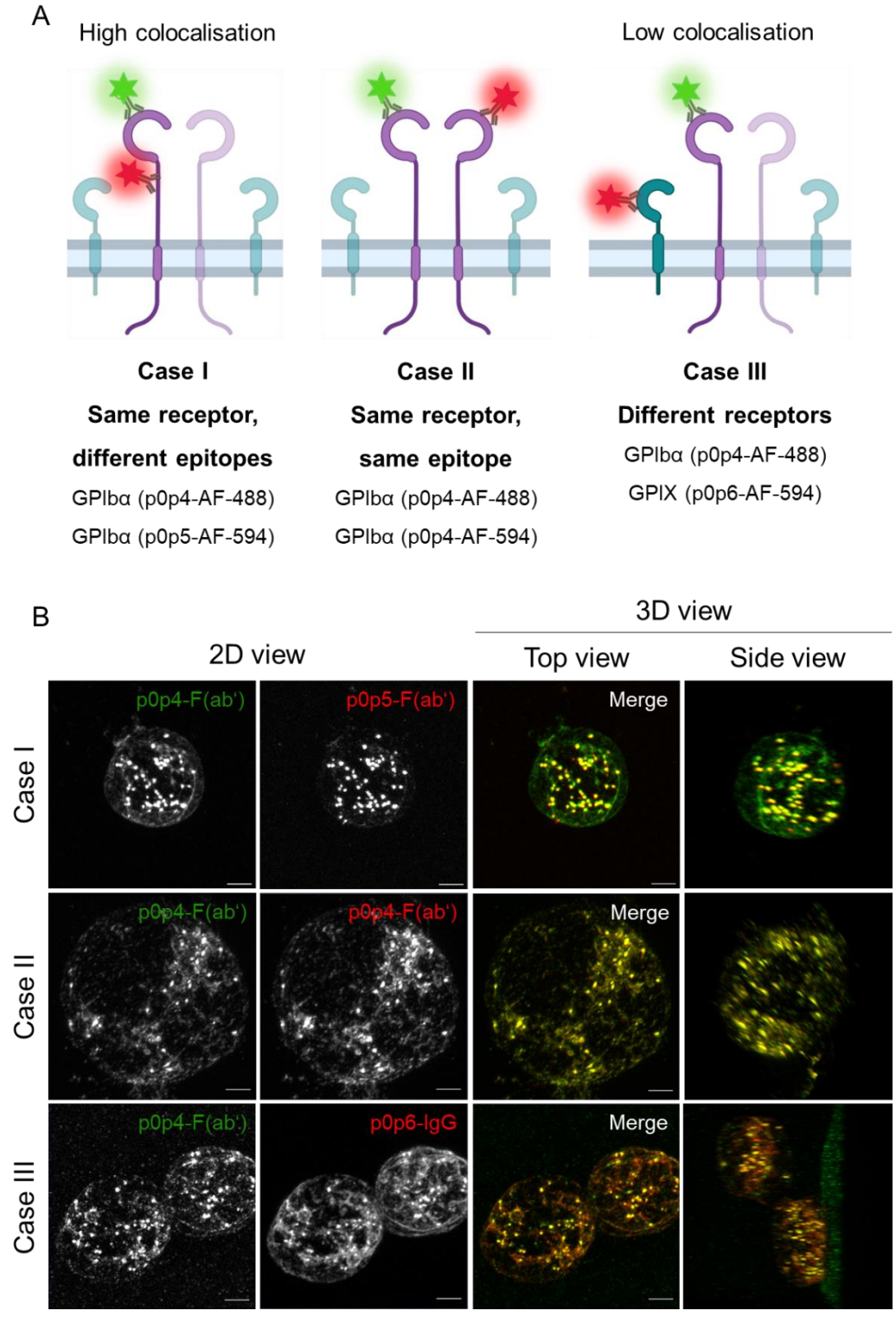

Figure 5.8. Using our new 10x ExM protocol to study the distribution of GPIbα on resting platelets. (**A**) Schematic representation of the colocalisation cases used for the study; case I (maximum colocalisation expected, left), case II (aim of the study, middle), and case III (minimum colocalisation expected, right). (**B**) Washed murine resting platelets were spread on glycine-coated coverslips, expanded 10x using the 10x MM-ExM protocol, and imaged using the AiryScan confocal microscope (Zeiss). The reconstructed images and 3D projections were obtained using

Zen Blue software (Zeiss). Representative 2D images (left) and 3D projections (right) of platelets stained according to case I (top), case II (middle) and case III (bottom). Merge images were taken to highlight the colocalisation for the different cases. Scale bar: 5 µm.

According to the literature GPIbα can interact in the platelet plasma membrane with GPVI (Arthur et al., 2005). However, there is no super-resolution data yet available demonstrating this interaction. We use our 10x MM-ExM protocol to label platelets for GPIbα and GPVI and observe the degree of colocalisation (**Figure 5.9**). According to the preliminary results, these two receptors colocalise on platelets, but as mentioned above, a colocalisation analysis is still required to ensure that these two molecules interact.

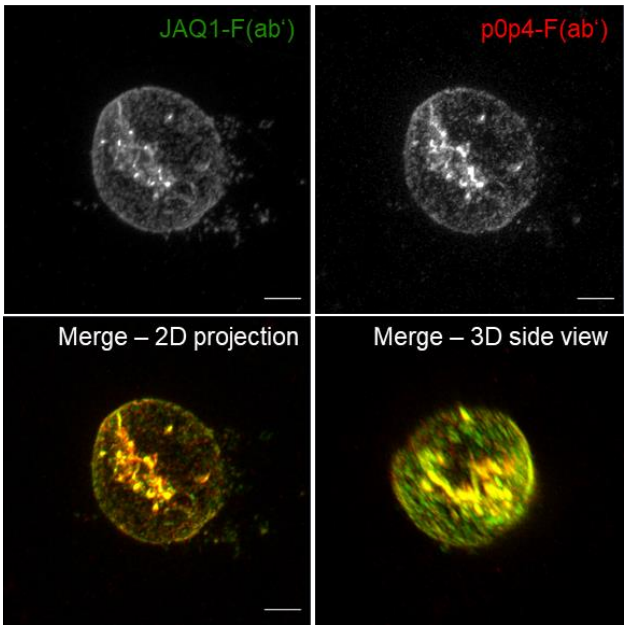

Figure 5.9. Using our new 10x ExM protocol to study the interaction of GPIbα and GPVI in platelets. Representative 2D and 3D projections of washed murine resting platelets were spread on glycine-coated coverslips, expanded 10x using the 10x MM-ExM protocol, and labelled with F(ab') fragments against GPVI (JAQ1) and GPIbα (p0p4) conjugated with AF-488 (green) and AF-594 (red), respectively. Image acquisition was performed using the AiryScan confocal microscope (Zeiss). The reconstructed images and 3D projections were obtained using Zen Blue software (Zeiss). Merge images were taken to highlight the colocalisation of the two receptors. Scale bar: 5 µm.

5.4 Discussion

Expansion microscopy is a relatively new microscopy technique that is constantly developing, with new protocols improving the labelling or increasing the sample size. We demonstrated that the best approach to reduce the signal loss during expansion is to label the sample after gelation and expansion. Additionally, we developed a new 10x expansion microscopy protocol that allowed us to expand platelets 10 times and post-gelationally label the sample with F(ab') fragments. The usage of F(ab') fragments is essential in our study to label nc-aggregates induced by anti-GPIbα IgG antibodies, but also to improve the imaging quality in general. The majority of platelet labelling has been done using IgG antibodies, which have a relatively high linkage error (of approximately 17 nm when using primary and secondary IgG antibodies) that lower the resolution gained through ExM. By using F(ab') fragments, we could decrease this linkage, and therefore improve the effective achieved resolution. F(ab') fragments, however, have the limitation of a reduced labelling density, which can result in dim images.

Signal loss is one of the biggest disadvantages of expansion microscopy, and previous protocols (Tillberg et al., 2016, Truckenbrodt et al., 2018) used proteinase K in the digestion buffer after sample labelling. We demonstrated that there is a significant loss of fluorescent signal upon digestion, but the IgG remained bright enough, while the F(ab') fragment was not visible. To minimise this loss, we implemented the labelling with antibodies (IgG and F(ab') fragment) conjugated with trifunctional anchors. The trifunctional anchors were first used in expansion microscopy by Shi and co-authors (Shi et al., 2021) proving higher retention of the labels. In this Chapter, we show that, in line with the previous publication, we were able to increase the fluorescence signal of IgG antibodies using trifunctional labels. However, for F(ab') fragments this approach was not successful, probably because the degree of labelling (DOL) we achieved for p0p4 F(ab') fragment was one-quarter of the DOL of the IgG. It was expected that F(ab')

fragments have a lower DOL than IgGs since they only have half the binding sites to fluorophores, but as a result of these low DOL, samples labelled with F(ab') fragments could not be visualised due to weak signals.

The main loss of fluorescent signal was caused by digestion, as also reported by other groups (Büttner et al., 2021, Shi et al., 2021). We tried a different approach in order to visualise the F(ab') fragments, known as post-gelation labelling, in which the labelling occurred upon gelation, denaturation and expansion when the platelets were embedded in the gel and expanded. This protocol is named 4x U-ExM (Gambarotto et al., 2019). By omitting the harsh digestion with the proteinase K and performing post-gelational labelling, we demonstrated that we were able to visualise 4x expanded platelets labelled with IgG and F(ab') fragments. In addition, post-gelational labelling increases the fluorescent signal when compared to regular pre-gelational labelling protocols, since the sample is already digested when labelled, so the digestion facilitates antibody binding to their epitopes.

Nevertheless, using the 4x U-ExM protocol expanded platelet size was not big enough to break the diffraction limit and to perform the colocalisation analysis. Therefore, we developed a new expansion microscopy protocol, following the principle of the U-ExM but using a monomer solution that allowed us to expand the sample 10x. To achieve the highest signal intensity, we tested different compositions of fixative as well as fixation and denaturation times. We called the new protocol mix and match expansion microscopy (MM-ExM). Using MM-ExM we proved that platelets labelled with IgG and F(ab') fragments were visualised without losing the fluorescent signal. Aside from that, the microscopic size of expanded platelets was approximately 10x larger than that of unexpanded platelets, reaching 20 µm in diameter. This was an improvement compared to the previous 10x protocol established by Truckenbrodt et al., with which we obtained a platelet size of around 15 µm in diameter. Aside from being faster, the MM-ExM

protocol produced more stable and firm hydrogels when compared to the 10x Truckenbrodt protocol, even though that was difficult to quantify.

In this Chapter we also show that resting, collagen- and fibrinogen-activated platelets, and nc-aggregates could be embedded in the 10x hydrogel and imaged. This is key for our project as the final aim is to visualise receptors' distribution in nc-aggregates caused by anti-GPIbα monoclonal antibodies. The three different colocalisation cases needed for studying GPIbα have already been imaged, and we are currently establishing the colocalisation analysis based on Manders' coefficient. The colocalisation analysis would provide insights into the receptor dynamic on single resting platelets, and since platelet nc-aggregates can already be imaged using ExM, the next step would be to compare the distribution of GPIb and the entire GPIb-IX-V receptor complex between single resting platelets and nc-aggregates. The image quality of ExM could be improved by combining it with another SR method, such as SIM, if after performing the colocalisation analysis we realised that the obtained images do not have enough resolution to visualize individual platelets within nc-aggregates.

CHAPTER 6

General discussion

6.1 Summary of results

Platelets play a wide variety of roles in both physiological and pathological processes including cardiovascular diseases (CVDs). As CVDs are still one of the leading causes of death worldwide (Roth et al., 2020a), platelets are often the target of novel therapies and it is, therefore, crucial to understand how platelets become activated. The collagen receptor GPVI and the vWF receptor GPIbα are two of the main glycoprotein receptors on the platelet plasma membrane and are involved in platelet activation. Therefore, understanding their signalling pathways, organisation, and conformation is important due to their potential role as antithrombotic targets.

Whereas in literature we find data on the GPVI downstream signalling pathway, less is known about GPVI organisation and conformation on the plasma membrane. Also, little is published about the GPIbα signalling cascade and localisation. This lack of knowledge and the recent developments in the super-resolution microscopy field have driven us to carry out this PhD thesis. The overall aim of this project was to develop and optimised super-resolution microscopy techniques for the study of platelet receptors, focusing on GPVI and GPIbα. We demonstrated that; 1) *d*STORM and SIM are the best methods to use for plasma membrane protein localisation in single platelets; 2) Rac does alter the GPVI signalling cascade but not receptor clustering and dimerisation; 3) expansion microscopy can be used to image receptors on single platelets and in nc-aggregates.

6.2 Choosing the best super-resolution microscopy methods for platelet imaging

The choice of which microscopy technique to use, whether super-resolution or not, is dependent on the question being asked and the tools that are available. Several super-resolution microscopy methods have been developed in recent years. Each of them has been optimised to solve different problems and therefore provides the user with different advantages (Montague et al., 2020). In our group in Birmingham, we have extensive

experience using *d*STORM, which is one of the best microscopy methods for studying receptor localisation because it relies on TIRF for optimal performance, making it ideal for looking at events occurring on the plasma membrane (Rust et al., 2006). *d*STORM data is then further amenable to performing cluster analysis to assess receptor distribution. However, like all techniques, it is not without its limitations. We, therefore, investigated DNA-PAINT as an alternative single molecule technique, for obtaining super-resolved images of platelets in TIRF mode and compared this to *d*STORM. In contrast to *d*STORM, PAINT has the benefit of being a super-resolution microscopy technique, which negates the problems associated with chromatic aberrations that are amplified in super-resolution imaging (Erdelyi et al., 2013), and decreases photobleaching (Pallikkuth et al., 2018). Additionally, PAINT permits multiplex labelling of the sample using the same fluorophore, this approach is called exchange-PAINT (Jungmann et al., 2014). Another drawback of *d*STORM is that it does not give absolute numbers of proteins. This is because it reports the localisations of fluorescent ‘blinks’, but each antibody can have several fluorophores attached and each fluorophore can blink multiple times. This behaviour is influenced by the photophysics of the dye and the buffer environment (Goossen-Schmidt et al., 2020), and therefore *d*STORM can only be used to report relative differences between treatments or areas within the cell. The same group which published Exchange-PAINT also developed a quantitative form of PAINT called qPAINT (Jungmann et al., 2016), a robust SR method that allows precise quantification and could be also useful for protein interaction studies. The biggest challenge with qPAINT is the number of controls and statistics analysis that need to be performed in order to obtain the quantification, therefore it is not a SR microscopy method easy to implement (Unterauer and Jungmann, 2022).

However, in our comparison of the two techniques in Chapter 3, using SQUIRREL analytical approach we obtained a lower image resolution in PAINT, due to the presence

of more artefacts than in *d*STORM super-resolved images. This artefact could be explained by; 1) the longer acquisition time required by PAINT compared to *d*STORM, which increases the risk of drifting; 2) PAINT reference images showing a higher unspecific background signal due to the imager strand freely diffusing in the imaging buffer, which could lead to errors in the software analysis; 3) the antibody's linkage error, which is significantly larger in PAINT due to the fluorophore coupled to a DNA oligo conjugated-IgG (30-40 nm) compared to normal primary and secondary standard labelling (17 nm) (Zwettler et al., 2020). The lower resolution obtained with PAINT than with *d*STORM is consistent with previous data where they also compared the resolution of microtubules using these two microscopy techniques (Früh et al., 2021). Nevertheless, PAINT has the potential to be a great tool for platelet imaging as it offers a range of advantages that other SR microscopy methods lack. The decrease in resolution of PAINT can be compensated by the possibility to image the entire GPVI signalling complex, instead of just one or two targets, and get real quantification data. We recommend the further optimisation of this method because of its great potential in platelet imaging.

An important objective of our project was to continue studying GPVI clustering using cluster analysis tools. The cluster analysis of GPVI was first implemented by Poulter and co-authors using Ripley's K-function-based cluster analysis (Poulter et al., 2017). However, several recent studies demonstrated that the density-based analysis approach, DBSCAN, is a better alternative for GPVI cluster analysis along collagen fibres than Ripley's K-function since it analyses the entire image instead of a small region of interest (Clark et al., 2019, Pallini, 2020). Therefore, as a continuation of those studies, we used DBSCAN cluster analysis for studying GPVI spatial location on the plasma membrane, validating their data. There are several other clustering methods, such as the topological mode analysis tool (ToMATo) developed to study integrin α2β1 clustering

of platelets on collagen (Pike et al., 2019), which we have started to use in GPVI cluster analysis.

We also demonstrated in Chapter 3 that SIM is one of the easiest methods to obtain stacks of super-resolved images that allows the visualisation of plasma membrane receptors and intracellular proteins, thus has been used in platelet imaging (Aslan et al., 2015, Pluthero and Kahr, 2018). Recent studies have used SIM in combination with TIRF (TIRF-SIM) to study receptor dynamics and perform live imaging, and increase the spatial resolution of SIM (Roth et al., 2020b, Ranjan and Chen, 2021, Wöllert and Langford, 2022). TIRF-SIM is the first commercially available method that allows super-resolution imaging of live cells and has a great potential for platelet imaging in order to visualise platelets spreading live, providing more insights about proteins dynamic.

The microscopy techniques mentioned above are designed to visualise platelets and other cells as a monolayer on a surface. However, one of the most peculiar characteristics of platelets is that they aggregate upon stimulation (Geratz et al., 1978). The platelets in these processes come close together, making it impossible to visualize their individual membranes and target molecules using a conventional epifluorescence, TIRF or confocal microscope. For these reasons, we implemented the usage of expansion microscopy (ExM) as a tool for platelet imaging. Currently, ExM is an emerging technology and many groups are developing their expansion microscopy protocols to overcome the limitations of the original protocol, such as fluorescence signal loss and the limited expansion of the sample (Truckenbrodt et al., 2018, Shi et al., 2021, Cho and Chang, 2022). Recently, our group in Würzburg published the first study performing expansion microscopy in platelets (Heil et al., 2022) using IgG antibodies to labelled platelet receptors. To move forward in the topic, this project aimed to image platelets labelled using fluorescently-tagged F(ab') fragments in order to avoid the higher linkage error of IgG and avoid nc-aggregation formation using anti-GPIbα antibodies

(Bergmeier et al., 2000). As described in Chapter 5, this was not possible using the most popular expansion microscopy protocols (Tillberg et al., 2016, Truckenbrodt et al., 2018), therefore we developed a new expansion microscopy protocol (MM-ExM) that allowed us to expand the sample 10x and labelled it with F(ab') fragments. This is the first protocol allowing the imaging of 10x expanded platelets immunostained with F(ab') fragments conjugated with fluorophores. We believe that our protocol is an important advancement for the ExM field, not only for platelet imaging, as many studies can benefit from labelling their samples with F(ab') fragments. To achieve a higher spatial resolution, ExM can be also used in combination for instance with *d*STORM (Xu et al., 2019, Zwettler et al., 2020) and SIM (Halpern et al., 2017).

Another method to increase ExM, and any other microscopy method, spatial resolution is to change the labelling strategy and use nanobodies, which are a new tool for imaging platelets (Bao et al., 2021). Nanobodies are recombinant variable domains of heavy-chain-only antibodies produced by camelids. They are a tenth of the size of an antibody, and more suitable for imaging than an IgG antibody since their small size allows them to penetrate the target tissue better and increase the precision of the image (Hassanzadeh-Ghassabeh et al., 2013). Because of their small size, they reduce the linkage error, reaching an average of 4 nm in combination with 10x ExM (Mikhaylova et al., 2015, Zwettler et al., 2020). In the Birmingham research group, we have developed the first nanobodies against human GPVI (Slater et al., 2021) that have been already used for imaging platelets under flow to study thrombus formation (Jooss et al., 2022). ExM, which is a great tool to image tissue and big and dense structures, could also be used in combination with nanobodies to study thrombus formation and obtain super-resolved images.

6.3 How does the actin cytoskeleton interact with GPIbα and GPVI signalling pathways?

Platelet aggregation and thrombus generation start with the adhesion of GPVI and GPIb-V-IX complex to their ligands. They have different ligands, GPVI binds to collagen, fibrin, laminin and adiponectin, while GPIbα (main ligand-binding subunit of GPIb-V-IX) binds to vWF, thrombin, leukocyte integrin αMβ2, and factors XI and XII among others (Andrews and Gardiner, 2016). Some data indicate that both glycoproteins activate the same signalling pathway leading to an increase in cytosolic calcium and activation of integrin αIIbβ3 which induces platelet aggregation (Ozaki et al., 2005). However, there is not a consensus in the literature regarding GPIbα signalling, with others reporting activation of the integrin αIIbβ3 being independent of GPIbα and induced by vWF binding directly to the integrin at high shear (Feng et al., 2006). Using transgenic mice lacking the GPIbα intracellular domain, Constantinescu-Bercu et al. demonstrated impaired GPVI signalling in response to CRP stimulation, resulting in reduced P-selectin expression and integrin αIIbβ3 activation, confirming that GPIbα is necessary to support GPVI signalling (Constantinescu-Bercu et al., 2021). This could explain that GPIbα does not directly activate integrin αIIbβ3 but supports GPVI in the activation of this integrin. Regarding the localisation of these glycoproteins, it has been proven by pull-down assays that GPVI can be associated with GPIbα in the platelet plasma membrane (Arthur et al., 2005). In Chapter 5, by using ExM we suggested that GPVI and GPIbα colocalise in resting platelets, supporting previous findings. Further experiments will be necessary to determine how the signalling of the two receptors might be regulated in platelets activated by different ligands or in platelets in a thrombus.

Another strong link between GPVI and GPIb-V-IX complex is the fundamental role that the actin cytoskeleton has on their signalling cascades and reorganisation. Also, activation of these two receptors results in significant modifications of platelet shape

because the actin cytoskeleton is reorganised (Goggs et al., 2015). GPIbα plasma membrane expression and distribution were altered by changes in the actin cytoskeleton induced by mouse platelets lacking filamin A (an actin-binding protein that controls the rearrangement of the actin cytoskeleton, and has a binding domain in the intracellular domain of GPIbα). The absence of filamin A also caused severe alteration in GPVI signalling, especially in Syk and PLCγ2 phosphorylation, demonstrating that another link between GPVI and GPIbα is their regulation by the cytoskeleton (Falet et al., 2010). In Chapter 4, we studied the role of the actin cytoskeleton by inhibiting Rac, a small Rho GTPase that controls actin redistribution and remodel (Moldovan et al., 1999). We observed that the disruption of the cytoskeleton mediated by Rac inhibition (using EHT1864) and cytochalasin D caused impaired human platelet aggregation upon GPVI ligand-stimulation. The same was observed in Rac1 deficient murine platelets upon collagen (Pleines et al., 2009). These data together suggest that the actin cytoskeleton is necessary for the correct aggregation of platelets mediated by GPVI, even though there is no evidence that this receptor directly interacts with the actin cytoskeleton. However, the disruption of the cytoskeleton causes dysfunction on the transportation and secretion of granules containing second-wave mediators necessary for aggregation, as well as impaired platelet remodelling and spatial relocation of different proteins that could potentially support platelet activation and aggregation downstream GPVI (Bury et al., 2016, Woronowicz et al., 2010). One of the molecules that could support GPVI is GPIbα, which directly interacts with the actin network via Filamin A, and has been demonstrated to be essential for GPVI-induced aggregation of platelets (Constantinescu-Bercu et al., 2021).

In Chapter 4, we described for the first time in human platelets that there is an effect on the GPVI downstream signalling pathway caused by the inhibition of Rac. We observed that the inhibition of Rac decreased phosphorylation levels of PLCγ2 in human, but not

in murine platelets, demonstrating that there are innate differences in the signalling pathway of both species. It was proposed by old literature that GPVI and GPIbα downstream cascades also share the activation of PLCγ2 (**Figure 6.1**). Nevertheless, one of the main differences between both signalling pathways is that GPVI induces a greater activation of PLCγ2 than GPIbα (Suzuki-Inoue et al., 2004). There is data reporting that Rac1 deficient platelets present an impaired phosphoinositide 3-kinase (PI3K) activation on platelets stimulated with vWF, however, there are no data yet available regarding PLCγ2 phosphorylation status (Delaney et al., 2012). As PLCγ2 is downstream PI3K in the GPIbα signalling cascade, we expect Rac inhibition to also decrease PLCγ2 activation on platelets stimulated with vWF. Unfortunately, we were unable to perform those experiments due to time constraints. Regarding the role of Rac on GPVI-mediated platelet spreading, we demonstrated that it affected the degree of spreading but not the adhesion. This is in line with previous studies that reported that platelets adhesion to vWF through GPIbα was also not altered in Rac1 deficient platelets (Delaney et al., 2012), meaning that the role of the cytoskeleton does not affect platelet adhesion to different ligands, including collagen, fibrinogen and vWF.

Surprisingly, we also observed that by disrupting the inhibition of Rac using EHT1864, we decreased only GPVI and GPV surface expression, whereas GPIbα surface levels were unaltered. These glycoprotein receptors have different auto-regulatory mechanisms for shedding due to the different metalloproteinases involved (ADAM10 in GPVI and GPV shedding, and ADAM17 in GPV and GPIbα shedding) (Gardiner et al., 2007, Bender et al., 2010) (**Figure 6.1**). We expected the actin cytoskeleton to have an important role in GPVI and GPIb-IX-V receptor complex cleavage because, as recently reported, actin polymerisation is crucial for GPIbα shedding (Zhou et al., 2022). The authors used jasplakinolide (a peptide that induces actin polymerisation and stabilisation; (Bubb et al., 2000)), which impaired thrombin-, but not collagen-induced platelet

aggregation, and promoted GPIbα but not GPVI shedding, suggesting that GPIbα shedding is dependent on actin polymerisation. The mechanism described indicates that calpain is activated by actin polymerisation, and this hydrolyses filamin A, which results in ADAM17-specific induced GPIbα shedding (Zhou et al., 2022). We hypothesize that a similar process, where the actin filaments are involved, could happen in the GPVI shedding induced upon Rac inhibition. However, we demonstrated that this process is exclusively mediated by ADAM10, by blocking the shedding with GI254023X (a specific ADAM10 inhibitor). GPVI interacts with calmodulin (CaM), a protein that accelerates actin polymerisation in human platelets (Piazza and Wallace, 1985). Of note, CaM also activates Rac (Elsaraj and Bhullar, 2008) and CaM inhibition induces GPVI shedding (Gardiner et al., 2004). The current hypothesis is that the inactivation and therefore dissociation of CaM from GPVI allows ADAM10 to easily reach the cleavage site and therefore induces GPVI shedding (Facey et al., 2016). With our study, Rac1 is now included in this picture, suggesting that Rac activity may be essential to keep CaM associated in the platelet surface to GPVI. As an alternative, Rac could also have a role in modulating ADAM10 activity through tetraspanins (Tspan). In platelets, Tspan15 forms a complex with ADAM10, and this molecular scissor is responsible for GPVI cleavage (Koo et al., 2022). In a recent study, Rac was shown to bind to the cytosolic domain of Tspan15 (Koo et al., 2020), even though the importance of Rac in this process is unknown. To fully understand the mechanisms that drive GPVI shedding from platelet plasma membranes, and the exact role Rac plays in this, more research is needed. Mapping the position of Rac1, ADAM10, Tspan15 and CaM relative to GPVI using super-resolution microscopy methods, such as exchange-PAINT (Jungmann et al., 2014), would be an interesting approach for further research on GPVI shedding, as it allows the visualisation of up to 8 target in the same sample. Yet, we started the optimisation of DNA-PAINT, as described in Chapter 3, however, the difficult optimisation

procedure did not allow us to implement exchange-PAINT for platelet imaging due to the limited length of the PhD.

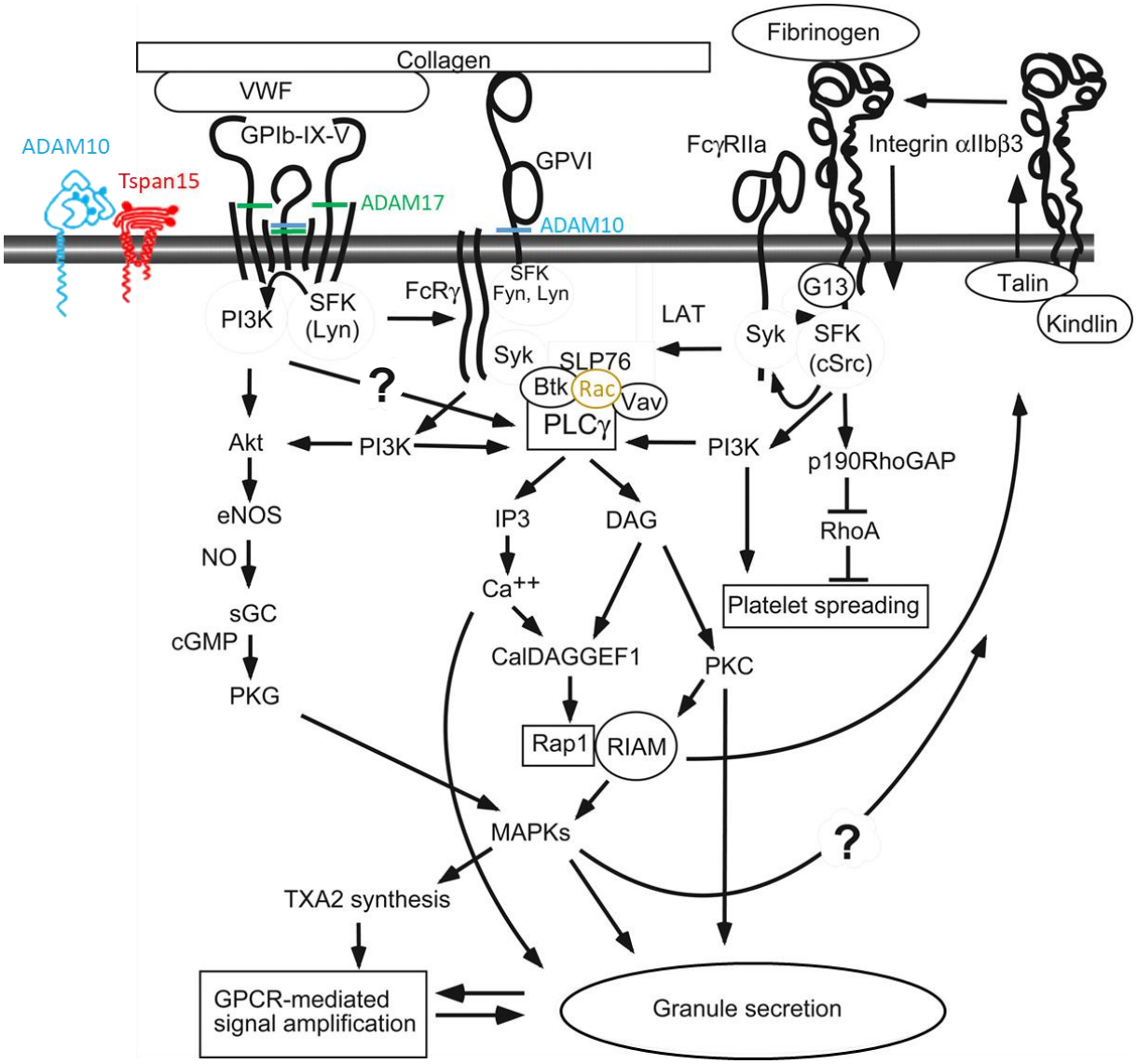

Figure 6.1. Schematic representation of the interaction of the signalling cascades of the GPIb-IX-V complex with GPVI and integrin αIIbβ3 on the platelet surface. Imaged modified from (Li et al., 2010), highlighting the localisation of Rac (yellow) downstream GPVI signalling pathway, upstream PLCγ2. The metalloproteinase ADAM10 (blue) interacts with Tspan15 (red) and is responsible for GPVI and GPV shedding, whereas ADAM17 (green) controls GPIbα and GPV shedding.

6.4 Challenges in analysing GPVI dimerisation and clustering in human platelets

The conformation of GPVI in resting and activated platelets has been extensively discussed in the past years (Clark et al., 2021a). The aim of this project was to provide some insights into GPVI conformation by using biophysical and super-resolution microscopy techniques. Miura and co-authors reported that only dimeric GPVI, and not monomeric GPVI, could bind to collagen fibres (Miura et al., 2002). More recently, this data was contradicted by our group (Clark et al., 2021b), demonstrating that GPVI dimerisation is not fundamental for GPVI binding to collagen, and therefore activation. The study reported that HEK293T cells transfected with GPVI missing the D2 domain (that contains the GPVI dimerisation site according to crystallography data (Horii et al., 2006, Slater et al., 2021)) were still able to bind fibrillar collagen. The main limitation of this study is that it did not involve platelets, so further research is needed in platelets to determine whether monomeric GPVI binds to collagen. However, this is challenging because platelets lack a nucleus that could allow the expression of modified versions of GPVI. Mouse models expressing a human copy of GPVI (Navarro et al., 2022), could be genetically modified and used to address this limitation of human platelets.

In 2007, Berlanga and co-authors were the first to propose that GPVI is dynamic and could dimerise or oligomerise using transfected HEK293T cells (Berlanga et al., 2007). A dimeric GPVI-specific F(ab') fragment was used to confirm this in platelets (Jung et al., 2009). Further studies also suggested that approximately 20% of GPVI was found as dimers in resting platelets, and there is an increase in GPVI dimerisation upon platelet activation with CRP, a GPVI ligand (Jung et al., 2012, Loyau et al., 2012). In Chapter 3 and 4, we studied GPVI dimerisation in human platelets using flow cytometry-based FRET analysis. We observed that, in line with the literature, GPVI was partially expressed as dimers in resting and CRP-activated platelets. In contrast, we did not find

an increase in FRET efficiency when platelets were stimulated with CRP, which would indicate an increase in GPVI dimerisation/oligomerisation on CRP-stimulated platelets. As we discussed in the previous section, we expected the cytoskeleton to have an effect on GPVI conformation, therefore we also studied the effect of disrupting the actin cytoskeleton using the Rac inhibitor EHT1864. We did not observe any significant change in GPVI dimerisation upon Rac inhibition. These results could be explained by the biophysical limitations of the technique used. In immunolabelled samples, antibody binding epitopes can be further than 10 µm, resulting in suboptimal FRET efficiency despite the receptors forming dimers. We performed a control experiment using the integrin αIIbβ3, which is a well-known dimer, indicating that the principle of the technique works in our hands. However, an ideal positive control for our flow cytometry-based FRET experiment studying GPVI dimerisation would be to use a cell line expressing dimeric GPVI-Fc and perform in that the FRET analysis using the same antibodies as in platelets.

With regard to the dynamics of GPVI, the receptor clusters on the platelet plasma membrane in solution, forming GPVI oligomers of up to 8 molecules upon convulxin stimulation (Horii et al., 2009), and large clusters along immobilised fibrillar collagen (Poulter et al., 2017). However, the mechanism that drives GPVI clustering is still unknown. One explanation could be the nature of collagen that contains several GPO and physically brings together GPVI molecules. Research conducted by our group in Birmingham has attempted to understand the mechanism underlying clustering and how to disrupt it. Pallini et al. demonstrated that by inhibiting two of the main tyrosine kinases downstream GPVI signalling pathway, Src and Syk, the cluster was not disrupted and therefore downstream signalling is not required to maintain the clusters once they are formed (Pallini et al., 2021). However, these clusters are in areas enriched in signalling proteins such as p-Syk, suggesting they are important for maintaining the signalling. A

similar scenario was reported by Clark et al., in which platelets were incubated with adenylyl cyclase-activating compounds forskolin, and adenosine, and GPVI clustering was not altered (Clark et al., 2019). Up to this point, collagen-induced GPVI clustering has been disrupted only by losartan (angiotensin II that inhibits TXA2 and GPVI) (Jiang et al., 2015). As part of this PhD project (Chapter 3 and 4), we also studied GPVI clustering and examined the effect of inhibiting Rac and, therefore, altering the actin cytoskeleton on GPVI clustering in human platelets. We expected the actin cytoskeleton somehow to play a role in GPVI clustering and lateral mobility, as it does, for instance, for the GPIb-V-IX receptor complex (Kasirer-Friede et al., 2002). It has been reported that polymerisation is essential for GPIb-IX-V complex centralisation on the platelet surface (Kovacsovics and Hartwig, 1996a). We demonstrated that pre-incubation with EHT1864 prior to spreading does not alter GPVI cluster density, area and size on human platelets that have spread on fibrillar collagen. Of note, the clustering analysis was performed in platelets that were partially and fully spread, suggesting that EHT1864 had less effect on those platelets. It would be ideal to analyse only platelets with filopodia extensions in order to guarantee that EHT1864 is acting, but due to their small size, the receptor density was too high for us to perform a colocalisation analysis on those platelets. To overcome this problem, a solution would be to use ExM in combination with *d*STORM (Xu et al., 2019).

Another limitation of this study is that GPVI dynamics could not be analysed in live platelets, as samples were imaged post-fixation. The implementation of appropriate microscopy techniques could be beneficial to provide broader information about clusters' dynamics. Therefore, we recommend for further studies the use a super-resolution microscopy technique that allows live imaging, such as TIRF-SIM. Additionally, *d*STORM and the DBSCAN cluster analysis provide qualitative analysis, which is useful for comparing different conditions but does provide an exact number of molecules. To

continue forward with the project we would like to perform the imaging using qPAINT to obtain a quantitative analysis that will indicate the exact number of GPVI molecules per cluster.

6.5 Concluding remarks

During this thesis, we have provided new insights into the GPVI and GPIb-IX-V complex signalling cascades and localisation, highlighting the special importance of the actin cytoskeleton, through Rac, in GPVI downstream signalling pathway and shedding in human platelets. We demonstrated the advantages but also the challenges of using super-resolution microscopy in platelets and suggest avenues for future work. Essentially, we have stressed the importance of choosing the right microscopy methods based on the question to be addressed.

CHAPTER 7: References

ABBE, E. 1873. Beiträge zur Theorie des Mikroskops und der mikroskopischen Wahrnehmung. *Archiv für Mikroskopische Anatomie,* 9**,** 413-468.

AKBAR, H., KIM, J., FUNK, K., CANCELAS, J. A., SHANG, X., CHEN, L., JOHNSON, J. F., WILLIAMS, D. A. & ZHENG, Y. 2007. Genetic and pharmacologic evidence that Rac1 GTPase is involved in regulation of platelet secretion and aggregation. *J Thromb Haemost,* 5**,** 1747-55.

AKBAR, H., SHANG, X., PERVEEN, R., BERRYMAN, M., FUNK, K., JOHNSON, J. F., TANDON, N. N. & ZHENG, Y. 2011. Gene targeting implicates Cdc42 GTPase in GPVI and non-GPVI mediated platelet filopodia formation, secretion and aggregation. *PloS one,* 6**,** e22117.

AL-TAMIMI, M., GRIGORIADIS, G., TRAN, H., PAUL, E., SERVADEI, P., BERNDT, M. C., GARDINER, E. E. & ANDREWS, R. K. 2011. Coagulation-induced shedding of platelet glycoprotein VI mediated by Factor Xa. *Blood,* 117**,** 3912.

AL-TAMIMI, M., MU, F. T., ARTHUR, J. F., SHEN, Y., MOROI, M., BERNDT, M. C., ANDREWS, R. K. & GARDINER, E. E. 2009a. Anti-glycoprotein VI monoclonal antibodies directly aggregate platelets independently of FcgammaRIIa and induce GPVI ectodomain shedding. *Platelets,* 20**,** 75-82.

AL-TAMIMI, M., MU, F. T., MOROI, M., GARDINER, E. E., BERNDT, M. C. & ANDREWS, R. K. 2009b. Measuring soluble platelet glycoprotein VI in human plasma by ELISA. *Platelets,* 20**,** 143.

ALSHEHRI, O. M., HUGHES, C. E., MONTAGUE, S., WATSON, S. K., FRAMPTON, J., BENDER, M. & WATSON, S. P. 2015a. Fibrin activates GPVI in human and mouse platelets. *Blood,* 126**,** 1601-1608.

ALSHEHRI, O. M., MONTAGUE, S., WATSON, S., CARTER, P., SARKER, N., MANNE, BHANU K., MILLER, JEANETTE L. C., HERR, ANDREW B., POLLITT, ALICE Y., O'CALLAGHAN, CHRIS A., KUNAPULI, S., ARMAN, M., HUGHES, CRAIG E. & WATSON, STEVE P. 2015b. Activation of glycoprotein VI (GPVI) and C-type lectin-like receptor-2 (CLEC-2) underlies platelet activation by diesel exhaust particles and other charged/hydrophobic ligands. *Biochemical Journal,* 468**,** 459-473.

ANDRE, P., DELANEY, S. M., LAROCCA, T., VINCENT, D., DEGUZMAN, F., JUREK, M., KOLLER, B., PHILLIPS, D. R. & CONLEY, P. B. 2003. P2Y12 regulates platelet adhesion/activation, thrombus growth, and thrombus stability in injured arteries. *J Clin Invest,* 112**,** 398-406.

ANDREWS, R. K. & GARDINER, E. E. 2016. Metalloproteolytic receptor shedding…platelets "acting their age". *Platelets,* 27**,** 512-8.

ANDREWS, R. K., KARUNAKARAN, D., GARDINER, E. E. & BERNDT, M. C. 2007. Platelet receptor proteolysis: a mechanism for downregulating platelet reactivity. *Arterioscler., Thromb., Vasc. Biol.,* 27**,** 1511.

ANDREWS, R. K., LÓPEZ, J. A. & BERNDT, M. C. 1997. Molecular mechanisms of platelet adhesion and activation. *Int J Biochem Cell Biol,* 29**,** 91-105.

ANDREWS, R. K., SUZUKI-INOUE, K., SHEN, Y., TULASNE, D., WATSON, S. P. & BERNDT, M. C. 2002. Interaction of calmodulin with the cytoplasmic domain of platelet glycoprotein VI. *Blood,* 99**,** 4219-4221.

ARTHUR, J. F., GARDINER, E. E., MATZARIS, M., TAYLOR, S. G., WIJEYEWICKREMA, L., OZAKI, Y., KAHN, M. L., ANDREWS, R. K. & BERNDT, M. C. 2005. Glycoprotein VI is associated with GPIb-IX-V on the membrane of resting and activated platelets. *Thromb. Haemostasis,* 93**,** 716.

ARTHUR, J. F., SHEN, Y., KAHN, M. L., BERNDT, M. C., ANDREWS, R. K. & GARDINER, E. E. 2007. Ligand binding rapidly induces disulfide-dependent dimerization of glycoprotein VI on the platelet plasma membrane. *J Biol Chem,* 282**,** 30434-41.

ASAZUMA, N., OZAKI, Y., SATOH, K., YATOMI, Y., HANDA, M., FUJIMURA, Y., MIURA, S. & KUME, S. 1997. Glycoprotein Ib-von Willebrand factor interactions activate tyrosine kinases in human platelets. *Blood, The Journal of the American Society of Hematology,* 90**,** 4789-4798.

ASLAN, J. E., ITAKURA, A., GERTZ, J. M. & MCCARTY, O. J. 2012. Platelet shape change and spreading. *Platelets and Megakaryocytes.* Springer.

ASLAN, J. E. & MCCARTY, O. J. 2013. Rho GTPases in platelet function. *J Thromb Haemost,* 11**,** 35-46.

ASLAN, J. E., RIGG, R. A., NOWAK, M. S., LOREN, C. P., BAKER-GROBERG, S. M., PANG, J., DAVID, L. L. & MCCARTY, O. J. T. 2015. Lysine acetyltransfer supports platelet function. *Journal of Thrombosis and Haemostasis,* 13**,** 1908-1917.

ATALAR, E., HAZNEDAROGLU, I. C., KILIC, H., OZER, N., COSKUN, S., OZTURK, E., AKSOYEK, S., OVUNC, K., KIRAZLI, S. & OZMEN, F. 2005. Increased soluble glycoprotein V concentration during the acute onset of unstable angina pectoris in association with chronic cigarette smoking. *Platelets,* 16**,** 329-333.

AURBACH, K., SPINDLER, M., HAINING, E. J., BENDER, M. & PLEINES, I. 2019. Blood collection, platelet isolation and measurement of platelet count and size in mice-a practical guide. *Platelets,* 30**,** 698-707.

BAI, Y., GUO, D., SUN, X., TANG, G., LIAO, T., PENG, Y., XU, J. & SHI, L. 2018. Balanced Rac1 activity controls formation and maintenance of neuromuscular acetylcholine receptor clusters. *Journal of Cell Science,* 131**,** jcs215251.

BAO, G., TANG, M., ZHAO, J. & ZHU, X. 2021. Nanobody: a promising toolkit for molecular imaging and disease therapy. *EJNMMI Research,* 11.

BEARDSLEY, D. S. & ERTEM, M. 1998. Platelet autoantibodies in immune thrombocytopenic purpura. *Transfus Sci,* 19**,** 237-44.

BENDAS, G. & SCHLESINGER, M. 2022. The GPIb-IX complex on platelets: insight into its novel physiological functions affecting immune surveillance, hepatic thrombopoietin generation, platelet clearance and its relevance for cancer development and metastasis. *Experimental Hematology & Oncology,* 11**,** 19.

BENDER, M., HAGEDORN, I. & NIESWANDT, B. 2011. Genetic and antibody-induced glycoprotein VI deficiency equally protects mice from mechanically and FeCl3-induced thrombosis. *Journal of Thrombosis and Haemostasis,* 9**,** 1423-1426.

BENDER, M., HOFMANN, S., STEGNER, D., CHALARIS, A., BOSL, M., BRAUN, A., SCHELLER, J., ROSE-JOHN, S. & NIESWANDT, B. 2010. Differentially regulated GPVI ectodomain shedding by multiple platelet-expressed proteinases. *Blood,* 116**,** 3347.

BENNETT, J. S. 2005. Structure and function of the platelet integrin alphaIIbbeta3. *The Journal of clinical investigation,* 115**,** 3363-3369.

BERGMEIER, W., BURGER, P. C., PIFFATH, C. L., HOFFMEISTER, K. M., HARTWIG, J. H., NIESWANDT, B. & WAGNER, D. D. 2003. Metalloproteinase inhibitors improve the recovery and hemostatic function of in vitro–aged or–injured mouse platelets. *Blood,* 102**,** 4229-4235.

BERGMEIER, W., PIFFATH, C. L., CHENG, G., DOLE, V. S., ZHANG, Y., VON ANDRIAN, U. H. & WAGNER, D. D. 2004. Tumor necrosis factor-alpha-converting enzyme (ADAM17) mediates GPIbalpha shedding from platelets in vitro and in vivo. *Circ Res,* 95**,** 677-83.

BERGMEIER, W., RACKEBRANDT, K., SCHRÖDER, W., ZIRNGIBL, H. & NIESWANDT, B. 2000. Structural and functional characterization of the mouse

von Willebrand factor receptor GPIb-IX with novel monoclonal antibodies. *Blood,* 95**,** 886-893.

BERGMEIER, W., SCHULTE, V., BROCKHOFF, G., BIER, U., ZIRNGIBL, H. & NIESWANDT, B. 2002. Flow cytometric detection of activated mouse integrin αIIbβ3 with a novel monoclonal antibody. *Cytometry: The Journal of the International Society for Analytical Cytology,* 48**,** 80-86.

BERLANGA, O., BORI-SANZ, T., JAMES, J. R., FRAMPTON, J., DAVIS, S. J., TOMLINSON, M. G. & WATSON, S. P. 2007. Glycoprotein VI oligomerization in cell lines and platelets. *J Thromb Haemost,* 5**,** 1026-1033.

BERNARD, J. & SOULIER, J. P. 1948. [On a new variety of congenital thrombocytary hemo-ragiparous dystrophy]. *Sem Hop,* 24**,** 3217-23.

BERNDT, M. C. & PHILLIPS, D. R. 1981. Interaction of thrombin with platelets: purification of the thrombin substrate. *Annals of the New York Academy of Sciences,* 370**,** 87-95.

BERNDT, M. C., SHEN, Y., DOPHEIDE, S. M., GARDINER, E. E. & ANDREWS, R. K. 2001. The vascular biology of the glycoprotein Ib-IX-V complex. *Thromb Haemost,* 86**,** 178-88.

BERTHOLD, M. R., CEBRON, N., DILL, F., GABRIEL, T. R., KÖTTER, T., MEINL, T., OHL, P., THIEL, K. & WISWEDEL, B. 2009. KNIME-the Konstanz information miner: version 2.0 and beyond. *AcM SIGKDD explorations Newsletter,* 11**,** 26-31.

BETZIG, E., PATTERSON, G. H., SOUGRAT, R., LINDWASSER, O. W., OLENYCH, S., BONIFACINO, J. S., DAVIDSON, M. W., LIPPINCOTT-SCHWARTZ, J. & HESS, H. F. 2006. Imaging Intracellular Fluorescent Proteins at Nanometer Resolution. *Science,* 313**,** 1642-1645.

BI, X., SU, Z., YAN, H., DU, J., WANG, J., CHEN, L., PENG, M., CHEN, S., SHEN, B. & LI, J. 2020. Prediction of severe illness due to COVID-19 based on an analysis of initial Fibrinogen to Albumin Ratio and Platelet count. *Platelets,* 31**,** 674-679.

BIGALKE, B., STELLOS, K., WEIG, H.-J., GEISLER, T., SEIZER, P., KREMMER, E., PÖTZ, O., JOOS, T., MAY, A. E., LINDEMANN, S. & GAWAZ, M. 2009. Regulation of platelet glycoprotein VI (GPVI) surface expression and of soluble GPVI in patients with atrial fibrillation (AF) and acute coronary syndrome (ACS). *Basic research in cardiology,* 104**,** 352-357.

BIZZOZERO, G. 1881. Su di un nuovo elemento morfologico del sangue dei mammiferi e della sua importanza nella trombosi e nella coagulazione. *L'Osservatore,* 17.

BOECKH-BEHRENS, T., GOLKOWSKI, D., IKENBERG, B., SCHLEGEL, J., PROTZER, U., SCHULZ, C., NOVOTNY, J., KREISER, K., ZIMMER, C., HEMMER, B. & WUNDERLICH, S. 2021. COVID-19-associated Large Vessel Stroke in a 28-year-old Patient : NETs and Platelets Possible Key Players in Acute Thrombus Formation. *Clin Neuroradiol,* 31**,** 511-514.

BOULAFTALI, Y., HESS, P. R., GETZ, T. M., CHOLKA, A., STOLLA, M., MACKMAN, N., OWENS, A. P., 3RD, WARE, J., KAHN, M. L. & BERGMEIER, W. 2013. Platelet ITAM signaling is critical for vascular integrity in inflammation. *J Clin Invest,* 123**,** 908-16.

BOURNE, J. H., BERISTAIN-COVARRUBIAS, N., ZUIDSCHERWOUDE, M., CAMPOS, J., DI, Y., GARLICK, E., COLICCHIA, M., TERRY, L. V., THOMAS, S. G., BRILL, A., BAYRY, J., WATSON, S. P. & RAYES, J. 2021. CLEC-2 Prevents Accumulation and Retention of Inflammatory Macrophages During Murine Peritonitis. *Frontiers in immunology,* 12**,** 693974-693974.

BOYLAN, B., CHEN, H., RATHORE, V., PADDOCK, C., SALACZ, M., FRIEDMAN, K. D., CURTIS, B. R., STAPLETON, M., NEWMAN, D. K., KAHN, M. L. & NEWMAN, P. J. 2004. Anti-GPVI–associated ITP: an acquired platelet disorder

caused by autoantibody-mediated clearance of the GPVI/FcRγ-chain complex from the human platelet surface. *Blood,* 104**,** 1350-1355.

BROCKMAN, J. M., SU, H., BLANCHARD, A. T., DUAN, Y., MEYER, T., QUACH, M. E., GLAZIER, R., BAZRAFSHAN, A., BENDER, R. L., KELLNER, A. V., OGASAWARA, H., MA, R., SCHUEDER, F., PETRICH, B. G., JUNGMANN, R., LI, R., MATTHEYSES, A. L., KE, Y. & SALAITA, K. 2020. Live-cell super-resolved PAINT imaging of piconewton cellular traction forces. *Nature Methods,* 17**,** 1018-1024.

BROWN, H. C., BECK, S., NAVARRO, S., DI, Y., SORIANO JEREZ, E. M., KACZMARZYK, J., THOMAS, S. G., MIRAKAJ, V., WATSON, S. P., NIESWANDT, B. & STEGNER, D. 2021. Antibody-mediated depletion of human CLEC-2 in a novel humanised mouse model. *bioRxiv***,** 2021.10.03.462933.

BUBB, M. R., SPECTOR, I., BEYER, B. B. & FOSEN, K. M. 2000. Effects of jasplakinolide on the kinetics of actin polymerization. An explanation for certain in vivo observations. *J Biol Chem,* 275**,** 5163-70.

BURKHART, J. M., VAUDEL, M., GAMBARYAN, S., RADAU, S., WALTER, U., MARTENS, L., GEIGER, J., SICKMANN, A. & ZAHEDI, R. P. 2012. The first comprehensive and quantitative analysis of human platelet protein composition allows the comparative analysis of structural and functional pathways. *Blood,* 120**,** e73-e82.

BURY, L., FALCINELLI, E., CHIASSERINI, D., SPRINGER, T. A., ITALIANO, J. E., JR. & GRESELE, P. 2016. Cytoskeletal perturbation leads to platelet dysfunction and thrombocytopenia in variant forms of Glanzmann thrombasthenia. *Haematologica,* 101**,** 46-56.

BÜTTNER, M., LAGERHOLM, C. B., WAITHE, D., GALIANI, S., SCHLIEBS, W., ERDMANN, R., EGGELING, C. & REGLINSKI, K. 2021. Challenges of Using Expansion Microscopy for Super-resolved Imaging of Cellular Organelles. *Chembiochem,* 22**,** 686-693.

CADROY, Y., HANSON, S. R., KELLY, A. B., MARZEC, U. M., EVATT, B. L., KUNICKI, T. J., MONTGOMERY, R. R. & HARKER, L. A. 1994. Relative Antithrombotic Effects of Monoclonal Antibodies Targeting Different Platelet Glycoprotein-Adhesive Molecule Interactions in Nonhuman Primates. *Blood,* 83**,** 3218-3224.

CAUWENBERGHS, N., MEIRING, M., VAUTERIN, S., VAN WYK, V., LAMPRECHT, S., ROODT, J. P., NOVÁK, L., HARSFALVI, J., DECKMYN, H. & KOTZÉ, H. F. 2000. Antithrombotic effect of platelet glycoprotein Ib–blocking monoclonal antibody Fab fragments in nonhuman primates. *Arteriosclerosis, thrombosis, and vascular biology,* 20**,** 1347-1353.

CHANG, J. B., CHEN, F., YOON, Y. G., JUNG, E. E., BABCOCK, H., KANG, J. S., ASANO, S., SUK, H. J., PAK, N., TILLBERG, P. W., WASSIE, A. T., CAI, D. & BOYDEN, E. S. 2017. Iterative expansion microscopy. *Nat Methods,* 14**,** 593-599.

CHEN, F., TILLBERG, P. W. & BOYDEN, E. S. 2015. Expansion microscopy. *Science,* 347**,** 543-548.

CHEN, W., LIANG, X., SYED, A. K., JESSUP, P., CHURCH, W. R., WARE, J., JOSEPHSON, C. D. & LI, R. 2016. Inhibiting GPIbalpha Shedding Preserves Post-Transfusion Recovery and Hemostatic Function of Platelets After Prolonged Storage. *Arteriosclerosis, Thrombosis, and Vascular Biology,* 36**,** 1821-1828.

CHEN, W., WILSON, M. S., WANG, Y., BERGMEIER, W., LANZA, F. & LI, R. 2022. Fast clearance of platelets in a commonly used mouse model for GPIbα is impeded by an anti-GPIbβ antibody derivative. *J Thromb Haemost,* 20**,** 1451-1463.

CHO, I. & CHANG, J.-B. 2022. Simultaneous expansion microscopy imaging of proteins and mRNAs via dual-ExM. *Scientific Reports,* 12**,** 3360.
CHOW, T. W., HELLUMS, J. D., MOAKE, J. L. & KROLL, M. H. 1992. Shear Stress-Induced von Willebrand Factor Binding to Platelet Glycoprotein Ib Initiates Calcium Influx Associated With Aggregation. *Blood,* 80**,** 113-120.
CHUNG, J., JEONG, D., KIM, G.-H., GO, S., SONG, J., MOON, E., HUH, Y. H. & KIM, D. 2021. Super-resolution imaging of platelet-activation process and its quantitative analysis. *Scientific reports,* 11**,** 1-18.
CLARK, J. C., DAMASKINAKI, F.-N., CHEUNG, Y. F. H., SLATER, A. & WATSON, S. P. 2021a. Structure-function relationship of the platelet glycoprotein VI (GPVI) receptor: does it matter if it is a dimer or monomer? *Platelets,* 32**,** 724-732.
CLARK, J. C., KAVANAGH, D. M., WATSON, S., PIKE, J. A., ANDREWS, R. K., GARDINER, E. E., POULTER, N. S., HILL, S. J. & WATSON, S. P. 2019. Adenosine and Forskolin Inhibit Platelet Aggregation by Collagen but not the Proximal Signalling Events. *Thrombosis and Haemostasis,* 119**,** 1124-1137.
CLARK, J. C., NEAGOE, R. A. I., ZUIDSCHERWOUDE, M., KAVANAGH, D. M., SLATER, A., MARTIN, E. M., SOAVE, M., STEGNER, D., NIESWANDT, B., POULTER, N. S., HUMMERT, J., HERTEN, D.-P., TOMLINSON, M. G., HILL, S. J. & WATSON, S. P. 2021b. Evidence that GPVI is Expressed as a Mixture of Monomers and Dimers, and that the D2 Domain is not Essential for GPVI Activation. *Thrombosis and Haemostasis*.
CLEMETSON, J. M., POLGAR, J., MAGNENAT, E., WELLS, T. N. C. & CLEMETSON, K. J. 1999. The Platelet Collagen Receptor Glycoprotein VI Is a Member of the Immunoglobulin Superfamily Closely Related to FcαR and the Natural Killer Receptors*. *Journal of Biological Chemistry,* 274**,** 29019-29024.
CLEMETSON, K. J. 2012. Platelets and primary haemostasis. *Thromb Res,* 129**,** 220-4.
COLLER, B. S., KALOMIRIS, E., STEINBERG, M. & SCUDDER, L. E. 1984. Evidence that glycocalicin circulates in normal plasma. *The Journal of clinical investigation,* 73**,** 794-799.
CONSTANTINESCU-BERCU, A., WANG, Y. A., WOOLLARD, K. J., MANGIN, P., VANHOORELBEKE, K., CRAWLEY, J. T. B. & SALLES-CRAWLEY, I. I. 2021. The GPIbα intracellular tail – role in transducing VWF- and collagen/GPVI-mediated signaling. *Haematologica*.
COXON, C. H., GEER, M. J. & SENIS, Y. A. 2017. ITIM receptors: more than just inhibitors of platelet activation. *Blood,* 129**,** 3407-3418.
CRANMER, S. L., ASHWORTH, K. J., YAO, Y., BERNDT, M. C., RUGGERI, Z. M., ANDREWS, R. K. & JACKSON, S. P. 2011. High shear–dependent loss of membrane integrity and defective platelet adhesion following disruption of the GPIbα-filamin interaction. *Blood,* 117**,** 2718-2727.
CULLEY, S., ALBRECHT, D., JACOBS, C., PEREIRA, P. M., LETERRIER, C., MERCER, J. & HENRIQUES, R. 2018. Quantitative mapping and minimization of super-resolution optical imaging artifacts. *Nature methods,* 15**,** 263-266.
DALY, M. E. 2011. Determinants of platelet count in humans. *Haematologica,* 96**,** 10.
DAMSTRA, H. G., MOHAR, B., EDDISON, M., AKHMANOVA, A., KAPITEIN, L. C. & TILLBERG, P. W. 2022. Visualizing cellular and tissue ultrastructure using Ten-fold Robust Expansion Microscopy (TREx). *eLife,* 11.
DAVÌ, G. & PATRONO, C. 2007. Platelet Activation and Atherothrombosis. *New England Journal of Medicine,* 357**,** 2482-2494.
DE CANDIA, E., HALL, S. W., RUTELLA, S., LANDOLFI, R., ANDREWS, R. K. & DE CRISTOFARO, R. 2001. Binding of Thrombin to Glycoprotein Ib Accelerates the Hydrolysis of Par-1 on Intact Platelets*. *Journal of Biological Chemistry,* 276**,** 4692-4698.

DE TOLEDO, M., SENIC-MATUGLIA, F., SALAMERO, J., UZE, G., COMUNALE, F., FORT, P. & BLANGY, A. 2003. The GTP/GDP Cycling of Rho GTPase TCL Is an Essential Regulator of the Early Endocytic Pathway. *Molecular Biology of the Cell,* 14**,** 4846-4856.

DELANEY, M. K., LIU, J., ZHENG, Y., BERNDT, M. C. & DU, X. 2012. The Role of Rac1 in Glycoprotein Ib-IX–Mediated Signal Transduction and Integrin Activation. *Arteriosclerosis, Thrombosis, and Vascular Biology,* 32**,** 2761-2768.

DEMMERLE, J., INNOCENT, C., NORTH, A. J., BALL, G., MÜLLER, M., MIRON, E., MATSUDA, A., DOBBIE, I. M., MARKAKI, Y. & SCHERMELLEH, L. 2017. Strategic and practical guidelines for successful structured illumination microscopy. *Nature Protocols,* 12**,** 988-1010.

DEMPSEY, G. T., VAUGHAN, J. C., CHEN, K. H., BATES, M. & ZHUANG, X. 2011. Evaluation of fluorophores for optimal performance in localization-based super-resolution imaging. *Nature methods,* 8**,** 1027-1036.

DENG, W., XU, Y., CHEN, W., PAUL, D. S., SYED, A. K., DRAGOVICH, M. A., LIANG, X., ZAKAS, P., BERNDT, M. C., DI PAOLA, J., WARE, J., LANZA, F., DOERING, C. B., BERGMEIER, W., ZHANG, X. F. & LI, R. 2016. Platelet clearance via shear-induced unfolding of a membrane mechanoreceptor. *Nature Communications,* 7**,** 12863.

DÉSIRÉ, L., BOURDIN, J., LOISEAU, N., PEILLON, H., PICARD, V., DE OLIVEIRA, C., BACHELOT, F., LEBLOND, B., TAVERNE, T., BEAUSOLEIL, E., LACOMBE, S., DROUIN, D. & SCHWEIGHOFFER, F. 2005. RAC1 inhibition targets amyloid precursor protein processing by gamma-secretase and decreases Abeta production in vitro and in vivo. *J Biol Chem,* 280**,** 37516-25.

DONG, J. F. 2005. Cleavage of ultra-large von Willebrand factor by ADAMTS-13 under flow conditions. *Journal of Thrombosis and Haemostasis,* 3**,** 1710-1716.

DORNIER, E., COUMAILLEAU, F., OTTAVI, J. F., MORETTI, J., BOUCHEIX, C., MAUDUIT, P., SCHWEISGUTH, F. & RUBINSTEIN, E. 2012. TspanC8 tetraspanins regulate ADAM10/Kuzbanian trafficking and promote Notch activation in flies and mammals. *J. Cell Biol.,* 199**,** 481.

DURÁN-SAENZ, N. Z., SERRANO-PUENTE, A., GALLEGOS-FLORES, P. I., MENDOZA-ALMANZA, B. D., ESPARZA-IBARRA, E. L., GODINA-GONZÁLEZ, S., GONZÁLEZ-CURIEL, I. E., AYALA-LUJÁN, J. L., HERNÁNDEZ-BARRALES, M., CUETO-VILLALOBOS, C. F., FRAUSTO-FIERROS, S. Y., BURCIAGA-HERNANDEZ, L. A. & MENDOZA-ALMANZA, G. 2022. Platelet Membrane: An Outstanding Factor in Cancer Metastasis. *Membranes,* 12**,** 182.

DÜTTING, S., HEIDENREICH, J., CHERPOKOVA, D., AMIN, E., ZHANG, S. C., AHMADIAN, M. R., BRAKEBUSCH, C. & NIESWANDT, B. 2015. Critical off-target effects of the widely used Rac1 inhibitors NSC23766 and EHT1864 in mouse platelets. *Journal of Thrombosis and Haemostasis,* 13**,** 827-838.

DWIVEDI, S., PANDEY, D., KHANDOGA, A. L., BRANDL, R. & SIESS, W. 2010. Rac1-mediated signaling plays a central role in secretion-dependent platelet aggregation in human blood stimulated by atherosclerotic plaque. *Journal of Translational Medicine,* 8**,** 128.

ELSARAJ, S. M. & BHULLAR, R. P. 2008. Regulation of platelet Rac1 and Cdc42 activation through interaction with calmodulin. *Biochimica et Biophysica Acta (BBA) - Molecular Cell Research,* 1783**,** 770-778.

EMMER, B. T., GINSBURG, D. & DESCH, K. C. 2016. Von Willebrand Factor and ADAMTS13. *Arteriosclerosis, Thrombosis, and Vascular Biology,* 36**,** 2281-2282.

ENGLERT, M., AURBACH, K., BECKER, I. C., GERBER, A., HEIB, T., WACKERBARTH, L. M., KUSCH, C., MOTT, K., ARAUJO, G. H. M., BAIG, A. A., DÜTTING, S., KNAUS, U. G., STIGLOHER, C., SCHULZE, H.,

NIESWANDT, B., PLEINES, I. & NAGY, Z. 2022. Impaired microtubule dynamics contribute to microthrombocytopenia in RhoB-deficient mice. *Blood Adv*.

ERDELYI, M., REES, E., METCALF, D., SCHIERLE, G. S. K., DUDAS, L., SINKO, J., KNIGHT, A. E. & KAMINSKI, C. F. 2013. Correcting chromatic offset in multicolor super-resolution localization microscopy. *Optics Express,* 21**,** 10978-10988.

ESTER, M., KRIEGEL, H.-P., SANDER, J. & XU, X. 1996. A density-based algorithm for discovering clusters in large spatial databases with noise. *Proceedings of the Second International Conference on Knowledge Discovery and Data Mining.* Portland, Oregon: AAAI Press.

EZUMI, Y., UCHIYAMA, T. & TAKAYAMA, H. 2000. Molecular Cloning, Genomic Structure, Chromosomal Localization, and Alternative Splice Forms of the Platelet Collagen Receptor Glycoprotein VI. *Biochemical and Biophysical Research Communications,* 277**,** 27-36.

FACEY, A., PINAR, I., ARTHUR, J. F., QIAO, J., JING, J., MADO, B., CARBERRY, J., ANDREWS, R. K. & GARDINER, E. E. 2016. A-Disintegrin-And-Metalloproteinase (ADAM) 10 Activity on Resting and Activated Platelets. *Biochemistry,* 55**,** 1187-1194.

FALATI, S., EDMEAD, C. E. & POOLE, A. W. 1999. Glycoprotein Ib-V-IX, a Receptor for von Willebrand Factor, Couples Physically and Functionally to the Fc Receptor γ-Chain, Fyn, and Lyn to Activate Human Platelets. *Blood,* 94**,** 1648-1656.

FALATI, S., GROSS, P., MERRILL-SKOLOFF, G., FURIE, B. C. & FURIE, B. 2002. Real-time in vivo imaging of platelets, tissue factor and fibrin during arterial thrombus formation in the mouse. *Nature medicine,* 8**,** 1175-1180.

FALET, H., POLLITT, A. Y., BEGONJA, A. J., WEBER, S. E., DUERSCHMIED, D., WAGNER, D. D., WATSON, S. P. & HARTWIG, J. H. 2010. A novel interaction between FlnA and Syk regulates platelet ITAM-mediated receptor signaling and function. *Journal of Experimental Medicine,* 207**,** 1967-1979.

FEITSMA, L. J., BRONDIJK, H. C., JARVIS, G. E., HAGEMANS, D., BIHAN, D., JERAH, N., VERSTEEG, M., FARNDALE, R. W. & HUIZINGA, E. G. 2022. Structural insights into collagen binding by platelet receptor glycoprotein VI. *Blood,* 139**,** 3087-3098.

FENG, S., LU, X., RESÉNDIZ, J. C. & KROLL, M. H. 2006. Pathological shear stress directly regulates platelet αIIbβ3 signaling. *American Journal of Physiology-Cell Physiology,* 291**,** C1346-C1354.

FINNEY, B. A., SCHWEIGHOFFER, E., NAVARRO-NÚÑEZ, L., BÉNÉZECH, C., BARONE, F., HUGHES, C. E., LANGAN, S. A., LOWE, K. L., POLLITT, A. Y., MOURAO-SA, D., SHEARDOWN, S., NASH, G. B., SMITHERS, N., REIS E SOUSA, C., TYBULEWICZ, V. L. & WATSON, S. P. 2012. CLEC-2 and Syk in the megakaryocytic/platelet lineage are essential for development. *Blood,* 119**,** 1747-56.

FÖRSTER, T. 1948. Zwischenmolekulare energiewanderung und fluoreszenz. *Annalen der physik,* 437**,** 55-75.

FOX, J. G., BARTHOLD, S., DAVISSON, M., NEWCOMER, C. E., QUIMBY, F. W. & SMITH, A. 2006. *The mouse in biomedical research: normative biology, husbandry, and models*, Elsevier.

FREIFELD, L., ODSTRCIL, I., FÖRSTER, D., RAMIREZ, A., GAGNON, J. A., RANDLETT, O., COSTA, E. K., ASANO, S., CELIKER, O. T. & GAO, R. 2017. Expansion microscopy of zebrafish for neuroscience and developmental biology studies. *Proceedings of the National Academy of Sciences,* 114**,** E10799-E10808.

FRÜH, S. M., MATTI, U., SPYCHER, P. R., RUBINI, M., LICKERT, S., SCHLICHTHAERLE, T., JUNGMANN, R., VOGEL, V., RIES, J. & SCHOEN, I. 2021. Site-Specifically-Labeled Antibodies for Super-Resolution Microscopy Reveal In Situ Linkage Errors. *ACS Nano,* 15**,** 12161-12170.

GAERTNER, F., AHMAD, Z., ROSENBERGER, G., FAN, S., NICOLAI, L., BUSCH, B., YAVUZ, G., LUCKNER, M., ISHIKAWA-ANKERHOLD, H., HENNEL, R., BENECHET, A., LORENZ, M., CHANDRARATNE, S., SCHUBERT, I., HELMER, S., STRIEDNIG, B., STARK, K., JANKO, M., BÖTTCHER, R. T., VERSCHOOR, A., LEON, C., GACHET, C., GUDERMANN, T., MEDEROS, Y. S. M., PINCUS, Z., IANNACONE, M., HAAS, R., WANNER, G., LAUBER, K., SIXT, M. & MASSBERG, S. 2017. Migrating Platelets Are Mechano-scavengers that Collect and Bundle Bacteria. *Cell,* 171**,** 1368-1382.e23.

GAMBAROTTO, D., ZWETTLER, F. U., LE GUENNEC, M., SCHMIDT-CERNOHORSKA, M., FORTUN, D., BORGERS, S., HEINE, J., SCHLOETEL, J.-G., REUSS, M., UNSER, M., BOYDEN, E. S., SAUER, M., HAMEL, V. & GUICHARD, P. 2019. Imaging cellular ultrastructures using expansion microscopy (U-ExM). *Nature Methods,* 16**,** 71-74.

GAO, Y., DICKERSON, J. B., GUO, F., ZHENG, J. & ZHENG, Y. 2004. Rational design and characterization of a Rac GTPase-specific small molecule inhibitor. *Proc Natl Acad Sci U S A,* 101**,** 7618-23.

GARDINER, E., ARTHUR, J. & ANDREWS, R. 2014. Targeting GPVI as a novel antithrombotic strategy. *Journal of Blood Medicine***,** 59.

GARDINER, E. E., ARTHUR, J. F., KAHN, M. L., BERNDT, M. C. & ANDREWS, R. K. 2004. Regulation of platelet membrane levels of glycoprotein VI by a platelet-derived metalloproteinase. *Blood,* 104**,** 3611-3617.

GARDINER, E. E., KARUNAKARAN, D., SHEN, Y., ARTHUR, J. F., ANDREWS, R. K. & BERNDT, M. C. 2007. Controlled shedding of platelet glycoprotein (GP)VI and GPIb?IX?V by ADAM family metalloproteinases. *Journal of Thrombosis and Haemostasis,* 5**,** 1530-1537.

GAY, L. J. & FELDING-HABERMANN, B. 2011. Contribution of platelets to tumour metastasis. *Nat Rev Cancer,* 11**,** 123-34.

GERATZ, J. D., TIDWELL, R. R., BRINKHOUS, K. M., MOHAMMAD, S. F., DANN, O. & LOEWE, H. 1978. Specific inhibition of platelet agglutination and aggregation by aromatic amidino compounds. *Thromb Haemost,* 39**,** 411-25.

GIBBINS, J., ASSELIN, J., FARNDALE, R., BARNES, M., LAW, C.-L. & WATSON, S. P. 1996. Tyrosine Phosphorylation of the Fc Receptor γ-Chain in Collagen-stimulated Platelets. *Journal of Biological Chemistry,* 271**,** 18095-18099.

GITZ, E., KOOPMAN, C. D., GIANNAS, A., KOEKMAN, C. A., VAN DEN HEUVEL, D. J., DECKMYN, H., AKKERMAN, J. W., GERRITSEN, H. C. & URBANUS, R. T. 2013. Platelet interaction with von Willebrand factor is enhanced by shear-induced clustering of glycoprotein Ibα. *Haematologica,* 98**,** 1810-8.

GOGGS, R., WILLIAMS, CHRISTOPHER M., MELLOR, H. & POOLE, ALASTAIR W. 2015. Platelet Rho GTPases–a focus on novel players, roles and relationships. *Biochemical Journal,* 466**,** 431-442.

GOOSSEN-SCHMIDT, N. C., SCHNIEDER, M., HÜVE, J. & KLINGAUF, J. 2020. Switching behaviour of dSTORM dyes in glycerol-containing buffer. *Scientific Reports,* 10.

GREENBERG, E. M. 2017. Thrombocytopenia: A Destruction of Platelets. *J Infus Nurs,* 40**,** 41-50.

GREINACHER, A., PECCI, A., KUNISHIMA, S., ALTHAUS, K., NURDEN, P., BALDUINI, C. & BAKCHOUL, T. 2017. Diagnosis of inherited platelet disorders on a blood smear: a tool to facilitate worldwide diagnosis of platelet disorders. *Journal of Thrombosis and Haemostasis,* 15**,** 1511-1521.

GREMMEL, T., FRELINGER, A. & MICHELSON, A. 2016. Platelet Physiology. *Seminars in Thrombosis and Hemostasis,* 42**,** 191-204.

GROSS, B. S., MELFORD, S. K. & WATSON, S. P. 1999. Evidence that phospholipase C-γ2 interacts with SLP-76, Syk, Lyn, LAT and the Fc receptor γ-chain after stimulation of the collagen receptor glycoprotein VI in human platelets. *European Journal of Biochemistry,* 263**,** 612-623.

GROZOVSKY, R., BEGONJA, A. J., LIU, K., VISNER, G., HARTWIG, J. H., FALET, H. & HOFFMEISTER, K. M. 2015. The Ashwell-Morell receptor regulates hepatic thrombopoietin production via JAK2-STAT3 signaling. *Nat Med,* 21**,** 47-54.

GUIDETTI, G. F., BERNARDI, B., CONSONNI, A., RIZZO, P., GRUPPI, C., BALDUINI, C. & TORTI, M. 2009. Integrin α2β1 induces phosphorylation-dependent and phosphorylation-independent activation of phospholipase Cγ2 in platelets: role of Src kinase and Rac GTPase. *Journal of Thrombosis and Haemostasis,* 7**,** 1200-1206.

GUSTAFSSON, M. G. L. 2000. Surpassing the lateral resolution limit by a factor of two using structured illumination microscopy. *Journal of Microscopy,* 198**,** 82-87.

HAINING, E. J., MATTHEWS, A. L., NOY, P. J., ROMANSKA, H. M., HARRIS, H. J., PIKE, J., MOROWSKI, M., GAVIN, R. L., YANG, J., MILHIET, P.-E., BERDITCHEVSKI, F., NIESWANDT, B., POULTER, N. S., WATSON, S. P. & TOMLINSON, M. G. 2017. Tetraspanin Tspan9 regulates platelet collagen receptor GPVI lateral diffusion and activation. *Platelets,* 28**,** 629-642.

HALLY, K., FAUTEUX-DANIEL, S., HAMZEH-COGNASSE, H., LARSEN, P. & COGNASSE, F. 2020. Revisiting Platelets and Toll-Like Receptors (TLRs): At the Interface of Vascular Immunity and Thrombosis. *Int J Mol Sci,* 21.

HALPERN, A. R., ALAS, G. C., CHOZINSKI, T. J., PAREDEZ, A. R. & VAUGHAN, J. C. 2017. Hybrid structured illumination expansion microscopy reveals microbial cytoskeleton organization. *ACS nano,* 11**,** 12677-12686.

HARPER, M. T. & POOLE, A. W. 2010. Diverse functions of protein kinase C isoforms in platelet activation and thrombus formation. *Journal of Thrombosis and Haemostasis,* 8**,** 454-462.

HARRISON, N., KOO, C. Z. & TOMLINSON, M. G. 2021. Regulation of ADAM10 by the TspanC8 Family of Tetraspanins and Their Therapeutic Potential. *International Journal of Molecular Sciences,* 22**,** 6707.

HARRISON, P. 2005. Platelet function analysis. *Blood reviews,* 19**,** 111-123.

HASSANZADEH-GHASSABEH, G., DEVOOGDT, N., DE PAUW, P., VINCKE, C. & MUYLDERMANS, S. 2013. Nanobodies and their potential applications. *Nanomedicine (Lond),* 8**,** 1013-26.

HEIJNEN, H. & VAN DER SLUIJS, P. 2015. Platelet secretory behaviour: as diverse as the granules … or not? *J Thromb Haemost,* 13**,** 2141-51.

HEIL, H. S., AIGNER, M., MAIER, S., GUPTA, P., EVERS, L. M. C., GÖB, V., KUSCH, C., MEUB, M., NIESWANDT, B., STEGNER, D. & HEINZE, K. G. 2022. Mapping densely packed αIIbβ3 receptors in murine blood platelets with expansion microscopy. *Platelets***,** 1-10.

HEILEMANN, M., VAN DE LINDE, S., SCHÜTTPELZ, M., KASPER, R., SEEFELDT, B., MUKHERJEE, A., TINNEFELD, P. & SAUER, M. 2008. Subdiffraction-Resolution Fluorescence Imaging with Conventional Fluorescent Probes. *Angewandte Chemie International Edition,* 47**,** 6172-6176.

HEINTZMANN, R. & HUSER, T. 2017. Super-Resolution Structured Illumination Microscopy. *Chem Rev,* 117**,** 13890-13908.

HELL, S. W. & WICHMANN, J. 1994. Breaking the diffraction resolution limit by stimulated emission: stimulated-emission-depletion fluorescence microscopy. *Optics Letters,* 19**,** 780-782.

HENSLER, M., FROJMOVIC, M., TAYLOR, R., HANTGAN, R. & LEWIS, J. 1992. Platelet morphologic changes and fibrinogen receptor localization. Initial responses in ADP-activated human platelets. *The American journal of pathology,* 141**,** 707.

HO-TIN-NOÉ, B., BOULAFTALI, Y. & CAMERER, E. 2018. Platelets and vascular integrity: how platelets prevent bleeding in inflammation. *Blood,* 131**,** 277-288.

HOCHREITER, B., KUNZE, M., MOSER, B. & SCHMID, J. A. 2019. Advanced FRET normalization allows quantitative analysis of protein interactions including stoichiometries and relative affinities in living cells. *Scientific Reports,* 9.

HOFFMEISTER, K. M., FELBINGER, T. W., FALET, H., DENIS, C. V., BERGMEIER, W., MAYADAS, T. N., VON ANDRIAN, U. H., WAGNER, D. D., STOSSEL, T. P. & HARTWIG, J. H. 2003. The clearance mechanism of chilled blood platelets. *Cell,* 112**,** 87-97.

HORII, K., BROOKS, M. T. & HERR, A. B. 2009. Convulxin forms a dimer in solution and can bind eight copies of glycoprotein VI: implications for platelet activation. *Biochemistry,* 48**,** 2907-14.

HORII, K., KAHN, M. L. & HERR, A. B. 2006. Structural basis for platelet collagen responses by the immune-type receptor glycoprotein VI. *Blood,* 108**,** 936-42.

HORVÁTH, G., PETRÁS, M., SZENTESI, G., FÁBIÁN, Á., PARK, J. W., VEREB, G. & SZÖLLŐSI, J. 2005. Selecting the right fluorophores and flow cytometer for fluorescence resonance energy transfer measurements. *Cytometry Part A,* 65A**,** 148-157.

HUANG, B., WANG, W., BATES, M. & ZHUANG, X. 2008. Three-dimensional super-resolution imaging by stochastic optical reconstruction microscopy. *Science,* 319**,** 810-3.

HUANG, C., WANG, Y., LI, X., REN, L., ZHAO, J., HU, Y., ZHANG, L., FAN, G., XU, J. & GU, X. 2020. Clinical features of patients infected with 2019 novel coronavirus in Wuhan, China. *The lancet,* 395**,** 497-506.

HUGHES, C. E., AUGER, J. M., MCGLADE, J., EBLE, J. A., PEARCE, A. C. & WATSON, S. P. 2008. Differential roles for the adapters Gads and LAT in platelet activation by GPVI and CLEC-2. *J Thromb Haemost,* 6**,** 2152-9.

ICHINOHE, T., TAKAYAMA, H., EZUMI, Y., ARAI, M., YAMAMOTO, N., TAKAHASHI, H. & OKUMA, M. 1997. Collagen-stimulated Activation of Syk but Not c-Src Is Severely Compromised in Human Platelets Lacking Membrane Glycoprotein VI. *Journal of Biological Chemistry,* 272**,** 63-68.

INDURUWA, I., MOROI, M., BONNA, A., MALCOR, J. D., HOWES, J. M., WARBURTON, E. A., FARNDALE, R. W. & JUNG, S. M. 2018. Platelet collagen receptor Glycoprotein VI-dimer recognizes fibrinogen and fibrin through their D-domains, contributing to platelet adhesion and activation during thrombus formation. *Journal of Thrombosis and Haemostasis,* 16**,** 389-404.

INOUE, O., OSADA, M., NAKAMURA, J., KAZAMA, F., SHIRAI, T., TSUKIJI, N., SASAKI, T., YOKOMICHI, H., DOHI, T., KANEKO, M., KURANO, M., OOSAWA, M., TAMURA, S., SATOH, K., TAKANO, K., MIYAUCHI, K., DAIDA, H., YATOMI, Y., OZAKI, Y. & SUZUKI-INOUE, K. 2019. Soluble CLEC-2 is generated independently of ADAM10 and is increased in plasma in acute coronary syndrome: comparison with soluble GPVI. *International Journal of Hematology,* 110**,** 285-294.

ITALIANO, J. E., JR., LECINE, P., SHIVDASANI, R. A. & HARTWIG, J. H. 1999. Blood platelets are assembled principally at the ends of proplatelet processes produced by differentiated megakaryocytes. *J Cell Biol,* 147**,** 1299-312.

JACKSON, D. E., WARD, C. M., WANG, R. & NEWMAN, P. J. 1997. The protein-tyrosine phosphatase SHP-2 binds platelet/endothelial cell adhesion molecule-1 (PECAM-1) and forms a distinct signaling complex during platelet aggregation:

evidence for a mechanistic link between PECAM-1-and integrin-mediated cellular signaling. *Journal of Biological Chemistry,* 272**,** 6986-6993.

JANDROT-PERRUS, M., BUSFIELD, S., LAGRUE, A. H., XIONG, X., DEBILI, N., CHICKERING, T., LE COUEDIC, J. P., GOODEARL, A., DUSSAULT, B., FRASER, C., VAINCHENKER, W. & VILLEVAL, J. L. 2000. Cloning, characterization, and functional studies of human and mouse glycoprotein VI: a platelet-specific collagen receptor from the immunoglobulin superfamily. *Blood,* 96**,** 1798-807.

JANDROT-PERRUS, M., CLEMETSON, K. J., HUISSE, M. G. & GUILLIN, M. C. 1992. Thrombin interaction with platelet glycoprotein Ib: effect of glycocalicin on thrombin specificity. *Blood,* 80**,** 2781-6.

JANUS-BELL, E., AHMED, M. U., RECEVEUR, N., MOURIAUX, C., NIESWANDT, B., GARDINER, E. E., GACHET, C., JANDROT-PERRUS, M. & MANGIN, P. H. 2021. Differential Role of Glycoprotein VI in Mouse and Human Thrombus Progression and Stability. *Thromb Haemost,* 121**,** 543-546.

JARVIS, G. E., ATKINSON, B. T., SNELL, D. C. & WATSON, S. P. 2002. Distinct roles of GPVI and integrin alpha(2)beta(1) in platelet shape change and aggregation induced by different collagens. *Br J Pharmacol,* 137**,** 107-17.

JENKINS, C. S., PHILLIPS, D. R., CLEMETSON, K. J., MEYER, D., LARRIEU, M. J. & LÜSCHER, E. F. 1976. Platelet membrane glycoproteins implicated in ristocetin-induced aggregation. Studies of the proteins on platelets from patients with Bernard-Soulier syndrome and von Willebrand's disease. *Journal of Clinical Investigation,* 57**,** 112-124.

JIANG, N., KIM, H.-J., CHOZINSKI, T. J., AZPURUA, J. E., EATON, B. A., VAUGHAN, J. C. & PARRISH, J. Z. 2018. Superresolution imaging of Drosophila tissues using expansion microscopy. *Molecular biology of the cell,* 29**,** 1413-1421.

JIANG, P., LOYAU, S., TCHITCHINADZE, M., ROPERS, J., JONDEAU, G. & JANDROT-PERRUS, M. 2015. Inhibition of Glycoprotein VI Clustering by Collagen as a Mechanism of Inhibiting Collagen-Induced Platelet Responses: The Example of Losartan. *PLOS ONE,* 10**,** e0128744.

JIMENEZ, A., FRIEDL, K. & LETERRIER, C. 2020. About samples, giving examples: Optimized Single Molecule Localization Microscopy. *Methods,* 174**,** 100-114.

JIROUŠKOVÁ, M., JAISWAL, J. K. & COLLER, B. S. 2007. Ligand density dramatically affects integrin αIIbβ3-mediated platelet signaling and spreading. *Blood,* 109**,** 5260-5269.

JOOSS, N. J., SMITH, C. W., SLATER, A., MONTAGUE, S. J., DI, Y., O'SHEA, C., THOMAS, M. R., HENSKENS, Y. M. C., HEEMSKERK, J. W. M., WATSON, S. P. & POULTER, N. S. 2022. Anti-GPVI nanobody blocks collagen- and atherosclerotic plaque–induced GPVI clustering, signaling, and thrombus formation. *Journal of Thrombosis and Haemostasis,* n/a.

JU, L., LOU, J., CHEN, Y., LI, Z. & ZHU, C. 2015. Force-induced unfolding of leucine-rich repeats of glycoprotein Ibα strengthens ligand interaction. *Biophysical journal,* 109**,** 1781-1784.

JUNG, S., TSUJI, K. & MOROI, M. 2009. Glycoprotein (GP) VI dimer as a major collagen-binding site of native platelets: direct evidence obtained with dimeric GPVI-specific Fabs. *Journal of Thrombosis and Haemostasis,* 7**,** 1347-1355.

JUNG, S. M., MOROI, M., SOEJIMA, K., NAKAGAKI, T., MIURA, Y., BERNDT, M. C., GARDINER, E. E., HOWES, J.-M., PUGH, N., BIHAN, D., WATSON, S. P. & FARNDALE, R. W. 2012. Constitutive Dimerization of Glycoprotein VI (GPVI) in Resting Platelets Is Essential for Binding to Collagen and Activation in Flowing Blood. *Journal of Biological Chemistry,* 287**,** 30000-30013.

JUNG, S. M., TAKEMURA, Y., IMAMURA, Y., HAYASHI, T., ADACHI, E. & MOROI, M. 2008. Collagen-type specificity of glycoprotein VI as a determinant of platelet adhesion. *Platelets,* 19**,** 32-42.

JUNGMANN, R., AVENDAÑO, M. S., DAI, M., WOEHRSTEIN, J. B., AGASTI, S. S., FEIGER, Z., RODAL, A. & YIN, P. 2016. Quantitative super-resolution imaging with qPAINT. *Nature Methods,* 13**,** 439-442.

JUNGMANN, R., AVENDAÑO, M. S., WOEHRSTEIN, J. B., DAI, M., SHIH, W. M. & YIN, P. 2014. Multiplexed 3D cellular super-resolution imaging with DNA-PAINT and Exchange-PAINT. *Nature Methods,* 11**,** 313-318.

JUNGMANN, R., STEINHAUER, C., SCHEIBLE, M., KUZYK, A., TINNEFELD, P. & SIMMEL, F. C. 2010. Single-Molecule Kinetics and Super-Resolution Microscopy by Fluorescence Imaging of Transient Binding on DNA Origami. *Nano Letters,* 10**,** 4756-4761.

KAHN, M. L., NAKANISHI-MATSUI, M., SHAPIRO, M. J., ISHIHARA, H. & COUGHLIN, S. R. 1999. Protease-activated receptors 1 and 4 mediate activation of human platelets by thrombin. *J Clin Invest,* 103**,** 879-87.

KAHR, W. H., PLUTHERO, F. G., ELKADRI, A., WARNER, N., DROBAC, M., CHEN, C. H., LO, R. W., LI, L., LI, R., LI, Q., THOENI, C., PAN, J., LEUNG, G., LARA-CORRALES, I., MURCHIE, R., CUTZ, E., LAXER, R. M., UPTON, J., ROIFMAN, C. M., YEUNG, R. S., BRUMELL, J. H. & MUISE, A. M. 2017. Loss of the Arp2/3 complex component ARPC1B causes platelet abnormalities and predisposes to inflammatory disease. *Nat Commun,* 8**,** 14816.

KAMYKOWSKI, J., CARLTON, P., SEHGAL, S. & STORRIE, B. 2011. Quantitative immunofluorescence mapping reveals little functional coclustering of proteins within platelet α-granules. *Blood,* 118**,** 1370-3.

KANAJI, T., RUSSELL, S. & WARE, J. 2002. Amelioration of the macrothrombocytopenia associated with the murine Bernard-Soulier syndrome. *Blood,* 100**,** 2102-2107.

KANAJI, T., WARE, J., OKAMURA, T. & NEWMAN, P. J. 2012. GPIbα regulates platelet size by controlling the subcellular localization of filamin. *Blood,* 119**,** 2906-2913.

KASIRER-FRIEDE, A., WARE, J., LENG, L., MARCHESE, P., RUGGERI, Z. M. & SHATTIL, S. J. 2002. Lateral Clustering of Platelet GP Ib-IX Complexes Leads to Up-regulation of the Adhesive Function of Integrin αIIbβ3. *Journal of Biological Chemistry,* 277**,** 11949-11956.

KHATER, I. M., NABI, I. R. & HAMARNEH, G. 2020. A Review of Super-Resolution Single-Molecule Localization Microscopy Cluster Analysis and Quantification Methods. *Patterns,* 1**,** 100038.

KING, C., RAICU, V. & HRISTOVA, K. 2017. Understanding the FRET Signatures of Interacting Membrane Proteins*. *Journal of Biological Chemistry,* 292**,** 5291-5310.

KISHIMOTO, A., TAKAI, Y., MORI, T., KIKKAWA, U. & NISHIZUKA, Y. 1980. Activation of calcium and phospholipid-dependent protein kinase by diacylglycerol, its possible relation to phosphatidylinositol turnover. *J Biol Chem,* 255**,** 2273-6.

KLAGES, B., BRANDT, U., SIMON, M. I., SCHULTZ, G. & OFFERMANNS, S. 1999. Activation of G12/G13 results in shape change and Rho/Rho-kinase–mediated myosin light chain phosphorylation in mouse platelets. *The Journal of cell biology,* 144**,** 745-754.

KOO, C. Z., HARRISON, N., NOY, P. J., SZYROKA, J., MATTHEWS, A. L., HSIA, H.-E., MÜLLER, S. A., TÜSHAUS, J., GOULDING, J., WILLIS, K., APICELLA, C., CRAGOE, B., DAVIS, E., KELES, M., MALINOVA, A., MCFARLANE, T. A., MORRISON, P. R., NGUYEN, H. T. H., SYKES, M. C., AHMED, H., DI MAIO,

A., SEIPOLD, L., SAFTIG, P., CULL, E., PLIOTAS, C., RUBINSTEIN, E., POULTER, N. S., BRIDDON, S. J., HOLLIDAY, N. D., LICHTENTHALER, S. F. & TOMLINSON, M. G. 2020. The tetraspanin Tspan15 is an essential subunit of an ADAM10 scissor complex. *Journal of Biological Chemistry,* 295**,** 12822-12839.

KOO, C. Z., MATTHEWS, A. L., HARRISON, N., SZYROKA, J., NIESWANDT, B., GARDINER, E. E., POULTER, N. S. & TOMLINSON, M. G. 2022. The Platelet Collagen Receptor GPVI Is Cleaved by Tspan15/ADAM10 and Tspan33/ADAM10 Molecular Scissors. *International Journal of Molecular Sciences,* 23**,** 2440.

KOVACSOVICS, T. & HARTWIG, J. 1996a. Thrombin-induced GPIb-IX centralization on the platelet surface requires actin assembly and myosin II activation. *Blood,* 87**,** 618-629.

KOVACSOVICS, T. J. & HARTWIG, J. H. 1996b. Thrombin-Induced GPIb-IX Centralization on the Platelet Surface Requires Actin Assembly and Myosin II Activation. *Blood,* 87**,** 618-629.

KOWATA, S., ISOGAI, S., MURAI, K., ITO, S., TOHYAMA, K., EMA, M., HITOMI, J. & ISHIDA, Y. 2014. Platelet demand modulates the type of intravascular protrusion of megakaryocytes in bone marrow. *Thromb Haemost,* 112**,** 743-56.

KRAUSE, M. & GAUTREAU, A. 2014. Steering cell migration: lamellipodium dynamics and the regulation of directional persistence. *Nature Reviews Molecular Cell Biology,* 15**,** 577-590.

KUWAHARA, M., SUGIMOTO, M., TSUJI, S., MIYATA, S. & YOSHIOKA, A. 1999. Cytosolic Calcium Changes in a Process of Platelet Adhesion and Cohesion on a von Willebrand Factor-Coated Surface Under Flow Conditions: Presented in part at the American Society of Hematology Meeting in Miami Beach, FL, December 4-8, 1998 (abstr no. 1423). *Blood,* 94**,** 1149-1155.

LAKOWICZ, J. R. 2006. *Principles of fluorescence spectroscopy*, Springer.

LAU, L. M., WEE, J. L., WRIGHT, M. D., MOSELEY, G. W., HOGARTH, P. M., ASHMAN, L. K. & JACKSON, D. E. 2004. The tetraspanin superfamily member CD151 regulates outside-in integrin alphaIIbbeta3 signaling and platelet function. *Blood,* 104**,** 2368-75.

LECUT, C., FEENEY, L. A., KINGSBURY, G., HOPKINS, J., LANZA, F., GACHET, C., VILLEVAL, J.-L. & JANDROT-PERRUS, M. 2003. Human platelet glycoprotein VI function is antagonized by monoclonal antibody-derived Fab fragments. *Journal of Thrombosis and Haemostasis,* 1**,** 2653-2662.

LEE, S., BATJIKH, I. & KANG, S. H. 2020. Toward Sub-Diffraction Imaging of Single-DNA Molecule Sensors Based on Stochastic Switching Localization Microscopy. *Sensors,* 20**,** 6667.

LI, J., YIN, W., JING, Y., KANG, D., YANG, L., CHENG, J., YU, Z., PENG, Z., LI, X., WEN, Y., SUN, X., REN, B. & LIU, C. 2019. The Coordination Between B Cell Receptor Signaling and the Actin Cytoskeleton During B Cell Activation. *Frontiers in Immunology,* 9.

LI, R. 2022. Recent advances on GPIb-IX-V complex. *Platelets,* 33**,** 809-810.

LI, Z., DELANEY, M. K., O'BRIEN, K. A. & DU, X. 2010. Signaling During Platelet Adhesion and Activation. *Arteriosclerosis, Thrombosis, and Vascular Biology,* 30**,** 2341-2349.

LIANG, X., SYED, A. K., RUSSELL, S. R., WARE, J. & LI, R. 2016. Dimerization of glycoprotein Ibα is not sufficient to induce platelet clearance. *Journal of Thrombosis and Haemostasis,* 14**,** 381-386.

LICKERT, S., SORRENTINO, S., STUDT, J.-D., MEDALIA, O., VOGEL, V. & SCHOEN, I. 2018. Morphometric analysis of spread platelets identifies integrin α(IIb)β(3)-specific contractile phenotype. *Scientific reports,* 8**,** 5428-5428.

LITJENS, P. E. M. H., KRONER, C. I., AKKERMAN, J. W. N. & VAN WILLIGEN, G. 2003. Cytoplasmic regions of the beta3 subunit of integrin alphaIIbbeta3 involved in platelet adhesion on fibrinogen under flow conditions. *Journal of Thrombosis and Haemostasis,* 1**,** 2014-2021.

LOYAU, S., DUMONT, B., OLLIVIER, V., BOULAFTALI, Y., FELDMAN, L., AJZENBERG, N. & JANDROT-PERRUS, M. 2012. Platelet glycoprotein VI dimerization, an active process inducing receptor competence, is an indicator of platelet reactivity. *Arteriosclerosis, thrombosis, and vascular biology,* 32**,** 778-785.

MAMMADOVA-BACH, E., OLLIVIER, V., LOYAU, S., SCHAFF, M., DUMONT, B., FAVIER, R., FREYBURGER, G., LATGER-CANNARD, V., NIESWANDT, B., GACHET, C., MANGIN, P. H. & JANDROT-PERRUS, M. 2015. Platelet glycoprotein VI binds to polymerized fibrin and promotes thrombin generation. *Blood,* 126**,** 683-91.

MANDERS, E., VERBEEK, F. & ATEN, J. 1993. Measurement of co-localization of objects in dual-colour confocal images. *Journal of microscopy,* 169**,** 375-382.

MANGIN, H. M., MARIE-BLANCHE, O., NICOLAS, R., NICOLAS LE, L., ALEXANDER, T. H., CLARE, W., XIMENA, S., STÉPHANE, L., ARNAUD, D., AMIR, K. B., JEANETTE, L. C. M., HELEN, P., CRAIG, E. H., ANDREW, B. H., ROBERT, A. S. A., DIEGO, M., MARTINE, J.-P., CHRISTIAN, G. & STEVE, P. W. 2018. Immobilized fibrinogen activates human platelets through glycoprotein VI. *Haematologica,* 103**,** 898-907.

MARSHALL, S. J., ASAZUMA, N., BEST, D., WONEROW, P., SALMON, G., ANDREWS, R. K. & WATSON, S. P. 2002. Glycoprotein IIb-IIIa-dependent aggregation by glycoprotein Ibα is reinforced by a Src family kinase inhibitor (PP1)-sensitive signalling pathway. *Biochemical Journal,* 361**,** 297-305.

MATKÓ, J., MÁTYUS, L., SZÖLLÖSI, J., BENE, L., JENEI, A., NAGY, P., BODNÁR, A. & DAMJANOVICH, S. 1994. Analysis of cell surface molecular distributions and cellular signaling by flow cytometry. *Journal of Fluorescence,* 4**,** 303-314.

MATTHEWS, A. L., NOY, P. J., REYAT, J. S. & TOMLINSON, M. G. 2017. Regulation of A disintegrin and metalloproteinase (ADAM) family sheddases ADAM10 and ADAM17: The emerging role of tetraspanins and rhomboids. *Platelets,* 28**,** 333-341.

MAYR, S., HAUSER, F., PETERBAUER, A., TAUSCHER, A., NADERER, C., AXMANN, M., PLOCHBERGER, B. & JACAK, J. 2018. Localization Microscopy of Actin Cytoskeleton in Human Platelets. *International journal of molecular sciences,* 19**,** 1150.

MCCARTY, O. J. T., LARSON, M. K., AUGER, J. M., KALIA, N., ATKINSON, B. T., PEARCE, A. C., RUF, S., HENDERSON, R. B., TYBULEWICZ, V. L. J., MACHESKY, L. M. & WATSON, S. P. 2005. Rac1 Is Essential for Platelet Lamellipodia Formation and Aggregate Stability under Flow. *Journal of Biological Chemistry,* 280**,** 39474-39484.

MCEVER, R. P. 2007. P-selectin/PSGL-1 and other interactions between platelets, leukocytes, and endothelium. *Platelets,* 2**,** 231-49.

MCEWAN, P. A., YANG, W., CARR, K. H., MO, X., ZHENG, X., LI, R. & EMSLEY, J. 2011. Quaternary organization of GPIb-IX complex and insights into Bernard-Soulier syndrome revealed by the structures of GPIbβ and a GPIbβ/GPIX chimera. *Blood,* 118**,** 5292-5301.

MICHELSON, A. D., CATTANEO, M., FRELINGER, A. & NEWMAN, P. 2019. *Platelets*, Academic press.

MIKHAYLOVA, M., CLOIN, B. M. C., FINAN, K., VAN DEN BERG, R., TEEUW, J., KIJANKA, M. M., SOKOLOWSKI, M., KATRUKHA, E. A., MAIDORN, M., OPAZO, F., MOUTEL, S., VANTARD, M., PEREZ, F., VAN BERGEN EN

HENEGOUWEN, P. M. P., HOOGENRAAD, C. C., EWERS, H. & KAPITEIN, L. C. 2015. Resolving bundled microtubules using anti-tubulin nanobodies. *Nature Communications,* 6**,** 7933.

MISTRY, N., CRANMER, S. L., YUAN, Y., MANGIN, P., DOPHEIDE, S. M., HARPER, I., GIULIANO, S., DUNSTAN, D. E., LANZA, F., SALEM, H. H. & JACKSON, S. P. 2000. Cytoskeletal regulation of the platelet glycoprotein Ib/V/IX-von willebrand factor interaction. *Blood,* 96**,** 3480-9.

MIURA, Y., TAKAHASHI, T., JUNG, S. M. & MOROI, M. 2002. Analysis of the interaction of platelet collagen receptor glycoprotein VI (GPVI) with collagen. A dimeric form of GPVI, but not the monomeric form, shows affinity to fibrous collagen. *J Biol Chem,* 277**,** 46197-204.

MOLDOVAN, L., IRANI, K., MOLDOVAN, N. I., FINKEL, T. & GOLDSCHMIDT-CLERMONT, P. J. 1999. The actin cytoskeleton reorganization induced by Rac1 requires the production of superoxide. *Antioxid Redox Signal,* 1**,** 29-43.

MOLLE, J., RAAB, M., HOLZMEISTER, S., SCHMITT-MONREAL, D., GROHMANN, D., HE, Z. & TINNEFELD, P. 2016. Superresolution microscopy with transient binding. *Current Opinion in Biotechnology,* 39**,** 8-16.

MONTAGUE, S. J., DELIERNEUX, C., LECUT, C., LAYIOS, N., DINSDALE, R. J., LEE, C. S. M., POULTER, N. S., ANDREWS, R. K., HAMPSON, P., WEARN, C. M., MAES, N., BISHOP, J., BAMFORD, A., GARDINER, C., LEE, W. M., IQBAL, T., MOIEMEN, N., WATSON, S. P., OURY, C., HARRISON, P. & GARDINER, E. E. 2018. Soluble GPVI is elevated in injured patients: shedding is mediated by fibrin activation of GPVI. *Blood Advances,* 2**,** 240-251.

MONTAGUE, S. J., LIM, Y. J., LEE, W. M. & GARDINER, E. E. 2020. Imaging Platelet Processes and Function—Current and Emerging Approaches for Imaging in vitro and in vivo. *Frontiers in Immunology,* 11.

MOOG, S., MANGIN, P., LENAIN, N., STRASSEL, C., RAVANAT, C., SCHUHLER, S., FREUND, M., SANTER, M., KAHN, M., NIESWANDT, B., GACHET, C., CAZENAVE, J. P. & LANZA, F. 2001. Platelet glycoprotein V binds to collagen and participates in platelet adhesion and aggregation. *Blood,* 98**,** 1038-46.

MOROI, M., FARNDALE, R. W. & JUNG, S. M. 2020. Activation-induced changes in platelet surface receptor expression and the contribution of the large-platelet subpopulation to activation. *Research and Practice in Thrombosis and Haemostasis,* 4**,** 285-297.

MOROI, M. & JUNG, S. M. 2004. Platelet glycoprotein VI: its structure and function. *Thrombosis research,* 114**,** 221-233.

MOROI, M., JUNG, S. M., OKUMA, M. & SHINMYOZU, K. 1989. A patient with platelets deficient in glycoprotein VI that lack both collagen-induced aggregation and adhesion. *The Journal of Clinical Investigation,* 84**,** 1440-1445.

MORTON, L., HARGREAVES, P., FARNDALE, R., YOUNG, R. & BARNES, M. 1995a. Integrin α 2 β 1-independent activation of platelets by simple collagen-like peptides: collagen tertiary (triple-helical) and quaternary (polymeric) structures are sufficient alone for α 2 β 1-independent platelet reactivity. *Biochemical Journal,* 306**,** 337-344.

MORTON, L. F., HARGREAVES, P. G., FARNDALE, R. W., YOUNG, R. D. & BARNES, M. J. 1995b. Integrin α2β1-independent activation of platelets by simple collagen-like peptides: collagen tertiary (triple-helical) and quaternary (polymeric) structures are sufficient alone for α2β1-independent platelet reactivity. *Biochem. J.,* 306**,** 337.

MURAI, T., MIYAUCHI, T., YANAGIDA, T. & SAKO, Y. 2006. Epidermal growth factor-regulated activation of Rac GTPase enhances CD44 cleavage by metalloproteinase disintegrin ADAM10. *Biochemical Journal,* 395**,** 65-71.

NAGY, P., VEREB, G., POST, J. N., FRIEDLÄNDER, E. & SZÖLLOŐSI, J. 2005. Novel single cell fluorescence approaches in the investigation of signaling at the cellular level. *Biophysical aspects of transmembrane signaling.* Springer.

NAVARRO, S., STARKE, A., HEEMSKERK, J. W. M., KUIJPERS, M. J. E., STEGNER, D. & NIESWANDT, B. 2022. Targeting of a Conserved Epitope in Mouse and Human GPVI Differently Affects Receptor Function. *International Journal of Molecular Sciences,* 23**,** 8610.

NEAGOE, R. A. I., GARDINER, E. E., STEGNER, D., NIESWANDT, B., WATSON, S. P. & POULTER, N. S. 2022. Rac Inhibition Causes Impaired GPVI Signalling in Human Platelets through GPVI Shedding and Reduction in PLCγ2 Phosphorylation. *International Journal of Molecular Sciences,* 23**,** 3746.

NEIL, M. A. A., JUŠKAITIS, R. & WILSON, T. 1997. Method of obtaining optical sectioning by using structured light in a conventional microscope. *Optics Letters,* 22**,** 1905-1907.

NEWLAND, S. A., MACAULAY, I. C., FLOTO, A. R., DE VET, E. C., OUWEHAND, W. H., WATKINS, N. A., LYONS, P. A. & CAMPBELL, D. R. 2007. The novel inhibitory receptor G6B is expressed on the surface of platelets and attenuates platelet function in vitro. *Blood, The Journal of the American Society of Hematology,* 109**,** 4806-4809.

NICOLAI, L., SCHIEFELBEIN, K., LIPSKY, S., LEUNIG, A., HOFFKNECHT, M., PEKAYVAZ, K., RAUDE, B., MARX, C., EHRLICH, A., PIRCHER, J., ZHANG, Z., SALEH, I., MAREL, A.-K., LÖF, A., PETZOLD, T., LORENZ, M., STARK, K., PICK, R., ROSENBERGER, G., WECKBACH, L., UHL, B., XIA, S., REICHEL, C. A., WALZOG, B., SCHULZ, C., ZHEDEN, V., BENDER, M., LI, R., MASSBERG, S. & GAERTNER, F. 2020. Vascular surveillance by haptotactic blood platelets in inflammation and infection. *Nature Communications,* 11**,** 5778.

NIESWANDT, B. 2001. Glycoprotein VI but not alpha2beta1 integrin is essential for platelet interaction with collagen. *The EMBO Journal,* 20**,** 2120-2130.

NIESWANDT, B., BERGMEIER, W., RACKEBRANDT, K., GESSNER, J. E. & ZIRNGIBL, H. 2000a. Identification of critical antigen-specific mechanisms in the development of immune thrombocytopenic purpura in mice. *Blood,* 96**,** 2520-2527.

NIESWANDT, B., BERGMEIER, W., SCHULTE, V., RACKEBRANDT, K., GESSNER, J. E. & ZIRNGIBL, H. 2000b. Expression and Function of the Mouse Collagen Receptor Glycoprotein VI Is Strictly Dependent on Its Association with the FcRγ Chain *. *Journal of Biological Chemistry,* 275**,** 23998-24002.

NIESWANDT, B., ECHTENACHER, B., WACHS, F.-P., SCHRÖDER, J., GESSNER, J. E., SCHMIDT, R. E., GRAU, G. E. & MÄNNEL, D. N. 1999a. Acute Systemic Reaction and Lung Alterations Induced by an Antiplatelet Integrin gpIIb/IIIa Antibody in Mice. *Blood,* 94**,** 684-693.

NIESWANDT, B., HAFNER, M., ECHTENACHER, B. & MÄNNEL, D. N. 1999b. Lysis of tumor cells by natural killer cells in mice is impeded by platelets. *Cancer Res,* 59**,** 1295-300.

NIESWANDT, B., KLEINSCHNITZ, C. & STOLL, G. 2011a. Ischaemic stroke: a thrombo-inflammatory disease? *J Physiol,* 589**,** 4115-23.

NIESWANDT, B., PLEINES, I. & BENDER, M. 2011b. Platelet adhesion and activation mechanisms in arterial thrombosis and ischaemic stroke. *Journal of Thrombosis and Haemostasis,* 9**,** 92-104.

NIESWANDT, B., SCHULTE, V., BERGMEIER, W., MOKHTARI-NEJAD, R., RACKEBRANDT, K., CAZENAVE, J. P., OHLMANN, P., GACHET, C. & ZIRNGIBL, H. 2001. Long-term antithrombotic protection by in vivo depletion of platelet glycoprotein VI in mice. *J Exp Med,* 193**,** 459-69.

NIESWANDT, B. & WATSON, S. P. 2003. Platelet-collagen interaction: is GPVI the central receptor? *Blood,* 102**,** 449-461.
NURDEN, A. T. & CAEN, J. P. 1975. Specific roles for platelet surface glycoproteins in platelet function. *Nature,* 255**,** 720-2.
OFFERMANNS, S., TOOMBS, C. F., HU, Y. H. & SIMON, M. I. 1997. Defective platelet activation in G alpha(q)-deficient mice. *Nature,* 389**,** 183-6.
OKAMOTO, K. & SAKO, Y. 2017. Recent advances in FRET for the study of protein interactions and dynamics. *Current opinion in structural biology,* 46**,** 16-23.
OVESNÝ, M., KŘÍŽEK, P., BORKOVEC, J., ŠVINDRYCH, Z. & HAGEN, G. M. 2014. ThunderSTORM: a comprehensive ImageJ plug-in for PALM and STORM data analysis and super-resolution imaging. *Bioinformatics,* 30**,** 2389-2390.
OZAKI, Y., ASAZUMA, N., SUZUKI-INOUE, K. & BERNDT, M. C. 2005. Platelet GPIb-IX-V-dependent signaling. *Journal of Thrombosis and Haemostasis,* 3**,** 1745-1751.
PALLIKKUTH, S., MARTIN, C., FARZAM, F., EDWARDS, J. S., LAKIN, M. R., LIDKE, D. S. & LIDKE, K. A. 2018. Sequential super-resolution imaging using DNA strand displacement. *PLoS One,* 13**,** e0203291.
PALLINI, C. 2020. *GPVI receptor spatial organisation and signalling in platelets*, University of, Birmingham.
PALLINI, C., PIKE, J. A., O'SHEA, C., ANDREWS, R. K., GARDINER, E. E., WATSON, S. P. & POULTER, N. S. 2021. Immobilized collagen prevents shedding and induces sustained GPVI clustering and signaling in platelets. *Platelets,* 32**,** 59-73.
PANDEY, D., GOYAL, P., DWIVEDI, S. & SIESS, W. 2009. Unraveling a novel Rac1-mediated signaling pathway that regulates cofilin dephosphorylation and secretion in thrombin-stimulated platelets. *Blood,* 114**,** 415-424.
PASQUET, J. M., GROSS, B., QUEK, L., ASAZUMA, N., ZHANG, W., SOMMERS, C. L., SCHWEIGHOFFER, E., TYBULEWICZ, V., JUDD, B., LEE, J. R., KORETZKY, G., LOVE, P. E., SAMELSON, L. E. & WATSON, S. P. 1999. LAT is required for tyrosine phosphorylation of phospholipase cgamma2 and platelet activation by the collagen receptor GPVI. *Mol Cell Biol,* 19**,** 8326-34.
PATEL-HETT, S., RICHARDSON, J. L., SCHULZE, H., DRABEK, K., ISAAC, N. A., HOFFMEISTER, K., SHIVDASANI, R. A., BULINSKI, J. C., GALJART, N., HARTWIG, J. H. & ITALIANO, J. E., JR. 2008. Visualization of microtubule growth in living platelets reveals a dynamic marginal band with multiple microtubules. *Blood,* 111**,** 4605-16.
PATEL, L., WILLIAMSON, D., OWEN, D. M. & COHEN, E. A. K. 2021. Blinking statistics and molecular counting in direct stochastic reconstruction microscopy (dSTORM). *Bioinformatics,* 37**,** 2730-2737.
PERIAYAH, M. H., HALIM, A. S. & MAT SAAD, A. Z. 2017. Mechanism Action of Platelets and Crucial Blood Coagulation Pathways in Hemostasis. *Int J Hematol Oncol Stem Cell Res,* 11**,** 319-327.
PIAZZA, G. A. & WALLACE, R. W. 1985. Calmodulin accelerates the rate of polymerization of human platelet actin and alters the structural characteristics of actin filaments. *Proc Natl Acad Sci U S A,* 82**,** 1683-7.
PIECHULEK, T., REHLEN, T., WALLISER, C., VATTER, P., MOEPPS, B. & GIERSCHIK, P. 2005. Isozyme-specific Stimulation of Phospholipase C-γ2 by Rac GTPases. *Journal of Biological Chemistry,* 280**,** 38923-38931.
PIKE, J. A., KHAN, A. O., PALLINI, C., THOMAS, S. G., MUND, M., RIES, J., POULTER, N. S. & STYLES, I. B. 2019. Topological data analysis quantifies biological nano-structure from single molecule localization microscopy. *Bioinformatics,* 36**,** 1614-1621.

PIKE, J. A., SIMMS, V. A., SMITH, C. W., MORGAN, N. V., KHAN, A. O., POULTER, N. S., STYLES, I. B. & THOMAS, S. G. 2021. An adaptable analysis workflow for characterization of platelet spreading and morphology. *Platelets,* 32**,** 54-58.

PLEINES, I., ECKLY, A., ELVERS, M., HAGEDORN, I., ELIAUTOU, S., BENDER, M., WU, X., LANZA, F., GACHET, C., BRAKEBUSCH, C. & NIESWANDT, B. 2010. Multiple alterations of platelet functions dominated by increased secretion in mice lacking Cdc42 in platelets. *Blood,* 115**,** 3364-73.

PLEINES, I., ELVERS, M., STREHL, A., POZGAJOVA, M., VARGA-SZABO, D., MAY, F., CHROSTEK-GRASHOFF, A., BRAKEBUSCH, C. & NIESWANDT, B. 2009. Rac1 is essential for phospholipase C-γ2 activation in platelets. *Pflügers Archiv - European Journal of Physiology,* 457**,** 1173-1185.

PLEINES, I., HAGEDORN, I., GUPTA, S., MAY, F., CHAKAROVA, L., VAN HENGEL, J., OFFERMANNS, S., KROHNE, G., KLEINSCHNITZ, C., BRAKEBUSCH, C. & NIESWANDT, B. 2012. Megakaryocyte-specific RhoA deficiency causes macrothrombocytopenia and defective platelet activation in hemostasis and thrombosis. *Blood,* 119**,** 1054-63.

PLUTHERO, F. G. & KAHR, W. H. A. 2018. Imaging Platelets and Megakaryocytes by High-Resolution Laser Fluorescence Microscopy. *Methods Mol Biol,* 1812**,** 13-31.

POLLITT, A. Y., GRYGIELSKA, B., LEBLOND, B., DÉSIRÉ, L., EBLE, J. A. & WATSON, S. P. 2010. Phosphorylation of CLEC-2 is dependent on lipid rafts, actin polymerization, secondary mediators, and Rac. *Blood,* 115**,** 2938-2946.

POLLITT, A. Y., POULTER, N. S., GITZ, E., NAVARRO-NUÑEZ, L., WANG, Y.-J., HUGHES, C. E., THOMAS, S. G., NIESWANDT, B., DOUGLAS, M. R., OWEN, D. M., JACKSON, D. G., DUSTIN, M. L. & WATSON, S. P. 2014. Syk and Src Family Kinases Regulate C-type Lectin Receptor 2 (CLEC-2)-mediated Clustering of Podoplanin and Platelet Adhesion to Lymphatic Endothelial Cells. *Journal of Biological Chemistry,* 289**,** 35695-35710.

POOLE, A., GIBBINS, J. M., TURNER, M., VAN VUGT, M. J., VAN DE WINKEL, J. G. J., SAITO, T., TYBULEWICZ, V. L. J. & WATSON, S. P. 1997. The Fc receptor γ-chain and the tyrosine kinase Syk are essential for activation of mouse platelets by collagen. *The EMBO Journal,* 16**,** 2333-2341.

POULTER, N. S., POLLITT, A. Y., DAVIES, A., MALINOVA, D., NASH, G. B., HANNON, M. J., PIKRAMENOU, Z., RAPPOPORT, J. Z., HARTWIG, J. H., OWEN, D. M., THRASHER, A. J., WATSON, S. P. & THOMAS, S. G. 2015. Platelet actin nodules are podosome-like structures dependent on Wiskott–Aldrich syndrome protein and ARP2/3 complex. *Nature Communications,* 6**,** 7254.

POULTER, N. S., POLLITT, A. Y., OWEN, D. M., GARDINER, E. E., ANDREWS, R. K., SHIMIZU, H., ISHIKAWA, D., BIHAN, D., FARNDALE, R. W., MOROI, M., WATSON, S. P. & JUNG, S. M. 2017. Clustering of glycoprotein VI (GPVI) dimers upon adhesion to collagen as a mechanism to regulate GPVI signaling in platelets. *Journal of Thrombosis and Haemostasis,* 15**,** 549-564.

QIAO, J., SCHOENWAELDER, S. M., MASON, K. D., TRAN, H., DAVIS, A. K., KAPLAN, Z. S., JACKSON, S. P., KILE, B. T., ANDREWS, R. K., ROBERTS, A. W. & GARDINER, E. E. 2013. Low adhesion receptor levels on circulating platelets in patients with lymphoproliferative diseases prior to receiving Navitoclax (ABT-263). *Blood,* 121**,** 1479.

QUACH, M. E., CHEN, W. & LI, R. 2018a. Mechanisms of platelet clearance and translation to improve platelet storage. *Blood,* 131**,** 1512-1521.

QUACH, M. E., DRAGOVICH, M. A., CHEN, W., SYED, A. K., CAO, W., LIANG, X., DENG, W., DE MEYER, S. F., ZHU, G., PENG, J., NI, H., BENNETT, C. M., HOU, M., WARE, J., DECKMYN, H., ZHANG, X. F. & LI, R. 2018b. Fc-

independent immune thrombocytopenia via mechanomolecular signaling in platelets. *Blood,* 131**,** 787-796.
QUEK, L., BOLEN, J. & WATSON, S. 1998. A role for Bruton's tyrosine kinase (Btk) in platelet activation by collagen. *Current biology,* 8**,** 1137-S1.
QUEK, L. S., PASQUET, J.-M., HERS, I., CORNALL, R., KNIGHT, G., BARNES, M., HIBBS, M. L., DUNN, A. R., LOWELL, C. A. & WATSON, S. P. 2000. Fyn and Lyn phosphorylate the Fc receptor γ chain downstream of glycoprotein VI in murine platelets, and Lyn regulates a novel feedback pathway. *Blood, The Journal of the American Society of Hematology,* 96**,** 4246-4253.
RABIE, T., STREHL, A., LUDWIG, A. & NIESWANDT, B. 2005. Evidence for a Role of ADAM17 (TACE) in the Regulation of Platelet Glycoprotein V. *Journal of Biological Chemistry,* 280**,** 14462-14468.
RABIE, T., VARGA-SZABO, D., BENDER, M., POZGAJ, R., LANZA, F., SAITO, T., WATSON, S. P. & NIESWANDT, B. 2007. Diverging signaling events control the pathway of GPVI down-regulation in vivo. *Blood,* 110**,** 529-535.
RADOMSKI, M. W., PALMER, R. & MONCADA, S. 1987. The anti-aggregating properties of vascular endothelium: interactions between prostacyclin and nitric oxide. *British journal of pharmacology,* 92**,** 639.
RAMAKRISHNAN, V., DEGUZMAN, F., BAO, M., HALL, S. W., LEUNG, L. L. & PHILLIPS, D. R. 2001. A thrombin receptor function for platelet glycoprotein Ib–IX unmasked by cleavage of glycoprotein V. *Proceedings of the National Academy of Sciences,* 98**,** 1823-1828.
RANJAN, R. & CHEN, X. 2021. Super-Resolution Live Cell Imaging of Subcellular Structures. *J Vis Exp*.
RAYES, J., SOUMAYA, J., SIÂN, L., ANGÈLE, G., SURASAK, W., VÉRONIQUE, O., CÉCILE, V. D., JERRY, W., BERNHARD, N., MARTINE, J.-P., STEVE, P. W. & BENOÎT, H.-T.-N. 2018. The contribution of platelet glycoprotein receptors to inflammatory bleeding prevention is stimulus and organ dependent. *Haematologica,* 103**,** e256-e258.
REDDY, E. C. & RAND, M. L. 2020. Procoagulant Phosphatidylserine-Exposing Platelets in vitro and in vivo. *Front Cardiovasc Med,* 7**,** 15.
RICHARDSON, J. L., SHIVDASANI, R. A., BOERS, C., HARTWIG, J. H. & ITALIANO JR, J. E. 2005. Mechanisms of organelle transport and capture along proplatelets during platelet production. *Blood,* 106**,** 4066-4075.
RIVERA, J., LOZANO, M. L., NAVARRO-NÚÑEZ, L. & VICENTE, V. 2009. Platelet receptors and signaling in the dynamics of thrombus formation. *Haematologica,* 94**,** 700-11.
ROMO, G. M., DONG, J.-F., SCHADE, A. J., GARDINER, E. E., KANSAS, G. S., LI, C. Q., MCINTIRE, L. V., BERNDT, M. C. & LÓPEZ, J. A. 1999. The glycoprotein Ib-IX-V complex is a platelet counterreceptor for P-selectin. *The Journal of experimental medicine,* 190**,** 803-814.
ROSSY, J., OWEN, D. M., WILLIAMSON, D. J., YANG, Z. & GAUS, K. 2013. Conformational states of the kinase Lck regulate clustering in early T cell signaling. *Nat Immunol,* 14**,** 82-9.
ROTH, G. A., MENSAH, G. A., JOHNSON, C. O., ADDOLORATO, G., AMMIRATI, E., BADDOUR, L. M., BARENGO, N. C., BEATON, A. Z., BENJAMIN, E. J., BENZIGER, C. P., BONNY, A., BRAUER, M., BRODMANN, M., CAHILL, T. J., CARAPETIS, J., CATAPANO, A. L., CHUGH, S. S., COOPER, L. T., CORESH, J., CRIQUI, M., DECLEENE, N., EAGLE, K. A., EMMONS-BELL, S., FEIGIN, V. L., FERNÁNDEZ-SOLÀ, J., FOWKES, G., GAKIDOU, E., GRUNDY, S. M., HE, F. J., HOWARD, G., HU, F., INKER, L., KARTHIKEYAN, G., KASSEBAUM, N., KOROSHETZ, W., LAVIE, C., LLOYD-JONES, D., LU, H. S., MIRIJELLO, A., TEMESGEN, A. M., MOKDAD, A., MORAN, A. E., MUNTNER, P., NARULA, J.,

NEAL, B., NTSEKHE, M., MORAES DE OLIVEIRA, G., OTTO, C., OWOLABI, M., PRATT, M., RAJAGOPALAN, S., REITSMA, M., RIBEIRO, A. L. P., RIGOTTI, N., RODGERS, A., SABLE, C., SHAKIL, S., SLIWA-HAHNLE, K., STARK, B., SUNDSTRÖM, J., TIMPEL, P., TLEYJEH, I. M., VALGIMIGLI, M., VOS, T., WHELTON, P. K., YACOUB, M., ZUHLKE, L., MURRAY, C., FUSTER, V., ROTH, G. A., MENSAH, G. A., JOHNSON, C. O., ADDOLORATO, G., AMMIRATI, E., BADDOUR, L. M., BARENGO, N. C., BEATON, A., BENJAMIN, E. J., BENZIGER, C. P., BONNY, A., BRAUER, M., BRODMANN, M., CAHILL, T. J., CARAPETIS, J. R., CATAPANO, A. L., CHUGH, S., COOPER, L. T., CORESH, J., CRIQUI, M. H., DECLEENE, N. K., EAGLE, K. A., EMMONS-BELL, S., FEIGIN, V. L., FERNÁNDEZ-SOLA, J., FOWKES, F. G. R., GAKIDOU, E., GRUNDY, S. M., HE, F. J., HOWARD, G., HU, F., et al. 2020a. Global Burden of Cardiovascular Diseases and Risk Factors, 1990–2019: Update From the GBD 2019 Study. *Journal of the American College of Cardiology,* 76**,** 2982-3021.

ROTH, J., MEHL, J. & ROHRBACH, A. 2020b. Fast TIRF-SIM imaging of dynamic, low-fluorescent biological samples. *Biomed Opt Express,* 11**,** 4008-4026.

RUGGERI, Z. M., ZARPELLON, A., ROBERTS, J. R., MC CLINTOCK, R. A., JING, H. & MENDOLICCHIO, G. L. 2010. Unravelling the mechanism and significance of thrombin binding to platelet glycoprotein Ib. *Thromb Haemost,* 104**,** 894-902.

RUST, M. J., BATES, M. & ZHUANG, X. 2006. Sub-diffraction-limit imaging by stochastic optical reconstruction microscopy (STORM). *Nature Methods,* 3**,** 793-796.

SABOOR, M., AYUB, Q., ILYAS, S. & MOINUDDIN 2013. Platelet receptors; an instrumental of platelet physiology. *Pak J Med Sci,* 29**,** 891-6.

SAMBRANO, J., CHIGAEV, A., NICHANI, K. S., SMAGLEY, Y., SKLAR, L. A. & HOUSTON, J. P. 2018. Evaluating integrin activation with time-resolved flow cytometry. *J Biomed Opt,* 23**,** 1-10.

SANTILLI, F., SIMEONE, P., LIANI, R. & DAVÌ, G. 2015. Platelets and diabetes mellitus. *Prostaglandins Other Lipid Mediat,* 120**,** 28-39.

SCHAKS, M., DÖRING, H., KAGE, F., STEFFEN, A., KLÜNEMANN, T., BLANKENFELDT, W., STRADAL, T. & ROTTNER, K. 2021. RhoG and Cdc42 can contribute to Rac-dependent lamellipodia formation through WAVE regulatory complex-binding. *Small GTPases,* 12**,** 122-132.

SCHNITZBAUER, J., STRAUSS, M. T., SCHLICHTHAERLE, T., SCHUEDER, F. & JUNGMANN, R. 2017. Super-resolution microscopy with DNA-PAINT. *Nature Protocols,* 12**,** 1198-1228.

SCHULTE, V., RABIE, T., PROSTREDNA, M., AKTAS, B., GRÜNER, S. & NIESWANDT, B. 2003. Targeting of the collagen-binding site on glycoprotein VI is not essential for in vivo depletion of the receptor. *Blood, The Journal of the American Society of Hematology,* 101**,** 3948-3952.

SCHURR, Y., SPERR, A., VOLZ, J., BECK, S., REIL, L., KUSCH, C., EIRING, P., BRYSON, S., SAUER, M., NIESWANDT, B., MACHESKY, L. & BENDER, M. 2019. Platelet lamellipodium formation is not required for thrombus formation and stability. *Blood,* 134**,** 2318-2329.

SELVADURAI, M. V. & HAMILTON, J. R. 2018. Structure and function of the open canalicular system - the platelet's specialized internal membrane network. *Platelets,* 29**,** 319-325.

SEVLEVER, D., JIANG, P. & YEN, S. H. 2008. Cathepsin D is the main lysosomal enzyme involved in the degradation of alpha-synuclein and generation of its carboxy-terminally truncated species. *Biochemistry,* 47**,** 9678-87.

SHARONOV, A. & HOCHSTRASSER, R. M. 2006. Wide-field subdiffraction imaging by accumulated binding of diffusing probes. *Proceedings of the National Academy of Sciences,* 103**,** 18911-18916.

SHATTIL, S. J. & NEWMAN, P. J. 2004. Integrins: dynamic scaffolds for adhesion and signaling in platelets. *Blood,* 104**,** 1606-15.

SHI, X., LI, Q., DAI, Z., TRAN, A. A., FENG, S., RAMIREZ, A. D., LIN, Z., WANG, X., CHOW, T. T., CHEN, J., KUMAR, D., MCCOLLOCH, A. R., REITER, J. F., HUANG, E. J., SEIPLE, I. B. & HUANG, B. 2021. Label-retention expansion microscopy. *Journal of Cell Biology,* 220.

SHRIMPTON , C. N., BORTHAKUR , G., LARRUCEA , S., CRUZ , M. A., DONG , J.-F. & LÓPEZ , J. A. 2002. Localization of the Adhesion Receptor Glycoprotein Ib-IX-V Complex to Lipid Rafts Is Required for Platelet Adhesion and Activation. *Journal of Experimental Medicine,* 196**,** 1057-1066.

SHUTES, A., ONESTO, C., PICARD, V., LEBLOND, B., SCHWEIGHOFFER, F. & DER, C. J. 2007. Specificity and mechanism of action of EHT 1864, a novel small molecule inhibitor of Rac family small GTPases. *J Biol Chem,* 282**,** 35666-78.

SIMON, D. I., CHEN, Z., XU, H., LI, C. Q., DONG, J., MCINTIRE, L. V., BALLANTYNE, C. M., ZHANG, L., FURMAN, M. I., BERNDT, M. C. & LÓPEZ, J. A. 2000. Platelet glycoprotein ibalpha is a counterreceptor for the leukocyte integrin Mac-1 (CD11b/CD18). *J Exp Med,* 192**,** 193-204.

ŠKERLE, J., HUMPOLÍČKOVÁ, J., JOHNSON, N., RAMPÍROVÁ, P., POLÁCHOVÁ, E., FLIEGL, M., DOHNÁLEK, J., SUCHÁNKOVÁ, A., JAKUBEC, D. & STRISOVSKY, K. 2020. Membrane Protein Dimerization in Cell-Derived Lipid Membranes Measured by FRET with MC Simulations. *Biophys J,* 118**,** 1861-1875.

SLATER, A., DI, Y., CLARK, J. C., JOOSS, N. J., MARTIN, E. M., ALENAZY, F., THOMAS, M. R., ARIËNS, R. A. S., HERR, A. B., POULTER, N. S., EMSLEY, J. & WATSON, S. P. 2021. Structural characterization of a novel GPVI-nanobody complex reveals a biologically active domain-swapped GPVI dimer. *Blood,* 137**,** 3443-3453.

SLATER, A., PERRELLA, G., ONSELAER, M.-B., MARTIN, E. M., GAUER, J. S., XU, R.-G., HEEMSKERK, J. W. M., ARIËNS, R. A. S. & WATSON, S. P. 2019. Does fibrin(ogen) bind to monomeric or dimeric GPVI, or not at all? *Platelets,* 30**,** 281-289.

SMETHURST, P. A., JOUTSI-KORHONEN, L., O'CONNOR, M. N., WILSON, E., JENNINGS, N. S., GARNER, S. F., ZHANG, Y., KNIGHT, C. G., DAFFORN, T. R., BUCKLE, A., MJ, I. J., DE GROOT, P. G., WATKINS, N. A., FARNDALE, R. W. & OUWEHAND, W. H. 2004. Identification of the primary collagen-binding surface on human glycoprotein VI by site-directed mutagenesis and by a blocking phage antibody. *Blood,* 103**,** 903-11.

SMITHERMAN, T. C., MILAM, M., WOO, J., WILLERSON, J. T. & FRENKEL, E. P. 1981. Elevated beta thromboglobulin in peripheral venous blood of patients with acute myocardial ischemia: direct evidence for enhanced platelet reactivity in vivo. *Am J Cardiol,* 48**,** 395-402.

SMYTH, E. M. 2010. Thromboxane and the thromboxane receptor in cardiovascular disease. *Clin Lipidol,* 5**,** 209-219.

SOMMER, C., STRAEHLE, C., KOTHE, U. & HAMPRECHT, F. A. Ilastik: Interactive learning and segmentation toolkit. 2011 2011. IEEE.

SØRENSEN, A. L., RUMJANTSEVA, V., NAYEB-HASHEMI, S., CLAUSEN, H., HARTWIG, J. H., WANDALL, H. H. & HOFFMEISTER, K. M. 2009. Role of sialic acid for platelet life span: exposure of beta-galactose results in the rapid

clearance of platelets from the circulation by asialoglycoprotein receptor-expressing liver macrophages and hepatocytes. *Blood,* 114**,** 1645-54.
STAATZ, W. D., RAJPARA, S. M., WAYNER, E. A., CARTER, W. G. & SANTORO, S. A. 1989. The membrane glycoprotein Ia-IIa (VLA-2) complex mediates the Mg++-dependent adhesion of platelets to collagen. *J Cell Biol,* 108**,** 1917-24.
STEFANINI, L., BOULAFTALI, Y., OUELLETTE, T. D., HOLINSTAT, M., DÉSIRÉ, L., LEBLOND, B., ANDRE, P., CONLEY, P. B. & BERGMEIER, W. 2012. Rap1-Rac1 circuits potentiate platelet activation. *Arteriosclerosis, thrombosis, and vascular biology,* 32**,** 434-441.
STRASSEL, C., MOOG, S., BAAS, M.-J., CAZENAVE, J.-P. & LANZA, F. 2004. Biosynthesis of platelet glycoprotein V expressed as a single subunit or in association with GPIb-IX. *European Journal of Biochemistry,* 271**,** 3671-3677.
SUGIYAMA, T., OKUMA, M., USHIKUBI, F., SENSAKI, S., KANAJI, K. & UCHINO, H. 1987. A Novel Platelet Aggregating Factor Found in a Patient With Defective Collagen-Induced Platelet Aggregation and Autoimmune Thrombocytopenia. *Blood,* 69**,** 1712-1720.
SULLAM, P. M., HYUN, W. C., SZÖLLÖSI, J., DONG, J.-F., FOSS, W. M. & LÓPEZ, J. A. 1998. Physical Proximity and Functional Interplay of the Glycoprotein Ib-IX-V Complex and the Fc Receptor FcγRIIA on the Platelet Plasma Membrane*. *Journal of Biological Chemistry,* 273**,** 5331-5336.
SUN, B., LI, J. & KAMBAYASHI, J. 1999. Interaction between GPIbalpha and FcgammaIIA receptor in human platelets. *Biochem Biophys Res Commun,* 266**,** 24-7.
SUOFU, Y., LI, W., JEAN-ALPHONSE, F. G., JIA, J., KHATTAR, N. K., LI, J., BARANOV, S. V., LERONNI, D., MIHALIK, A. C., HE, Y., CECON, E., WEHBI, V. L., KIM, J., HEATH, B. E., BARANOVA, O. V., WANG, X., GABLE, M. J., KRETZ, E. S., DI BENEDETTO, G., LEZON, T. R., FERRANDO, L. M., LARKIN, T. M., SULLIVAN, M., YABLONSKA, S., WANG, J., MINNIGH, M. B., GUILLAUMET, G., SUZENET, F., RICHARDSON, R. M., POLOYAC, S. M., STOLZ, D. B., JOCKERS, R., WITT-ENDERBY, P. A., CARLISLE, D. L., VILARDAGA, J. P. & FRIEDLANDER, R. M. 2017. Dual role of mitochondria in producing melatonin and driving GPCR signaling to block cytochrome c release. *Proc Natl Acad Sci U S A,* 114**,** E7997-e8006.
SUZUKI-INOUE, K., FULLER, G. L., GARCÍA, Á., EBLE, J. A., PÖHLMANN, S., INOUE, O., GARTNER, T. K., HUGHAN, S. C., PEARCE, A. C. & LAING, G. D. 2006. A novel Syk-dependent mechanism of platelet activation by the C-type lectin receptor CLEC-2. *Blood,* 107**,** 542-549.
SUZUKI-INOUE, K., INOUE, O., DING, G., NISHIMURA, S., HOKAMURA, K., ETO, K., KASHIWAGI, H., TOMIYAMA, Y., YATOMI, Y., UMEMURA, K., SHIN, Y., HIRASHIMA, M. & OZAKI, Y. 2010. Essential in vivo roles of the C-type lectin receptor CLEC-2: embryonic/neonatal lethality of CLEC-2-deficient mice by blood/lymphatic misconnections and impaired thrombus formation of CLEC-2-deficient platelets. *J Biol Chem,* 285**,** 24494-507.
SUZUKI-INOUE, K., KATO, Y., INOUE, O., KANEKO, M. K., MISHIMA, K., YATOMI, Y., YAMAZAKI, Y., NARIMATSU, H. & OZAKI, Y. 2007. Involvement of the snake toxin receptor CLEC-2, in podoplanin-mediated platelet activation, by cancer cells. *J Biol Chem,* 282**,** 25993-6001.
SUZUKI-INOUE, K., TULASNE, D., SHEN, Y., BORI-SANZ, T., INOUE, O., JUNG, S. M., MOROI, M., ANDREWS, R. K., BERNDT, M. C. & WATSON, S. P. 2002. Association of Fyn and Lyn with the proline-rich domain of glycoprotein VI regulates intracellular signaling. *Journal of Biological Chemistry,* 277**,** 21561-21566.

SUZUKI-INOUE, K., WILDE, J. I., ANDREWS, R. K., AUGER, J. M., SIRAGANIAN, R. P., SEKIYA, F., RHEE, S. G. & WATSON, S. P. 2004. Glycoproteins VI and Ib-IX-V stimulate tyrosine phosphorylation of tyrosine kinase Syk and phospholipase Cgamma2 at distinct sites. *Biochemical Journal,* 378**,** 1023-1029.

TAKAYAMA, H., HOSAKA, Y., NAKAYAMA, K., SHIRAKAWA, K., NAITOH, K., MATSUSUE, T., SHINOZAKI, M., HONDA, M., YATAGAI, Y., KAWAHARA, T., HIROSE, J., YOKOYAMA, T., KURIHARA, M. & FURUSAKO, S. 2008. A novel antiplatelet antibody therapy that induces cAMP-dependent endocytosis of the GPVI/Fc receptor γ-chain complex. *Journal of Clinical Investigation,* 118**,** 1785-1795.

TAM, J. & MERINO, D. 2015. Stochastic optical reconstruction microscopy (STORM) in comparison with stimulated emission depletion (STED) and other imaging methods. *Journal of Neurochemistry,* 135**,** 643-658.

TEFFERI, A. & PARDANANI, A. 2019. Essential Thrombocythemia. *New England Journal of Medicine,* 381**,** 2135-2144.

THOMAS, S. G. 2019. The structure of resting and activated platelets. *Platelets***,** 47-77.

THOMAS, S. G., CALAMINUS, S. D., AUGER, J. M., WATSON, S. P. & MACHESKY, L. M. 2007. Studies on the actin-binding protein HS1 in platelets. *BMC cell biology,* 8**,** 1-8.

THON, J. N. & ITALIANO, J. E. 2010. Platelet Formation. *Seminars in Hematology,* 47**,** 220-226.

THORLEY, J. A., PIKE, J. & RAPPOPORT, J. Z. 2014. Chapter 14 - Super-resolution Microscopy: A Comparison of Commercially Available Options. *In:* CORNEA, A. & CONN, P. M. (eds.) *Fluorescence Microscopy.* Boston: Academic Press.

TIEDT, R., SCHOMBER, T., HAO-SHEN, H. & SKODA, R. C. 2007. Pf4-Cre transgenic mice allow the generation of lineage-restricted gene knockouts for studying megakaryocyte and platelet function in vivo. *Blood,* 109**,** 1503-1506.

TILBURG, J., BECKER, I. C. & ITALIANO, J. E. 2022. Don't you forget about me(gakaryocytes). *Blood,* 139**,** 3245-3254.

TILLBERG, P. W., CHEN, F., PIATKEVICH, K. D., ZHAO, Y., YU, C. C., ENGLISH, B. P., GAO, L., MARTORELL, A., SUK, H. J., YOSHIDA, F., DEGENNARO, E. M., ROOSSIEN, D. H., GONG, G., SENEVIRATNE, U., TANNENBAUM, S. R., DESIMONE, R., CAI, D. & BOYDEN, E. S. 2016. Protein-retention expansion microscopy of cells and tissues labeled using standard fluorescent proteins and antibodies. *Nat Biotechnol,* 34**,** 987-92.

TRUCKENBRODT, S., MAIDORN, M., CRZAN, D., WILDHAGEN, H., KABATAS, S. & RIZZOLI, S. O. 2018. X10 expansion microscopy enables 25-nm resolution on conventional microscopes. *EMBO reports,* 19**,** e45836.

TRUCKENBRODT, S., SOMMER, C., RIZZOLI, S. O. & DANZL, J. G. 2019. A practical guide to optimization in X10 expansion microscopy. *Nat Protoc,* 14**,** 832-863.

TSUJI, M., EZUMI, Y., ARAI, M. & TAKAYAMA, H. 1997. A novel association of Fc receptor gamma-chain with glycoprotein VI and their co-expression as a collagen receptor in human platelets. *J Biol Chem,* 272**,** 23528-31.

TWOMEY, L., G. WALLACE, R., M. CUMMINS, P., DEGRYSE, B., SHERIDAN, S., HARRISON, M., MOYNA, N., MEADE-MURPHY, G., NAVASIOLAVA, N., CUSTAUD, M.-A. & P. MURPHY, R. 2019. Platelets: From Formation to Function. IntechOpen.

TYAGI, T., JAIN, K., GU, S. X., QIU, M., GU, V. W., MELCHINGER, H., RINDER, H., MARTIN, K. A., GARDINER, E. E., LEE, A. I., TANG, W. H. & HWA, J. 2022. A guide to molecular and functional investigations of platelets to bridge basic and clinical sciences. *Nature Cardiovascular Research,* 1**,** 223-237.

UNDAS, A. & ARIËNS, R. A. S. 2011. Fibrin Clot Structure and Function. *Arteriosclerosis, Thrombosis, and Vascular Biology,* 31**,** e88-e99.

UNTERAUER, E. M. & JUNGMANN, R. 2022. Quantitative Imaging With DNA-PAINT for Applications in Synaptic Neuroscience. *Frontiers in Synaptic Neuroscience,* 13.

VALLI, J., GARCIA-BURGOS, A., ROONEY, L. M., VALE DE MELO E OLIVEIRA, B., DUNCAN, R. R. & RICKMAN, C. 2021. Seeing beyond the limit: A guide to choosing the right super-resolution microscopy technique. *Journal of Biological Chemistry,* 297**,** 100791.

VARGA-SZABO, D., BRAUN, A. & NIESWANDT, B. 2009. Calcium signaling in platelets. *Journal of Thrombosis and Haemostasis,* 7**,** 1057-1066.

VEREB, G., NAGY, P., & SZÖLLO, J. 2011. Flow cytometric FRET analysis of protein interaction. In Flow Cytometry Protocols. *Humana Press* 371-392.

VIGNOLI, A., GIACCHERINI, C., MARCHETTI, M., VERZEROLI, C., GARGANTINI, C., DA PRADA, L., GIUSSANI, B. & FALANGA, A. 2013. Tissue Factor Expression on Platelet Surface during Preparation and Storage of Platelet Concentrates. *Transfus Med Hemother,* 40**,** 126-32.

VU, T.-K. H., HUNG, D. T., WHEATON, V. I. & COUGHLIN, S. R. 1991. Molecular cloning of a functional thrombin receptor reveals a novel proteolytic mechanism of receptor activation. *Cell,* 64**,** 1057-1068.

WAGNER, C. L., MASCELLI, M. A., NEBLOCK, D. S., WEISMAN, H. F., COLLER, B. S. & JORDAN, R. E. 1996. Analysis of GPIIb/IIIa receptor number by quantification of 7E3 binding to human platelets.

WANG, Y., YU, Z., CAHOON, C. K., PARMELY, T., THOMAS, N., UNRUH, J. R., SLAUGHTER, B. D. & HAWLEY, R. S. 2018. Combined expansion microscopy with structured illumination microscopy for analyzing protein complexes. *Nat Protoc,* 13**,** 1869-1895.

WEISS, L. J., DRAYSS, M., MANUKJAN, G., ZEITLHÖEFLER, M. J., KLEISS, J., WEIGEL, M. L., HERRMANN, J., MOTT, K., BECK, S., BURKARD, P., LAM, T. T., ALTHAUS, K., BAKCHOUL, T., FRANTZ, S., MEYBOHM, P., NIESWANDT, B., WEISMANN, D. & SCHULZE, H. 2022. Uncoupling of platelet granule release and integrin activation suggests GPIIb/IIIa as therapeutic target in COVID-19. *Blood Adv*.

WERNER, M. & HANNUN, Y. 1991. Delayed accumulation of diacylglycerol in platelets as a mechanism for regulation of onset of aggregation and secretion. *Blood,* 78**,** 435-444.

WESTMORELAND, D., SHAW, M., GRIMES, W., METCALF, D. J., BURDEN, J. J., GOMEZ, K., KNIGHT, A. E. & CUTLER, D. F. 2016. Super-resolution microscopy as a potential approach to diagnosis of platelet granule disorders. *J Thromb Haemost,* 14**,** 839-49.

WHITE, J. G. 1981. Morphological studies of platelets and platelet reactions. *Vox Sang,* 40 Suppl 1**,** 8-17.

WIENS, K. M., LIN, H. & LIAO, D. 2005. Rac1 Induces the Clustering of AMPA Receptors during Spinogenesis. *The Journal of Neuroscience,* 25**,** 10627-10636.

WILLIAMSON, D., PIKOVSKI, I., CRANMER, S. L., MANGIN, P., MISTRY, N., DOMAGALA, T., CHEHAB, S., LANZA, F., SALEM, H. H. & JACKSON, S. P. 2002. Interaction between Platelet Glycoprotein Ibα and Filamin-1 Is Essential for Glycoprotein Ib/IX Receptor Anchorage at High Shear*. *Journal of Biological Chemistry,* 277**,** 2151-2159.

WILLIAMSON, D. J., OWEN, D. M., ROSSY, J., MAGENAU, A., WEHRMANN, M., GOODING, J. J. & GAUS, K. 2011. Pre-existing clusters of the adaptor Lat do not participate in early T cell signaling events. *Nat Immunol,* 12**,** 655-62.

WOJTUKIEWICZ, M. Z., SIERKO, E., HEMPEL, D., TUCKER, S. C. & HONN, K. V. 2017. Platelets and cancer angiogenesis nexus. *Cancer Metastasis Rev,* 36**,** 249-262.

WOLF, M. E., LUZ, B., NIEHAUS, L., BHOGAL, P., BÄZNER, H. & HENKES, H. 2021. Thrombocytopenia and Intracranial Venous Sinus Thrombosis after “COVID-19 Vaccine AstraZeneca” Exposure. *Journal of Clinical Medicine,* 10**,** 1599.

WÖLLERT, T. & LANGFORD, G. M. 2022. Super-Resolution Imaging of the Actin Cytoskeleton in Living Cells Using TIRF-SIM. *Methods Mol Biol,* 2364**,** 3-24.

WORONOWICZ, K., DILKS, J. R., ROZENVAYN, N., DOWAL, L., BLAIR, P. S., PETERS, C. G., WORONOWICZ, L. & FLAUMENHAFT, R. 2010. The platelet actin cytoskeleton associates with SNAREs and participates in alpha-granule secretion. *Biochemistry,* 49**,** 4533-42.

XU, H., TONG, Z., YE, Q., SUN, T., HONG, Z., ZHANG, L., BORTNICK, A., CHO, S., BEUZER, P. & AXELROD, J. 2019. Molecular organization of mammalian meiotic chromosome axis revealed by expansion STORM microscopy. *Proceedings of the National Academy of Sciences,* 116**,** 18423-18428.

YAGUCHI, A., LOBO, F., VINCENT, J. L. & PRADIER, O. 2004. Platelet function in sepsis. *Journal of thrombosis and haemostasis,* 2**,** 2096-2102.

ZAHID, M., MANGIN, P., LOYAU, S., HECHLER, B., BILLIALD, P., GACHET, C. & JANDROT-PERRUS, M. 2012. The future of glycoprotein VI as an antithrombotic target. *J. Thromb. Haemostasis,* 10**,** 2418.

ZAID, Y., PUHM, F., ALLAEYS, I., NAYA, A., OUDGHIRI, M., KHALKI, L., LIMAMI, Y., ZAID, N., SADKI, K., BEN EL HAJ, R., MAHIR, W., BELAYACHI, L., BELEFQUIH, B., BENOUDA, A., CHEIKH, A., LANGLOIS, M. A., CHERRAH, Y., FLAMAND, L., GUESSOUS, F. & BOILARD, E. 2020. Platelets Can Associate with SARS-Cov-2 RNA and Are Hyperactivated in COVID-19. *Circ Res,* 127**,** 1404-18.

ZHANG, W., DENG, W., ZHOU, L., XU, Y., YANG, W., LIANG, X., WANG, Y., KULMAN, J. D., ZHANG, X. F. & LI, R. 2015. Identification of a juxtamembrane mechanosensitive domain in the platelet mechanosensor glycoprotein Ib-IX complex. *Blood, The Journal of the American Society of Hematology,* 125**,** 562-569.

ZHOU, K., XIA, Y., YANG, M., XIAO, W., ZHAO, L., HU, R., SHOAIB, K. M., YAN, R. & DAI, K. 2022. Actin polymerization regulates glycoprotein Ibα shedding. *Platelets,* 33**,** 381-389.

ZUCKER-FRANKLIN, D. & KAUSHANSKY, K. 1996. Effect of thrombopoietin on the development of megakaryocytes and platelets: an ultrastructural analysis. *Blood,* 88**,** 1632-8.

ZWETTLER, F. U., REINHARD, S., GAMBAROTTO, D., BELL, T. D. M., HAMEL, V., GUICHARD, P. & SAUER, M. 2020. Molecular resolution imaging by post-labeling expansion single-molecule localization microscopy (Ex-SMLM). *Nat Commun,* 11**,** 3388.

CHAPTER 8: Appendix

8.1 List of abbreviations

4x	Four times
10x	Ten times
°C	Degrees Celsius
AA	Acrylamide
ACD	Acid citrate dextrose
AcX	Acryloyl-X
ADAM	A disintegrin and metalloproteinase
ADP	Adenosine diphosphate
AMR	Ashwell-Morell receptor
APS	Ammonium peroxodisulfate
ATP	Adenosine triphosphate
AU	Arbitrary units
AUC	Area under the curve
bp	Base pair
BPM	Beats per minute
BRET	Bioluminescence resonance energy transfer
BSA	Bovine serum albumin
Btk	Bruton’s tyrosine kinase
Ca^{2+}	Calcium cation
CaM	Calmodulin
CBD	Collagen-binding domain
CD	Cluster of differentiation
Cdc42	cell division cycle 42
CLEC-2	C-type lectin-like receptor 2
COVID-19	Coronavirus disease 2019
CRP	Collagen-related peptide
DAG	Diacylglycerol
DBSCAN	Density-based spatial Clustering of applications with noise
DDM	n-dodecyl-β-D-maltoside
DIC	Differential interference contrast
DMAA	N,N-dimethylacrylamide
DMSO	Dimethylsulfoxide

*d*STORM	*Direct* stochastic optical reconstruction microscopy
DTS	Dense tubular system
ECM	Extracellular matrix
EDTA	Ethylenediaminetetraacetic acid
EHT1864	2-(4-morpholinylmethyl)-5-[[5-[[7-(trifluoromethyl)-4-quinolinyl]thio]pentyl]oxy]-4H-pyran-4-one, dihydrochloride
ExM	Expansion microscopy
F	Factor
FA	Formaldehyde
F(ab')	Fragment antigen binding
FcR	Fc receptor
FCS	Fluorescence correlation spectroscopy
FITC	Fluorescein-isothiocyanate
FOV	Field of view
FRET	Fluorescence resonance energy transfer
GAP	GTPase-activating proteins
GAPDH	Glyceraldehyde 3-phosphate dehydrogenase
GEF	Guanine nucleotide exchange factor
GP	Glycoprotein
GPCR	G-protein coupled receptor
GPO	Glycine-proline-hydroxyproline
GTP	Guanine triphosphate
h	Hour
HSC	Hematopoietic stem cell
HEPES	N-2-Hydroxyethylpiperazine-N'-2-ethanesulfonic acid
HRP	Horseradish peroxidase
ICAM-2	intercellular adhesion molecule 2
Ig	Immunoglobulin
IL-4R	Interleukin 4 receptor
IP_3	Inositol-1.4.5-trisphosphate
ITAM	Immunoreceptor tyrosine-based activation motif
ITIM	Immunoreceptor tyrosine-based inhibitory motifs
JAM	Junction adhesion molecule
kDa	Kilodalton
KO	Knockout

LAT	Linker of activated T cells
LRR	Leucine-rich repeat
MAb	Monoclonal antibody
MFI	Mean fluorescence intensity
MK	Megakaryocytes
MSD	Mechanosensory domains
MT	Microtubules
NA	Numerical aperture
Nb	Nanobody
Nc-aggregation	Non-classical aggregation
NEM	N-ethylmaleimide
NOD2	Nucleotide-binding oligomerisation domain 2
ns	Not significant
NSC23776	N6-[2-[[4-(Diethylamino)-1-methylbutyl]amino]-6-methyl-4-pyrimidinyl]-2-methyl-4,6-quinolinediamine trihydrochloride
OCS	Open canicular system
PAGE	Polyacrylamide gel electrophoresis
PAINT	Point Accumulation in Nanoscale Topography
PALM	Photoactivated localisation microscopy
PAR	Protease activation receptor
PBS	Phosphate buffered saline
PE	Phycoerythrin
PF4	Platelet factor 4
PFA	Paraformaldehyde
PGI_2	Prostacyclin
PI3K	Phosphoinositide-3-kinase
PIP_2	Phosphatidylinositol-4,5-bisphosphate
PIP_3	phosphatidylinositol-3,4,5-trisphosphate
PLC	Phospholipase C
PRP	Platelet rich plasma
PS	Phosphatidylserine
PVDF	Polyvinylidene difluoride
pY	Tyrosine phosphorylation
Rac1	Ras-related C3 botulinum toxin substrate 1
RBC	Red blood cell

Rho	Ras homolog
ROI	Region of interest
rpm	Rotations per minute
RT	Room temperature
SARS-CoV-2	Severe acute respiratory syndrome coronavirus 2
SD	Standard deviation
SDS	Sodium dodecyl sulfate
SEM	Standard error of the mean
SFK	Src family tyrosine kinase
sGPVI	Soluble GPVI
SH	Src homology
SIM	Structured illumination microscopy
SLP-76	SH2 domain-containing leukocyte protein of 76 kDa
SMLM	Single-molecule localisation microscopy
SR	Super-resolution
STED	Stimulated emission depletion microscopy
Syk	Spleen tyrosine kinase
TAE	Tris-acetate-EDTA
TBS	Tris-buffered saline
TEMED	Tetramethylethylenediamine
TF	Tissue factor
Tg	Transgenic
TIRF	Total internal reflection fluorescence
TLR	Toll-like receptor
TPO	Thrombopoietin
TRIS	Tris(hydroxymethyl)aminomethane
Tspan	Tetraspanin
TTP	Thrombotic thrombocytopenic purpura
TxA2	Thromboxane A2
U-ExM	Ultrastructure expansion microscopy
vWF	Von Willebrand factor
WASP	Wiskott-Aldrich syndrome protein
WT	Wildtype
Y	Tyrosine

8.2 Acknowledgements

This PhD project was funded by the European Union's Horizon research and innovation programme under the Marie Skłodowska-Curie grant agreement (No. 766118). During the time of my PhD I was based in the Institute of Cardiovascular Sciences at the University of Birmingham, United Kingdom, in the research Group of Prof Steve P. Watson for almost 2 years, in the Institute of Experimental Biomedicine at the Rudolf Virchow Centre, University of Würzburg, Germany, in the research group of Prof Bernhard Nieswandt for 2 years, and in the Department of Biotechnology, at the University of Rijeka, Croatia, in the research group of Prof Antonija Jurak Begonja for 3 months.

First, I would like to thank all my supervisors for giving me the opportunity to perform my PhD in their groups and for all the support over the 4 years. A big thanks goes to Dr Natalie Poulter, my primary supervisor, for the continuous virtual support throughout my PhD journey. Due to her maternity leave, the COVD-19 pandemic and my several placements we barely spent time in person, but you were always there for me via ZOOM. You always supported me in a scientific and personal manner, and without you, I could not have completed my PhD. Thanks, Steve Watson, for taking over the role of being my primary supervisor during my first year of my PhD, for your great scientific feedback, continuous encouragement and positive attitude inside and outside the lab. I would also like to thank my supervisors in Würzburg, Bernhard and David, for all the support, help and scientific guidance and discussion, and my supervisor in Rijeka, Antonijia Jurak, for allowing me to spend 3 months in her laboratory, and learn new techniques.

I also would like to thank the following people that contributed with their help and support during my PhD:

From Birmingham: Chiara, Jo, Lourdes, and Gina for teaching me all the techniques and everything I needed to know about the lab. Thanks for your enormous patience and for the great fun we had inside and outside the lab. Dee and Jeremy, from COMPARE, for teaching me how to use all the microscopes and for the help and support to acquire and analyse the super-resolution microscopy data. The lab technicians Beata, Lourdes and Ying for taking care of everything we need and smoothly running the lab. To all my colleagues, and in special to Evie, Luis, Hilaire, Vanessa, Chris, Amanda and Josh for all the support and laughs.

From Würzburg: a special thanks to Dr Irina Pleines, the expert on Rac1 in platelets, for all the scientific help. To Stefano, for always withdrawing blood and for the long hours of scientific and personal discussions. To the imaging facility, Prof Katrin Heinze for her valuable support and expertise in expansion microscopy, Prateek and Luise for helping me to perform and analyse the expansion microscopy data, and all the Heinze members. Also, thanks to all of the technicians, especially Stefanie Harttman for generating all the F(ab') fragments. Helena, Timo, Zoltan, Vanessa and all the Nieswandt's and Stegner's members for their help and great time spent together.

From Rijeka, to Ana and Ivana for helping to adapt and for making my placement in Croatia the best part of the PhD. Also, thanks to Prof Elizabeth Gardiner, from Australia for the generous provision of the anti-GPVI antibodies.

To my parents, this PhD and anything that I have achieved in life is thanks to you. Thank you for all your unconditional love and support, and for all the sacrifices that you have made for my happiness. To my friends, Veronica, Alvaro, Claudia, Roberto, and Alba, for distracting me from work and listening to me complaining about the challenges of the PhD. To Till, thank you for your patience and for being always there for me.

8.3 List of publications

d'Alessandro, E., Becker, C., Bergmeier, W., Bode, C., Bourne, J. H., Brown, H., Buller, H. R., Ten Cate-Hoek, A. J., Ten Cate, V., van Cauteren, Y. J. M., Cheung, Y. F. H., Cleuren, A., Coenen, D., Crijns, H. J. G. M., de Simone, I., Dolleman, S. C., Klein, C. E., Fernandez, D. I., Granneman, L., van T Hof, A., **Neagoe, R.A.I.**, Renske, H.O … Scientific Reviewer Committee (2020). Thrombo-Inflammation in Cardiovascular Disease: An Expert Consensus Document from the Third Maastricht Consensus Conference on Thrombosis. *Thrombosis and haemostasis*, 120(4), 538–564.

Scheller, I., Beck, S., Göb, V., Gross, C., **Neagoe, R. A. I.**, Aurbach, K., Bender, M., Stegner, D., Nagy, Z., & Nieswandt, B. (2021). Thymosin β4 is essential for thrombus formation by controlling the G-actin/F-actin equilibrium in platelets. *Haematologica*, 10.3324/haematol.2021.278537.

Clark, J. C., **Neagoe, R. A. I**., Zuidscherwoude, M., Kavanagh, D. M., Slater, A., Martin, E. M., Soave, M., Stegner, D., Nieswandt, B., Poulter, N. S., Hummert, J., Herten, D.-P., Tomlinson, M. G., Hill, S. J., & Watson, S. P. (2021). Evidence that GPVI is Expressed as a Mixture of Monomers and Dimers, and that the D2 Domain is not Essential for GPVI Activation. *Thrombosis and Haemostasis*, 121(11), 1435–1447.

Neagoe, R. A. I., Gardiner, E. E., Stegner, D., Nieswandt, B., Watson, S. P., & Poulter, N. S. (2022). Rac Inhibition Causes Impaired GPVI Signalling in Human Platelets through GPVI Shedding and Reduction in PLCγ2 Phosphorylation. *International journal of molecular sciences*, 23(7), 3746.

8.5 Affidavit

I hereby confirm that my thesis entitled “Development of techniques for studying the platelet glycoprotein receptors GPVI and GPIb localisation and signalling” is the result of my own work. I did not receive any help or support from commercial consultants. All sources and / or materials applied are listed and specified in the thesis.

Furthermore, I confirm that this thesis has not yet been submitted as part of another examination process neither in identical nor in similar form.

Würzburg, November 2022 _____

Neagoe, Raluca Alexandra Iulia

8.6 Eidesstattliche Erklärung

Hiermit erkläre ich an Eides statt, die Dissertation “Entwicklung von Methoden zur Untersuchung zur der Lokalisation und Signaltransduktion der Thrombozytenrezeptoren GPVI und GPIb” eigenständig, d.h. insbesondere selbständig und ohne Hilfe eines kommerziellen Promotionsberaters, angefertigt und keine anderen als die von mir angegebenen Quellen und Hilfsmittel verwendet zu haben.

Ich erkläre außerdem, dass die Dissertation weder in gleicher noch in ähnlicher Form bereits in einem anderen Prüfungsverfahren vorgelegen hat.

Würzburg, November 2022 _____

Neagoe, Raluca Alexandra Iulia